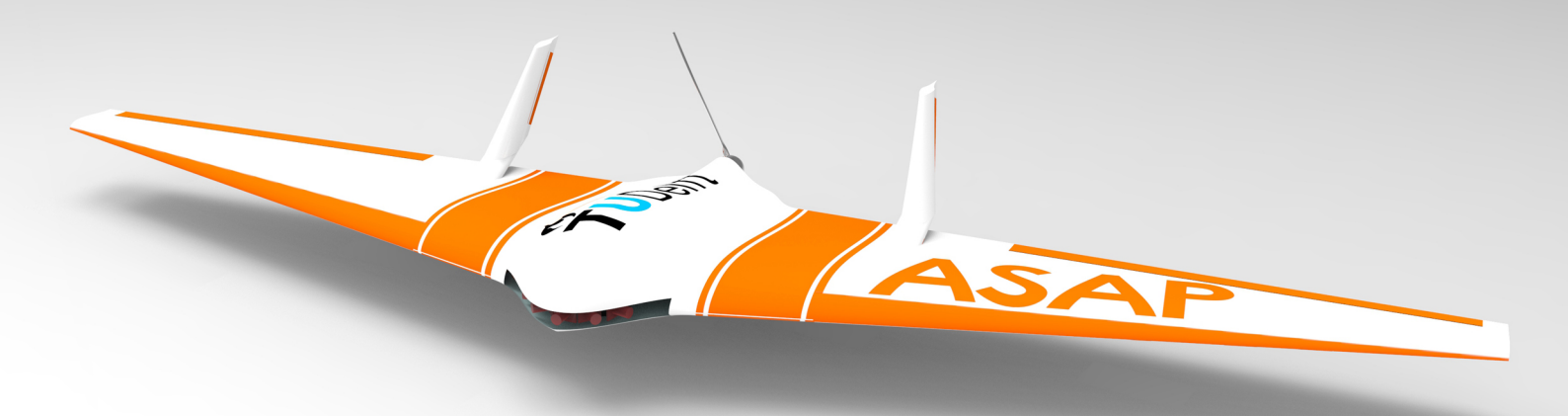
Final Report

Design Synthesis Exercise - Spring 2014

Group 03:

All-Weather All-Polymer Search and Rescue UAV





FINAL REPORT

DESIGN SYNTHESIS EXERCISE - SPRING 2014

by



D. van den Bergen 4078047

- Quality Control - Structures &
- Structures & Materials Department



T. Blondeel 4160681

 Performance & Propulsion Department



B. Durieux 1274279

- Control & Stability Department



D.N.E. Maxence 4104854

- External Communications
- Aerodynamics Department



J.M. van Mourik Broekman 1517759

- Chairman
- Aerodynamics Department



T.J.E. Schouten 4104463

- Quality Control
- Performance & Propulsion Department



S. Vial 4111303

- Chief Engineer - Structures &
- Structures & Materials
 Department



R.S. de Wit 4091639

- Lead Engineer Structures & Materials Department



M. Wolken 4009703

- Structures & Materials Department



N.J. van Wonderen 4170466

- Chief Engineer
- Control & Stability Department

Date: May 23rd, 2014

Supervisor: T.J. Dingemans, J.A. Melkert, D. Zarouchas



CHANGE RECORD

Issue	Date	Pages affected former document	Pages affected new document	Brief description of changes
1.1	23-May-2014	All		New document
1.2	26-June-2014	ix-xi	xv-xvii	Adjusted summary
		xvii-xviii	xiii-xiv	Expanded list of symbols
		1	1	Mission statement adjusted
		6	8	Figure 3.2 is altered
		_	9	Added paragraph detection of victims
		9	11	Changed shape to prismatic shape
		9	12	Expanded Table 3.5
		9	12	Adjusted Subsystems: Battery system
		19	22	Selected a new heated pitot tube
		23	24	Leeway vector figure
		25	26	Stall velocity added
		25	29	Fairing at wingtip
		32	36	Added waterproof description
		_	33	Correction mean time between failure
		_	33	Added error detection
		34		Correction of faulty value MTBF
		_	35	Added description about Hard time vs on
				condition maintenance
		34	38	Update Figure 5.2
		37	40	Update End of Life of Payload
		42	47	Altered Figure 6.3
		43	49	Explanation creep due to plasticizers added
		44	49	Explanation about sinking added
		45	50	Altered Figure 6.5b
		45	51	Constituents coating added
		46	51	Determination impact toughness adjusted
		_	52	Added paragraph adhesives
		47	54	Explanation added reference systems
		47	54	Elastic axis added
		49-50	56-58	Figures converted to black and white
		_	59-60	Stress adhesive bonding added
		52	61	Stress evasive method added
		54	63	Explanation impact toughness added
		_	64	Thickness optimization added
		55	64	Figure 6.21 minimum thickness changed
		59	70	Figure 8.2 enlarged to increase readability
		64	74	Camber line added to the airfoil cross sections
		64	76	An additional explanation of the sharpnes paramater Δy
		66	78	Wing twist explained as an option to reduce tip stall

68	80	Additional motivation for the use of
		elevons
78	83	Height and width of tail
37	87-92	MAI: correcting comments
37	92	MAI: Battery integration
84	95	Weight budget revision: included
		sensitivity and polymer content
_	90	MAI Adhesive bonding added
90	95	Sensitivity of design to weight budget
89	97	Included information about bulk
		purchasing of items
86	100	Table containing cost estimation results in
		Euro
90	103	Changed waste percentage piechart and
		text
92	104	Figure CO2 emission changed for
		readability
100	112	Changed formulation for PERF-10
101	116-117	Added risk descriptions in text
129-130	_	Removed Risk appendix
All	All	Spell check of content
		•

PREFACE

This is the fourth and final report in a series for the Spring 2014 Design Synthesis Exercise (DSE). This report is preceded by the Project Plan, the Baseline Report and the Mid Term Report.

The DSE concludes the Bachelor Aerospace Engineering (BSc AE) at Delft University of Technology. As the final project, it is a multi-disciplinary assignment combining all courses and projects preceding it in the BSc AE. New subjects are introduced such as an extensive literature study, project management, sustainability, production of aerospace systems and cost & business strategy.

In the first place, the design team would like to thank T.J. Dingemans, J.A. Melkert and D. Zarouchas for composing the assignment, monitoring the progress and acting as critical customers. Second, special thanks to R. Moleman from Koninklijke Nederlandse Redding Maatschappij (KNRM) for providing valuable information on (Dutch) Search And Rescue (SAR) and the (future) role of Unmanned Aerial Systems (UASs).

CONTENTS

List of Tables							
List of Tables List of Abbreviations Summary 1 Introduction 2 Baseline Report and Mid-Term Report Recap 2.1 Market Analysis 2.1.1 Targeted Customers. 2.1.2 Design Goals 2.2 Mission Analysis 2.3 List of Requirements 2.4 Concepts 2.5 Trade-Off 2.5.1 Payload 2.5.2 Energy Storage 2.5.3 Configuration 3 Subsystem characteristics 3.1 Hard- and Software Interaction 3.1.1 Hardware interaction 3.1.2 Software interaction 3.2 Payload 3.3 Detection of victims 3.4 Motor	Preface iv						
List of Abbreviations Summary 1 Introduction 2 Baseline Report and Mid-Term Report Recap 2.1 Market Analysis .	viii						
Summary 1 Introduction 2 Baseline Report and Mid-Term Report Recap 2.1 Market Analysis . 2.1.1 Targeted Customers. 2.1.2 Design Goals . 2.2 Mission Analysis 2.3 List of Requirements 2.4 Concepts 2.5 Trade-Off . 2.5.1 Payload . 2.5.2 Energy Storage . 2.5.3 Configuration 3 Subsystem characteristics 3.1 Hard- and Software Interaction . 3.1.1 Hardware interaction . 3.1.2 Software interaction . 3.2 Payload . 3.3 Detection of victims . 3.4 Motor .	X						
1 Introduction 2 Baseline Report and Mid-Term Report Recap 2.1 Market Analysis . 2.1.1 Targeted Customers . 2.1.2 Design Goals . 2.2 Mission Analysis . 2.3 List of Requirements . 2.4 Concepts . 2.5 Trade-Off . 2.5.1 Payload . 2.5.2 Energy Storage . 2.5.3 Configuration . 3 Subsystem characteristics 3.1 Hard- and Software Interaction . 3.1.1 Hardware interaction . 3.1.2 Software interaction . 3.1.2 Software interaction . 3.2 Payload . 3.3 Detection of victims . 3.4 Motor .	xii						
2 Baseline Report and Mid-Term Report Recap 2.1 Market Analysis 2.1.1 Targeted Customers. 2.1.2 Design Goals 2.2 Mission Analysis 2.3 List of Requirements 2.4 Concepts 2.5 Trade-Off 2.5.1 Payload 2.5.2 Energy Storage 2.5.3 Configuration 3 Subsystem characteristics 3.1 Hard- and Software Interaction 3.1.1 Hardware interaction 3.1.2 Software interaction 3.2 Payload 3.3 Detection of victims 3.4 Motor	xv						
2.1 Market Analysis 2.1.1 Targeted Customers. 2.1.2 Design Goals 2.2 Mission Analysis 2.3 List of Requirements 2.4 Concepts 2.5 Trade-Off 2.5.1 Payload 2.5.2 Energy Storage 2.5.3 Configuration 3 Subsystem characteristics 3.1 Hard- and Software Interaction 3.1.1 Hardware interaction 3.1.2 Software interaction 3.2 Payload 3.3 Detection of victims 3.4 Motor	1						
2.5 Trade-Off 2.5.1 Payload 2.5.2 Energy Storage 2.5.3 Configuration 3 Subsystem characteristics 3.1 Hard- and Software Interaction 3.1.1 Hardware interaction. 3.1.2 Software interaction 3.1.2 Software interaction 3.2 Payload 3.3 Detection of victims. 3.4 Motor.	3 3 3 3 4						
3.1 Hard- and Software Interaction	4 4 4 4						
3.9 Autopilot, computer and SSD	11 15 17 19						
4 Operations & Logistics 4.1 Mission Duration, Search Pattern and Swarm Operations. 4.1.1 Mission Duration. 4.1.2 Flight pattern. 4.1.3 Swarm search operation 4.2 Take-off. 4.3 Landing. 4.4 Stationkeeping 4.5 Storage	21 21 21 23 24 25						

CONTENTS

5	5 Life Cycle	29
	5.1 Reliability, Availability, Maintainability and Safety (RAMS)	
	5.1.1 Reliability	
	5.1.2 Maintainability	
	5.1.3 Availability	
	5.1.4 Safety	
	5.2 End of Life disposal	
G	6 Materials and structure	41
	6.1 Biodegradable polymers	
	6.1.1 Bio fibers	
	,	
	0	
	6.1.4 Adhesives	
	6.2 Structure	
	6.2.1 Loads and Stresses in wings	
	6.2.2 Deflection wings	
	6.2.3 Wing fuselage interaction	
	6.2.4 Stresses within fuselage	
	6.2.5 Impact toughness regarding hail	
	6.2.6 Thickness optimization	
	6.3 Conclusion on materials and structure	
7	7 Internal Layout	63
^	O Flight Denfermence and Association	0.5
	8 Flight Performance and Aerodynamic Characteristics	65
	8.1 Additional requirements	
	8.2 Flight Performance	
	8.3 Airfoil Selection	
	8.4 Planform Parameters	
	8.5 Final Flight Performance and Aerodynamic Characteristics	
	8.5.1 Airfoil trade-off	
	8.5.2 Stability analysis	
	8.6 Final wing planform selection	
	8.6.1 Elevons	
	8.7 Final parameters and characteristics	
9	9 Manufacturing, Assembly and Integration	85
	9.1 Manufacturing	
	9.1.1 Molding of composites	
	9.1.2 components	
	9.2 Assembly	
	9.2.1 Mechanical fastening	
	9.2.2 Adhesive bonding	
	9.2.3 Attachment of separate wings (Connection A & B)	
	9.2.4 Attachment Fuselage top panel to wings (Connection A and	
	9.2.5 Attachment of Fairing	
	9.2.6 Attachment of tails and rudder	
	9.2.7 Attachment of elevons	
	9.3 Integration	
	10 Budget allocation	93
	10.1 Weight budget	
	10.1.1 Component Weigths	
	10.1.2 Sensitivity of the design	
	10.1.3 Polymer content of final design	

CONTENTS

10.2.1 Resea 10.2.2 Finar 10.2.3 Total 10.2.4 Manu 10.2.5 Open	get	n (RDTE) Cost	Estimate	 	
	cap				
12.2 Rule of M 12.3 Structures 12.4 Requirem 12.4.1 Desig 12.4.2 Desig 12.5 Risk Analy 12.5.1 Missi	nd Validation nce tool			 	
	esign & Development Logic planning				
14.1 Conclusio	Recommendations on				
0 - 1	ircraft Manufacturing				133
A EIO-LCA for As B Personal Appe	· ·				133 136
B.1 D. van der B.2 T. Blondee B.3 B. Durieu: B.4 D.N.E. Ma B.5 J.M. van M B.6 T.J.E. Scho B.7 S. Vial B.8 R.S. de Wi	n Bergen				
	Vonderen				

LIST OF FIGURES

1	The internal layout of the ASAP UAV	XVI
3.1	The Hardware Block Diagram of the ASAP UAV	5
3.2	The Software Block Diagram of the ASAP UAV	6
	Electrical interaction between the battery and the subsystems	11
	The lay-out Autonomous SAR All Polymer (ASAP) Unmanned Aerial Vehicle (UAV)'s computer .	12
	The autopilot's data flow	12
	The data handling of the engine control unit	13
3.7	The data are assistant false. See 8 April and a d	13
	The data processing of the See&Avoid payload	14
	The data processing of the imaging payload	14
	Communication block diagram	17
3.11	Rain attention in function of band frequency	19
4.1	The Leeway vector which describes the velocity and direction of the victim in the water	22
4.2	The leeway in knots for different objects in water for different wind speeds	22
4.3	The expanding square search pattern around the datum	23
4.4	The flight pattern relative to the ground. The UAV starts at the left bottom. A: No wind. B:	
	Downwind. C: Upwind.	23
4.5	*	24
	(, F, F	
5.1	Redundancy for components with an MTBF of 50 and 100 hours	31
	UAV maintenance interval timeline, indicating the amount of missions between the mainte-	
	nance activities. Black indicates maintenance or overhaul and grey indicates scheduled inspec-	
		36
		00
6.1	The effect of temperature on PLA and PLA/Flax composites	42
	Creep strain versus time at 0.45 MPa with test temperature: (a) 30°C, (b) 40°C, and (c) 50°C for	
	different levels of hydrocarbon liquid concentration (C)	43
6.3	Stress–strain curves of a PLLA/30%Flax composite compared to other thermoplastic composites.	
	Water absorption of pure polymers and composites	47
	Curing cycles for several curing temperatures	51
	Fatigue strength of simple lap joints made with a cold-cured epoxy adhesive.	51
	Reference frames used for the structural tool	52
	Forces and moments on the skin with thickness 2.0 during cruise flight	53
	Stress distribution in the wings during cruise flight, with a skin thickness of 2.0 mm	54
	Stress distribution in the wings during launch with a skin thickness of 2.0 mm	55
	Stress distribution in the wings during landing with a skin thickness of 2.0 mm $$	55
	Stress distribution in the wings during launch with a skin of thickness 2.0 mm, without vertical	
	forces	56
6.14	Von Mises stress distribution from root (left) to tip (right) in the top front spar during launch	
	with constant skin thickness 2.0 mm	56
6.15	Deflections with a 2 mm skin thickness and compound material	57
6.16	Several loading conditions with their stress components	57
	Effects on peel stress due to secondary bending	58
	Stress calculations surrounding defects in the skin	59
	Stress distribution top panel fuselage	59
	Diagram for calculating the impact stresses due to hail	60
	Minimum thickness required for hail impacts with a diameter of 5.1 cm	61

LIST OF FIGURES ix

7.1 7.2	The internal layout of the ASAP UAV	63 64
8.2 8.3 8.4 8.5 8.6 8.7	The iterative process to optimize the design for mission performance	65 66 67 70 70
	Airfoil candidates	71 72
	$\frac{C_{L_{max}}}{C_{l_{max}}}$ in function of ΔY and Λ_{LE} for high-aspect ratio wings without twist	72
8.11 8.12 8.13	Stability of a reflex airfoil	76 77 78 80
9.1 9.2 9.3	Trade-off table for the assembly of the ASAP UAV	87 88
	ample) [103]	89 89 90 90
	Pie-chart showing the mass-percentage of the UAV in terms of recyclable, biodegradable and waste creating	
12.1	Distribution of Forces and Moments along the span of the wing box	106
	The post-DSE project design and development logic flow diagram	
14.2	The internal layout of the ASAP UAV	120
	waste creating	121

LIST OF TABLES

3.1	Amount of pixels of a human head and the Line Of Sight (LOS) per service altitude	7
3.2	Specifications of the Hacker A30-14L V3 brushless Direct Current (DC) motor	8
3.3	Specifications of the Hacker X-40 SB-Pro brushless DC motor controller	8
3.4	Specifications of the GWS Park HPX F servo	9
3.5	Battery specifications	10
3.6	Required voltages	10
3.7	Specifications of the EO camera's video footage	15
3.8	Specifications of the thermal camera's video footage	15
3.9	Specifications of the NavStik Main Board	16
3.10	Specifications of the NavStik Interface Board	16
	Specifications of the STWD100NYWY3F Watchdog timer	16
	Specifications of the Samsung MicroSDXC Pro 64GB	16
	Link budget for both frequencies of the ASAP UAV	18
3.14	Properties of the Eagle Tree Prandtl-Pitot Tube	19
4.1		24
4.2	Advantages and disadvantages of landing methods for the ASAP UAV	26
- 1	P. II	20
5.1	Failure category per components per mission	30
5.2	Expected MTBF and reliability of catastrophic failure category parts, and total UAV Reliability .	31
5.3	Expected MTBF and reliability of catastrophic failure category parts, and total UAV Reliability.	32
5.4	Expected MTBF and reliability of catastrophic, critical and moderate failure category parts, and	20
	total Mission Reliability	32
5.5	Maintenance procedure and characteristics for the UAV subsystems	35
6.1	Material properties of PLA polymers	41
6.2	Material properties of Rayon and Flax	43
6.3	Material properties of scutched Flax fibers	43
6.4	Material properties of 30% short fiber flax composites	45
6.5	Material properties of continuous fiber composites	46
6.6	The effects of Triacetin on PLA and a 40% PLA/FLAX composite	46
6.7	Biodegradability of bio composite PLA/ramie in the Baltic Sea and compost	48
6.8	Specifications of different hail sizes	49
6.9	Several adhesives and their properties	50
6.10	Table relevant parameters for optimized skin thickness	61
7.1	Dimensions and volumes of different part of the ASAP UAV	64
8.1	The planform parameters, the effect of an increase of these parameters and the effect particular to the ASAP UAV	72
0.2		73 75
	Airfoil trade-off table	75 75
	Weight distribution of all elements, including their respective Center of Gravity (c.g.) location .	75 70
	Elevon characteristics	79
	The final aerodynamic and planform parameters for the ASAP UAV	82
	The final aerodynamic and planform parameters for the ASAP UAV	83
9.1	Definition of the trade-off criteria of the assembly	86
	Assembly methods	87
10.1	Component weight breakdown	93

LIST OF TABLES xi

10.2 Cost for Commercial off-the-shelf (COTS) systems on board of the ASAP UAV	96
10.3 Total cost per phase of design as well as service contract price per flight hour for the ASAP UAV,	
per number of UAV sales, in US dollar	98
10.4 Total cost per phase of design as well as service contract price per flight hour for the ASAP UAV,	
per number of UAV sales, in Euro	99
$10.5\ \hat{\text{Comparison}}$ between Baseline Report (BR) Cost Budget and Final Report (FR) Cost Estimation .	99
12.1 Constants for the verification of the flight performance tool	
12.2 Performance tool verification results	104
12.3 Material properties of several calculated composites and existing composites	
12.4 Verification results for the structures tool	106
12.5 Derived requirements compliance matrix	108
12.5 Mission requirements for the SAR UAV (continued)	109
12.6 Customer requirement matrix	110
12.6 Customer and mission requirements for the SAR UAV	
12.7 Structural Mission Risk Analysis	112
12.8 Power and Performance Mission Risk Analysis	
12.9 Control Mission Risk Analysis	113
12.10On-board Systems Mission Risk Analysis	113
12.11Mission Consequence Risk Map	114
14.1 The final aerodynamic and planform parameters for the ASAP UAV	122
A.1 The Economic Input-Output Life Cycle Assessment (EIO-LCA.) result	134
A.1 (continued)	135

LIST OF ABBREVIATIONS

a.c. ALRE ALU AOA AR ASAP	Aerodynamic center Aircraft Launch & Recovery Equipment Arithmetic Logical Unit Angle of Attack Aspect Ratio Autonomous SAR All Polymer	KNRM LOS M.A.C. MicroSD MTBF	Koninklijke Nederlandse Redding Maatschappij Line Of Sight Mean Aerodynamic Chord Micro Secure Digital Mean Time Between Failure
BER	Bit-Error Rate	MTBM	Mean Time Between Maintenance
Bft	Beaufort	MTR	Mid-Term Review
BR	Baseline Report	n.p.	Neutral Point
CEF	Cost Escalation Factor	PCB	Printed Circuit Board
CFD	Computational Fluid Dynamics	PLA	Polylactic Acid
c.g.	Center of Gravity	PP	Poly-propylene
COTS	Commercial off-the-shelf	PPI	Producer Price Index
CPU	Central Processing Unit	RAM	Random Access Memory
CU	Control Unit	RAMS	Reliability, Availability, Maintainability,
DC	Direct Current		Safety
DoD	Depth of Discharge	RDTE	Research, Development, Testing & Eval-
DSE	Design Synthesis Exercise		uation
EIO-LCA.	Economic Input-Output Life Cycle As-	RoI	Return on Investment
	sessment	S&A	See and Avoid
EIRP	Effective Isotropic Radiated Power	SAR	Search And Rescue
EO	Electro-Optical	SD	Secure Digital
EOL	End Of Life	SNR	Signal to Noise Ratio
F/C	Flight Computer	SSD	Solid State Drive
FEM	Finite Element Method	UAS	Unmanned Aerial System
FPGA	Field-Programmable Gate Array	UAV	Unmanned Aerial Vehicle
GNC	Guidance, Navigation and Control	UED	Ultra Ever Dry
GPS	Global Positioning System	USD	US Dollar
ICAO	International Civil Aviation Organisation	UV	Ultra Violet

LIST OF SYMBOLS

δ	Sheet thickness [m]	D_b	Induced drag box plane [N]
ϵ	Angle of twist [deg]	$D_{i,m}$	Induced drag monoplane [N]
η_0	fiber orientation efficiency factor [-]	dV	Airspeed difference $[km/hr]$
η_L	fiber length efficiency factor [-]	E	Youngs Modulus [GPa]
η_{LTD}	Life-time degradation efficiency [-]	e	Oswald factor [-]
Γ	Dihedral angle [deg]	E_f	fiber Young's modulus [GPa]
Λ	Sweep [deg]	E_r	Resin Young's modulus [GPa]
λ	Taper [-]	E_{D_m}	Energy-mass density $\left[\frac{Wh}{kg}\right]$
λ	Wavelength [m]	E_{D_m}	Energy-volume density $\left[\frac{Wh}{l}\right]$
		E_{tot}	Total Young's Modulus [GPa]
ω_s^{max}	Maximum deflection skin [m]	F_{land}	Force during landing [N]
Φ	Bank angle [deg]	FH	Flight hours [hrs]
$ ho_c$	material density of the composite $[\frac{kg}{m^3}]$	G_m	Shear modulus [dB]
$ ho_f$	material density of the fibers $[\frac{kg}{m^3}]$	G_R	receiver antenna gain [dB]
$ ho_r$	material density of the resin $\left[\frac{kg}{m^3}\right]$	G_T	Transmitter antenna gain [dB]
σ	Normal stress [Pa]	Н	Endurance [hr]
σ	Ratio between height and width box wing [-]	i_w	Incidence angle [deg]
σ_d^{max}	Maximum dynamic stress [Pa]	k	fiber efficiency factor [-]
	•	K_t	Stress intensity factor [-]
σ_f	fiber tensile strength [Pa]	L	Lift [N]
σ_{tot}	Total tensile strength [Pa]	L/D	Lift over Drag ratio [-]
σ_{um}	Matrix stress at fiber failure strain [Pa]	L_P	absorptive propagation loss [dB]
τ_a	Shear stress adhesive [Pa]	L_{rail}	Length of the rail launch system [m]
a	Acceleration of the UAV $[m/s^2]$	L_R	receiving signal loss from the receiver antenna through the amplifier [dB]
A_0	Operational availability [%]	L_T	Signal loss [dB]
A_a	Achieved availability[%]	m	Mass of the UAV [kg]
A_i	Inherent availability [%]	MDT	Maintenance Down Time [hrs]
AR	Aspect ratio [-]		Mean time between Failures [hrs]
b	Wing span [m]		Time to repair [hrs]
$C_{d,0}$	zero-lift drag coefficient [-]	n	Load factor [-]
$C_{d,i}$	Induced drag coefficient [-]	N_i	Noise

N_{Rep}	Number of repair activities [-]	C_r	Root chord [m]
P	Power [W]	C_t	Tip chord [m]
P_{req}	Required power [W]	$C_{L_{\max}}$	3D lift coefficient [-]
P_T	Transmitted power [W]	$C_{l_{ m max}}$	2D maximum lift coefficient [-]
q	Dynamic pressure [Pa]	$C_{l_{des}}$	2D design lift coefficient [-]
R	Quantifiable reliability [%]	$C_{l_{\delta_A}}$	Moment coefficient per deflection of ailerons
R	Range [km]		[-]
S	Surface area wing $[m^2]$	$C_{m_{ac}}$	Moment coefficient around a.c. [-]
s_{land}	Landing distance [m]	i_w	Incidence angle [deg]
t	Time over which reliability is measured [hrs]	C_m	Moment coefficient [-]
T_{g}	Glass transition temperature [°C]	В	Bandwidth [Hz]
	of Sum of total repair time [hrs]	b	Width of a joint [m]
υ υ	Poisson ratio [-]	D	Diameter nut [mm]
	Fiber volume fraction [-]	d	Average Flax fiber diameter [dB]
V_f		F	Noise factor
V_r	Resin volume fraction [-]	h	Amount of hours [hr]
V_{endur}	ance Airspeed for optimum endurance $[m/s]$	k	Boltzmann constant [$m^2kgs^{-2}K^{-1}$]
V_{max}	Maximum airspeed $[m/s]$	L	Fiber length of Flax [dB]
V_{min}	Minimum airspeed $[m/s]$	L	Overlap length [m]
V_{range}	Airspeed for optimum range $[m/s]$	P	Load [N]
v_{releas}	$_{e}$ Release velocity of the UAV at take-off $[m/s]$	R	distance between the transmitter and the re-
v_{wind}	Wind velocity [m/s]	It	ceiver [m]
W	Weight [N]	SD	Secure Digital
W/S	Wing loading $[N/m^2]$	SSD	Solid state drive
\dot{P}	Roll rate [deg/s]	T	Temperature [K]
λ	Failure rate [1/hr]	t	Sheet thickness [m]

SUMMARY

In 2013 the KNRM performed approximately 2000 search and rescue missions without the use of UAVs. The total costs rounded up to 15 million euros. A lot of research is done with respect to UAVs as applications for SAR missions, reducing the need for expensive helicopters. This will drastically reduce the costs for SAR missions and may improve the speed and efficiency with which victims can be located. In addition, these UAVs could be placed on many different types of ships, making it possible for the UAV to be at the victims location within seconds. Looking at polymers, one can see a drastic trend in the aerospace industry for low weight solutions. Polymers are becoming multifunctional, making it possible to have electric circuits, light sources or even actuators all made from polymer. Therefore it is an interesting practice to design an all-polymer UAV. An extra challenge was introduced by creating this UAV out of biodegradable materials to diminish waste after end of life of the UAV. A working title was adapted: the Autonomous, Search, All-Polymer UAV (ASAP UAV).

The purpose of this report is to provide a detailed design of an all-weather, all polymer, Search UAV that is capable of station keeping and can fly with wind speeds up to 7 Beaufort (Bft) with gusts of 9 Bft. Already in the midterm report the configuration, a flying wing, was selected and in this report a more elaborated design will be shown.

This report begins first by a recap of the midterm report and summarizes why the flying wing configuration was chosen. Because the mission of the UAV is to locate a person at mid sea the payload and the subsystems are crucial. The description of all the subsystems present, motor, batteries, payload and others, are shown with their respective mass and power. The ASAP UAV can provide a live video stream with visual and thermal image equipment within 43 kilometers from the launch ship independent of weather conditions. This is due to its limits of staying within the line of sight of this ship. The See & Avoid system prevents mid-air collisions and an advanced Global Positioning System (GPS) guidance and navigation system allows for autonomous flight and search operations. The autopilot, which includes the flight computer and Guidance, Navigation and Control (GNC), is the open-source autopilot NavStik, developed at Delft University of Technology. The payload systems require a 2.4 GHz S-band frequency in order to support a stable video feed while the UAV will require a 430 MHz UHF-band in order to communicate with the ground-station.

The UAV will be deployed from a SAR ship by a rail launch system. The launch velocity equals 22 m/s. The length of the rail is 4 meter and this will result in an acceleration load of 5.1 g during take-off on the UAV's structure. After launch the UAV tries to locate the victim at a cruise speed of 29.2 m/s. During flight, which can take up to 3 hours, the UAV will continuously communicate with the ground station while exchanging flight statistics and imaging data. Once the victim is found it will either circle at the minimum drag speed of 22 m/s or, at high wind speeds, fly upwind to minimize ground velocity and remain above the victim. At the end of the mission the UAV will perform a belly landing on water using the fairing under the airframe. The reinforced faring is designed for minimal induced forces during landing on the structure. Afterwards the UAV can be retrieved and prepared for the next mission.

The life cycle consists of the manufacturing, operation and disposal of the UAV. The methods with which these three phases are fulfilled have significant influence on the design. A maintenance schedule is created describing post flight inspection, inspection for every 10 flights and a scheduled replacement of parts to guarantee safe operation of the UAV during lifetime.

One of the main objectives is to design a UAV with a maximal polymer content. For environmental concerns, bio-based materials are used: flax reinforced poly-lactic acid (PLA) since this composite is both bio-based and biologic degradable. The main advantage is, compared to petrochemical polymer materials, their capacity to diminish the high fossil feedstock dependency. Additionally the use of natural fibers allows the composite to overcome important drawbacks of the polymer matrix and opens access to alternative lightweight and low cost materials. This reduces fuel consumption and CO_2 emissions with respect to the current restrictive legislative standards worldwide. For integrated design, monocoque structure was chosen. The thickness of

this monocoque will be $2.0\ mm$ throughout the entire span of the UAV because this is a minimum thickness required for injection molding. Using this combination of PLA and natural flax fibers enables the UAV's air-frame to disintegrate within approximately 18 months in water. Looking at the deflections and stresses it is possible to use a PLA/Flax compound containing 30% chopped flax fibers. This will still only result in a deflection of $4\ mm$ at the wing tip which was confirmed using Finite Element Method (FEM) methods. The total polymer content of the UAV is over 80vol% and, when only considering the structure and propulsion system, over 98vol%.

The internal layout is arranged in such a way that the use of internal volume is maximized. Also, the mass distribution to achieve controllability of the system is taken into account. The total volume of the batteries is 3.8 liter, of which three liters are placed inside the wing. The residual 0.8 liter is stored inside the body, enclosing the imaging payload. In front of this imaging payload the See & Avoid subsystem is located with a reserved margin for electrical components. The internal layout of the ASAP UAV can be seen in Figure 1. In

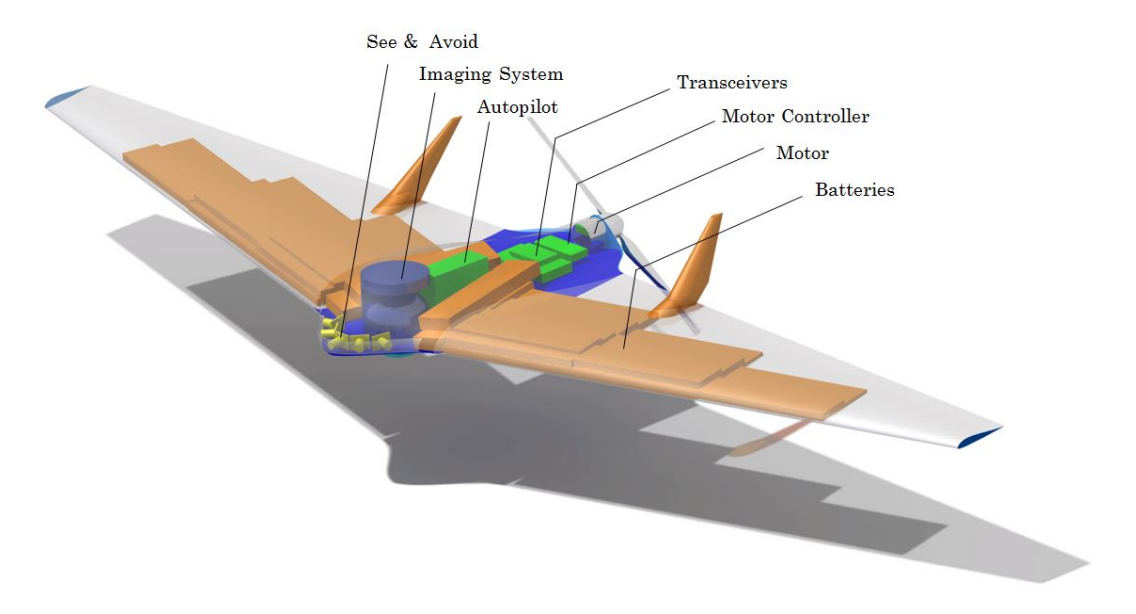


Figure 1: The internal layout of the ASAP UAV

order to estimate performance during the mission the flight and aerodynamic characteristics are determined. All different flight phases have been examined and a thorough sensitivity analysis is performed to identify the influence of wing parameters. The design goals are conflicting since the UAV should be able to find the victim as fast as possible while still being capable of slow flight after the victim is found. Another conflict arises from the fact that the speed range is increasing as the design is more resistant to wind gusts. An optimization is performed to be able to fulfill the complete mission of the UAV and to meet all the requirements set. The choice was made to design for a higher speed range and gust resilience giving a compact wing planform. The result is that the minimum speed of the UAV is higher than intended but still low enough to facilitate slow flight or circling. A reflex airfoil, MH-81, has been chosen since no horizontal tail is present to guarantee the neutral stability of the aircraft. A double fin rudder has been added to the UAV to ensure directional control during flight. A complete stability analysis is made to evaluate full controllability of the aircraft during all phases of the mission.

The manufacturing, assembly and integration of the UAV is designed to optimize cost and labor efficiency. The body will be manufactured by injection molding into three parts, 2 main parts consisting of a half wing and part of the bottom of the fuselage section and one part being the top part of the fuselage. The two main parts are joined by adhesive bonding using a symmetric joint to reduce stress concentrations and improve waterproof capability. The top fuselage part is easy removable using bolts to access all internal systems without disassembling the complete UAV. Finally the control surfaces and systems are integrated into the UAV structure using multiple integration methods of which Velcro and pin inserts are examples.

The tools used for designing the UAV are verified using analytical models. The final design has been verified using the derived requirements and has been validated using the customer requirements. It can be concluded that all customer requirements have been achieved to a large extent.

The cost of the ASAP UAV consists not only of the purchase price of a single UAV, but also of the research and development cost, the ground station, launcher and other general operating costs. The cost estimation is performed using empirical relations modified for small UAVs. These relations include estimates for inflation over time. The cost of the Unmanned Aerial System (UAS) will decrease to just over €100,000 per year after ten to a hundred sales due to learning effects, re-usability of injection molds and the fact that research and development costs can be divided among multiple UAV sales. An increase in sales will not bring down the cost much further. A contracting system is also being considered with the cost per flight hour lower than €200.- per hour. Mr. Moleman, head of operations of the KNRM, has expressed his general interest in the design due to its low cost and innovative solution and considers the ASAP UAS a viable addition for a Search & Rescue mission.

A sustainable development strategy is also implemented in this report. This focuses on the design, production and social sustainable aspects. Sustainability thus not only involves the materials (biodegradable) or how the end of life is defined, but sustainability will also be linked to the performed Reliability, Availability, Maintainability, Safety (RAMS) analysis. It is concluded that 27 % of the complete UAV degrades over time while it is recyclable for 68 %. The resulting waste is a mere 5 % of the UAV's total mass.

It can be concluded that the ASAP UAV fulfills all customer requirements except the capability to land on ship. The landing procedure is set by making the UAV able to land on the water surface. The biodegradable bio-composite used is novel to the aerospace industry and current research of these composites worldwide is increasing. These composites are an option to alternative, lightweight and low-cost materials while diminishing the oil dependency. The capability of the UAV to operate at 9 Bft with gusts up to 12 Bft is unique in the commercial UAV market.

Due to the restricted amount of time available for the design of the ASAP UAV, a number of aspects require further research and testing. The design team recommends the following aspects to be evaluated during post-DSE phase: Structural analysis of the UAV during take-off and landing and the results of different types of impact loading should be evaluated. The fatigue life of the bio-composites PLA/flax is still unclear and needs further research, although fatigue is not considered critical for the low-load ASAP UAV. Aerodynamic performance should be verified, validated and optimized using CFD, wind tunnel test and / or flight tests. Extensive controllability tests should be performed in heavy weather conditions and the autopilot must be programmed to cope with these conditions. The hydrophobic coating should be tested for durability and anti-icing performance. Production and assembly tests should be performed before the UAV can finally be checked for legislative compliance.

1

INTRODUCTION

New types and applications of polymers are being discovered and developed at breakneck speed. It seems that polymers can be used in a diverse selection of non-structural applications. Polymer batteries, solar panels, light sources and actuators have already been developed. A different emerging technology in the aerospace industry is the Unmanned Aerial System (UAS). The exploration of possible UAS' applications has only yet begun and there are numerous ways UAS could better human life.

The problem is twofold; first, it takes approximately 10-15 years for a new material and technology to be applied on commercial aerospace products. The testing required is costly and time consuming. Second, a number of challenges still remain in UAS development. A few examples are increase of range, all-weather operations and automated see and avoid.

An increase of knowledge on polymers is needed to provide lightweight, cheap and biodegradable solutions for aerospace challenges. In addition, extended use of a Unmanned Aerial System (UAS) could lead to a reduction of risk of human life and an increase of general wellfare. To increase knowledge on polymers and UAS, existing or near future technologies need to be applied in real products. As the UAS market does have less barriers than the commercial aerospace market, it is a perfect test bed for new aerospace materials and technologies. In addition, by presenting a design challenge for a product which is viable for application in the near future, it is expected that practical knowledge is obtained.

The purpose of this report is to present the design of the ASAP UAV. This UAV is an all-polymer biodegradable autonomous UAV with which a person can be located in sea in any weather conditions, which can transfer its location to its remote command center and is deployable from a ship. In addition its support equipment, construction, maintenance, disposal and operation will be presented. Furthermore, the report will show not only the results but also the design process in order to create a better understanding of the challenges one faces during the design of a UAS and the application of polymers in the aerospace industry. Although a complete UAS design has been made, a number of aspects of the design, such as testing, vibrational loading, have not been (extensively) treated. A plan is made however in order to evaluate these aspects after the design.

This report consists of fourteen chapters. The second chapter contains the recap of the Baseline and Mid-Term report. The third chapter contains the sub-system characteristics and the sub-system interactions. Operations and logistics is discussed in the fourth chapter. The fifth chapter contains the life-cycle analysis of the ASAP UAV. Chapter 6 contains the material study, the material selection and the structural analysis of the final design. The internal lay-out is discussed in the seventh chapter. The flight performance and aerodynamic characteristics of the final design is discussed in Chapter 8. The ninth chapter contains manufacturing, assembly and integration plan. In Chapter 10 and 11 the budget allocation and the sustainability of the design are discussed. Chapter 12 contains the verification and validation of the final design. The post DSE plan is discussed in Chapter 13. Finally, Chapter 14 gives the conclusion and recommendations for future research.

BASELINE REPORT AND MID-TERM REPORT RECAP

The following chapter contains the recap of the most important points of the Baseline Report [1] and the Mid-Term Report [2]. The conclusions from the market analysis are discussed in Section 2.1 and the mission analysis is shortly discussed in Section 2.2. Subsequently the Mid-Term Report is reviewed; in Section 2.3 a concise review of the requirements is done, in Section 2.4 the different concepts are discussed and in Section 2.5 the trade-off and its results are provided.

2.1. MARKET ANALYSIS

In order to gain an understanding of possible customer's wishes, needs and requirements, a market analysis has been performed in the Baseline Report. For the full analysis, see [1].

2.1.1. TARGETED CUSTOMERS

SAR work is usually performed by the air force, the navy, the interior ministry or the transport ministry. In addition, due to the fact that oil & gas companies have begun drilling in areas that are no longer covered by national emergency services, private operators have started providing SAR services.

Additionally private commercial vessels interested in providing an extra security provision to their ships are potential customers. In total there are over 100.000 commercial vessels operated over the world [3]. Finally, a future spin-off could be to use the ASAP UAV as an intelligent source for commercial vessels operated in areas sensitive to hijackers (e.g. Horn of Africa). To conclude, the list of possible customers is:

- Air Force
- Navy
- Governmental departments
- · Public foundations responsible for SAR missions
- Private SAR companies
- Private shipping companies

2.1.2. DESIGN GOALS

With the current technology used for SAR missions, the amount of fuel, manpower and money required is relatively high. In addition there is a risk for loss of human life due to the fact that the SAR vehicles are manned. Furthermore, well organized SAR missions have a success rate of approximately 75% [4]. As a result, the ASAP UAV should be an improvement in terms of required labor, cost, efficiency, and especially ecological footprint and operational possibilities.

The use of biodegradable polymers to construct the UAV and the usage of batteries as the source of power, will make the UAV a unique and sustainable solution for SAR missions. In addition, the capability of flying in severe weather conditions will reduce the risk of loss of human life. Finally, the purchase price as well as the maintenance cost will be significantly lower than current SAR vehicles.

2.2. MISSION ANALYSIS

A specific mission profile must be chosen in order to generate a complete list of requirements that can be used to verify and validate the design. From the market analysis and after consultation with the KNRM (personal consultation, 2014) and the customers, the search objectives are narrowed down to victims who are still alive; the KNRM indicates to stop the SAR mission when the chances of survival have diminished, which is after 3

hours. With this statement, a firm mission procedure can be made. All actions and choices, which are taken and made during this procedure, are given in in the mission analysis from the baseline report.

2.3. LIST OF REQUIREMENTS

The requirements generated in the Baseline Report and the Mid-Term Report will be used to verify and validate the design in Chapter 12. A number of requirements have been added due to increased knowledge about the design and objectives. The complete list of requirements can be found Chapter 12.

2.4. CONCEPTS

During the preliminary design phase many different concepts were generated and evaluated [2]. Three groups of concepts were generated, namely fixed-wing aircraft, rotorcraft and hybrids [2].

Subsequently, the concepts were qualitatively evaluated. The first step in this concept evaluation was discarding the non-viable options; the rotorcraft and the helicopter based hybrids. The viable options were subsequently evaluated by a strawman concept evaluation. The resulting three concepts were:

- · Conventional aircraft with simplified tail
- Flying wing with small empennage
- High-low box wing

2.5. TRADE-OFF

Not only the configurations, but also the payload and energy storage needed to be chosen for the ASAP UAV. The options for these different design aspects can be evaluated separately and with their own criteria.

The trade-off method was chosen as follows; all criteria are assigned a weight on a scale from one to ten. This weight is based on the importance of the specific criterion. The higher the weight, the more important the criteria is considered. All aspects of the proposed design are graded based on their performance on each specific criterion. The products of the weights and grades are added and form the total score of the design option. For a complete explanation of the trade-off and the different criteria used to evaluate the payload, energy storage system and configuration, see the Mid-Term Report [2].

2.5.1. PAYLOAD

The result from the payload trade-off was inconclusive. There are two camera systems that perform significantly better than the others; the M1-D gimbal from SPI CORP and the Cobalt 90 from FLIR. The M1-D gimbal from SPI CORP has the better score, however, when the size of the gimbal system will be a limiting factor, the Cobalt 90 from FLIR will be preferred over the M1-D. This is further elaborated in Section 3.2.

2.5.2. ENERGY STORAGE

For the energy storage the result was very conclusive; the lithium-polymer based battery system had the highest score by far. It scores best on all the different criteria and it is the best option considering the requirement concerning the polymer content.

2.5.3. CONFIGURATION

An extra measure that takes the sensitivity of each criterion into account was added to the configuration trade-off method. Every configuration is given an average score, but also a best and a worst possible score. This allows the design team to take the sensitivity of each design into account when making a decision. It should be noted that in the sum of all criteria, the upper and lower limit of the sensitivity are not viable because an alteration that excels in one criterion can underperform in another. The design that performs best on the trade-off analysis is the flying wing and this design will also be chosen as the final configuration.

SUBSYSTEM CHARACTERISTICS

The ASAP UAV comprises several kinds of subsystems. Most of them are explained in the Mid-Term report [2]. The main subsystems comprising the ASAP UAV are described in this chapter. First, the hard- and software architecture is explained in section 3.1. This is followed by the sections describing the subsystems in detail: Section 3.2 describing the payload, Section 3.4 describing the motor and corresponding systems and Section 3.5 describing the battery sizing of the ASAP UAV. The chapter continues describing the electrical interactions in Section 3.7 and the data handling of the UAV in Section 3.8. Finally the UAV flight computer (Section 3.9) and the communication system sizing (Section 3.10) are described. The redundancy of the sub-systems will be discussed in Chapter 5.

3.1. HARD- AND SOFTWARE INTERACTION

Interaction among the sub-systems happens through both physical and digital processes. These processes are described in the subsequent subsections. Section 3.1.1 describes the interaction of the hardware while the software interaction is explained in Section 3.1.2.

3.1.1. HARDWARE INTERACTION

The interaction among the hardware components happens on multiple levels. Figure 3.1 shows the interaction among the components. The specific workings of all parts is explained further in this chapter.

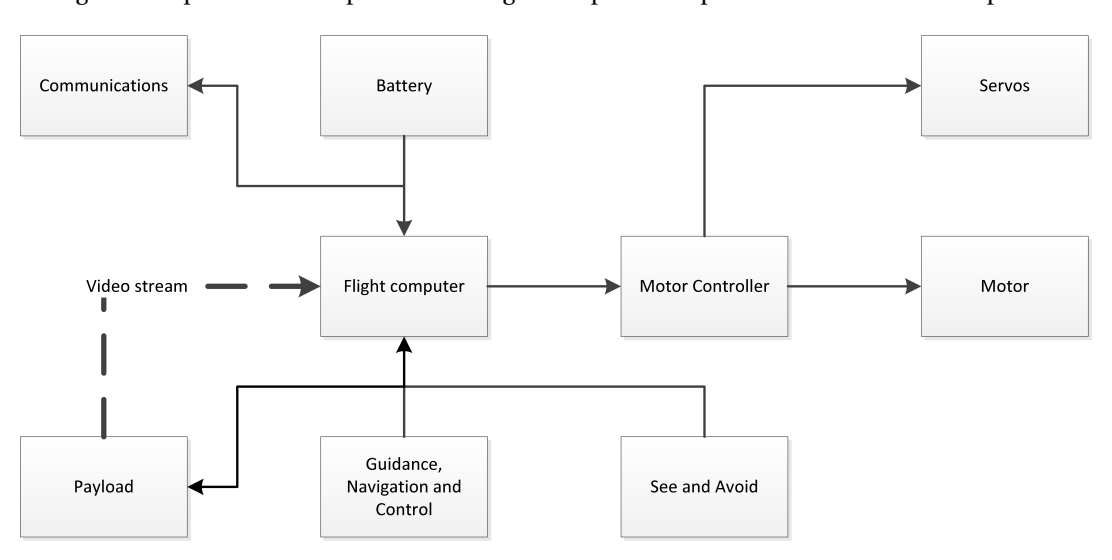


Figure 3.1: The Hardware Block Diagram of the ASAP UAV

3.1.2. SOFTWARE INTERACTION

The flight computer is the center of the hardware structure. All sensor components generate data and send this to this flight computer. The data is processed and the motor, servo and imaging subsystem settings are changed accordingly. The GNC and See and Avoid (S&A) produce direct input for the flight computer regarding the current attitude and position compared to the desired attitude and position. The battery sends information about capacity and current discharge rate. The imaging system updates the flight computer about the current camera attitude and the computer sets the desired camera attitude. The flight computer has to be programmed in such a way that the UAV can fly autonomously. Therefore a state of the art S&A sequence is required in order to avoid collisions. During the landing phase, when the S&A system is pointed

upwards, the imaging payload should have a S&A sequence. Besides this, it has to be possible for the operator to control the UAV manually in order to check certain points of the flight path. Therefore a manual take-over sequence and an operator warning sequence, which alarms the operator about reaching the LOS, the battery State of Charge and the UAV's flight envelope boundaries, should be written. In order to recognize drowning victims, also a person recognition software has to be programmed. A failure mode response sequence has to be written in order to land the UAV safely on water during a mishap. For example when the engine fails during flight, the UAV should switch to an active glide mode and perform a controlled landing onto the water surface. In Figure 3.2 the software interactions between the subsystems can be seen.

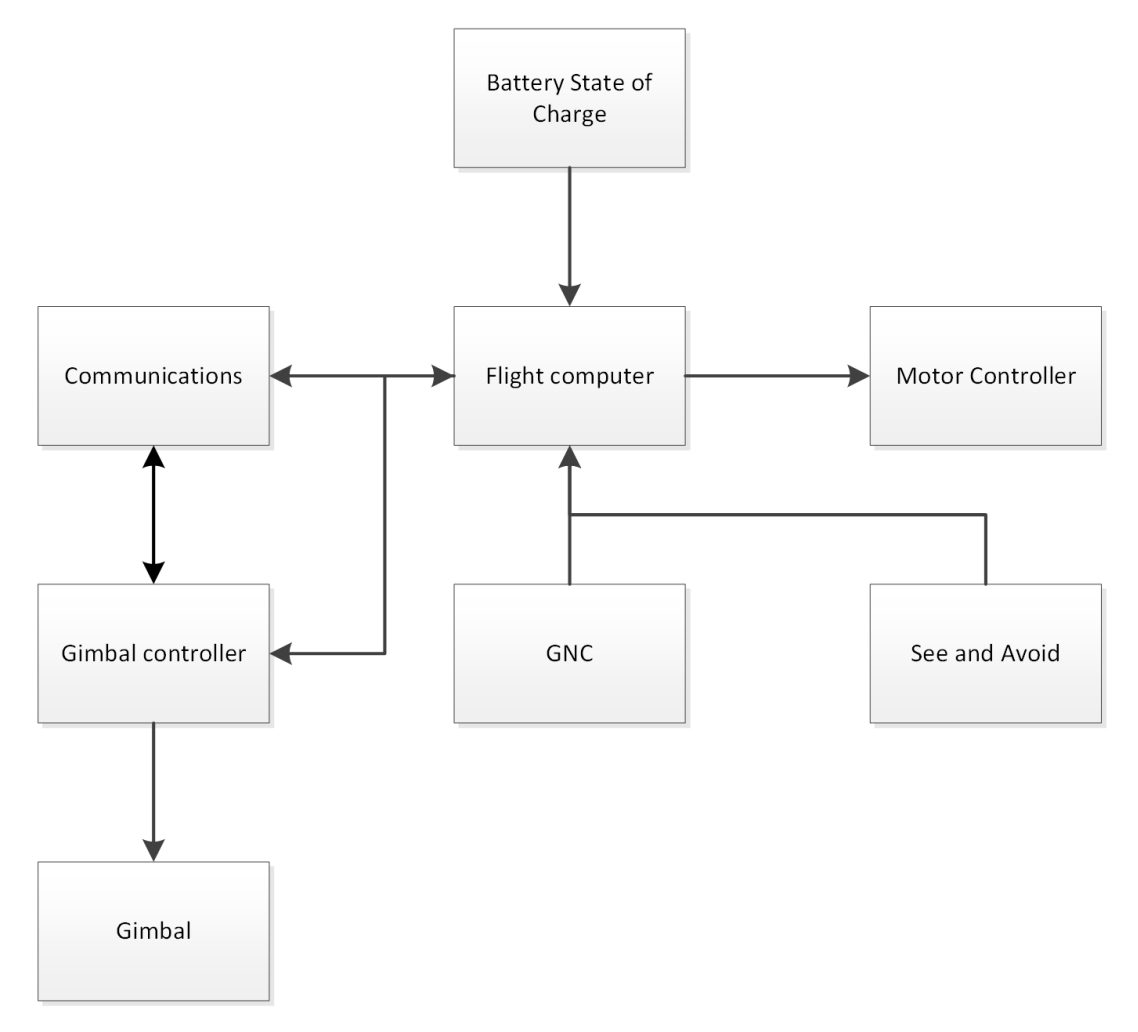


Figure 3.2: The Software Block Diagram of the ASAP UAV

3.2. PAYLOAD

The payload of the ASAP UAV consists of the imaging system and is present to detect victims and the S&A system for collision avoidance. The purpose of the imaging payload is to detect the victim by means of a thermal and an Electro-Optical (EO) camera. Multiple off-the-shelf systems are analyzed and compared in a trade-off table to find the solution that fits the needs of the mission best [2]. The Cobalt 90 scores best in weight and dimensions and the M1-D scores significantly better on price and thermal resolution. After consideration it was decided that the M1-D is simply too large to be implemented into the design. Due to its size the aerodynamics of the UAV were disturbed to such an extent that it was no longer a viable option.

The Cobalt is thus chosen due to its confine dimensions and relative low weight. The Cobalt 90 is an imaging system of approximately 0.65 kg with a diameter of 9 cm. It consists of a stabilizing micro turret, a pointing laser, infrared sensor and a normal camera (color video) which can provide stable imagery both during day-time as nighttime. The only drawback is that it is costly; Commercial off-the-shelf (COTS) price for the Cobalt

90 is approximately \$30,000. The system is capable of rotating for 360 degrees and tilting 180 degrees. The large field of view makes it very suitable for the mission to be flown. Operating conditions are from $-20^{\circ}C$ and $60^{\circ}C$, the resolution is 320x240pixels for the thermal camera and 768x494pixels for the EO camera and the system is operable in low light conditions. A vibrational damping system is incorporated in the system to ensure a stable video image.

The International Civil Aviation Organisation (ICAO) mandates, regarding international rules of air traffic, that each aerial vehicle must contain a S&A system with a field of regard of at least $\pm 110^\circ$ in azimuth direction. Aerial vehicles usually contain multiple sensors for their collision avoidance system. This method is feasible for larger aircraft but will be too heavy for the ASAP UAV. A theoretical approach is therefore used to scale the subsystem for the ASAP UAV. The S&A system will consist of 5 cameras, each 1.2 Megapixels, a Field-Programmable Gate Array (FPGA) and a vibration damping mount. This system has a total weight of 200 grams and consumes less than 5 W. These estimations were already described in the Mid-Term Review (MTR) [2]. To fulfill the requirements set to S&A the UAV needs to detect any incoming element and derive direction and speed of this object. The detection time before collision should be at least 20 seconds and the line of sight of the UAV should be approximately 2000 meters [5].

The system function for this S&A system will be by detecting and evaluating potential collisions. When multiple threats are present, they should be prioritized and a decision has to be made accordingly. Manoeuvres are commanded and executed so that collisions can be avoided.

Life vests, buoys, communication devices, etc. were also considered as extra SAR equipment. However, incorporating these would drive the design of the UAV to an unacceptable level. When however the risk exist that the UAV is becoming too heavy to land on the water, self-inflating bladders or balloons with CO_2 charges attached to them can be implemented. A balloon with a CO_2 charge is compact and lightweight and could easily be implemented into the design to assure the UAV's float worthiness.

3.3. DETECTION OF VICTIMS

The main feature of the imaging payload is detecting a victim in the water. The most recognizable part of a drowning person is the head, which can be approximated by a 21.4x21.4cm square, for an adult [6]. Therefore, the amount of pixels of the head is required to be as high as possible. Besides that, the UAV has to stay within the LOS of the ship and an altitude between the 50 and 150 m [1]. Since the imaging system is limited by its resolution and the LOS, it is required to choose a suitable service altitude. In Table 3.1, the required values per service altitude can be seen. The swath width angle and the swath height angle are assumed to be 36.8° and

Altitude	EO camera	thermal camera	LOS
[<i>m</i>]	[pixels]	[pixels]	[<i>km</i>]
50	16	3.2	25.2
80	12.3	2.5	32
100	7.9	1.6	35.7
150	1.8	0.4	43.7

Table 3.1: Amount of pixels of a human head and the LOS per service altitude.

 18.9° [1]. In order to detect a head only a few pixels are required for a thermal camera, since these cameras can detect a temperature difference of $0.2\,^\circ\text{C}$ [7]. On the other hand it is unknown if it is possible to detect a head existing of for example 10 pixels. The only way to obtain this knowledge is testing the EO camera. It can be concluded that a lower service altitude is beneficial for detecting victims, however then the UAV has to stay closer to the ship due to the reduced LOS. Also it can be concluded that at altitudes above $100\,\mathrm{m}$ it is almost impossible to detect any victims. The exact service altitude depends on the mission. The camera could however be 'whiskered' in order to obtain a smaller swath angle and therefore a better quality video at a larger swath width. The mission and the camera whiskering is elaborated in Chapter 4.

3.4. MOTOR

Since the ASAP UAV is to be made of mostly polymers it is impractical to use engines that produce a lot of heat, such as combustion engines. Therefore, the most suitable engine for the ASAP UAV is an DC electric motor. In the midtermreport a certain DC electric motor was already chosen, namely the Hacker A30-14L-V3 brushless DC motor [8] [9]. In Table 3.2 the specifications of this motor can be found. A corresponding engine

Table 3.2: Specifications of the Hacker A30-14L V3 brushless DC motor

Motor characteristics	Hacker A30-14L-V3
Peak power	500 <i>W</i> for 15 <i>s</i>
Nominal power	382W
Operating voltage	11V
Motor velocity constant	800 RPM/Volt
Poles	14
Physical characteristics	
Weight	143 <i>gr</i>
Diameter	37.2 <i>mm</i>
Length	40mm
Motor attachments	
Suggested controller	40 A Brushless
Suggested propeller	36 <i>cm</i> diameter
	18cm displacement per rotation

controller was also selected: the Hacker X-40 SB-Pro brushless DC motor controller. The specifications of this engine controller, which can control servos as well, are given in Table 3.3 [10].

Table 3.3: Specifications of the Hacker X-40 SB-Pro brushless DC motor controller

Controller characteristics	Hacker X-40 SB-Pro
Operating voltage	7.4 <i>V</i> to 22.2 <i>V</i>
Peak power	888 <i>W</i>
Physical characteristics	
Weight	43 <i>gr</i>
Dimensions	75x28x10 <i>mm</i>
Servos	
Control voltage	5.5 <i>V</i>
Maximum number of servos	6

3.4.1. SERVOS

In order to control angular position, velocity and acceleration, servomotors are required. A servo consists of a motor coupled to a sensor for position feedback. The chosen type of servomotor is the GWS Park HPX F servo and its specifications can be seen in Table 3.4 [11]. For the ASAP UAV a total of six servos is required: two for each elevon and one for each rudder.

3.5. BATTERY

One of the core subsystems of the ASAP UAV is the battery. Section 3.5.2 will describe the sizing of the batteries after a determination of the battery degradation during operational life in Section 3.5.1.

Servo characteristics	GWS Park HPX F
Modulation	Digital
Torque	$4.8V$: $2.66kg \cdot cm$
	$6.0V$: $3.02kg \cdot cm$
Speed	$4.8V: 0.06sec/60^{\circ}$
	$6.0V$: $0.05sec/60^{\circ}$
Physical characteristics	
Weight	19 <i>gr</i>
Dimensions	27x13x25 <i>mm</i>
Casing	Polymer

Table 3.4: Specifications of the GWS Park HPX F servo

3.5.1. BATTERY LIFETIME

Battery capacity degrades during its life cycle and the magnitude of degradation depends on the Depth of Discharge (DoD) [12]. Furthermore, typical lithium based batteries have a maximum life of two to three years [13]. The total usable lifespan depends on the acceptable battery energy capacity.

As explained in the MTR the ASAP UAV is designed to fly a mission daily. The battery capacity is reduced to 70% of its original if the batteries are discharged completely (a DoD of 100%) within 300 to 500 charge cycles [12]. If the batteries are used on shorter missions with, for example a maximum DoD of 50%, the same reduction as the 100% DoD occurs after more than 1200 cycles.

Since the battery weight is one of the driving factors in the weight estimation, a capacity of 85% of the original is considered tolerable while more margin is considered unacceptable for the design. Hence, the battery mass sizing is based on a capacity of 85% of the manufacturer specifications. This design goal implies that the life span of the battery itself depends on the mission duration. When a constant DoD of 100% is used, the battery life depends on the charge cycle degradation and may be less than one year. On the other hand, when short missions are performed, the battery life is limited by its storage time of a couple of years [13].

For the ASAP UAV it is assumed that on average no full discharge cycles occur. Therefore, the battery degradation is supposed not to go below 90% before it is replaced. That leaves 5% of the battery capacity as spare capacity for possible alterations further in the design cycle.

3.5.2. BATTERY SPECIFICATIONS

The type of battery used for the ASAP UAV is a lithium-polymer battery [14]. The main advantage of such batteries is that they come in any size and prismatic shape. Important properties of the UAV's battery are the weight and the volume. The battery weight is calculated with Equation 3.1.

$$W_{battery} = \frac{P_{req}h}{E_{Dm}\mu_{LTD}} \tag{3.1}$$

Where P_{req} is the total required power of all systems, which equals 360W, h is the required amount of flight hours, which equals three hours, E_{Dm} is the energy-mass density and μ_{LTD} is the Life-time degradation efficiency. The battery volume is calculated with Equation 3.2.

$$V_{battery} = \frac{P_{req}h}{E_{Dv}\mu_{LTD}} \tag{3.2}$$

Where E_{Dv} is the energy-volume density. A manufacturer of batteries is Amicell, this company manufactures custom designed Lithium-polymer batteries in custom shapes [15]. The specifications of the battery can be seen in Table 3.5 [15].

3.6. Battery configuration

The amount of cells is defined in this following section. A choice is made considering the amount of cells, the number of serial cells per string and the number of parallel strings. The required power to feed the engine is

Characteristic	Result
Battery type	Lithium-polymer
Battery voltage	3.7 V
C-rate	0.33
Resistance per cell	$0.003~\omega$
Energy density (mass)	$250 \frac{Wh}{kg}$
Energy density (volume)	$333 \frac{Wh}{I}$
Degradation efficiency	0.85
Battery weight	5.1 <i>kg</i>
Battery volume	$3.82 \ dm^3$

Table 3.5: Battery specifications

360 W. It is beneficial to limit the power loss of the UAV. This way, the efficiency of the UAV is higher and the heat loss is lower. This is important since a high temperature of bio composites has a negative influence on the mechanical properties. The total power loss by the internal resistance is calculated by Equation 3.3.

$$P_t = \frac{P_r^2 R_c}{V_c^2 n} {(3.3)}$$

Where P_r is the required power, R_c is the internal resistance of each cell, V_c is the voltage of each cell and n are the number of cells. The cell specified in Table 3.5 has a small internal resistance. When 30 cells are used, the power that is lost due to heat is only 0.95 W.

3.7. ELECTRICAL INTERACTIONS

An important part of the UAV is the electrical interaction among all subsystems. Every subsystem requires its own amount of voltage. In Table 3.6 the required voltage for each sub-system is given. It can be seen that most

Component	Voltage [V]
See & Avoid system	7.5 [5]
S-band antenna	32 [16]
UHF-band antenna	16-22.2 [17]
S-band transceiver	3.3-5.5 [18]
UHF-band transceiver	9-16 [19]
Engine	11 [9]
Controller	7.5-22.2 [10]
Servos	4.8-6 [11]
Flight computer	12 [20]
Imaging system	12 [21]
Solid state drive	3.3 or 5 or 12 [22]
Sensors	12 [20]
Pitot heater	12 [23]
LEDs	4 [24]

Table 3.6: Required voltages

sub-systems need a higher voltage than the battery gives. This can be solved by connecting several battery sections in series. When six battery sections are connected, this will result in a voltage five times higher than the initial battery voltage: 22.2V. Subsequently this voltage can be converted to the required voltage by a buck converter, which decreases the voltage, or a boost convert, which increases the voltage. The engine and servos are the only systems not requiring a converter since the engine control unit serves as a DC-to-DC converter. The solid state drive requires different voltages although most solid state drives are capable of converting 12V to other voltages [25]. The resulting total electrical system is given in Figure 3.3. As can be seen in the figure, only three buck converters and one boost converter are required. Due to the high efficiency (90% or higher) and the small required amount of amperes, the power used by the converters are negligible

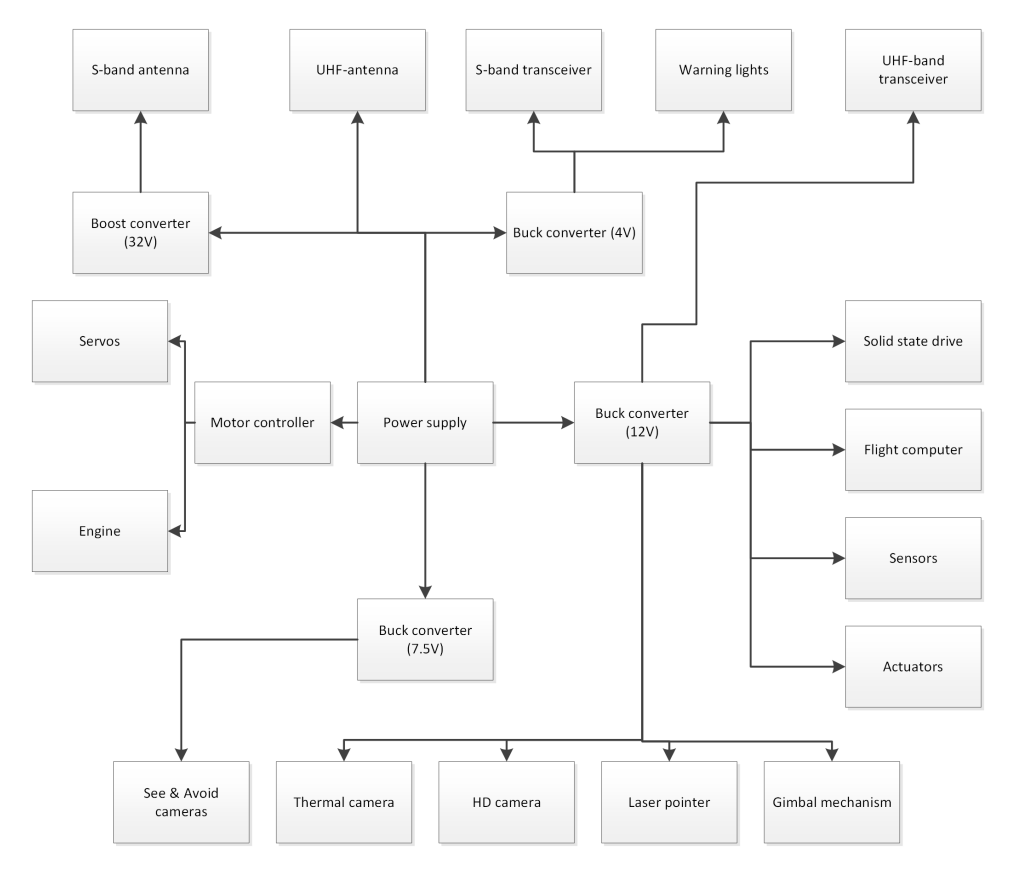


Figure 3.3: Electrical interaction between the battery and the subsystems

compared to the UAV's total required power [26]. The block 'Power Supply" in the figure is the sequence of battery sections.

3.8. Data Handling

The entire UAV is controlled by the flight computer. The flight computer exists of the Central Processing Unit (CPU), the Random Access Memory (RAM), a watchdog timer and a Solid State Drive (SSD). Important parts of the computer's data handling are:

- *CPU*: The CPU is the part of the hardware within the computer that carries out the instructions of the computer by performing simple arithmetical, logical and input/output operations. The Arithmetic Logical Unit (ALU) inside the CPU is responsible for the arithmetical and logical operations, while the Control Unit (CU) extracts information from the memory and executes them and therefore is responsible for the input/output operations [27].
- *CPU cache*: The CPU cache is the part of the core that is used by the CPU to temporarily store copies of information in order to reduce the time to access memory. This is due to the fact that the cache is a smaller and faster memory on which only small parts of information can be stored [28].
- *Clock*: The computing power of the computer depends mainly on the clock speed of the core clock. The faster the clock speed, the faster the CPU can process the data.

The RAM and the SSD are the two main components of the UAV's memory. Since the flight computer can store faster data on the RAM than on the SSD, the RAM is always used as temporarily working memory. On the other hand, when the UAV is shut down, the information stored on the RAM will be erased and therefore a SSD is always required. Generally speaking, the amount of information that can be stored on the RAM is less than on the SSD. However, when the RAM is full, the CPU can use a small part of the SSD as extra working memory. This temporarily memory is called the virtual memory [28].

The watchdog timer is a timer that is used to detect and recover from software and hardware malfunctions. Normally, the CPU resets the watchdog timer in order to prevent it from timing out. However, when in case of a software or hardware malfunction, the CPU will be unable to reset the watchdog timer and therefore the latter one will time out. When this happens the system will be placed in a safe mode and the normal system operations will be restored [28]. In Figure 3.4 the on-board computer lay-out can be seen. The lines connecting components are the data buses inside the computer.

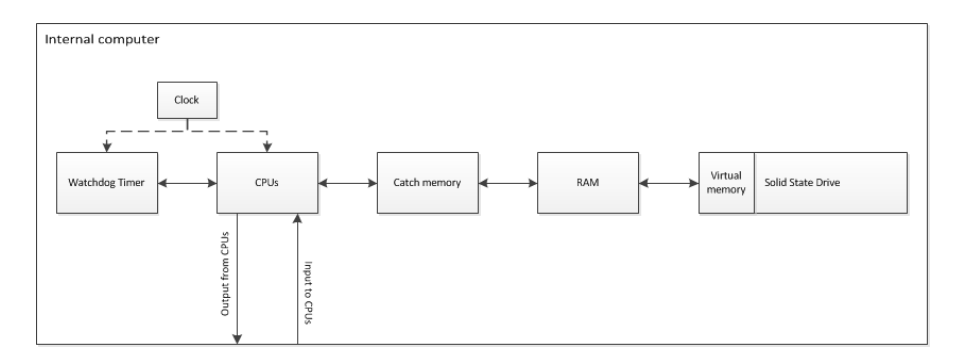


Figure 3.4: The lay-out ASAP UAV's computer

Autopilot data flow: the discussed flight computer handles the data of all the sub-system. In Figure 3.5 the data flow of the autopilot can be seen. The CPU sends input to the guidance loop, such as the required

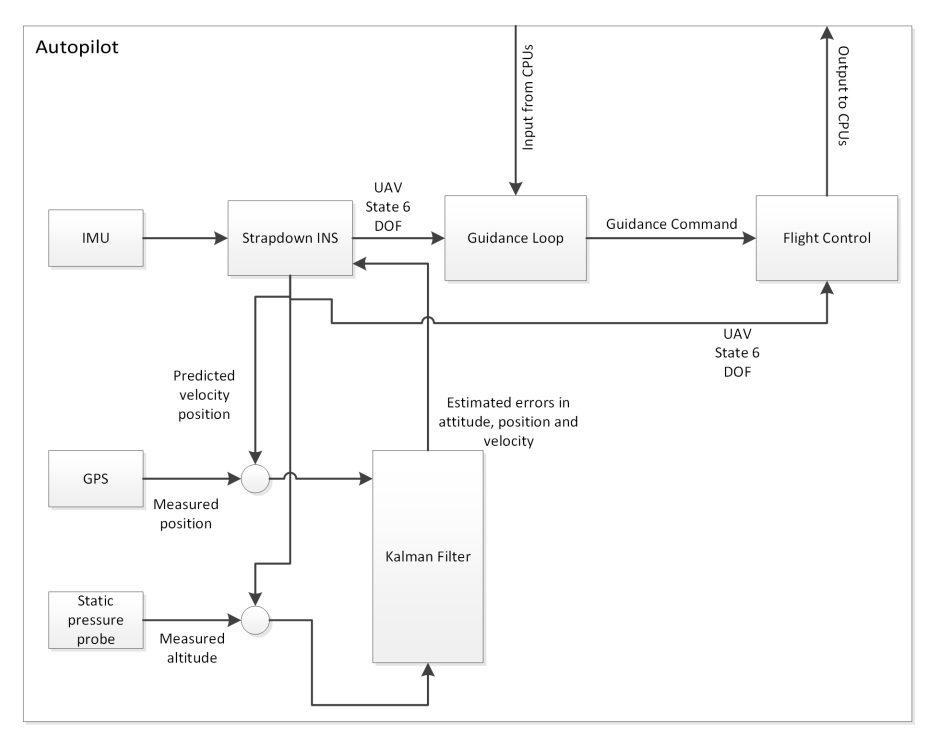


Figure 3.5: The autopilot's data flow

fly path, and together with the data from the Inertial Navigation System (INS) a guidance command will be formed. After that the guidance command and the data of the INS will be processed by the flight control loop and finally the calculated control responses will be send back to the CPU. The data of the INS results from the filtered data from the Inertial Measurement Unit (IMS) (3-axis gyro, 3-axis accelerometer and a compass), the GPS and the static pressure probe [2].

Engine controller data flow: all required responses are send by the CPU to the engine controller unit. In Figure 3.6 the processing of the control data can be seen. The CPU sends the required control responses to

the engine control unit, after which the required controls will be send to the engine and the servos. The servos also measure the applied controls, which will be send back to the CPU by the engine control unit.

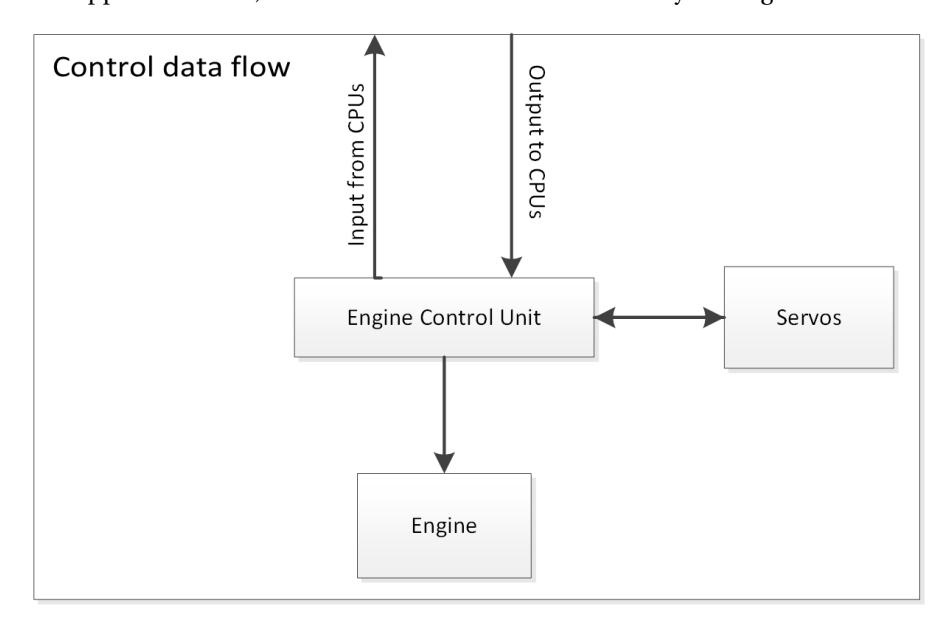


Figure 3.6: The data handling of the engine control unit

Communication data flow: Figure 3.7 shows the data flow from and to the S-band and UHF-band transceiver where the dashed lines represent the information received by the antennas.

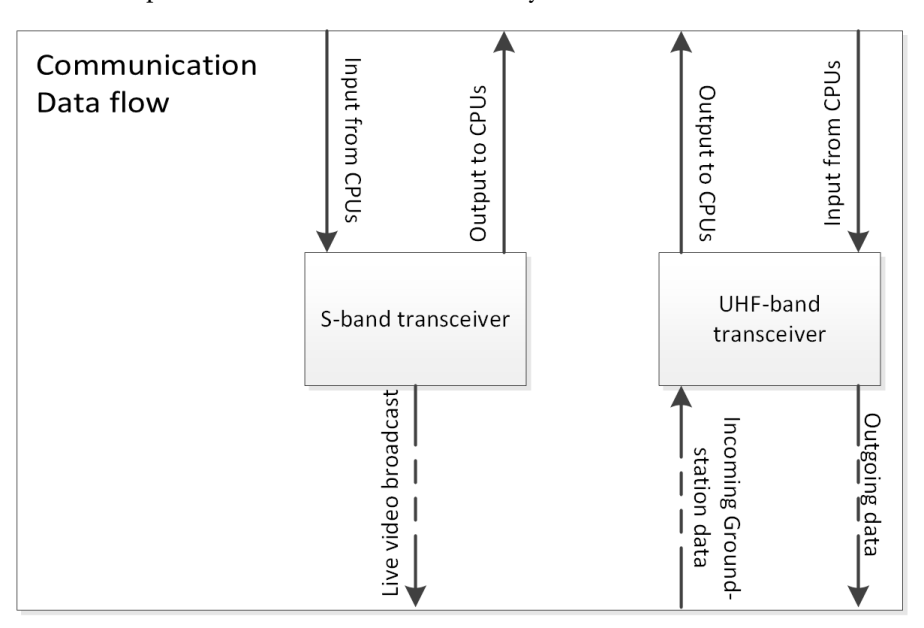


Figure 3.7: The communication data flow

See&Avoid data flow: Figure 3.8 shows the data handling of the See & Avoid payload. Here the FPGA board and the five cameras are of-the-shelf systems. The FPGA possesses its own CPU and RAM. However, the FPGA board of the See & Avoid system can be incorporated in the aircraft's flight computer [2].

Imaging data flow: in Figure 3.9 the data handling of the last subsystem can be seen. The camera control unit, which contains a separate CPU, processes the data received from the cameras and the gimbal's gyro and sends this to the UAV's computer. Also the camera control unit receives and processes information about the required gimbal attitude and sends it to the gimbal attitude controller [2].

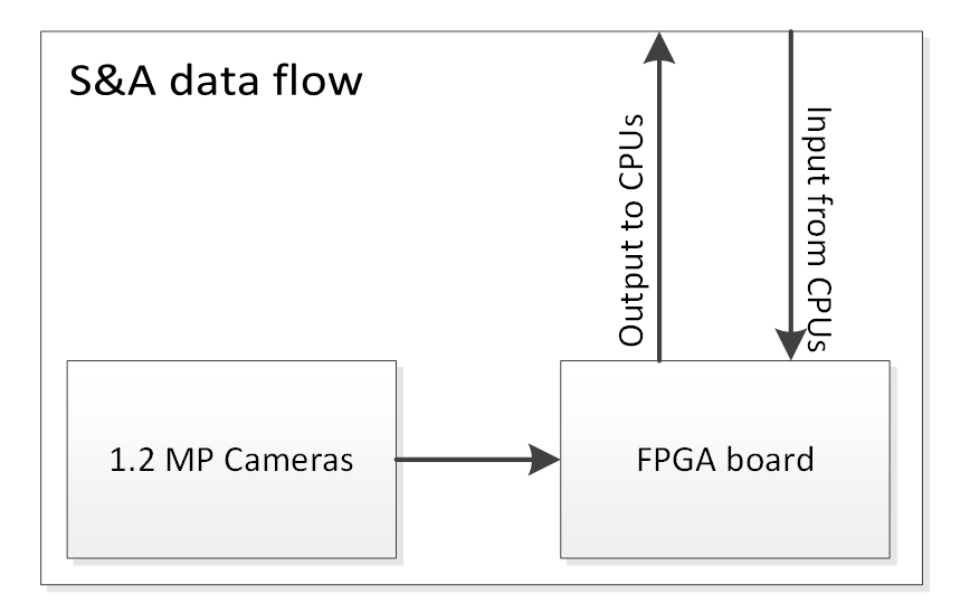


Figure 3.8: The data processing of the See&Avoid payload

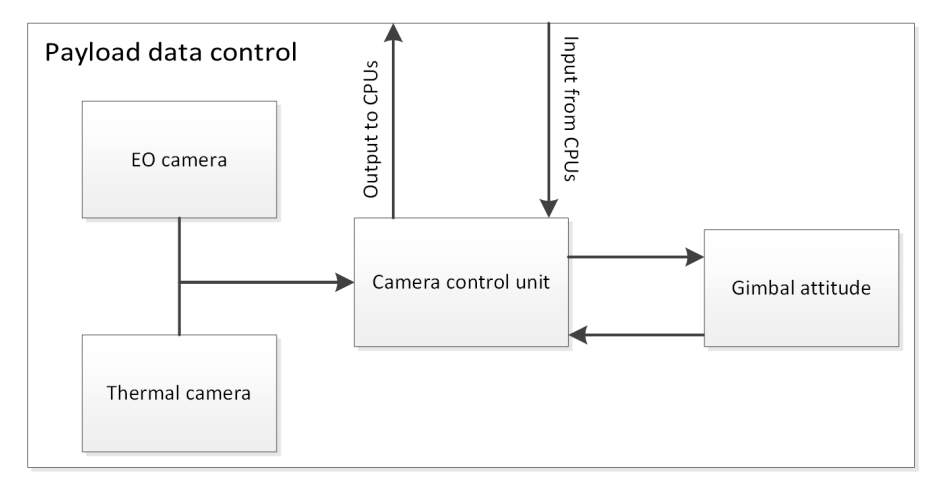


Figure 3.9: The data processing of the imaging payload

Data rate: the main function of the SSD is to store all the flight data during one mission. Also, when the connection between the ground-station and the UAV is temporarily lost, the UAV should be able to store a maximum of fifteen minutes of video on its SSD. There has been chosen for this maximum amount of video, because it can be watched back easily at the ground-station. The data rates, which determine the size of the SSD, are the data rates of both cameras. The specifications of the EO camera's video footage are given in Table 3.7. In order to have a decent video quality, a frame rate of 24 fps and a color depth of 10 bits (1024 different

Specification	Value
Resolution	768x494
Color depth	10 bits [29]
Frame rate	24 fps [30]
Bit rate	273.2 Mbps [31]
Compressed bit rate	2 Mbps [32]
Quality	RGB 4:4:4
Required 15 minute memory	225 MB

Table 3.7: Specifications of the EO camera's video footage

colors) is required. The resulting memory for a fifteen minute video is 225 MB. The compression of the video footage takes place inside the Cobalt 90's motherboard. The specifications of the thermal imaging system are given in Table 3.8. Since for thermal cameras only a small amount of different colors are needed, the

Specification	Value
Resolution	320x240
Color depth	4 bits
Frame rate	24 fps [30]
Bit rate	27.7 Mbps [31]
Compressed bit rate	400 kbps [32]
Quality	RGB 4:4:4
Required 15 minute memory	45 MB

Table 3.8: Specifications of the thermal camera's video footage

color depth will only be 4 bits (14 different colors). The resulting required 15 minute memory for the thermal camera's video footage is 45 MB giving a total required memory for the video footage of 270 MB per fifteen minutes.

3.9. AUTOPILOT, COMPUTER AND SSD

The autopilot, which includes the flight computer and GNC, is the open-source autopilot NavStik. In Table 3.9 the properties of the main board of the NavStik can be seen [33] [20]. Besides the main board an extra interface board is also needed, in order to connect the main board to the communication system, payload, engine controller and the SSD. In Table 3.10 the properties of the interface board can be seen [20]. In order to improve the flight computer a watchdog timer has to be added. A small and usable watchdog timer is the STWD100NYWY3F [34]. The characteristics of this Watchdog can be seen in Table 3.11 Besides these characteristics the voltage of this watchdog timer is regulated by the NavStik Main board and the power usage is negligible.

The flight computer's software, the flight data and the temporary 270 MB video footage have to be stored on the SSD of the ASAP UAV. A light-weight and small variety of SSD are the Micro Secure Digital (MicroSD) cards. The required voltage of the SD card is regulated by the flight computer. The Secure Digital (SD) card that will be used is the Samsung MicroSDXC Pro 64GB. The properties of this SD card can be found in Table 3.12 [35]. In order to get the flight computer and therefore the interaction between the ASAP UAV's subsystems operational, the UAV's software has to be programmed and stored on the flight computer and the SSD. An advantage is that a replaceable SD card simplifies the implementation of a software upgrade.

Table 3.9: Specifications of the NavStik Main Board

Autopilot characteristics	SkyCircuits SC2
input voltage	4.5V-14V
Required power	1~W
Temperature range	-20°C till 60°C
Mass	5.4 g
Length	59 <i>mm</i>
Width	18 <i>mm</i>
Height	15 <i>mm</i>
CPU	Cortex M4 with FPU and DSP
Clock speed	168 MHz
RAM	192 kB
On-board flash memory	16 Mb
Sensors	3-axis gyro
	3-axis accelerometer
	3-axis magnetometer
	Barometer
	Differential pressure sensor
	GPS
	Power level sensor

Table 3.10: Specifications of the NavStik Interface Board

Board characteristics	NavStik interface board
input voltage	4.5V-14V
Required power	1 <i>W</i>
Temperature range	-20°C till 60°C
Mass	8.6 g
Length	$41 \ mm$
Width	35 <i>mm</i>
Height	5 <i>mm</i>
Channels	12
Ports	SD card port
	USB port

Table 3.11: Specifications of the STWD100NYWY3F Watchdog timer

Watchdog characteristics	STWD100NYWY3F Watchdog
Temperature range	-20°C till 60°C
Mass	2.9 g
Length	$2.9 \ mm$
Width	1.6 <i>mm</i>
Height	$1.05 \ mm$
Time-out period	1.6s

Table 3.12: Specifications of the Samsung MicroSDXC Pro 64 GB

SD card characteristics	Samsung MicroSDXC Pro 64GB
Capacity	64 <i>GB</i>
Weight	0.5 gr
Reading speed	70 MB/s
Writing speed	20 <i>MB</i> / <i>s</i>

3.10. COMMUNICATION SYSTEM

The payload systems require a 2.4 GHz S-band frequency in order to support a stable video feed, while the UAV's control systems will require a 430 MHz UHF-band in order to communicate with the ground-station [2]. Both the S-band and UHF-band frequencies are only usable inside the LOS range, which has a maximum value of 43.71 km at 150m flight altitude and a minimum value of 25.14 km at 50m flight altitude [2]. Therefore these signals will be send to the SAR ship and subsequently send to the on-shore ground station. Figure 3.10 is a simple representation of the communication between the ground-station and the UAV. The UHF-band antenna is a small plate, which could be placed anywhere on the UAV. The S-band antenna, on the other hand, is a small fin. An optimal position for this antenna is in the middle of the fuselage above the engine.

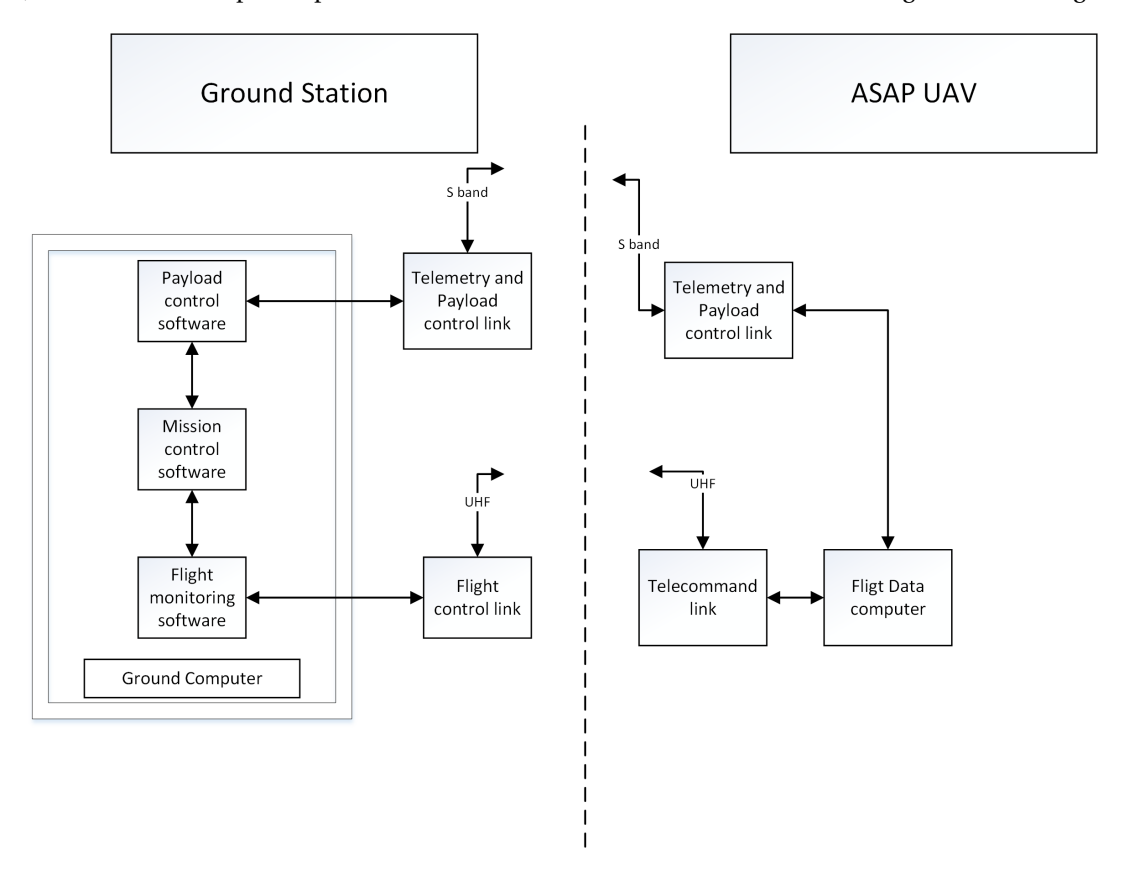


Figure 3.10: Communication block diagram

Now the link budget will be calculated for both the UHF- and S-band frequencies by first calculating the Signal to Noise Ratio (SNR). The signal strength *Si* can be found using Equation 3.4 [36].

$$Si = P_T G_T L_T L_P G_R L_R \left(\frac{\lambda}{4\pi R}\right)^2 \tag{3.4}$$

- P_T = transmitted power
- G_T = transmitter antenna gain
- L_T = signal loss through the transmitter antenna
- L_P = absorptive propagation loss
- G_R = receiver antenna gain

- L_R = receiving signal loss from the receiver antenna through the amplifier
- λ = wavelength of the carrier signal (length)
- R = distance between the transmitter and the receiver

The term $(\frac{\lambda}{4\pi R})^2$ denotes the free space loss, which in this case is calculated with the wavelength over the maximum LOS distance R of 43.71km. This way the link budget will be calculated for the maximum allowed parameters of the ASAP UAV. Some of the parameters indicating signal loss may consist of smaller individual losses within that element: L_T consists of the pointing loss $L_{T,Point}$, the component line loss $L_{T,Line}$

and the radome loss $L_{T,Radome}$. The latter denotes the loss caused by the casing around the antenna's and transceivers. L_T , G_T and G_T will be added up to represent the Effective Isotropic Radiated Power (EIRP) which would be the theoretical radiated power if it were distributed uniformly in all directions. With the signal strength known, the noise Ni can be found using Equation 3.5 [36].

$$Ni = ktBF (3.5)$$

- $k = Boltzmann's constant (1.38054 * 10^{-23})$
- process
- T = ambient absolute temperature
- F = noise factor
- B = effective noise bandwidth of the receiving

All of these values were calculated or evaluated for UHF-band and S-band communication systems. Table 3.13 represents all of the relevant values which make up the components of Si and Ni. Note that this only represents the downlink budget where data is transferred from the UAV (transmitter) to the ground control station (receiver). This is due to the fact that most parameters are known for the on-board communication systems, while yet little is known from the ground control station. The post-DSE phase will incorporate a further analysis of the available ground control stations, along with their communicative specifications. This will allow for an upload link-budget analysis. The precipitation absorption represents the signal loss due ob-

Table 3.13: Link budget for both frequencies of the ASAP UAV

Category	Parameter	430MHz UHF-band [37] [36]	2.4GHz S-band [36] [18] [16]
	Transmitted power $P_T[dBm]$	30	45
	Transmitter component line loss $L_{T,Line}[dB]$	-1.0	-1
Transmitter	Transmitter pointing loss $L_{T,Point}[dB]$	-0.5	-0.5
mansmitter	Transmitter radome loss $L_{T,Radome}[dB]$	-0.5	-0.5
	Antenna transmitter gain $G_T[dBi]$	-3.8	-5
	Free space loss $[dB]$	-117.92	-132.86
Propagation	Atmospheric absorption $L_{P,Atm}[dB]$	-0.44	-0.44
	Precipitation absorption $L_{P,Precip}[dB]$	≈ 0.0	≈0.0
	Receiver peak antenna gain $G_R[dBi]$	10.0	12.0
	Receiver polarization loss $L_{R,Polar}[dB]$	-3.0	-3.0
Receiver	Receiver pointing loss $L_{R,Point}[dB]$	0.0	0.0
Receiver	Receiver radome loss $L_{R,Radome}[dB]$	-0.5	-0.5
	Receiver component line loss $L_{R,Line}[dB]$	-1.0	-1.0
	Spreading implementation loss $L_{R,spread}[dB]$	-1.2	-1.2
	Thermal noise density kT [dbM/Hz]	-173.8	-173.8
Noise	Receiver noise bandwidth BW (1MHz) [dBHz]	53	66
	Receiver Noise Figure NF $[dB]$	2.0	0.9
	Available SNR	28.94	
Total	Required SNR	10	19.7
	Link margin	18.94	9.7

stacles and weather effects. Though there are near to no large objects at sea that may obstruct a transmission signal, the rain attenuation factor is of particular interest for the ASAP UAV due to its all-weather requirement. Fortunately, Figure 3.11 [36] shows that the rain attenuation is negligible at band frequencies below 5GHz, even in the worst weather conditions. All of the other minor contributions to the signal noise were estimated according to the general link budget analysis of UAVs [36]. The required SNR was taken at 10~dB, which is a typical value for UAV communication systems [36]. A more specific calculation of the required SNR can be made using the Bit-Error Rate (BER) of the entire communication system. Because of some uncertainties concerning the ground control station, an accurate estimate for the BER cannot yet be made. The link margin is especially good for the UHF-band frequency, which is almost twice the required SNR. The S-band link margin is lower but close to the required SNR, which makes it a very reasonable link budget.

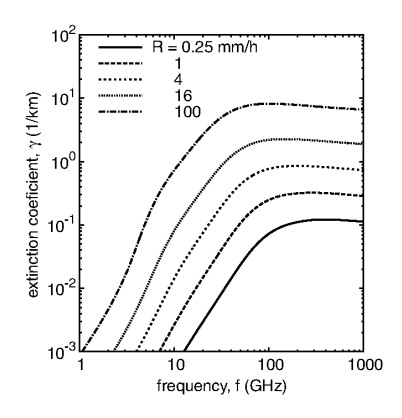


Figure 3.11: Rain attention in function of band frequency

There is an option to make some part of the antenna polymer-based, e.g. the supporting structure. Though entirely polymer-based antennas are still in development, they could be suitable for aerial applications in the near future, e.g. the ASAP UAV [38].

3.11. WARNING LIGHTS

In order to let the victim know he has been found, a set of colored led lights are added to the ASAP UAV's wingtips. These lights can be switched on by the flight computer as soon as a drowning person has been found. The colors of these lights will be red on the left wingtip and green on the right wingtip, which are the international navigation lights. The required voltage for a typical led light is about 4.2 V (2.2 Volts for the led light and 2 Volts for the resistor) [24]. In order to be visible, five red led lights are added to the left wingtip and five green led lights are added to the right wingtip. The power consumption of these 10 led lights is about 35 Watts [24]. In order to reduce the total power consumption, the led lights will flicker.

3.12. PITOT TUBE

In order to measure the dynamic pressure and therefore the velocity of the UAV, a Pitot tube has to be placed on the nose of the UAV above the See & avoid system. A suitable Pitot tube for the ASAP UAV, is the UAV Factory's heated Pitot-Static Tube. In Table 3.14 the properties of the Pitot tube can be seen [23]. The heater

Table 3.14: Properties of the Eagle Tree Prandtl-Pitot Tube

Disease le manuscrite : Engle Tree Bren del Bissasse

Pitot tube properties	Eagle Tree Prandtl-Pitot tube
Weight	58 gr
Length	23 cm
Diameter	10 <i>mm</i>
Power	19 <i>W</i>

of the Pitot tube is only switched on, when the outside temperature is below the freezing point of water.

OPERATIONS & LOGISTICS

This chapter will describe the operations and the logistics of the ASAP UAV. The chapter will commence describing the general operations and flight patterns of the UAV in Section 4.1. This is followed by the take-off and landing operations in Section 4.2 and 4.3, respectively. Section 4.4 will discuss the stationkeeping after victim localization, and the storage logistics of the UAV will be treated in Section 4.5.

4.1. MISSION DURATION, SEARCH PATTERN AND SWARM OPERATIONS

The largest mission segment of the ASAP UAV is searching for the victim. The performance of the UAV during this search operation will be described in Chapter 8. This section will first describe the search pattern for a single UAV, followed by the multi-UAV search operation.

4.1.1. MISSION DURATION

The duration of the mission is one of the most critical design parameters. In Chapter 2 it was mentioned that a mission duration of 3 hours is required. Although the total mission duration is 3 hours, the average mission duration has been estimated to be 2 hours. This too is an important design input for a number of parameters that must be taken into account during design, such as depth of discharge of the batteries and reliability of the UAV.

4.1.2. FLIGHT PATTERN

There is a distinction made between several flight patterns during search. The UAV can fly at cruise velocity to a designated area in which the victim is expected or the UAV can fly a pattern in order to maximize the search area. The first described pattern is a simplistic one. A signal is sent containing coordinates, which are corrected for wind and current effects, of the alleged location of the victim. Currents near the surface of large bodies of water are dominated by the wind in direction and are no larger than two to three m/s [39] [40]. This means the victim can drift more than ten kilometers per hour. The UAV should be aware of this drift and the direction in order to locate the victim as soon as possible.

The drift of an object in water is standardized by using the concept of leeway. Leeway is the victim's velocity vector relative to the victim's downwind direction as can be seen in Figure 4.1 [41]. The effect of leeway is prevalent up to depths of 1.0 m. Also it includes uncertainties since wind is not constant, neither in direction nor in magnitude. A plot showing leeway for different objects in water is shown in Figure 4.2. From this one can see that the victim will move with approximately 2 knots (or 1 meter per second) in 7 Bft winds. During gusts this leeway will increase for a short amount of time. A typical pattern for small search areas is an expanding square search which, as the name suggest, is a square pattern expanding around the datum (usually the corrected location where the victim was last reported) as shown in Figure 4.3 [42].

The second flight pattern is much more interesting in terms of operations. The Royal Netherlands Sea Rescue Institution (Dutch: KNRM) uses aircraft to extend the search area around their vessels. One of these patterns is shown in Figure 4.4 A [42]. This flight pattern can be used when the search area is very large. The spacing of the pattern is defined by the imaging resolution which results in a swath area of 100 meters by 50 meters. The path shown in figure A is strongly influenced by the wind. In no-wind conditions the pattern can be followed exactly. For downwind the turns (vertical paths in the figure) will be larger meaning the spacing will be larger. However, this will be accounted for by the drift of the victim since the victim will move in the same direction. As a matter of fact, the entire search area is moving in the downwind direction. The result is that the pattern will remain functional for windy conditions since the UAV is moving with the search area. The track relative to the ground however will appear compressed, extended or skewed. This phenomenon can cause confusion for an operating crew, since all modern-day location determination is ground-fixed. In this

Ö 2 6 8 12

Leeway

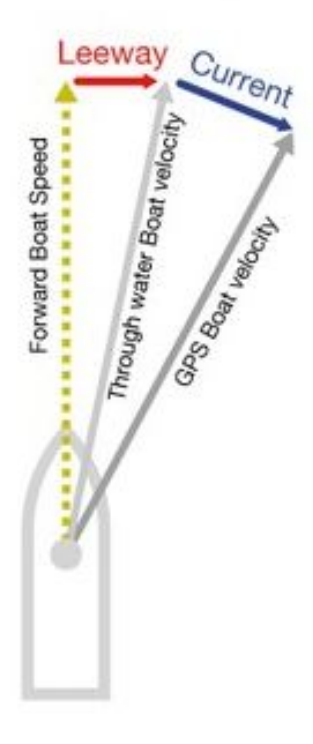


Figure 4.1: The Leeway vector which describes the velocity and direction of the victim in the water

Liferafts, Survival Craft and Persons in the Water (PIWs)

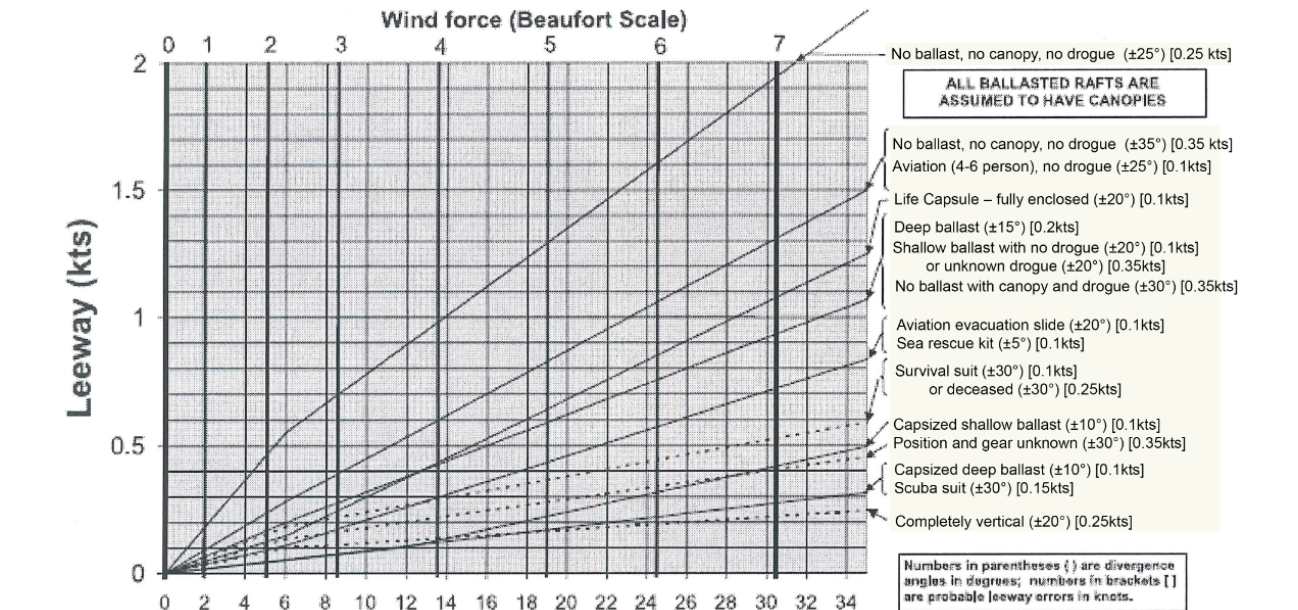


Figure 4.2: The leeway in knots for different objects in water for different wind speeds

14 16 18 20 22 24 26 28

Wind speed (kts)

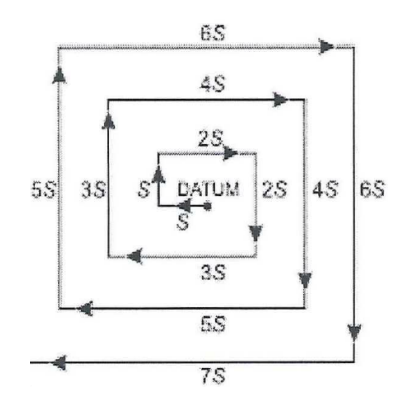


Figure 4.3: The expanding square search pattern around the datum

case the search area is moving with the UAV. This phenomenon is depicted in Figure 4.4. Figure 4.4 A shows the situation without any wind. For downwind (B), the ground pattern appears extended while for upwind (C) the path is compressed. In A and B the location of the victim is shown by the dot. As one can see in both cases the victim is found after the second turn. The location of the victim in Figure 4.4 C is shown for three. As one can see the victim will be discovered with this ground track due to the moving search area. Every flight

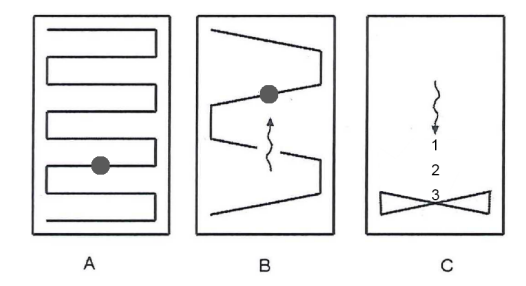


Figure 4.4: The flight pattern relative to the ground. The UAV starts at the left bottom. A: No wind. B: Downwind. C: Upwind.

pattern is more or less influenced by the weather. Severe winds can limit the performance of the UAV in such a way that flying the described patterns is not useful. This paragraph will look into the sensitivity of the flight patterns. The deviations from a certain flight path increase as the wind is increasing in magnitude. As can be seen in Figure 4.5 the wind speed is increasing as altitude increases [43]. This directly means that it may be favorable to fly at a lower altitude to decrease the influence of the wind. A drawback of a lower altitude is that the communication system on the UAV is limited by line of sight as mentioned in Chapter 3. An optimum needs to be found. In general one would like to fly as high as possible until the influence of the wind becomes too dominant. By decreasing the altitude the effective range of the UAV is lowered, directly influencing the possibilities of finding the victim as fast as possible in a large search area. The range of the UAV will be equal to 315 kilometers at cruise velocity as described in Chapter 8 while the line of sight will be limited to only 43 kilometers for a flight altitude of 150 meters. For every mission the command center will calculate the most optimal routing towards the search area. In order to remain capable of transmitting a direct video link to the ground station a ship should always be within the aforementioned 43 kilometers. As explained in Chapter 3 the video feed will be forwarded from the ship to the ground control station. A last consideration to increase the search area can be to use so-called camera whiskering. This whiskering is the quick rotation of the camera from side to side in order to point the imaging system beyond the edges of the fixed vision. However, the video quality and detection reliability could suffer from this constant rotation. In addition it is uncertain whether the Flir Cobalt-90 is capable of performing this whiskering. More research is necessary for this complicated method of imaging as will be described in Chapter 13.

4.1.3. SWARM SEARCH OPERATION

In the case of multiple victims or a very large search area it will be beneficial to search using multiple ASAP UAVs. In order to make the search as effective as possible the UAVs should be aware of the pattern of other UAVs. An example is that multiple UAVs fly side-by-side, spaced in such a way that gaps are prevented. This

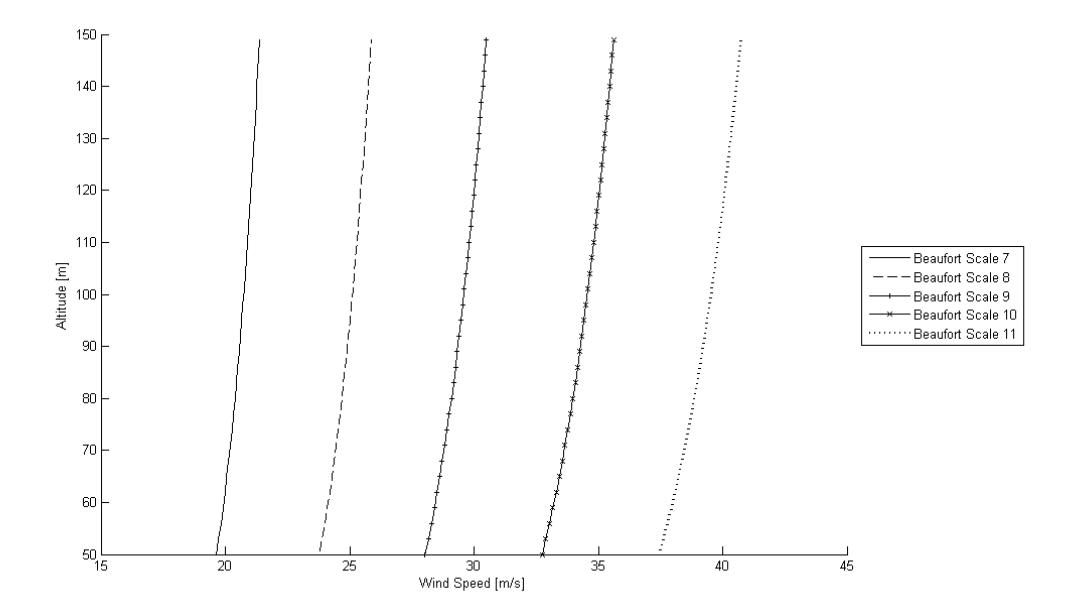


Figure 4.5: The wind velocity profile for different magnitudes (Beaufort scale)

maneuver is called a track-search. The idea of effective range is also an issue for multiple UAV usage, since neither one should be more than 43 kilometers from a command center (either aboard a vessel or on land). An additional point of consideration is that the UAVs should not intrude other search terrain nor circle the same victim after localization. This circling will be further explained in Section 4.4. As with the single UAV operation, the ground station's computer will calculate the most optimum route to the last known location of multiple victims, or create a pattern to scan a large area as effective as possible.

4.2. TAKE-OFF

This section will cover the take-off. Since the UAV will be launched from a ship, there are limitations to the take-off maneuver. First, a trade-off between different catapults is performed, followed by the explanation of the forces exerted on the UAV during launch. In Table 4.1 this trade-off can be seen.

Criteria	Weight	Troy	Robotic	Eli
Maximum launch velocity	10	8	3	5
Dimensions	8	8	2	8
Mass	4	5	1	8
Total points		164	50	146

Table 4.1: Trade-off between different launch systems

Table 4.1 compares three different take-off systems respectively Troy [44], Robonic [45] and Eli [46]. The different trade-off criteria are dimensions of the system, maximum launch velocity and mass. The most important criteria is the launch velocity that can be achieved by the system. In the dimensions criteria the length, width and height are taken into account. Mass is the least important criteria because the launch system does not have to moved. The minimum launch velocity is 18.4 m/s, which is the stall speed. A small safety factor of 0.92 is used, therefore a minimum launch velocity of 20 m/s is required. It is desired to have a slightly higher launch velocity to increase the difference between stall and launch velocity.

SECTION 4.3. LANDING 25

The maximum launch velocity of Troy, Robonic and Eli are respectively 30,20 and 22 m/s, with a side note that the length of the Troy is 6 m instead of 4 m when the maximum velocity is reached. Both Eli and Troy consist out of a 4 m long bar, while the Robonic is a very large launch system. The mass of Eli is 25 kg and the mass of Troy is 85 kg. The Robonic launcher mass is 255 kg, which is very large in comparison to the other systems.

Using the trade off in Table 4.1 the rail launch of Troy pneumatic catapult is chosen to operate on a ship for the ASAP UAV. The UAV is placed on a rail where a battery operated air compressor helps to accelerate the UAV to the desired speed over a very short take off distance along a rail. The angle of the launcher is 12 degrees with respect to the ship. This angle is just below the stall angle to maximize the lift coefficient while avoiding stall. The size of the launcher should be small enough to fit on most ships and this will result in a very high acceleration. The equation used to determine the launcher length is given in Equation 4.1 [36].

$$L_{rail} = \frac{V_{release}^2}{2a} \tag{4.1}$$

In Equation 4.1 L_{rail} is the length of the rail, $V_{release}$ is the release speed at the end of the launcher and a is the average acceleration during the launch. The length of the chosen catapult is 4 meter, therefore the take-off force on the UAV is 5.1g. This force is used in the calculation of the structure in Section 6.2. The chosen rail launcher shall fit partly (2-3m) on the boat. The other part of the aluminum beam will protrude over the edge of the ship. This will vary from ship to ship.

The minimum launch velocity is set at 20 m/s, while the launch velocity is 22 m/s. This is above the stall velocity of 18.4 m/s. When the wind velocity is larger than 2 m/s, the UAV has to be launched into headwind. The wave's at the surface of the sea are mainly caused by the wind [39]. Therefore the wave's velocity direction is the same as the wind velocity. When the UAV has to take-off into headwind, the front of the ship is first to reach the wave. This is favorable for the stability of the boat, since front of the ship cuts through the waves.

4.3. LANDING

After the mission is performed, the UAV needs to be recovered. Because of the extreme weather conditions, it will be difficult and dangerous to land on the ship. The other solution is landing on the water. However this is only possible when the UAV floats and in order to float, the UAV's volume has to be higher than its mass. As can be found in Chapter 8, this is the case for the ASAP UAV. A water landing can be done in several ways. These ways are:

- Deep stall:
 - Deep stall is a technique where the UAV will go into stall and the stabilizer will keep the UAV in stall where it would normally prevent this. The drag of the wing will act as a way to slowly descent. However, the UAV could enter in a spin when going into the deep stall and the maneuver could become uncontrollable. It will be difficult to keep control of the UAV when landing in severe weather conditions.
- Parachute:
 - The next option considered is a parachute. At the end of the mission the UAV will deploy a parachute and glide down gently. The UAV will descend and touchdown in the water and subsequently can be recovered. An advantage of this solution is the low landing velocity, but disadvantages are the sensitivity in bad weather conditions and the additional weight and volume of the parachute in the UAV.
- Inflatable device:
 - An inflatable device can also be used to land. This device should be placed along the entire bottom of the UAV, next to the fairing and the camera. It is not desirable to land in the water with the nose down. When this happens the UAV will have the tendency to flip over. Therefore the UAV should have landing surfaces after the c.g.. Hence the inflatable devices are next to the fairing and the camera. A disadvantage of these inflatable devices is the storage. These devices will cover the complete length of the bottom and will therefore be difficult to store. The fuselage has to be watertight which results in an extra compartment in the bottom of the fuselage for these devices. The impact force will act on the inflatable devices instead of the structure, therefore the fairing and camera will have to be less impact resistant.
- Landing on a fairing:

 It is also possible to land on the fairing and the camera casing, so no external devices are necessary. The

camera will be protected using a transparent polymer, like Polylactic Acid (PLA). If the camera will be used to land, an impact resistant polymer can be used. Then it will act as protection for the camera and as landing surface. The fairing should also be designed to withstand the impact loads during landing. At first the UAV has to hit the water with the fairing, thereafter the angle between the UAV's neutral line and the water can be minimized. A distributed impact load will act on the fairing and the camera, which can be calculated using FEM analysis.

The advantages and disadvantages of each method are described in Table 4.2 The ASAP UAV will land on the

Landing method	Major advantage	Major disadvantage
Deep stall	Simple system	Possibly uncontrollable in heavy weather conditions.
Inflatable device	No impact resistant structure is needed	Complicated system. Extra compartments at the underside of the UAV.
Parachute	Low landing velocity	Parachute is payload and brings extra volume and mass. Possibly very sensitive in heavy wind conditions.
Fairing & camera casing	No additional systems needed	Impact resistant structure is necessary.

Table 4.2: Advantages and disadvantages of landing methods for the ASAP UAV

fairing and camera casing. This method is chosen because no extra systems are necessary to perform the landing. Another advantage is that this landing method can also be performed in severe weather conditions. The maximum angle of a wave is 5.8 degrees and the stall angle of the UAV is 15 degrees [47]. The UAV shall land into headwind, which decreases the ground velocity. This will significantly decrease the force of the wave on the UAV. Therefore it is still possible to land on the fairing in severe conditions.

When there is no wind, the minimal landing velocity is 18.4 m/s equal to the stall speed. Wind makes it easier for the UAV to land because the velocity with respect to the ground is lower. The effective landing velocity should be higher than the stall velocity to prevent sudden stall. As mentioned before, an effective landing velocity (airspeed) of 20 m/s will be used.

$$F_{and} = \frac{0.5 * m * v^2}{s_{land}} \tag{4.2}$$

$$n = \frac{F_{land}}{m * g} \tag{4.3}$$

The point load on the fairing can be estimated by Equation 4.2. In this equation m is the mass, v is the landing velocity, s_{land} is the landing distance and F_{land} is the force exerted on the fairing. In equation 4.3 the load factor n during landing is determined. The landing velocity is 20 m/s, mass is 10 kg and the landing distance is estimated as 5 m. The landing distance is relatively small, but is used as extreme value. The point force is calculated at 400 N, therefore the load factor at landing is 4.1. During launch a load of 5.1 g acts on the structure, therefore the fairing should survive a load of 4.1 g. The forces on the structure are elaborated in Section 6.2. FEM analysis and tests should be performed to finalize the landing design.

The shape of the fairing can have the shape of the hull of a ship, inspired by seaplanes [48]. Also at the wing tips extra drop shaped symmetric winglet can be added. These extra winglets will protrude below the wing in order to provide stability during landing. A disadvantage of these extra landing fairings are the drag induced on the UAV. There is also the possibility that one of the winglets sticks in the water instead of float over it. This is possible because these fairings are fairly small, maximum of 2 cm. When the water slows down one of these winglets, the UAV turns and crashes. Because of this uncertainty it is chosen not to use these winglets.

After the UAV has landed on the water, it should be returned to the ship. According to Mr. R. Moleman, (head operations, KNRM) their ships are maneuverable up to waves with a height of 10 meters, which indicates that it is possible to retrieve the UAV in severe weather conditions. There are two retrievement methods, which

are dependent on the ship. KNRM ships have a tilt valve at the aft of the ship. This valve is used to get the victims out of the water, therefore this can also be used to retrieve the UAV.

In the case the ships do not contain these valves, the UAV can be retrieved using a small ship or by using two retrieval poles equipped with nets. These nets can enclose both wings and the UAV can be raised out of the water. From these small ships the UAV can easily be retrieved. An elaborate study in the behavior of a ship or small boat in 7 Beaufort is needed, since the retrievement of the UAV should not endanger the crew.

4.4. STATIONKEEPING

When a victim is located, the UAV should be able to keep station above the victim. There are two possibilities to perform station keeping; flying in circles and using headwind to hover. The endurance velocity of the UAV is determined to be 22.2 m/s, which can be found in Chapter 8. Therefore, it is the velocity at which the UAV should perform a slow circling flight above the victim. There are three wind velocity ranges in which the UAV can perform station keeping, respectively $v_{wind} = 0 \text{ m/s}$, $0 < v_{wind} < 22.2 \text{ m/s}$ and $22.2 \le v_{wind} < 40.2 \text{ m/s}$. The altitude at which the UAV will operate during station keeping is 150 m. This is the maximum height of the UAV, whereby the camera angle is at its minimum.

At a wind velocity of $v_{wind} = 0$ m/s the UAV will fly perfect circles at a bank angle of 20 degrees. The radius of the circle is 138 m at an endurance velocity of 22.2 m/s. The angle at which the camera is operating with respect to the UAV is 63 degrees.

Due to a wind velocity range of $0 < v_{wind} < 22.2$ m/s the circular flight will become, due to the windy conditions, elliptical. W.r.t. the ground the UAV is faster on one side of the ellipse and slower on the other side. Half a circle is flown in a certain amount of time at $v_{endurance}$. This time, necessary to fly half a circle, is multiplied by the wind speed to calculate the deviation with respect to the initial end point of the circle. Since the deviation of the UAV with respect to the victim cannot be too large, the whole ellipse should shift in opposite direction of the deviation. This shift should make the victim the center of the ellipse and therefore minimize the maximum distance to the UAV.

The bank angle at which the UAV operates in a turn is set at 20 degrees. If the bank angle is decreased, the turn radius is larger but the drag is decreased and thus power required. If the bank angle is increased, the turn radius decreases and the drag increases exponentially. The camera angle and the bank angle should, when added up, not exceed 90 degrees. If the bank angle is set at 20 degrees, the camera angle will vary between 42 and 67 degrees. Therefore the total camera angle w.r.t. the UAV varies between 62 and 87 degrees.

Due to a wind velocity equal to or higher than the endurance velocity, thus a wind speed from $22.2 \le v_{wind} < 40.2$, it will be possible to hover. The UAV will fly with the same velocity as the wind at which the UAV will perform station keeping and will operate right above the victim, so that the UAV can focus its camera on the victim. The endurance time of the UAV will decrease, because the velocity is higher than the endurance velocity. The maximum wind velocity is the same as the maximum velocity of the UAV, which is calculated at 40.2 m/s. If the wind velocity is greater than 40.2 m/s, the UAV cannot perform station keeping.

4.5. STORAGE

The transport container of the ASAP UAV has the function to protect the UAV from the environment whenever it is not flying. This includes protection from shocks, acceleration loads, vibrations and chemical and thermal degradation. While the container has to fulfil all these requirements, it should also be easily accessible. When the UAV is required it should be up in the air as soon as possible. These requirements can be fulfilled by using a box. This box will be filled with soft foam. In order to completely encase the UAV, the foam will be formed to the shape of the UAV. Due to the foam the UAV will be protected against shocks, acceleration loads and vibrations. The box will be used in a humid environment on sea. When the UAV is in the box it is desired to have it in a non-moisturized environment. This will be done by putting moisture absorbers in the box. When the UAV is needed, it will be extracted out the box as a whole. Thereafter the UAV is put on the rail launch system. A detailed design will be made in the post DSE phase 13.

LIFE CYCLE

In this chapter the life cycle of the ASAP UAV is discussed. The life cycle consists of the manufacturing, operation and disposal of the UAV, which are described in Section 5.1. The manner in which these three 'phases' are fulfilled has a big influence on the design. In addition it is of importance for a number of different parties, such as the manufacturer and the owner, as they are responsible for the manufacturing, operation and disposal of the UAV as elaborated in Section 5.2.

5.1. Reliability, Availability, Maintainability and Safety (RAMS)

A RAMS analysis is necessary to predict the performance of the design during operations and whether or not it fulfills the requirements set by the design team. When unfulfilled requirements are discovered, the design is altered accordingly. First the reliability is described in Section 5.1.1. It contains information regarding how the UAV will perform its mission considering failure rate. Then the availability is elaborated in Section 5.1.3, followed by the maintainability in Section 5.1.2. The safety of the UAV is documented in Section 5.1.4.

5.1.1. RELIABILITY

Reliability defines how often the UAV experiences a failure within a given time frame. The operational reliability of the different components of the UAV is evaluated in order to determine if redundancy should be added. To choose the redundancy measures, the consequences of the failure of a component are taken into account. Here a distinction is made between Mission Reliability and UAV Reliability. Mission Reliability expresses how often a mission cannot be (completely) performed. The UAV Reliability however, denotes how often the UAV will be completely lost. By differentiating between these reliabilities the amount of redundancy required can be minimized and therefore reduce the financial and carbon cost of the design. The failure categories are defined as follows:

- · Catastrophic; the UAV becomes uncontrollable and does not respond to commands. This leads to the loss of the UAV and creates a potential danger. In general aviation terms this is called a 'class-A mishap'.
- Critical; the UAV cannot sustain flight but is able to perform a controlled landing.
- · Moderate; the UAV can continue flight, but cannot perform its mission as required.
- Minor; the UAV can perform its mission, possibly with a compromise on efficiency.

UAV Reliability consists solely of failures in the 'catastrophic' category. Mission Reliability however, consists of the first three categories. Note that when a UAV is lost, the mission cannot be completed. Therefore the category 'catastrophic' is also included.

The ASAP UAV consists of a large number of parts that can all experience failure. These parts can be considered to be arranged in series due to the fact that if one part fails, the entire UAV experiences the described failure category. Therefore, the total reliability (R_{tot}) is defined by the product of the individual reliabilities, as is expressed in Equation 5.1. As can be seen in Equation 5.2, the reliability of a single part is defined by the flight duration (t), which is assumed to be 2 hours, and the incident rate (λ) . The incident rate is defined in Equation 5.3 and is dependent on the Mean Time Between Failure (MTBF) value of the part.

$$R_{tot} = \prod_{i=1}^{N} R_i \tag{5.1}$$

$$R_i = \exp[-\lambda \cdot t] \tag{5.2}$$

$$R_{i} = exp[-\lambda \cdot t]$$

$$\lambda = \frac{1}{MTBF}$$
(5.2)

To conclude, reliability is dependent on the MTBF of the individual components, and the flight duration, which is two hours on average. Therefore, to determine the UAV Reliability and the Mission Reliability, the 30 Chapter 5. Life Cycle

components of the UAV have been examined with respect to the failure category and their MTBF. The results have been provided in Table 5.1.

Table 5.1: Failure category per components per mission

Part	Failure category	MTBF	Part Relia- bility	Reasoning
Flight	Catas-	5000	0.9996	The UAV becomes completely uncontrollable if the
Computer	trophic			flight computer fails.
GNC	Catas- trophic	5000	0.9996	If the GNC system fails the UAV is not aware of its position, attitude and flight path. As this might cause danger, the engine is programmed to shut off and the UAV will crash.
Motor	Catas-	4000	0.9995	The motor controller sends input to the motor and to
Controller	trophic			the servos. If the controller fails, the UAV becomes uncontrollable.
Servos	Critical	500	0.9960	The servo failure type determines the outcome. If the servo is stuck in a deflected position the UAV might not be controllable. If it is not stuck a controlled landing is possible.
See and Avoid	Critical	5000	0.9996	An immediate landing will be necessary to mitigate risk.
Motor	Critical	4000	0.9995	Active glide mode will be activated and a controlled landing will be performed.
Payload	Moderate	2000	0.9990	If the payload does not work, the mission cannot be completed.
Catapult	Moderate	1500	0.9987	If the catapult fails, the mission cannot be started.
Communi- cations	Moderate	2000	0.9990	Dependent on the type of failure, the mission can or cannot be completed.
Batteries	Minor	40.000	0.99995	If a battery fails, only a part of the power is lost. The mission can therefore be continued, but with less duration and range.
Wiring	Catas- trophic	5000	0.9996	The wiring failure affects a component, which results in a catastrophic failure.
	Critical or Moderate	2000	0.9990	The wiring failure affects a component, which results in a critical or moderate failure.
Airframe	Catas-	4000	0.9995	The airframe fails in a manner by which the UAV
mmunic	trophic			becomes uncontrollable.
	Critical or	2000	0.9990	The airframe fails in a manner by which it is still
	Moderate			controllable but cannot continue its mission

Note that the failure category of a wiring or airframe failure has been split up into two. The reason is that a wiring failure can result in a failure of any other part. If a wiring failure shuts down the flight computer, the result is catastrophic, whereas if a battery is shut down, the UAV is able to continue its mission. The same goes for the airframe; a minor crack can occur, or the entire wing could fail.

DETERMINATION OF MTBF VALUES

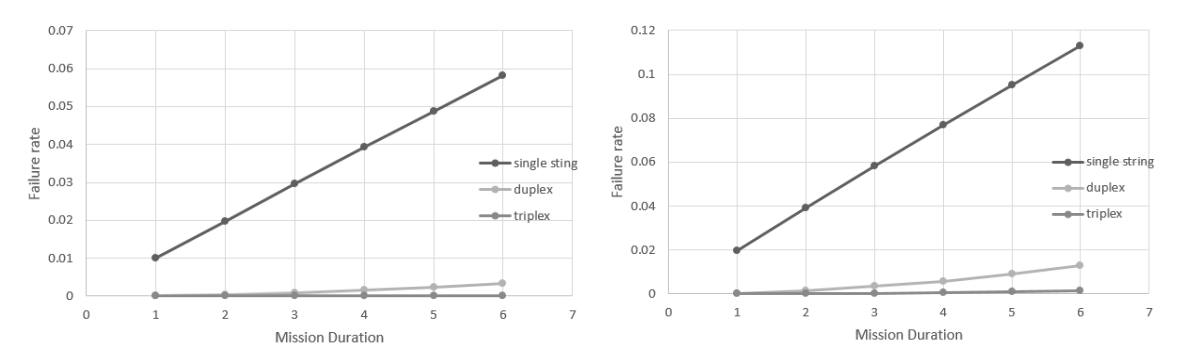
Most manufacturers are reluctant to share information about the failure rate of their products. Hence, the MTBF is unknown of most products. However, a reliable reference is found [36] containing the range of typical MTBF values for all parts. For each part the MTBF value of an average quality part is approximated. The reason for this is that parts that reach the chosen MTBF will most likely not be expensive, but reliable enough for this application. Therefore, during the post-DSE phase, described in Chapter 13, only the parts that reach the defined MTBF should be selected. In addition the reliability of the different parts should be tested, verified and validated. This process is also described in Chapter 13.

REDUNDANCY

MTBF

Reliability

Now that the failure category the different parts has been examined, a substantiated redundancy approach is constructed. The possible redundancy measures that can be taken are to add so-called 'duplex' or 'triplex' parts. These are parts that are identical to the primary parts and only come into action when that part fails. The effect of duplex and triplex parts can be viewed in Figure 5.1a and 5.1b. As can be seen, the effect of adding a duplex part is much larger than when a triplex part is added. In addition, the effectiveness of a redundancy measure increases as the reliability decreases, as can be concluded from the comparison between Figure 5.1a, which shows the effect on a part with a MTBF of 50 hours, and Figure 5.1b, showing the effect on a part with a MTBF of 100 hours. It is concluded that the most efficient redundancy measure is to add duplex redundancy to the parts with the lowest MTBF. Note that the size and especially weight of the components should be taken into account, as the storage space and weight for additional parts and batteries is limited.



(a) Redundancy for components with a MTBF of 50 hours. (b) Redundancy for components with a MTBF of 100 hours.

Figure 5.1: Redundancy for components with an MTBF of 50 and 100 hours.

As noted before, the values of the UAV Reliability and Mission Reliability are evaluated separately to minimize the required redundancy measures. The reliability values are determined using the content of Table 5.1 and Equations 5.1, 5.2 and 5.3. The result for the UAV Reliability is given in Table 5.2, whereas the result for the Mission Reliability is provided in Table 5.4.

Subsystem Flight Computer Motor Controller GNC Wiring Airframe Total

4000

0.9995

5000

0.9996

5000

0.9996

4000

0.9995

908

0.9978

Table 5.2: Expected MTBF and reliability of catastrophic failure category parts, and total UAV Reliability

5000

0.9996

The result of the UAV reliability analysis is that every 908 hours one ASAP UAV will be lost. Compared to the average Class-A mishap rate of UAVs, which is between 10^1 - 10^3 per 100.000 flight hours [36], this is an average result. Another way to view the result is that, with an average mission duration of 2 hours, every 450 missions an UAV is lost. With a cost estimate of over \$35,000,- per UAV, as described in Table 10.2 in Chapter 10, the design team considers this too rate high so redundancy should be added.

As concluded before, the most efficient redundancy measure is to add duplex parts to the parts with the lowest MTBF. In this case, these are the airframe and the motor controller. As a second airframe cannot be added, and the airframe design already contains a safety margin as explained in Chapter 6, its reliability cannot be adjusted. A duplex motor controller can be added however. This is a moderately heavy component, with a weight of 43 g [10]. The flight computer, GNC and wiring all have the same MTBF. The lightest components are the flight computer and the GNC. These are both attached to the autopilot (NavStick) as has been described in Chapter 3, which has a weight of 10 g. Using Equation 5.4 the part reliability after redundancy is calculated. The results are combined in Table 5.3

$$R_{tot,part} = 1 - \prod_{i=1}^{N} (1 - R_i)$$
 (5.4)

32 Chapter 5. Life Cycle

Table 5.3: Expected MTBF and reliability of catastrophic failure category parts, and total UAV Reliability

Redundancy	Total MTBF	Effect [%]	Additional weight [g]
No redundancy	908	-	=
Motor controller	1176	29.5	43
Autopilot	1428	57.3	10
Motor controller & autopilot	2220	144.5	53

As can be concluded from the table, the total efficiency when combining redundancy measures is larger than the sum of the individual components. This is therefore the most effective solution. In addition, the design team considers this level of reliability necessary, mainly out of a quality versus price standpoint. When these measures are taken an ASAP UAV is lost on average every 2220 hours, or approximately 1100 missions, compared to 908 without the redundancy.

Now that the redundancy is designed for the UAV Reliability, the new values should be taken into account when evaluating the Mission Reliability. In addition, it should be noted that the UAV contains 6 servos, consisting of 3 pairs of duplex redundant servos, this is further elaborated in Chapter 8.

Redundant components will not increase the MTBF when failure is not detected. By using the current sensing capability of the auto pilot, the output of the motor controller is verified. When the current output does not correspond with the desired value, it is considered non-functional. Then the back-up controller is activated and command center is notified of this happening. The auto-pilots are frequently polling each other's state and based on an algorithm it is decided which computer controls the UAV.

At the servos, small angular measurement chips are applied. If the servo deflection does not correspond with required input, the servo is not functioning and backups are used, either a backup servo or a backup plan to control the UAV without the faulty servo-control surface combination. A suitable angular sensor is manufactured by Bourns and measures only a couple of mm^3 [49].

Table 5.4: Expected MTBF and reliability of catastrophic, critical and moderate failure category parts, and total Mission Reliability

Subsys- tem	Autopilot (redun- dant)	Motor Con- troller (redun- dant)	Servos (redun- dant)	See and Avoid	Motor	Payload	Catapult
MTBF Reliability	$6.24 \cdot 10^6 \\ 0.9999997$	$8.00 \cdot 10^6$ 0.9999998	$4.17 \cdot 10^4 \\ 0.999952$	5000 0.9996	4000 0.9995	2000 0.9990	1500 0.9987
Subsys- tem	Commu- nications	Wiring (Cat.)	Wiring (Crit. & Mod.)	Airframe (Cat.)	Airframe (Crit. & Mod.)	Total	-
MTBF Reliability	1000 0.998	5000 0.9996	2000 0.9990	4000 0.9995	2000 0.9990	245 0.9919	-

It can be concluded that on average, with the current redundancy measures, an ASAP UAV cannot complete its mission once every 245 hours. This is considered a good result by the design team, and no further redundancy measures will be taken.

LIGHTNING STRIKE PROTECTION

One of the derived requirements is that the UAV needs to remain operational after being struck by lightning. This will require additional design efforts and will add weight to the design, add complexity to the manufacturing process and will most likely decrease the polymer content of the UAV. The resources required should be weighed against the likelihood and result of a lightning strike.

On average, an passenger aircraft is struck by lightning once a year [50]. Furthermore, these aircraft have

an average amount of flight hours of between 2000 and 3200 hours. This would suggest they are struck on average once every 2600 hours. This value is not valid for the ASAP UAV, as its flight profile differs greatly. It can be found that less than 5 % of aircraft lightning strikes occur below 2000 ft. [51] due to the fact that most lightning strikes occur when a aircraft passes through clouds. A simple calculation shows that on average the UAV will be struck by lightning every 52.000 flight hours. This value is so large that the resources do not weigh up against the added complexity and decreased polymer content. A decision is therefore made not to pursue lightning protection.

5.1.2. MAINTAINABILITY

The life-time of the ASAP UAV depends on the different products placed on the UAV. The warranty of the expensive electrical products e.g. the camera, see & avoid and motor, is regulated by legislation. This legal warranty is stated as two years, after two years the quality of the products cannot be guaranteed. Therefore it is decided to design for a life-time of two years. The maintenance strategy includes scheduled inspections and maintenance intervals. Most incorporated off-the-shelf solutions are not properly documented for use with the ASAP UAV as explained in Chapter 3. In order to guarantee availability of the UAV at all times, all parts have to be in good condition. Maintenance can be scheduled based on part age or on number of missions performed. As the latter is most likely the critical case for a UAV that is used daily, the maintenance schedule is driven by the number of missions performed.

Four maintenance related activities are considered for each component. The most vulnerable and mission critical components are inspected after each mission during the post flight inspection in order to verify the integrity and functionality of the components. This procedure should not take too long and is performed by a single operator. This inspection or maintenance activity is low tech, however the operator is required to possess some basic knowledge about the UAV maintenance.

Inspection intervals are scheduled for most components. This activity is a more in-depth inspection compared to the post-flight inspection. The purpose of this activity is to ensure the integrity and functionality of the UASs. During this inspection the UAV's fuselage has to be opened. This activity is performed by trained personnel and is not likely to happen off-shore. The inspection interval depends on the nature of deterioration of the inspected system. As for some systems the degradation depends on the number of missions or its intensity, while others deteriorate over time.

Maintenance activities are scheduled for systems that are subjected to wear. Like the scheduled inspection, the maintenance interval depends on the nature of deterioration of the system. Typical maintenance activities are the replacement of worn components, or precautionary replacing of components.

Some systems may be difficult to inspect, have a determinant life span or are too inexpensive to be subjected to tests. These systems have a replacement schedule. Typical for these systems is the lack of extensive maintenance activities.

A supplement to the scheduled inspections and maintenance is the test flight or flight envelope test. This is a procedure where the UAV performs a demanding test mission to validate its compliance with the flight envelope and operating conditions. Furthermore the functionality of several subsystems can be tested. A flight test is performed between every 50 flights or every six months.

SYSTEM MAINTENANCE

In this subsection, all maintenance activities are described. For the most important subsystems, there is an elaboration on the origin of the maintenance activities. The result for all subsystems is summarized in Table 5.5.

The fuselage of the UAV is inspected visually after every mission in order to spot obvious damage on the structure. Due to the nature of the mission and the harsh landing conditions the structure requires regular inspections. Also, biopolymers suffer from environmental degradation, further elaborated in Chapter 6. As such, the combination of structural loads and environmental impacts pose serious demands on the fuselage.

Notorious locations of stress concentrations are inspected, both the inside and the outside of the structure. After 200 landings, the structural integrity of the UAV cannot be guaranteed and either a specialized sonar

34 Chapter 5. Life Cycle

inspection for micro cracks is necessary or the fuselage has to be replaced. The latter is likely to be the cheaper option and thus preferred.

As mentioned before, polymers suffer from environmental conditions even when no mission is performed. Therefore a cap of 1 year is enforced, the fuselage is replaced after 1 year or after 200 missions.

As the battery system is one of the key elements of the UAV and is prone to degradation [13], regular inspection is required. Every ten missions, the shape of the battery should be inspected to ensure no gas-forming has taken place. During the missions, information about the battery voltage and current drawn is analyzed, hence the state of the battery is derived. This helps to predict the remaining life time of the battery. The charge cycles and life time of batteries is explained in Section 3.5.1, based on the expected life it is advised to replace the batteries after 200 full charge cycles or when the batteries are one year old.

Servos are important components for control of the UAV and, as explained in the MTR [2], they are cheap and relatively light. After each mission the functionality of the servos is verified by deflecting all control surfaces. Also, the control surfaces are checked for play. As the servos are inexpensive, precautionary replacement of the servos is favored over maintenance. For convenience, the servos are replaced with the fuselage after 200 flights.

The **motor** consists of four parts that are to be considered for maintenance. The bearings are particularly vulnerable to corrosion or debris, caused by salt water. The coils of the motor are insulated and therefore not vulnerable to water. Magnets are corrosion vulnerable and the sensors for brushless DC motors are vulnerable to water. Hence the electronics inside the motor have to be water proof. Furthermore the bearings and magnets have to be rinsed with water and treated with water repelling lubricant after each mission. As the motor is relatively inexpensive, it is precautionary replaced after ten missions. However, when all components seem to be in good condition, the motor is overhauled by replacing the bearings.

The **propeller** is the cheapest component of the UAV. Typical fixed pitch, polymer propellers cost a few dollar per piece. Since the propeller is crucial for the performance and is prone to damage from the landing impact, it is replaced after every mission.

Coating The coating protects the fuselage from environmental damage and it can also be applied to other exposed subsystems like the motor, for protection against corrosion. The quality of the coating may deteriorate over time due to environmental conditions such as Ultra Violet (UV) radiation, rain or temperature fluctuations. It is also prone to contact damage during handling, launch and impacts during flight or landing. Therefor the coating is inspected every 10 flights using dyed water. Damage can be repaired by locally reapplying the coating. Every 50 flights the coating is entirely reapplied to ensure continuous protection.

The **payload** is the most important system on board of the UAV. The gimbal is designed for UAV surveillance missions [21] and comes with two years warranty. Therefore it is assumed it will last two years. After each flight it is inspected for scratches and cracks since it shoul remain waterproof for all the flights. Further performance is measured during the flight envelope tests. If any maintenance has to be performed, it is send back to the manufacturer either for repairs or for warranty replacement.

MAINTENANCE INTERVAL

With all the maintenance and inspection intervals known, the life cycle for maintenance of the UAV is plotted in Figure 5.2. Easily identifiable are the major maintenance activities every year or 200 flights. Using this figure, one sees that when one has to consider to replace the entire UAV, it is best to do that right before the major maintenance activities. All routines incorporated to reduce the environmental impact of part replacement are described in Section 5.2.

5.1.3. AVAILABILITY

The availability of the UAV represents the time the UAV is available to perform a mission compared to the down time for maintenance. Based on this ratio, one can estimate the amount of UAV one should possess to be able to be responsive at all times.

Table 5.5: Maintenance procedure and characteristics for the UAV subsystems

	Maintenance characteristics	Post flight	Inspection interval	Maintenance interval	Scheduled replacement
Fuselage	Prone to damage due to operating conditions. Both obvious visible cracks and invisible micro cracks in the fibers may occur.	Inspect for structural integrity.	10 flights, inspection of inner structure. Flight envelope test.	Not Applicable (N.A.)	200 landings or 1 year - replacement.
Battery	Functional deterioration over time and through usage. Damage is often visible.	N.A.	10 Flights or weekly visual inspection and voltage check	N.A.	Scheduled 200 flights or annual replacement.
Servos	Lifespan deteriorates when pushed to its limits. End of life not easily predictable.	Check for control surface play and servo functionality.	Flight envelope test.	N.A.	Replacement with fuselage.
Motor	Structural and functional deterioration over time, decreased life time when operated at its limit.	Rinse with fresh water, grease bearings.	N.A.	Overhaul by replacing bearings every ten flights.	Replacement after ten flights when necessary.
Propeller	Prone to damage during landing. Easy to inspect and replace.	N.A.	N.A.	N.A.	Replacement after every flight.
Fuselage	Functional deterioration over time and through contact with objects. Scratches in the coating can be made visible with dyed water.	Visual inspection for scratches.	Inspect coating every ten flights.	N.A.	Re-apply coating every 50 flights.
Payload	Image quality and correct rotation of the gimbal can be verified.	Camera lens inspection for scratches. Gimbal structure integrity inspection.	Flight envelope test for functionality.	Possible scheduled overhaul, interval to be determined.	N.A.
Flight electron- ics	Impossible to inspect for structural deterioration or to maintain.	N.A.	Flight envelope test for functionality.	Annual software update	N.A.
Commu- nications	Impossible to inspect for structural deterioration or to maintain. Antenna damage is visible at inspection.	Visual antenna inspection.	Flight envelope test.	N.A.	N.A.
Wiring	Easy to inspect, vulnerability depends on the quality of fastening.	N.A.	10 flights connector inspection.	50 flights wiring integrity inspection and maintenance.	N.A.
S&A	Image quality can be verified.	Camera lens inspection for scratches.	Flight envelope test for functionality.	N.A.	N.A.

36 Chapter 5. Life Cycle

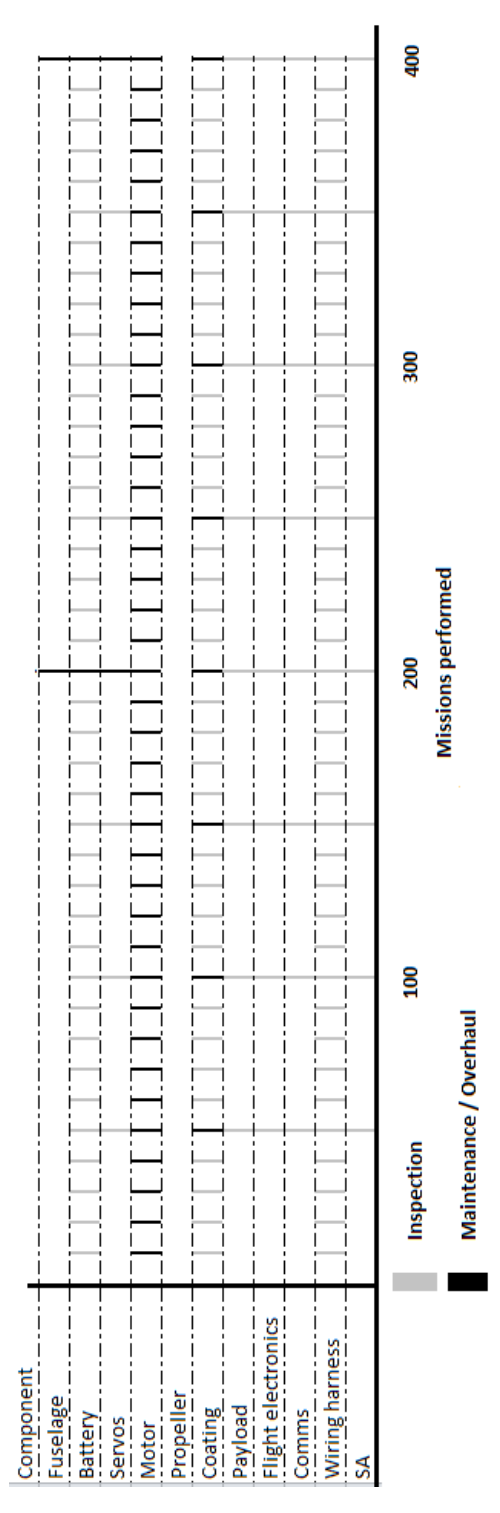


Figure 5.2: UAV maintenance interval timeline, indicating the amount of missions between the maintenance activities. Black indicates maintenance or overhaul and grey indicates scheduled inspection.

MAINTENANCE INTERVAL

As explained in Section 5.1.2, the UAV requires maintenance every 10, 50 and 200 missions. It is safe to assume that, regardless of the type of work, the UAV is out of service for a day. When performing a mission on a daily basis, after 10 days the UAV is out for maintenance for one day. According to [36], the availability depends on the Mean Time Between Maintenance (MTBM) and the maintenance duration. As explained, the MTBM is 10 days and the maintenance down time (MDT) is 1 day. Using Equation 5.5, the availability is 91%.

$$A = \frac{MTBM}{MTBM + MDT} \tag{5.5}$$

UAV AVAILABILITY

In order to ensure 100% availability for a single UAV mission, one needs 2 UAVs. For multiple parallel missions, the sum of the availabilities of all owned UAVs (n) should be more than the amount of missions one can perform simultaneously (x), as shown in Equation 5.6. The closer the sum to the desired availability, the more accurate the maintenance activities have to be scheduled.

$$\sum_{n} A(n) > x \tag{5.6}$$

5.1.4. SAFETY

In a study conducted by the Massachusetts Institute of Technology regarding the safety of operating UAVs [52], there are two kinds of safety aspects considered: UAV mid-air collisions with other air-traffic and UAV collision with the ground. The first risk is obviated with the mission boundary conditions and the S&A system that is integrated. The risk of UAV ground collisions is of particular interest as requirement CUS-22 states (Section 12.4.2) that the UAV must be safely disposable. Two other safety aspects can be derived from requirement CUS-22. One is the safety regarding the physical disposal of the UAV or its replaced parts. The other is implied by the human interaction during launch and landing.

Safety regarding UAV with ground collision is mainly dependent on the accuracy of the auto pilot and the functioning of the GNC-system and actuators. As long as the UAV can determine its position accurately, and no flight-critical components malfunction, the UAV will not crash. Therefore this first aspect of safety depends on the reliability of the UAV's subsystems. As explained in Section 5.1.1, the ground collisions are caused by critical failures. Given the extensive measures to minimize the critical failure rate of the UAV, the chance for ground collision is minimal.

Safety regarding the full or partial disposal of the UAV depends on the used material, fabrication process and overall layout of the UAV. In order to ensure the safety of workers involved with the decomposition of the UAV, a number of precautions have to be incorporated.

First, the amount of chemicals that can cause toxic substances during decomposition or manufacturing should be kept to a minimum. If these chemicals are present, the workers should be aware of them and act accordingly. Second, wherever there are dangerous components incorporated in the UAV, their removal should be safe and easy. It is also desired to limit or even avoid the use of these objects, e.g. spring loaded systems, sharp materials or high voltage setups. The incorporation of these safety advises is elaborated upon in Sections 9.1 and 5.2. No pre-tension systems are required for the UAV and the bio based materials pose little danger to the workers. This is elaborated upon in Section 9.1.

Intense human interaction is present during launch and landing phases of the UAV's mission. During launch, operators have to prepare the UAV for its mission and place the UAV on the launch system. When the UAV is installed at the launch system, there is the potential danger of rotating propellers and a faulty launch may result in serious worker injuries. Therefore safety measures are incorporated during launch to prevent contact with the propeller and make sure that a faulty launch will result in a crash with the water instead of the boat. Furthermore the propeller cannot turn on whenever the UAV is neither in flight nor safely attached to the launch system. This decision algorithm is programmed in the auto-pilot.

As described in Section 4.3, the UAV lands on the water. The UAV might land in the close proximity of either the launch ship or the victim, without posing any threat to the ship, operators or the victim. Therefore the UAV must use distance buffers when landing. This landing procedure and safety measures are described in Chapter 4. Test flights have to prove if these buffers are sufficient to guarantee operational safety.

38 Chapter 5. Life Cycle

5.2. END OF LIFE DISPOSAL

Some parts of the UAV have to be replaced or repaired on both scheduled and unscheduled intervals. Since sustainability is a large aspect of the project [2], the waste disposal of the UAV has to be considered.

There are two forms of waste to be considered. When the UAV crashes at sea and is unrecoverable, it has to degrade by itself. However when waste is produced during maintenance or when the UAV fully or partially reaches its End Of Life (EOL), the maintenance crew is in charge of the disposal method.

This section covers the parts that are replaced during maintenance as these parts are the main contributors to waste. Other subsystems are not incorporated in this analysis because they are too complex at his design phase, and their specifications are not disclosed by their manufacturers. Therefore these parts are not incorporated in this analysis.

The two components that are subjected to frequent replacement are the motor and the propeller. The propeller is constructed out of polymer and is therefore a viable candidate for either bio-based degradation or melting down the propeller for re-usage. One option is to buy an off-the-shelf solution for the propeller, the downside is that one has no control over the manufacturing-or recycling process. Another solution is to fabricate a set of propellers together with the construction of the fuselage. If the latter is viable, this option is preferred over an off-the-shelf solution as the material selection, manufacturing process and degradation capabilities are controlled. Self-manufactured propellers are explained in Section 9.1.

These propellers are likely to break during landing and remain non-retrievable. As mentioned before, the propeller is fabricated out of bio-based polymers and a degradation accelerator is incorporated so it will not pose any danger to the environment when it is not retrieved after a mission. Chapter 6 elaborates on this technique.

The motor needs replacement every ten flights. As the most sensitive part of the motor are the bearings due to wear, it is possible to replace the bearings instead of the entire motor. The motor copper windings are insulated by the manufacturer but its durability is uncertain. Applying the hydrophobic coating to the copper windings during maintenance is therefore included in the maintenance routine.

The permanent magnet in the motor is the only unprotected part of the motor. Since the magnets are vulnerable for corrosion, the magnets have to be coated as well which will also help to lengthen its lifespan. This approach changes the nature of the maintenance interval for the motor. Instead of replacing the motor every ten flights, it is now overhauled every ten flights, given that it does not take substantially more time for the worker to overhaul the motor compared to replacing the motor.

Whenever the UAV is not retrieved after a mission, the motor is difficult to dispose. As the main components are insulated copper wires, coated magnets and a coated metal casing, it is unlikely that it will degrade by itself.

The batteries are polymer based and supplied by a manufacturer. The main chemicals in lithium polymer based batteries are Cobaltite, Carbon, Lithium, Copper and Aluminum bonded on polymer [53]. Copper is soluble in water but is regarded as a contamination at sea, hence its presence in the battery should be minimized [54] [55]. Aluminum occurs naturally in water but is difficult to dissolve. However, it is not considered as toxic [56]. The other elements, Cobaltite, Carbon and Lithium are part of the chemical reaction in the battery [53] and its chemical form changes during the battery cycle. The elements react with water but are not considered toxic [57].

For the polymer electrolyte and electrodes there is no information on the degradation. As batteries as a whole are not considered harmful and can be recycled [57] it is desirable to retrieve the batteries after a crash and recycle them at all time as they are fully recyclable [58].

Servos contain a DC motor, gearing, electronics and a casing. They consist of various metals and plastics. As this is an off-the-shelf solution, no information is known about the exact composition of the parts of the servos. Due to the low price of servos, they are simply replaced as maintenance and overhaul activities are regarded as economic undesirable. To ensure simple replacement, the fuselage is designed to allow easy

access to the servos. Like the motor, servos consist of numerous non-degradable parts, hence decomposition at sea is unlikely.

The fuselage is subjected to numerous sorts of loads with random magnitude and frequency. The fuselage is designed to last at least a year or 200 flights as it is difficult to guarantee full functionality and integrity after time. The fuselage materials are also subjected to environmental influences.

As the fuselage needs periodic replacement, the other components that are contained within the fuselage need to be transferred to the new fuselage. Therefore the fuselage is designed to allow for easy access. This is described in detail in Chapter 7. When the old fuselage is replaced, it is left to degrade with biologic waste as it is fully bio-degradable.

Like the propeller, there are degradation accelerators incorporated in the polymer fuselage that help speed up the degradation process after a crash. The fuselage will be fully decomposed into environmental friendly waste within a short window of time. Section 6 elaborates upon this technique.

The coating protects the fuselage from environmental influences, mainly ice and water. The coating may suffer from scratches occurring during operation or handling on the ground. The scratches are made visible using dyed water. Where necessary, it is repaired with a repair kit. Every 50 flights, right before the flight envelope test, the coating is re-applied as a precaution to wear. The properties of the hydrophobic coating are extensively described in Chapter 6.

All off-the-shelf-solutions, like the payload and flight electronics, as well as the servos, consist for a large part of electronics and non-degradable components. While the UAV is designed to completely decompose into environmental friendly substances after a crash, these electronics cannot be designed as such since there are no alternatives that do comply with the desire to be fully biologic decomposable. It cannot be guaranteed that these components do not have an impact on the environment the UAV crashes in. Therefore it is always desirable to retrieve the UAV when possible, even after a crash. The UAV will then decompose under controlled circumstances and reusable components will be extracted.

As the imaging payload is expensive and has a reasonable MTBF, it is possible to re-use it on a new UAV. This reduces the total amount of waste. All other electronics can be decomposed where most resources can be retrieved like the servo motor, gearing and all the polymer casings. Only the unrecyclable components in the subsystems are to be regarded as waste.

MATERIALS AND STRUCTURE

Important requirements set by the customers are the 95% polymer content and the use of biodegradable materials. This chapter treats a variety of possible materials, which could be used for the structure and for protective coatings. Possible substances or micro-organisms, which are able to degrade the UAV at its end-of-life, are also investigated. The structure of the ASAP UAV is of course directly linked to the material chosen. The structure should be designed in such a way that the ASAP UAV can bear all its loads for the given amount of time with the materials used. If this is not possible in a way the material selection should be reconsidered.

6.1. BIODEGRADABLE POLYMERS

As discussed in the MTR [2] the most applicable bio-degradable polymers for the ASAP UAV are PLAs. These are thermoplastic aliphatic polyesters, which are derived from natural substances like corn starch or sugarcane. The main component of these polymers is lactic acid ($C_3H_6O_3$). PLAs have a large range of derivatives. The most common derivative is Poly-L-lactic Acid (PLLA), which is the product resulting from the polymerization of L-lactide [59]. The properties of these PLAs can be seen in Table 6.1 [60]. Polylactide polymers are

Polymer	Tensile strength	Young's modulus	Density	Glass Transition Temperature T_g
	[MPa]	[GPa]	$[g/cm^2]$	[°C]
PLA	60	3.5	1.25	56
PLLA	75	4.14	1.3	63

Table 6.1: Material properties of PLA polymers

stiff and brittle materials, and it is therefore necessary to use plasticizers to improve the elongation and impact properties. The polylactide is fully biodegradable. The degradation occurs by hydrolysis to lactic acid, which is metabolized by micro-organisms to water and carbon monoxide. By composting together with other biomass the degradation occurs within two weeks, and the material has fully disappeared within 3–4 weeks [61].

When comparing PLA to Poly-propylene (PP), one of the most used non-biodegradable thermoplastic, it can be seen that generally, the pure PLA has better mechanical properties than pure PP. The Young's modulus of PP is between 1-2.5 GPa compared to the 3.5 GPa of PLA and a yield strength of 32.9 MPa compared to 50 MPa of PLLA. However, the failure in polymer components can occur at relatively low stress levels, far below the tensile strength because of four major reasons: cyclic stresses or fatigue, long term stress or creep rupture, the presence of structural flaws and environmental structural degradation [62].

ENVIRONMENTAL STRUCTURAL DEGRADATION

Polymer degradation in nature has multiple reasons of which some are unwanted for the structural integrity of the product. A list of the most important influences considering degradation is listed below.

- · Thermal activation
- hydrolysis
- biological activity

The degradation caused by heat (Thermal activation) in the UAV becomes higher when the environmental temperature is higher. During production of the composite parts in the UAV, the thermoplastic material and the fibers will be heated to be molded in the preferred shape. During this process, the temperature will be higher than at any other time during the mission. Fast heating and cooling during the production process

will keep thermal degradation during production to a minimum. During the mission, most of the heat is generated by the motor, the batteries and radiation from the sun. Heat dissipation will exist of radiation and convection to the flowing air. In Figure 6.1 the Young's modulus decrease, due to the temperature can be seen for PLA, a PLA/Flax composite (PLA/Flax I) and a crystallized PLA/Flax (PLA/Flax II). From Figure 6.1 there

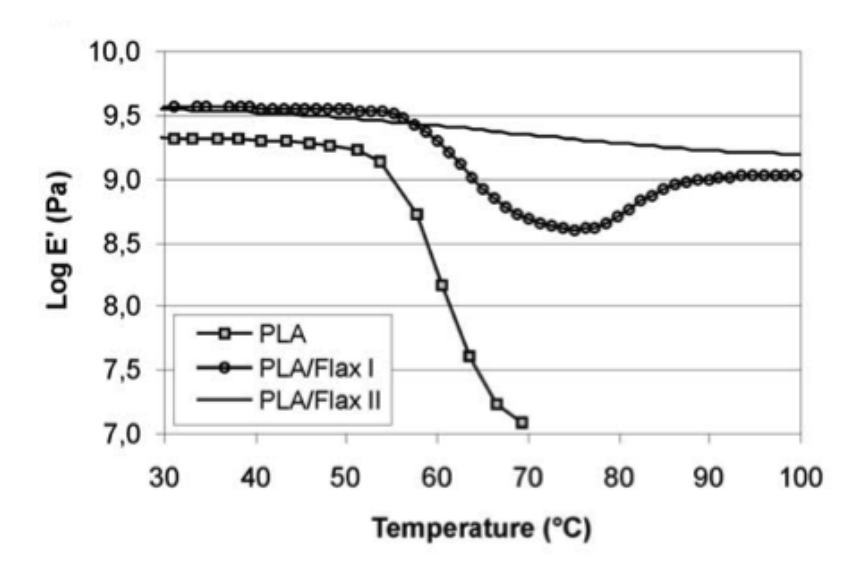


Figure 6.1: The effect of temperature on PLA and PLA/Flax composites

can be concluded that reinforcing PLA with Flax fibers is beneficial for the thermal behaviour of PLA.

The influence of water, (hydrolysis), is an important aspect considering the mechanical properties of PLA. During the first period, when water absorption level is still low, the Young's modulus of the material rises due to the plasticizing effect of the water. When the composite becomes saturated this effect reverses and the composite gets a lower Young's modulus. Humidity ageing tests showed that the tensile modulus was reduced from 9 GPa to 2.5 GPa after 1000 h exposure time at 95% humidity and 38°C, while the tensile strength was reduced by 70% [63]. A coating can be used to limit the effect caused by water absorption.

Bio composite materials can degrade under influence of biological activity. When enzymes are added to the composite (or when it is placed in a composing environment) the UAV will start degrading at an increased speed. This will dissolve the bio composite completely. This process takes 3-4 weeks[64].

CREEP FAILURE

Creep is an important failure mode of polymers and it implies the slow movement and permanent deformation under the influence of mechanical stresses. Besides that, the rate of creep is determined by the polymer's stiffness and therefore also the temperature and moisture content. In Figure 6.2 the effect of creep at various absorbed liquid contents and temperatures can be seen [65]. Figure 6.2 is the result of a tested piece of PLA, which was loaded for sixty minutes by a tensile force resulting in a constant stress of 0.45 MPa. Next, the tested piece is unloaded after which the piece of PLA recovers itself slowly. After 12 minutes the PLA is recovered, although the PLA never recovers completely to its original state. A higher temperature will increase the effect of creep. Up to the T_g the moisture content negatively affects creep as well, but above the T_g it will improve the creep behavior of PLA. The used moisture for the test was hydrocarbon liquid [65]. It is concluded that the stresses during the ASAP UAV's missions will result in a significant amount of plastic deformation after only a small amount of flights. A way to decrease the rate of creep, is using reinforcements inside the structure.

6.1.1. BIO FIBERS

In order to reinforce a polymer, a certain fiber is needed. In the MTR already two suitable fibers were mentioned [2]. These fibers are Rayon (Viscose) and Flax. Viscose fibers are synthetic cellulosic fibers extracted from wood, bamboo or cotton pulp. Flax fibers, on the other hand, are natural cellulosic fibers, which are extracted from Flax stems. In Table 6.2 the material properties of both fibers can be found. In order to choose the most suitable fiber, the most crucial material property has to be determined. The maximum Von Mises

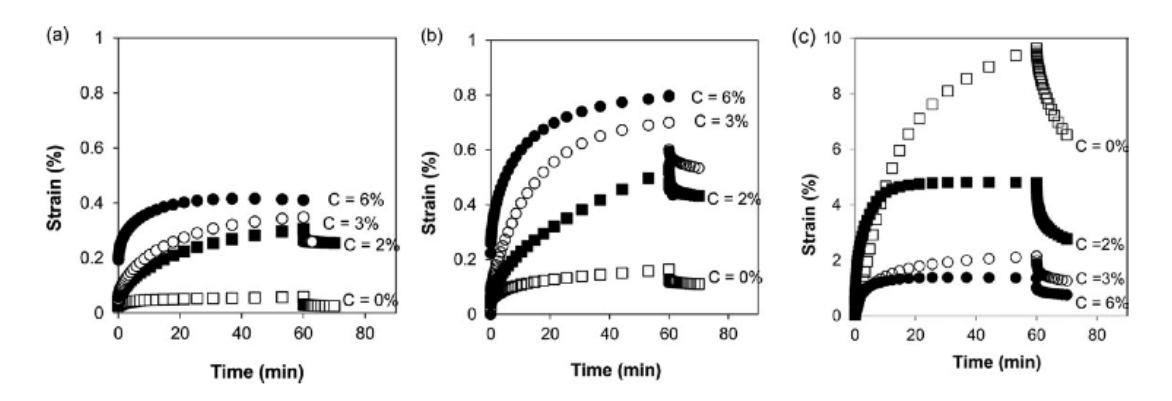


Figure 6.2: Creep strain versus time at 0.45 MPa with test temperature: (a) 30° C, (b) 40° C, and (c) 50° C for different levels of hydrocarbon liquid concentration (C).

Table 6.2: Material properties of Rayon and Flax

Fiber	Tensile strength	Young's modulus	Density
	[MPa]	[GPa]	$[g/cm^2]$
Flax	500	80	1.4
Rayon	770	60	1.52

stress is particularly low [2], even when it is compared to the tensile strength of pure PLA. Therefore, the tensile strength is not a crucial property. However, due to the fact that polymers and therefore also the matrix of composites are susceptible for fatigue and creep, the stiffness and therefore the Young's modulus will be a crucial property. Flax is less affected by fatigue and creep than Rayon, due to its higher Young's modulus. Besides that, Flax is the lighter of the two fibers as well. In Table 6.3 the properties of scutched Flax fibers can be seen.

Table 6.3: Material properties of scutched Flax fibers

Property	Value
Density	$1.3 \ g/cm^2$
Tensile strength	500 <i>MPa</i>
Tensile modulus	80 <i>GPa</i>
Diameter	$80 \mu m [66]$
Strain	2% [67]

6.1.2. BIO COMPOSITES

Advanced polymer composites containing carbon and glass fibers have been utilized extensively in the aerospace, automotive, and construction industries. Since the matrices and the fiber reinforcements in these advanced composites are based on mineral resources, their long term sustainability is problematic. While recycling may be a viable strategy, the complicated mixed morphology of composite materials makes them inherently difficult to recycle. In comparison, several so called bio-composites have been developed that offer certain environmental advantages at the end of their useable cycle when composites are landfilled or incinerated. The structure of the ASAP UAV is designed to be biodegradable as far as possible by using biodegradable resin and fibers.

RULE OF MIXTURE

An important law for the properties of composites is the Rule of Mixture. With the Rule of Mixture the Young's modulus, tensile strength and density of the composites is calculated. In Equation 6.1 the rule of mixture of

the Young's modulus can be seen [66].

$$E_{tot} = \eta_0 \eta_L E_f V_f + E_r V_r \tag{6.1}$$

In this equation the η_0 is the fiber orientation efficiency, η_L is the fiber length efficiency, E_f is the Young's modulus of the fiber, V_f is the volume fraction of the fibers, E_r is the Young's modulus of the resin and the V_r . From the 'shear lag' theory of Cox-Krenchel an expression for η_L can be found in Equation 6.2.[66].

$$\eta_L = 1 - \frac{\tanh(\beta L/2)}{\beta L/2} \tag{6.2}$$

 β is defined by Equation 6.3.

$$\beta = \frac{2}{d} \left(\frac{2G_m}{E_f} ln \left[\pi / (X_i V_f) \right] \right)^{\frac{1}{2}}$$
(6.3)

Where d is the fiber diameter, L is the fiber length and G_m is the shear modulus. For X_i , the calculation of Thomas and Vlug [68] is used and equals 4 (dimensionless).

Also the same principle can be used to calculate the tensile stress of the composite. The Rule of Mixture for the tensile stress can be found in Equation 6.4.

$$\sigma_c = \eta_0 \eta_L \sigma_f V_f + \sigma_{um} V_r \tag{6.4}$$

Where σ_f is the tensile stress of the fiber and σ_{um} is the matrix stress at fiber failure strain. The calculation for σ_{um} can be found in Equation 6.5 [66].

$$\sigma_{um} = E_m \frac{\sigma_f}{E_f} \tag{6.5}$$

Finally, in Equation 6.6 the calculation for the composite material density can be found.

$$\rho_c = \rho_f V_f + \rho_r V_r \tag{6.6}$$

Where ρ_f is the material density of the fiber and the ρ_m is the density of the resin.

CHOPPED AND CONTINUOUS FIBERS

Composites can be produced with both continuous and discontinued fibers. Both have advantages and disadvantages over the other. Composites existing of PLA and chopped fibers are defined by the length of the fiber, the orientation efficiency and the length efficiency. For chopped fibers, the orientation efficiency is close to 0.3 The length efficiency is dependent on the length of the fibers and this reaches 95% for fibers of a length of 2.0mm. This is obtained using Equation 6.2. The maximal length used for the chopped composites is considered to be 2.0mm When the fibers are longer, it increases the difficulty for injection molding, while the mechanical properties improve little.

An advantage of chopped fibers over continuous fibers is the manufacturability. More complex shapes are possible, reproducibility is better and work intensity is lower. Another advantage of chopped fibers are water absorbance characteristics. When chopped fibers absorb water, the specific fiber is lost but the integrity of the entire structure is unaltered. For continuous fibers, the whole length of the fiber will absorb water and loose mechanical properties. Disadvantages are that the yield stress and the Young's modulus are lower.

The Rule of Mixture only can be applied for a maximum chopped fiber content of 30%, since that is about the maximum chopped fiber content that the resin effectively can impregnate [61]. A list of composites from thermoplastics and chopped fibers will be listed in Table 6.4. They vary in fiber length and components. The Young's modulus, tensile strength and density are calculated using the Equations 6.1, Equation 6.4 and Equation 6.6 respectively. Notice that fibers with a longer fiber length than 2.0mm will not have a much higher stiffness and strength. In Figure 6.3 a typical stress-strain curve for a short fibered PLLA/30%Flax composite can be seen together with other composites. In the figure it can be seen that the stiffness of PLA/Flax composites is comparable to Glass/PP composites and is much stronger than Hemp/PP and Jute/PP. Also, there can be concluded that PLA/Flax is more brittle compared to the other composites.

Table 6.4: Material properties of 30% short fiber flax composites

Compos-	Fiber length	Tensile stress	Young's	Density
ite	[mm]	[MPa]	modulus [<i>GPa</i>]	$[g/cm^2]$
Flax/PLA	0.5	40.6	6.5	1.3
Flax/-	0.5	44.8	7.2	1.33
PLLA				
Flax/PLA	1	50.2	8	1.3
Flax/-	1	53.8	8.6	1.33
PLLA				
Flax/PLA	2	55.9	8.9	1.3
Flax/-	2	58.5	9.4	1.33
PLLA				
Flax/PLA	3	57	9.1	1.3
Flax/-	3	60	9.6	1.33
PLLA				
Flax/PLA	6.5	58	9.4	1.3
Flax/-	6.5	62	9.8	1.33
PLLA				

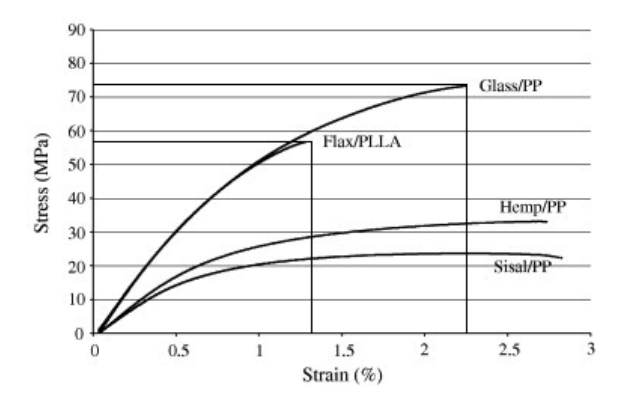


Figure 6.3: Stress-strain curves of a PLLA/30%Flax composite compared to other thermoplastic composites.

Besides chopped fibers, also long continuous fibers can be used. A main advantage of continuous fibers is that the composite can be reinforced in certain directions. Therefore, these composites are generally speaking much stronger in a certain direction than composites with chopped fibers. However, in other directions these composites can be much weaker compared to chopped fiber composites. On the other hand, when the continuous fibers are woven, these composites will have a more overall strength and are still stronger than chopped fiber composites. The strength of these continuous fiber composites also depends on the weave technique. A significant difference between short fiber composites and continuous fiber composites is the fact that they can contain a higher fiber content. Typical fiber contents of these composites are 30% or 40% [67]. In Table 6.5 several Flax/PLA and Flax/PLLA composites with continuous fibers can be found. Where

Composite	Tensile stress	Young's modulus	Density
	[MPa]	[GPa]	$[g/cm^2]$
PLA/30%Flax (UD)	165	26.3	1.3
PLLA/30%Flax (UD)	168	26.8	1.33
PLA/30%Flax (BA)	90.1	14.4	1.3
PLLA/30%Flax (BA)	93.1	14.8	1.33
PLA/30%Flax (woven)	78.3	12.5	1.3
PLLA/30%Flax (woven)	81.1	13	1.33
PLA/40%Flax (UD)	213	34	1.31
PLLA/40%Flax (UD)	215	34.5	1.34
PLA/40%Flax (BA)	113	18.1	1.31
PLLA/40%Flax (BA)	116	18.5	1.34

Table 6.5: Material properties of continuous fiber composites

'UD' is the abbreviation of unidirectional and 'BA' is the abbreviation of bi-axial. For the woven composites an orientation efficiency of 0.4 has been assumed. However at this moment the use of PPLA/Flax is not yet applied in the market and only PLA/flax composite are made. Due to the unavailability of PLLA/flax composites in the market it will from now on be discarded as on option for the UAV.

99.2

101.5

15.8

16.2

1.31

1.34

PLASTICIZERS

PLA/40%Flax (woven)

PLLA/40%Flax (woven)

Generally all composites with PLA are brittle connections and therefore have a low fracture toughness. A plasticizer can be used in order to increase the elongation of the material and therefore the impact strength. However, this will result in a decrease of the Young's modulus and the tensile stress. A typical plasticizer is Triacetin. In Table 6.6 the effect of Triacetin on PLA and 40% Flax/PLA composite can be seen [61]. Notice that the properties in Table 6.6 of PLA are different, since the PLA used in the previous tables are based on the data given by the manufacturer, while the data in Table 6.6 [61] are results from independent tests of the material from the same manufacturer [61]. As can be seen, when a PLA/FLAX composite is blended with 5%

Material	Tensile stress [MPa]	Young's modulus [GPa]	Elongation [%]
PLA	50.3	3.4	2
PLA/5%Tri	41.7	3	2.2
PLA/10%Tri	43.6	3.4	1.8
PLA/15%Tri	37.2	1.8	2.6
PLA/40%Flax	44.1	7.3	0.9
PLA/5%Tri/40%Flax	43.2	7.3	1.4
PLA/10%Tri/40%Flax	29.5	5.4	1.1
PLA/15%Tri/40%Flax	16.6	2.4	2.3

Table 6.6: The effects of Triacetin on PLA and a 40% PLA/FLAX composite

Triacetin, the maximum elongation will increase about 35%, while the tensile stress decreases about 2%. The decrease in Young's modulus, due to the plasticizer, is negligible small [61]. However, due to the decrease in Young's modulus, the composite will suffer more from creep.

WATER ABSORPTION BY BIO COMPOSITES

Since water can act as a plasticizer, absorbed moisture in composites can influence both the dimensional stability and the mechanical properties. Mechanisms of water uptake in a composite include diffusion through the matrix, capillarity through natural fibers or movement via porosities in the matrix or at the fiber-matrix interface. Consequently, water absorption depends not only on the relative hydrophilic character of the fiber and the matrix but also on the fiber-matrix interphase and the morphology of the composites. Interphase morphology can be influenced by voids, fibrillation and diffusion of additives to the fiber-matrix interface. Composite morphology can vary according to processing conditions: for example, fibers are generally more aligned in direction in injection-molded composites than in compression-molded products.

In general, bio composite mechanical properties should decrease as water uptake increases, e.g. Young's modulus and tensile strength. However the loss of modulus can be reduced at high fiber contents due to the opposing effects of the matrix plasticization by water an fiber reinforcement [69]. This effect is clearly demonstrated in Figure 6.4 [70]. A proposed solution to the problem of moisture is a PLLA layer on top of the

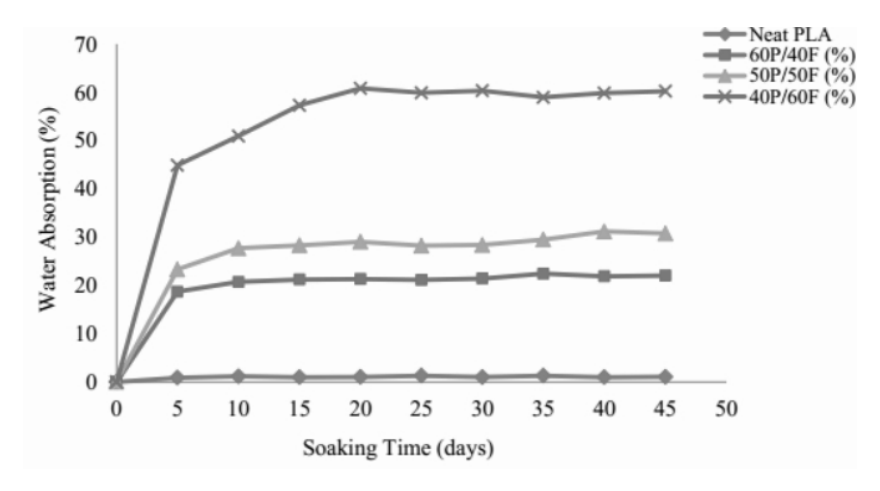


Figure 6.4: Water absorption of pure polymers and composites

product. Pure PLLA absorbs less water than the composite. This protects the structural component with a solution of a bio-polymer. The moisture absorbance characteristics can be improved without changing the mechanical properties by means of acetylation. A last option is a hydrophobic coating, this will be applied on the finished product and repel the water to keep the structural integrity of the airframe.

BIODEGRADATION OF BIO COMPOSITES

At the end of life of the UAV, the bio composite structure will biodegrade. However, here there are two options to be considered either the UAV structure will be replaced in maintenance or the structure can be biodegraded at a compost facility or the UAV crashes into sea and is not able to be retrieved. In the first case, an industrial compost facility can be used where the PLA/flax composite is degraded. Here, the temperature is mainly above 60° and high moisture concentration ensures quick degradation of the bio composite. Here the composite is degraded in about 60° to 80° days. According to the literature, natural fibers are degraded biologically because organisms recognize the cellulose and hemicelluloses in the cell wall and can hydrolyze them into digestible units using specific enzyme systems. Among all microorganisms involved the fungi are the most attractive for the cellulose fibers [71].

In the other case, the UAV crashed into the sea and sunk and therefore is not retrievable, the degradation occurs at a far slower speed because of the lack of high temperatures and lower concentration of enzymes, fungi and bacterial life.

Due to the lack of literature for the biodegradability of the bio composite PLA/flax a study on the bio composite PLA/ramie has been used as a reference [71]. Here, samples of the bio composite were placed 2 meters

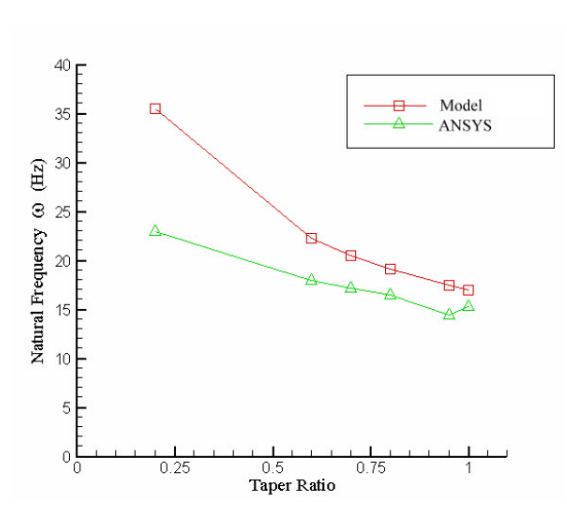
deep at the Baltic Sea to examine the biodegradability in seawater. Because the same resin is used as in PLA/flax composite and the fibers are both bio fibers with comparable mechanical properties, the use of this reference is justified. In this article it is shown that even at a sea of low temperature, average Baltic Sea temperature is only $14\,^\circ$ Celsius, the bio composite disintegrates at sea after $18\,$ months, see Figure $6.7\,$ [71]. In this article, the temperature of the compost was only between $3\,$ and $19\,^\circ$ Celsius which explains the long degradation time of the compost in comparison with other sources found. Due to the fact that PLA/flax composites degrade in seawater, it is not necessary to implement capsules with enzymes, which were discussed in the Mid-Term-report [2], inside the UAV's structure.

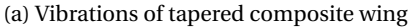
Polym	Weight changes of polymer samples [%]/incubation time [months]										
TOTYL	ner samples	1 3 4 6 8 9 12 15 18 24					24				
R/E	Sea water	+0.4	-	-4.6	-5.5	-	-16.2	-40.4	-92.4	disintegration	
NE	compost	+1.9	-1.9	-2.8	-	-33.9	-	-54.1	-87.5	disintegrat	on

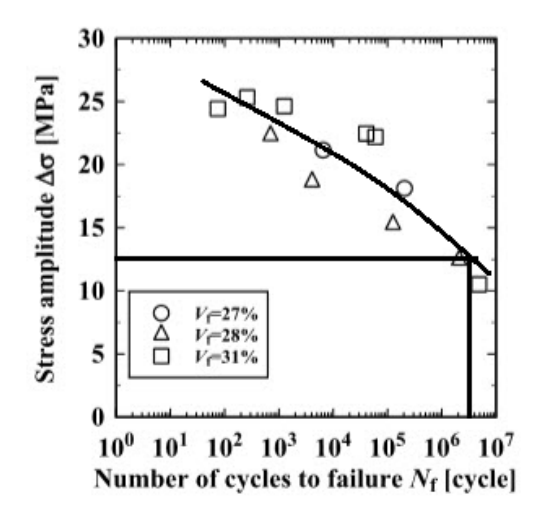
Table 6.7: Biodegradability of bio composite PLA/ramie in the Baltic Sea and compost

FATIGUE

To determine if the PLA suffers of fatigue an estimate is made in order to determine the number of cycles the wing experiences. To do so, not only the operating time is important, but also the vibration the wing is subjected to. A reference study was used where the composite tapered wings are evaluated on their vibrational behavior [72]. For these calculations graphite composite has been used with an E modulus of 200 GPA of the fibers which are stiffer as the flax fibers. The result of the vibration model created in this article can be seen in Figure 6.5a [72]. Looking at the 0.25 taper ratio of the ASAP UAV the graph results in a vibration of 34 Hz







(b) Fatigue test of PLA/jute composite for various fiber content

of the wing. Because of the lower stiffness of the bio composite a frequency of 30 Hz is assumed during the flight. When evaluating this for the expected lifetime of the structure, 200 missions of in average 2 hours, this gives in total 1,440,000 cycles. As a reference for the fatigue of PLA/flax composite, PLA/Jute has been used because no fatigue tests can be found for the PLA/flax composite. The results of this test can be seen in Figure 6.5b [73]. The assumption made to use this s-n curve can be justified because the jute fibers have similar properties as the flax fibers and have only a slightly lower mechanical properties as flax.

In the region of 1.5 million cycles, as discussed above, the maximum stress before failure is around 12.5 MPa. As can be seen later in this chapter this is far below the stresses working on the UAV which are around 1.5 MPa. However still the effects of fatigue cannot be neglected since the mechanical properties can decrease as discussed above by environmental degradation. The failure of the PLA/jute composite is described as follows: 'fatigue cracks in PLA resin initiate and propagate from specimen surface until the cracks get to jute spun yarns;

stress concentration at the crack tip engenders breakage of jute filaments. Therefore, the fatigue property of our composite would be dominated by that of PLA' [73]. Since the PLA/flax composite will be made of the same resin, this justifies even more the comparison with the PLA/jute composite.

IMPACT STRENGTH

The impact strength of the material is important considering hail storms. The size and speed of the hail determines the kinetic energy of the ball. This again determines the diameter required to sustain certain hail. When hail becomes larger, the falling speed is higher as well. Some hail specification are given in Table 6.8 [74]. Section 6.2.5 will use these energies to compute the hail stone size the structure can withstand.

diameter (cm)	speed (m/s)	energy (J)
2.5	22.3	1.36
3.2	25	5.42
3.8	27.4	10.85
4.5	29.6	18.96
5.1	32	29.8
6.4	35.7	71.9
7	37.8	109.8
7.6	39.6	162.7

Table 6.8: Specifications of different hail sizes

MATERIALS CONCLUSION

To conclude, the ASAP UAV is made of the bio composite PLA/Flax. However, the flax fibers can be used in either continuous or chopped way. The application of how the fibers will be used will be determined when the stresses and the deflections of the UAV are known. With the knowledge of these stress and deflections, the necessity of the use of continuous fibers can be determined and the location of them. The option also exist of making a hybrid, where different part are made with different processes and fiber layout. The main advantages of bio composites are, as compared to the petrochemical polymer materials, their capacity to diminish the high fossil feedstock dependency. Additionally, the use of natural fibers allows compensating some of the important drawbacks of the polymer matrix.

6.1.3. COATING

When searching for a coating for the ASAP UAV, there are a few important requirements to consider. These requirements are salt water resistance, durability, compatibility with polymers/composites and it should not be hazardous for the environment.

After the UAV has performed its mission, it will land in the water near the ship and is retrieved. The coating of the UAV should be able to prevent the skin of the UAV from getting wet, to prevent degradation of the skin by salt water to extend the life-time. For the coating, it is preferred to have a large durability to prevent the need of repainting the whole UAV after each mission. As the UAV fuselage will consist out of polymer composites, it should be possible for the coating to adhere to these products. The last important property for the coating are the environmental issues. The product should not be hazardous to the environment.

Ultra Ever Dry (UED) is chosen as coating for the ASAP UAV[75]. This coating is selected for its high resistance against salt water and durability. Steel coated with UED was immersed in salt water for 30 days without any corrosion effect. The UAV will land in the water after the mission has been performed. The time in the water per mission will be around 15 to 30 minutes. Without corrosion of the coating, the UAV could perform 1440 missions.

The UED coating is susceptible to environmental conditions such as UV. This coating offers approximately one year of outdoor life before a new coating at the top would be required. The weather conditions in which the UAV will operate are significantly worse than normal outside conditions, which decreases the life-time of the coating. UED consist out of two materials; the bottom coat bonds to most materials and acts as a primer. It provides a consistent material for the top coat to bond while interacting with the top coat to assemble the

surface. It is stated that the coating adheres to plastics. In the post DSE phase 13 testing of the coating on flax/PLA composites should be performed. This has to be done because the coating can degrade the material.

UED surface protection is more abrasion resistant than other super hydrophobic materials, registering a result of 30 cycles with a CS-10 wheel and 1000g load on the Taber Abraser [76] before droplets no longer roll off the coating at a slope of 5 degrees from horizontal. The coating may still be super hydrophobic at this point, but droplets might get stuck in the abraded area, and may not roll off until the area is tilted to a greater degree. So the coating is abrasive resistant although the coating should not be damaged by sharp surfaces, so it has to be handled with care. Nails can scratch the coating, so gloves will be needed to prevent this. If the coating is removed due to repeated or severe abrasion, it can be reapplied.

Sustainability of the coating can be divided into the manufacturing method and mission performance. Both layers will be sprayed on the skin of the UAV. These liquid materials can be toxic if inhaled, so good protection is needed e.g. face mask, gloves and spray suit. Whatever cannot be saved for recovery or recycling should be handled as hazardous waste and sent to an approved incinerator or disposed in a resource conservation and recovery act approved waste facility. When the layer is sprayed on the UAV, the thickness of the layer will only be $1.6 \cdot 10^-2$ mm. Because the layer is abrasive resistant, the amount of coating released per mission is minimal, so it does has not have any effect on the environment. It could be hazardous for fish in large quantities because the coating is silica based, but the released coating per mission is negligible.

6.1.4. ADHESIVES

In order to bond several parts of the UAV, it is possible to use an adhesive. There are two kinds of adhesives, namely films and pastes/liquids. In Table 6.9 several adhesives and their properties can be found [77],[78],[79]. the adhesives discussed in Table 6.9 are epoxy adhesives.

Adhesive	type	Shear strength [MPa]	Peel strength [N/mm]
$300\frac{g}{m^2}$ Tencate EF72	Film	36	7.3
EP31	Paste/Liquid	31.7	7.0
Scotch Weld EC-2792 B/A	Paste/Liquid	38.6	10.5

Table 6.9: Several adhesives and their properties

Other important aspects of adhesive bonding are the curing cycle of the process and the durability of the bond.

CURING TIME

The curing of the adhesive bonds is done by constantly heating the structure inside an oven to a certain temperature. However the most suitable curing temperature and its corresponding curing time depend on the materials being joined. There has been showed that untreated Flax fibers can retain their strength during an exposure of 120 minutes at a temperature of 170° C [66]. On the other hand, the T_g of PLA is around 60° C [61]. Therefore it is preferred to have a curing temperature slightly below the T_g of PLA, in order to retain the same structural properties. In Figure 6.6 several curing cycles, which depend on the optimal curing temperature and the corresponding curing time, of the Tencate EF72 adhesive can be seen [77]. The curing time of the EP31 and the Scotch Weld EC-2792 B/A adhesive at room temperature is around 24 hours for the EP31 adhesive and 7 days for the Scotch Weld EC-2792 B/A adhesive [78],[79].

DURABILITY

The durability of a bonded joint depends on the properties both of the adhesive and of the materials being joined. The adhesive used to bond the joint will be affected by several aspects, e.g. high temperatures, powerful solvents or water. Also the durability of the bonded joint depends on the effects, of the same aspects, on the materials being joined. Another important aspect is the quality of the pretreatment, since a poor pretreatment will decrease the durability of the bond dramatically.

SECTION 6.2. STRUCTURE 51

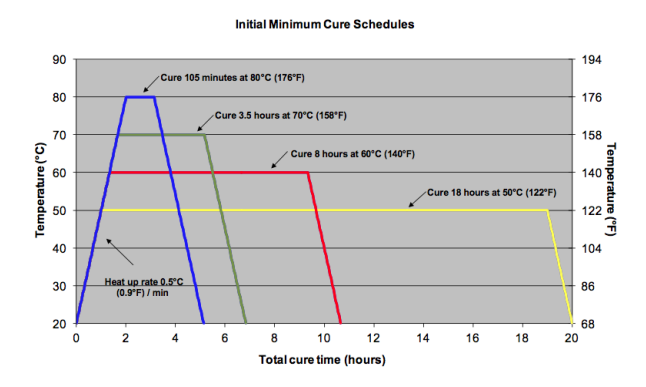


Figure 6.6: Curing cycles for several curing temperatures.

The bonded joints may need to resist sustained loads. Joint in which peel stresses are at a minimum give the best durability. The fatigue testing of simple lap shear joints made with epoxy adhesives will often fail at approximately 30% of the short-term measured breaking load. In Figure 6.7 the fatigue strength of simple lap joints with a cold-cured epoxy adhesive can be seen [80].

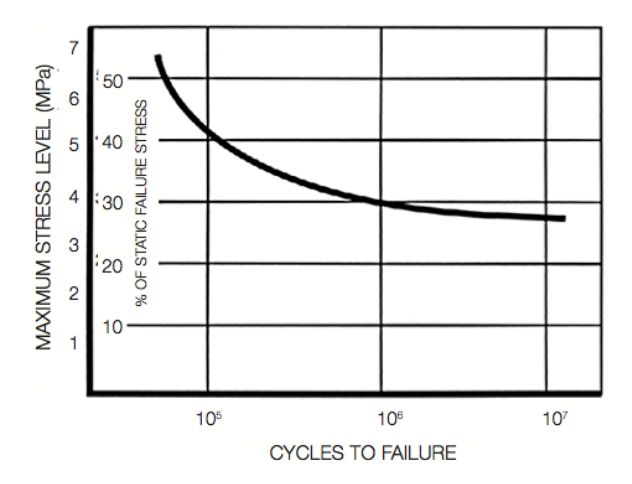
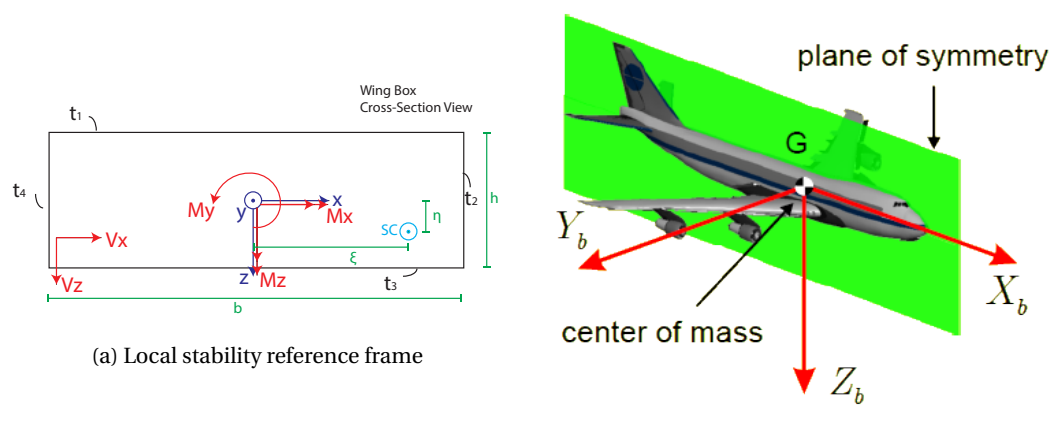


Figure 6.7: Fatigue strength of simple lap joints made with a cold-cured epoxy adhesive.

6.2. STRUCTURE

In this section the structural layout of the ASAP UAV is described. First the loads are discussed and the stresses and deflections induced for the different material types. Finally, a complete layout is given of the different parts and their properties. The method of approaching this is to first have a look at the wings them self. As the lift capabilities of the fuselage section are relatively low, the main focus will be on the wings and the connection between wings and fuselage. The wing box is divided into multiple sections in which a local axis-system is used. This local axis-system is shown in Figure 6.8a and is based on the global axis system shown in Figure 6.8b [81]. This reference system will also be used in the following figures.



(b) Body fixed reference frame system

Figure 6.8: Reference frames used for the structural tool

The global reference system that is used is based on the body axis reference system. This implies that the positive x-axis points towards the nose of the airplane, the positive y-axis points towards the starboard wing of the airplane and the positive z-axis is nadir pointed. The local reference system uses the same orientation as the global axis system, the origin of this reference changes constantly however. Because a finite element method will be used, the wing box is divided into multiple sections. The wing will be analyzed from tip to root, meaning that after each iteration the reference system moves into the negative y-axis. When the wing box is symmetric, the shear center will be at the same position as the origin of the reference system, meaning that the local reference system moves along the elastic axis system.

6.2.1. LOADS AND STRESSES IN WINGS

Figure 6.9 shows the distribution of forces and moments along the span of the wing during cruise flight. The forces in x-direction and the moment around the z-axis is zero. This is because there is no propulsion system located on the wing and there are no forces acting in the y-direction making also the moment around the z-axis zero. The force in z-direction gradually increases due to the elliptical wing distribution. It is, however, counteracted by the weight of the batteries. Due to this force, the moment around the x-axis also increases in a correct manner. A peculiar situation occurs however when looking at the moment around the y-axis. This can be explained by the movement of the local axis. Because the moments are computed around the local reference system. The weights of the structure and batteries are modelled as being distributed equally over the x-axis. This is only when the wing box is symmetric and this is indeed the case. The only attribute to the moment around the y-axis is thus the lift which acts on the front spar of the wing box. Looking at Figure 6.9, one can see first an increase in moment around the y-axis, after which it decreases rapidly. This is due to the sweep of the wing. Due to this sweep, the local axis system also moves in positive x-axis. During each cross section, the lift force is shifted to the origin of the axis system and the moment is added (each iteration). This means that the moment will first increase due to this shift, the resultant force (which is created by adding the lift every section) will counteract this moment due to the sweep of the wing.

Looking from the tip, the moment first increases after which it decreases again. This can be explained by the fact that the local axis system moves into the direction of the positive x-axis when the wing is further analyzed. Due to the increase in resultant shear force (which is placed in the middle), which overcomes the torque due to the lift at a certain point. As the lift is acting on the front spar and the axis system is placed in the center of the cross-section, this deviation occurs.

Figure 6.10 shows the stress distribution in the wing during cruise flight. The highest stress concentration occurs at the root in compression and is approximately 1.5 MPa for skin thicknesses of 2.0 mm throughout the wing box. A thickness of 2.0 mm is chosen as this is the minimum thickness for injection molding. There is, however, a difference between thin-walled injection molding and conventional injection molding. With thin-walled injection molding, parts with thicknesses as low as 0.5 mm can be produced. Applications of parts with these kind of thicknesses are however for food packaging, plastic packaging, electronic protection or cell phone components [82]. Normal injection molding requires a minimum thickness of 2.0 mm, making

SECTION 6.2. STRUCTURE 53

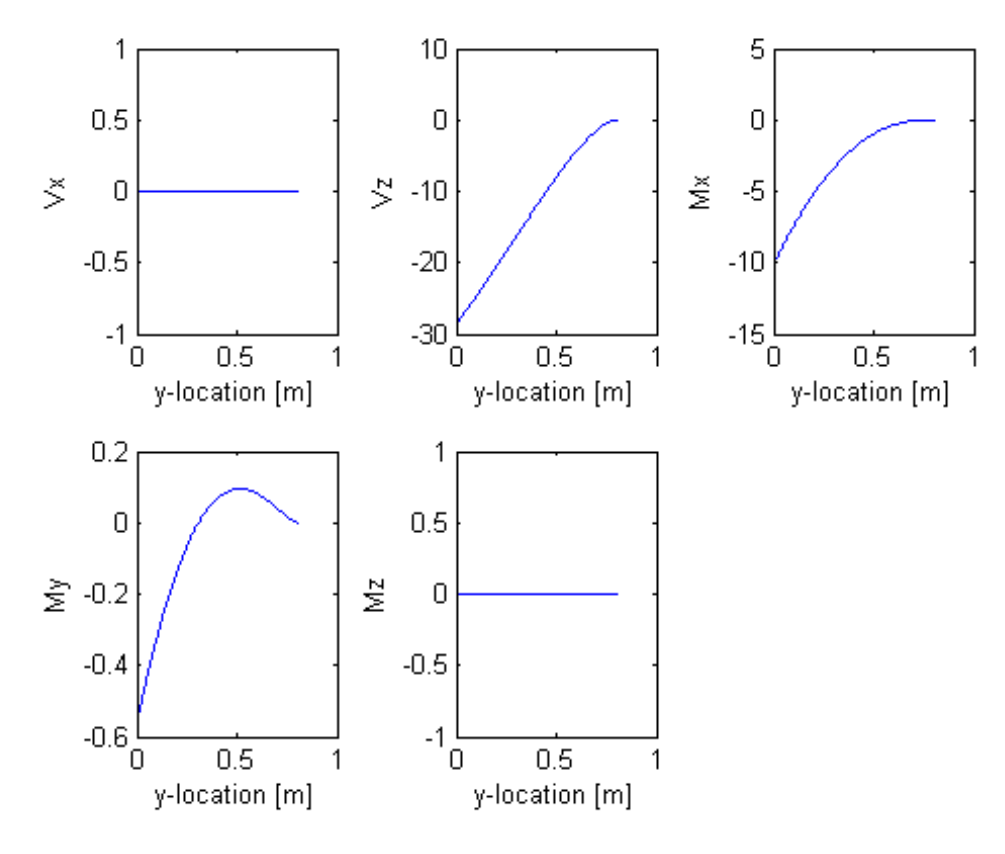


Figure 6.9: Forces and moments on the skin with thickness 2.0 during cruise flight

mechanical parts, automotive parts, chairs and tables and many other. Although it is possible to use the thin-walled injection method, it is preferred to use the conventional method. The composite used, contains fibers with lengths of 2.0 mm. Making the thickness much smaller than this value could cause the fibers to get entangled or aligned in a particular direction making the material anisotropic. This could however be applied for stress intensive parts but this is mainly dependent on the manufacturer. Section 6.2.6 will go further into detail regarding the thickness optimization, disregarding the minimum thickness requirement. As the stresses in the wing are low compared to the 56 Mpa tensile strength of PLA/flax, the most critical phase

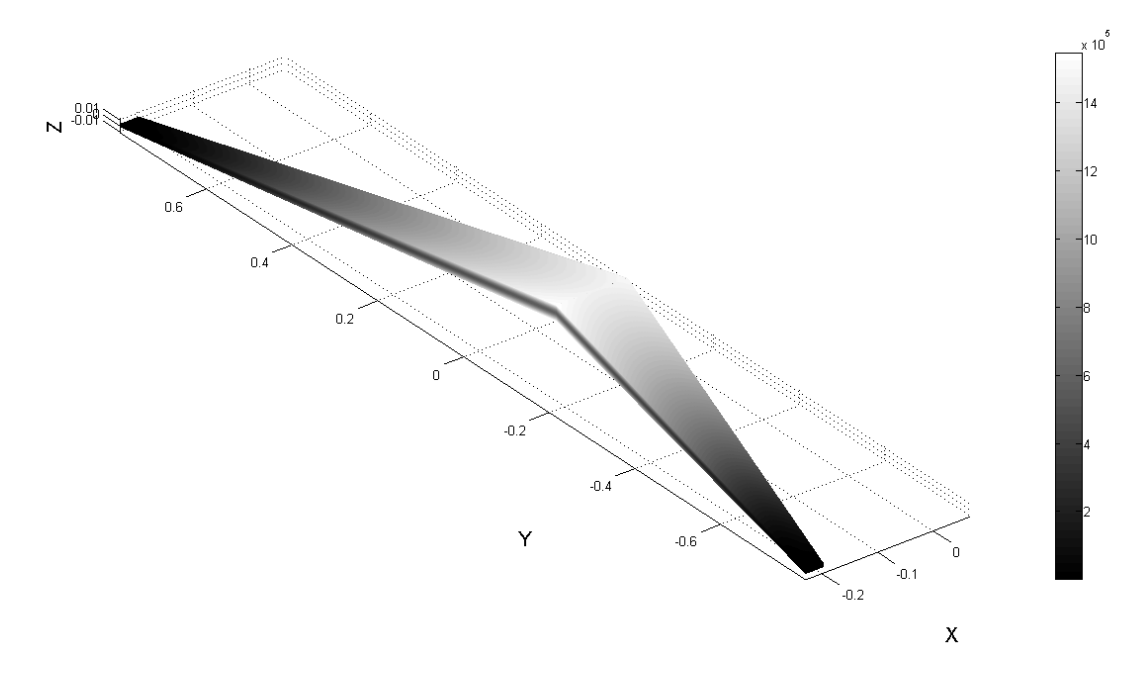


Figure 6.10: Stress distribution in the wings during cruise flight, with a skin thickness of 2.0 mm

of the mission is the design goal. The flight envelope for gusts is considered, the result however showed that this was insignificant. It was approximately 1.04g during gusts of 9 Bft. The most critical phases are thus the take-off and landing. During take-off, the structure and weight inside the wings is subjected to an acceleration of 5.1 times the gravitational constant, as explained in Section 4.2. Adding a safety factor of 1.25 to that results in an acceleration of approximately 6.4 times the gravitational constant. Having the catapult be attached to the fuselage gives the following Von Mises stress distribution as is shown in Figure 6.11. It is assumed that the force due to the acceleration acts in the x-plane and that the fuselage has no further effects on the wings. Looking at the top rear part of the wings, there is compression present and tension in the lower front spar. This distribution is not symmetric due to the forces present in z-direction. The maximum stress is approximately 3.9 MPa.

The last step is to look at the landing of the UAV. It was determined that a deceleration of 4.1g is present during the landing, as explained in Section 4.3. Adding a safety margin of 1.25 results in a deceleration of approximately 5.2 times the gravitational constant. The forces mainly act in the x-direction of the body-axis system of the UAV, because the velocity in x-direction is reduced from stall speed to zero. It is again assumed that the fuselage takes the impact load and only the deceleration acts on the wings. Figure 6.12 shows the landing with a deceleration of 5.2g in x-direction. The maximum stress during landing is 3.4 MPa in compression. It stands out that this has the opposite effect as the launch mode. To make the effect of the landing and launch phase more apparent, the forces in z-direction are disabled in Figure 6.13. Figure 6.13 clearly shows the rapid increase of both tension and compression stresses up to 2.4 [MPa]. This figure clearly deviates from Figure 6.11. Since the vertical forces are turned off, no Torque is present which explains the main difference. This is during take-off, meaning compression forces are located in the rear of the wing box and tension at the leading edge.

From these figures it can be concluded that the launch phase is most critical. All of these stresses were calculated with constant thickness of 2.0 mm. It is however possible to let this thickness change gradually over

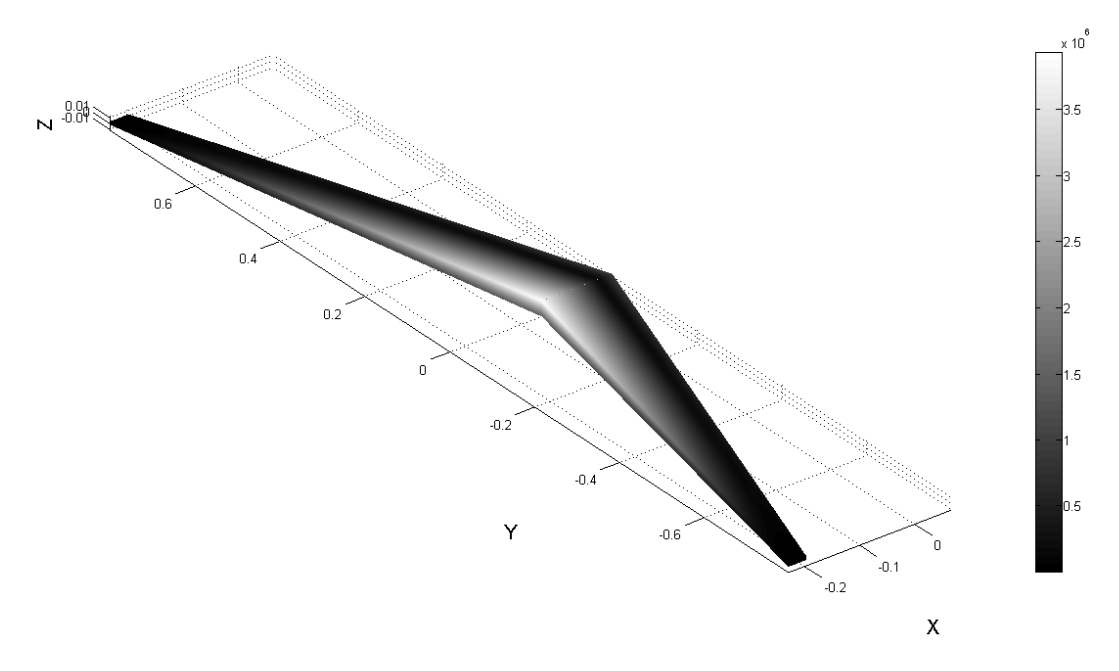


Figure 6.11: Stress distribution in the wings during launch with a skin thickness of 2.0 mm

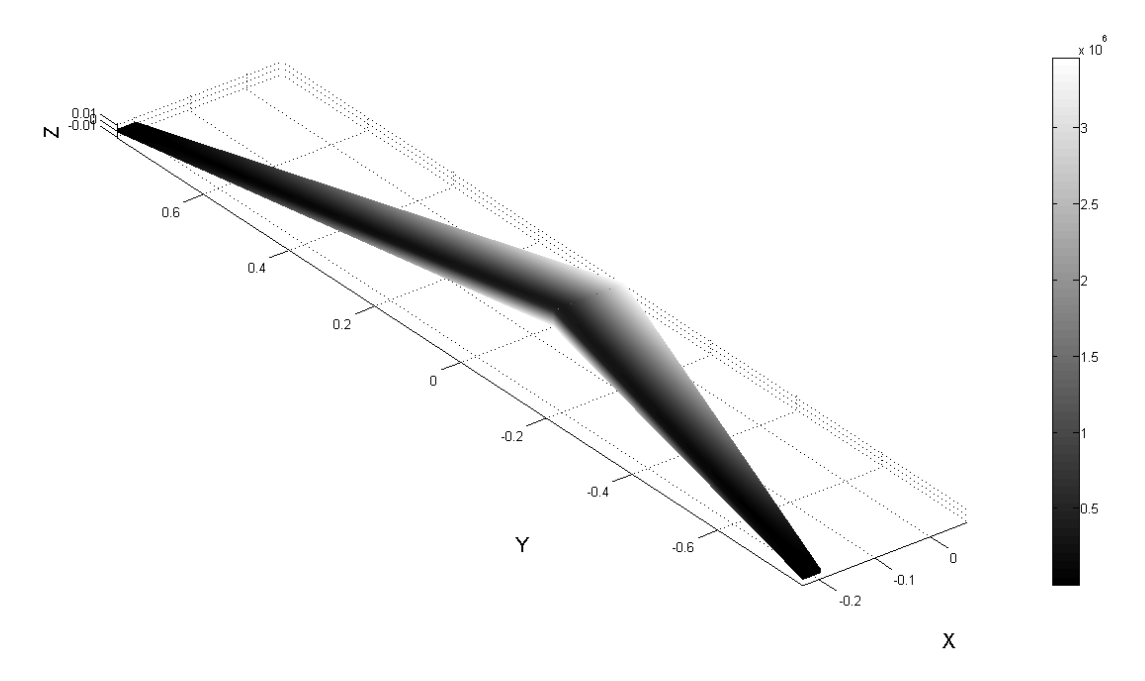


Figure 6.12: Stress distribution in the wings during landing with a skin thickness of 2.0 mm

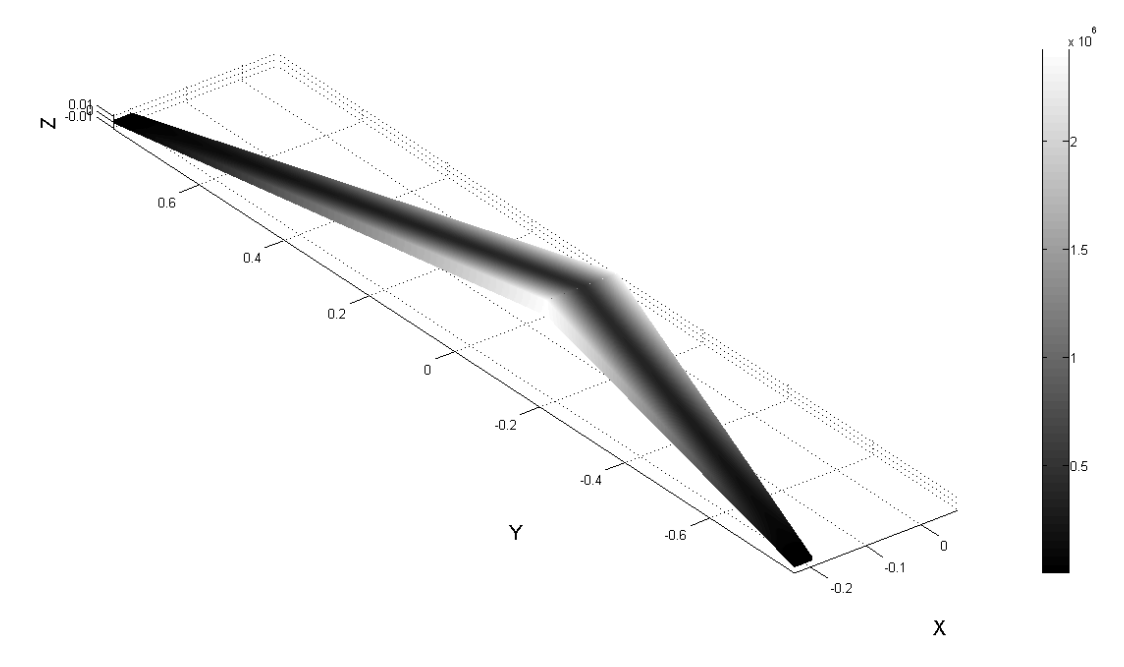


Figure 6.13: Stress distribution in the wings during launch with a skin of thickness 2.0 mm, without vertical forces

the span of the wing. Near the root, stresses are higher meaning thicknesses should be larger. The minimum thickness for a composite material is 2.0 [mm] [83]. Figure 6.11 shows that during launch, the Von Mises stress changed most rapidly on the rear spar in the upper corner. Figure 6.14 shows the distribution of this Von Mises along the span of the wing. Normal stresses are the main contributions to the Von Mises stress.

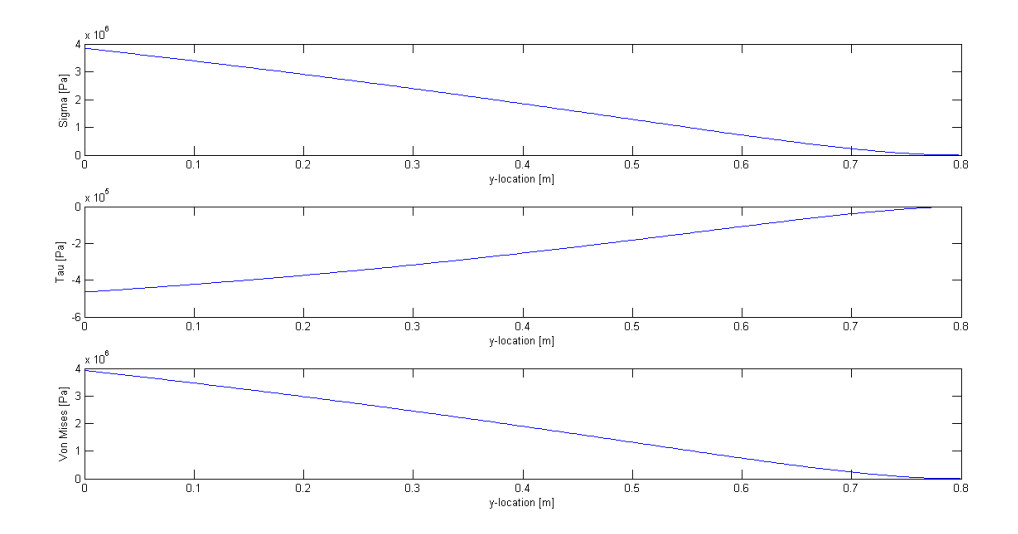


Figure 6.14: Von Mises stress distribution from root (left) to tip (right) in the top front spar during launch with constant skin thickness $2.0 \, \mathrm{mm}$

One can see from Figure 6.14 that the normal stress increases almost linear with respect to the distance y m. This can be explained by the increase in moments around x- and z-axis. After varying the thickness with respect to the span, using a minimum 2.0 mm, it is observed that the weight increases linearly but the maximum stress decreases exponentially. However, considering the stresses only, a thickness of more then 2 mm is not necessary.

SECTION 6.2. STRUCTURE 57

6.2.2. DEFLECTION WINGS

Next to the stresses present during normal flight, take-off and landing, the deflections are also an important factor 6.1. The deflections were calculated with the help of Abaqus/CAE 6.13 and are shown in Figure 6.15. The force distribution was verified using the Matlab code for structures. The deflections were calculated



Figure 6.15: Deflections with a 2 mm skin thickness and compound material

using the Young's modulus 8.9 GPa. What stands out, is that the maximum deflection at the tips is only 4.2 mm. A deflection of 4.2 mm over a total wing length of 80.1 cm means that the strain is much smaller than the maximum strain of 1.4%. Looking at the deflections, it is possible to use the compound material, because the deflections are, just as the stresses, limited.

6.2.3. WING FUSELAGE INTERACTION

For the interaction of the wing with the fuselage, different bonding methods might be considered. The primary focus in this section will be on the stress distribution of both nuts/bolts and adhesive bonding. First adhesive bonding is considered, as was explained in Section 6.1.4. The different loading conditions will be discussed and the stresses that might occur in these joints. Second, the stress distribution using nuts and bolts will be examined. Peak stresses might occur and should be considered.

ADHESIVE BONDING

There are multiple different methods aspects influencing the design for bonded joints. It is important to pay attention to the joint geometry, adhesive selection, present stresses and manufacturing conditions. Stresses may vary from tensile, compression, shear or peal stresses. Making sure these loads are aligned with the greatest strengths of the adhesive is key. These loading types are shown in Figure 6.16 [80]. Figure 6.16 also shows the stress distribution when such a joint is loaded in the indicated manner. For tension, compression

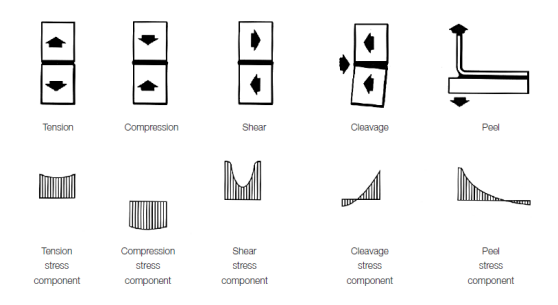


Figure 6.16: Several loading conditions with their stress components

and shear stresses adhesive bonding is very effective. The stress is greatest near the edges when shear stress is applied. This indicates that cracks will most likely start near the edges. Peak stresses will occur due to

cleavage and peel stresses. They cause the applied force to be aligned in a single line of high stress [80]. The design of the ASAP UAV does not have to cope with the cleavage and peel stresses as are indicated in Figure 6.16. When using a simple lap joint however, peel stresses can still occur. This is indicated in Figure 6.17 [80]. These peel stresses should be incorporated during designing the manufacturing method. The figures

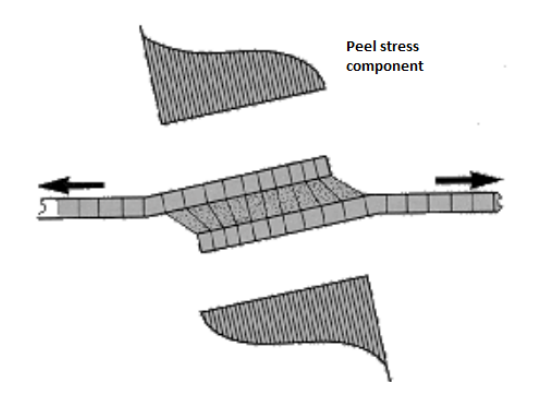


Figure 6.17: Effects on peel stress due to secondary bending

also indicate the reason why cracks will most often start at the edges of the bond. The type of loading in this design, is shear loading. Shear stresses are governed by Equation 6.7.

$$\tau_a = \frac{P}{Lb} \tag{6.7}$$

The adhesive shear stress (τ_a) is dependant on the load (P), the overlap length (L) and the width of the joint (b). But because the substrate will deform, the shear stresses will be concentrated near the end of the overlap (also shown in Figure 6.16). The upper limit on the strength a joint is able to withstand is given in Equation 6.8 [84].

$$P_{max} = \tau_{V} \cdot Lb \tag{6.8}$$

The maximum joint strength possible (P_{max}) is dependant on the yield stress of the adhesives and the geometry of the joint. This maximum strength will however in practice never be reached due to the limits for the adhesives shear strains. Next to this, peel stresses and failure of the substrate will also play a role. Peel stresses should always be avoided. These peel stresses occur due to secondary bending. The joint type should be chosen to be able to cope with these peel stresses or should try to minimize these. When the yield stress of the adhesive is known, one can compute the minimum thickness or the minimum overlap length of a joint with Equation 6.9 [80]. From calculations it follows that using adhesive bonding will not be a problem when looking at the stress levels.

$$\tau = \sigma \cdot \frac{t}{l} \tag{6.9}$$

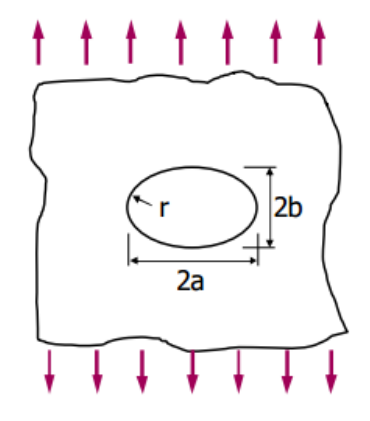
The normal stress was calculated in Section 6.2.1, the maximum shear stress is known from reference and the thickness of the sheet (t) and the overlap length (l) have to be assumed or calculated. Because the stresses are relatively low, the maximum shear strength for adhesive bonding will not be reached. The maximum shear stress of the adhesive is approximately 38 MPa. The maximum normal stress that occurs only during launch is 3.9 MPa. With a overlap length of 2 cm, and a thickness of 1 mm, the shear stress is only 0.2 MPa.

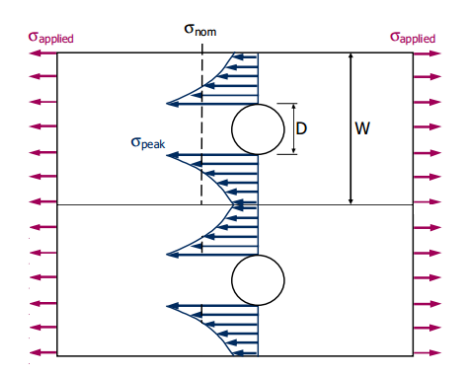
BOLTS AND NUTS

For assembling the UAV, bolts may have to be used. Typically, the holes used for bolting cause weak spots in the structure. It is thus important to know how the stress behaves around these weak spots. Figure 6.18 shows how the stress behaves in the vicinity of a hole and the different parameters used in Equation 6.10. Equation 6.10 gives the stress concentration factor. The stress concentration factor depends on the geometry of the hole. The ASAP UAV may have a bolt/nut connection meaning that the holes which will be located in the skin are circular. Circular holes indicate a stress concentration factor of 3. This implies that the peak stress will be three times larger than the nominal stress. Avoiding these peak stresses can be either by making the holes oval, decreasing the stress concentration factor. Another solution would be to put the bolts on pre-tension, decreasing the fatigue life of the bolt.

$$K_{t} = \frac{\sigma_{peak}}{\sigma_{nom}} = 1 + 2\frac{a}{b} \rightarrow \sigma_{nom} = \frac{W}{W - D} \cdot \sigma_{applied}$$
(6.10)

SECTION 6.2. STRUCTURE 59





(b) Stress distribution in the vicinity of a hole

(a) Parameters used surrounding a hole

Figure 6.18: Stress calculations surrounding defects in the skin

The tensile strength of PLA/Flax is 56 MPa, looking however at the fatigue criteria described in Section sec:fatigue, the maximum stress near the end of life of the UAV is approximately 12.5 MPa. Looking at the stresses present during launch and using nuts with a diameter of 3 mm, Equation 6.10 gives a minimum pitch between nuts of 2.4 cm. This pitch is based on just the holes. Putting the nuts on pre-tension could even increase this pitch but when this is used, the pre-tension effects should be further analyzed during the post-DSE phase.

6.2.4. Stresses within fuselage

The stresses within the fuselage were determined using Abaqus/CAE 6.13, due to its complex shape. Figure 6.19 gives the stress distribution for the fuselage during normal flight conditions for the top panel. Figure 6.19

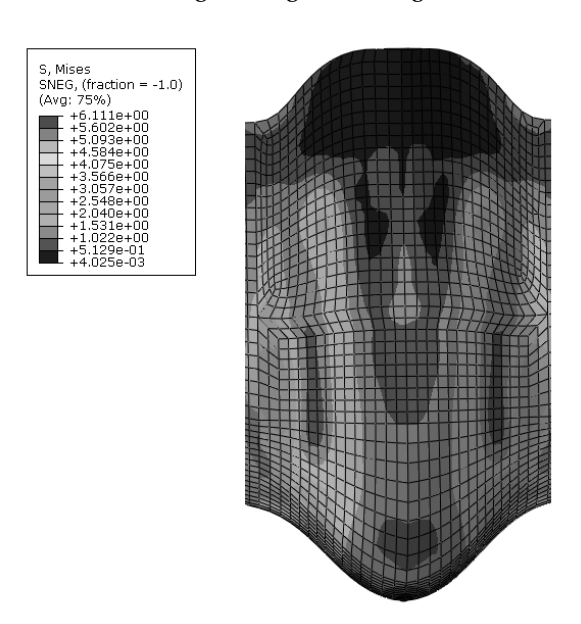


Figure 6.19: Stress distribution top panel fuselage

shows that the nominal stress at the connection between wings and fuselage is approximately 1.5 MPa, just as the Matlab structures code computed. There are, however, local stress increases due to the interaction. At certain weak points, the structure has the tendency to buckle causing an increase in stress. In Section 9.1.2, these peak stresses are deliberately avoided for the connection cuts during assembly. Figure 6.19 also shows the increase in stress at the leading edge where the wing is connected to the body. The stress could reach values up to 5 MPa. This is still less than 10% from its maximum tensile strength and under 50% of the tolerable stress for creep, as explained in Section 6.1.2. This is however during cruise flight, during launch

the stresses could reach higher values. To avoid problems, a local increase in thickness of the skin can be applied to make it better cope with the increase in stresses. However this could also be an error in mesh in the program. The exact cause should be further investigated during the post-DSE phase.

6.2.5. IMPACT TOUGHNESS REGARDING HAIL

One of the key requirements is that the UAV is all-weather. All-weather includes extreme wind conditions but also hail storms. Section 6.1.2 already discussed the individual diameters of hail stones with their respective velocities and energies. These kinetic energies are used to calculate the maximum stresses at the point of impact to determine if the material breaks. Because the individual energies, velocities and diameters before impact are given, the masses of the individual hail stones can be computed. Computing the maximum deflection and stresses could then be calculated assuming Hooke's law to remain valid under dynamic loading and that the elasticity modulus retains it value. Figure 6.20 shows the individual parameters used for calculating the impact stresses and strains due to hail. Figure 6.20 assumes that the skin is a simply supported square

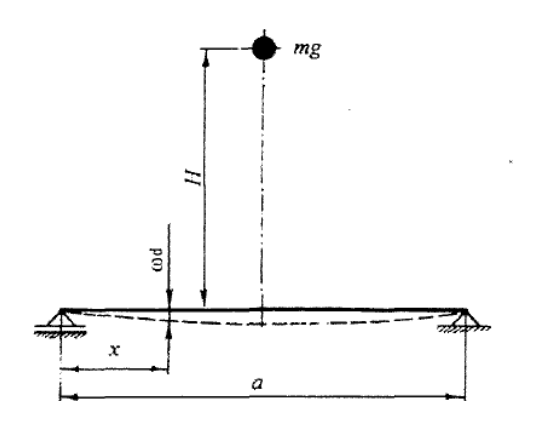


Figure 6.20: Diagram for calculating the impact stresses due to hail

plate and that the entire kinetic energy of the ball is transformed into potential energy, due to deformation of the skin. In reality, the skin will locally deform. For simplicity, the acceleration the skin acquires due to the impact is neglected.

To compute this surface stress, the deflection is needed. Equation 6.11 [85] gives the maximum deflection (ω_s^{max}) at the center, depending on the thickness (δ) , cylindrical rigidity of the plate (D), Young's modulus (E) and the Poisson ratio (v).

$$\omega_s^{max} = 0.01160 \cdot a^2 \frac{mg}{D} \to D \approx \delta^3 \frac{E}{12(1 - v^2)}$$
 (6.11)

With the deflection, the stress can be computed using Equation 6.12 [85]. The equation depends on the coefficient of mass reduction (α), the ratio of the mass of the skin over the mass of the hail (β) and the height (H), computed using the energy of the hail.

$$\sigma_d^{max} = k_d \cdot \sigma_s \to k_d = 1 + \sqrt{1 + \frac{2H}{(1 + \alpha\beta)\omega_s^{max}}} \cdot \sigma_s^{max}$$
 (6.12)

The dynamic stress is given by the multiplication of the dynamic coefficient with the static stress. The name **dynamic stress** is given because these are stresses due to **dynamic forces** or impacts of hail. The only unknown is the static stress. The static stress at the center of a square plate is given by Equation 6.13 [85]. The poisson ratio (ν) has a value of 0.4 [66].

$$\sigma_s^{max} = \frac{mg}{\delta^2} \left((1 - \nu) \left(0.485 \ln \frac{a}{2\delta} + 0.52 \right) + 0.48 \right) \cdot 0.7424 \pi \frac{1 + \nu}{3 + \nu}$$
 (6.13)

For all different sizes of hail, the dynamic stresses are computed and compared with the tensile strength of PLA/flax. With these formulae, the minimum thickness can be computed when looking at the fracture toughness of the material. The most common hail stone sizes, range from 5 mm to 5.1 cm in diameter [86]. Figure 6.21 shows how the dynamic stresses vary with the diameter thickness of hail. Indicated is the maximum

SECTION 6.2. STRUCTURE 61

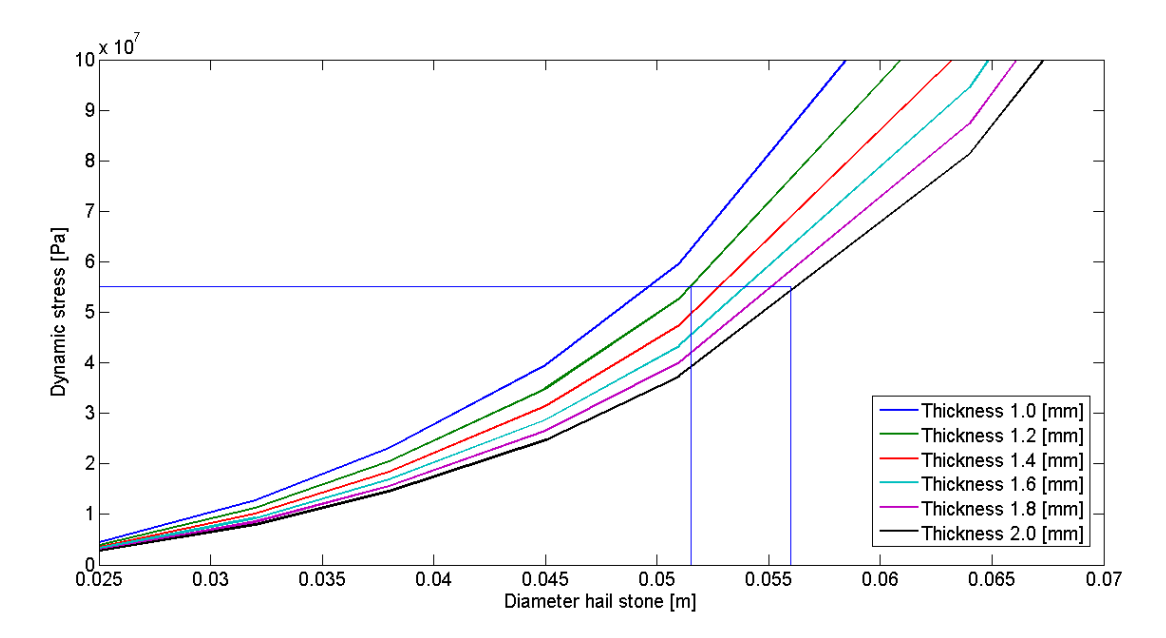


Figure 6.21: Minimum thickness required for hail impacts with a diameter of 5.1 cm

common occurring diameter of hail (5.1 cm) and the maximum tensile strength of PLA/flax. Designing for a diameter of 5.1 cm and adding a safety factor of 1.5, the minimum thickness of material needed to have no fracture is 1.2 mm. Because injection molding is still the limiting factor, the minimum thickness is kept on 2 mm. This concludes that the UAV with minimum thickness of 2 mm will also be able to cope with hail up to 5.6 cm in diameter.

6.2.6. THICKNESS OPTIMIZATION

In the case that the skin can be optimized, disregarding the manufacturing minimum skin thickness, a weight reduction can be achieved. This implies that the design will no longer be overdesigned, something which should be avoided. Table 6.10 gives the relevant parameters for skin thickness optimization. What clearly

Description	Unit	Original	Optimized for hail	Combined	Optimized for Stress
Skin thickness	[mm]	2	1.2	$1.2 \rightarrow 2.0$	$1.2 \to 2.1$
Maximum stress	[MPa]	3.9	6.4	4.6	3.69
Wing tip deflection	[mm]	4.2	7.4	5.5	5.2
Connection wing-fuselage	[-]	Sustains	Breaks	Breaks	Sustains
Hail diameter	[cm]	5.6	5.1	≥ 5.1	≥ 5.1
Wing weight reduction	[%]	0	38	15	12

Table 6.10: Table relevant parameters for optimized skin thickness

stands out is that reducing the thickness of the skin, the maximum Von Mises stress will increase as will the deflection. The problem is however with the connection of the wings to the fuselage. When bolts are used, the peak stress will be larger than the tensile strength (12. MPa) near the end-of-life of the UAV due to fatigue properties. This implies that with a constant skin thickness of 1.2 mm, the UAV will fail due to weakening of the skin when no skin parts are replaced. The solution is a varying skin thickness. Letting the thickness depend on the chord, or spanwise position, will imply lower maximum Von Mises stresses/deflections and a weight reduction. Because the maximum Von Mises stress is still the most important aspect, either the highest stresses should be avoided during manufacturing, nuts and bolts should be avoiding for joining methods or the thickness should be increased even more. When nuts and bolts are used, the optimal thickness is shown in Table 6.10 and equals a varying thickness of 1.2 mm to 2.1 mm.

6.3. CONCLUSION ON MATERIALS AND STRUCTURE

The thickness of the wings will be $2.0\ mm$ throughout the entire span of the UAV made of the bio composite PLA/flax. This is because of the minimum thickness requirement for injection molding. Using this combination of PLA and natural fibers enables the UAV to disintegrate within approximately 18 months. Looking at the deflections and stresses, it is possible to have the material made from a PLA/Flax compound containing 30% chopped flax fibers and still only have a deflection of $4\ mm$ at the wing tip.

Looking at the stress levels they turn out to be below the maximum stress level for fatigue at the number of cycles the structure makes before replacement. With a nut pitch of $2.4\ cm$, the peak stresses will be far below the tensile strength and the elongation beneath its maximum of 1.4%. Cuts for assembly intentionally avoid higher stress intensive spots, avoiding further weakening of the structure. With the minimum thickness of $2\ mm$, the UAV will be able to cope with hail impacts equal to or greater than $5.6\ cm$ in diameter. When injection molding is not the limiting factor, an optimal thickness variation will be $1.2\ mm$ from the tip to $2.1\ mm$ towards the root of the UAV. With these thicknesses, the UAV is able to be bonded with bolts/nuts and is capable of withstanding hail impacts with a diameter equal or greater than $5.1\ cm$.

INTERNAL LAYOUT

In Figure 7.1 the internal layout of the ASAP UAV is shown. Each subsystem is placed inside the body of the aircraft, with exception of the batteries. The volume inside the body is not sufficient to store all the batteries, hence most are placed inside the wings. As mentioned in Chapter 6, this will also cause bending relief which is beneficial for the structural design. The total volume of the batteries is 3.8 liter, if which three liters are

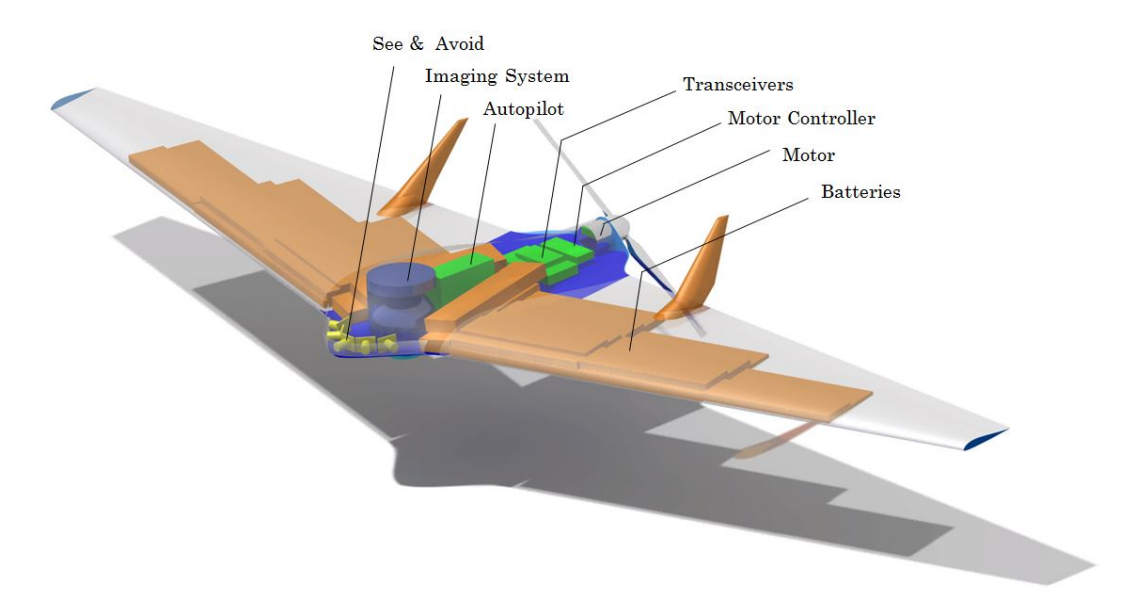


Figure 7.1: The internal layout of the ASAP UAV

placed inside the wing. The residual 0.8 liter is stored inside the body, enclosing the camera. In front of the camera the see and avoid subsystem, with extra space reserved for the electrical components (Printed Circuit Board (PCB)s, harddisks, etc.) that come with this system. The autopilot, which consists of two PCBs on top of each other (see Chapter 3), is placed aft of the camera. The electrical motor and propeller are located at the rear of the fuselage. Right in front of these is the motorcontroller. Between the motorcontroller and the flight computer the UHF and S-band transceivers are placed. Note that the servos are not displayed in Figure 7.1 and 7.2, which shows a front view with section cut. Finally, the sizes and volumes of each part of the ASAP UAV are displayed in Table 7.1.

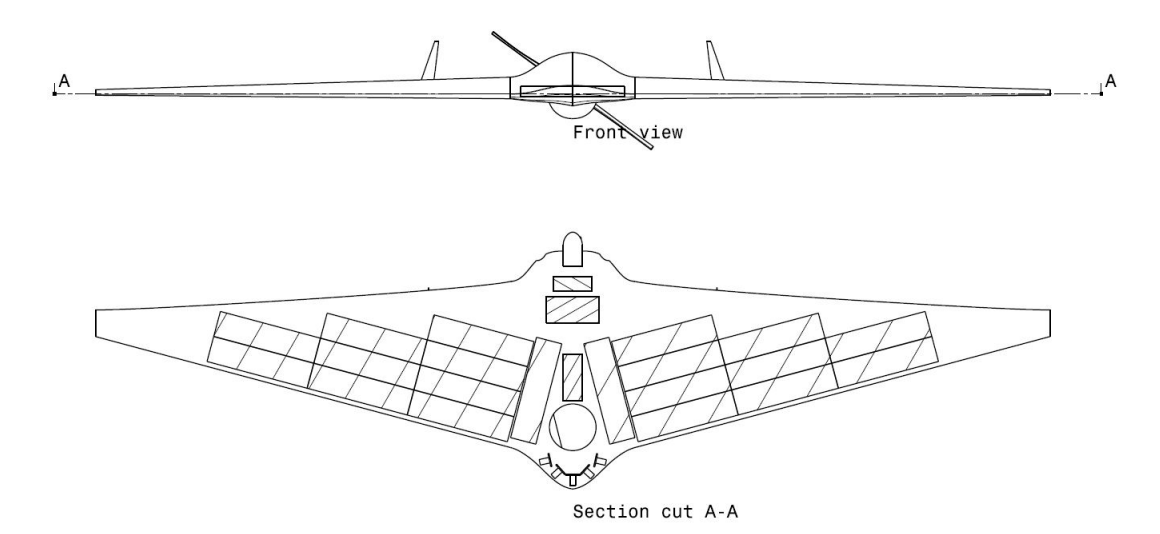


Figure 7.2: Front view with section cut showing placement of several subsystems $\,$

Table 7.1: Dimensions and volumes of different part of the ASAP UAV

Part	Dimension [cm x cm x cm]	Volume [L]
Comoro	8.89 x 8.89 x 11.43	0.9033
Camera	***************************************	
Motor	$3.27 \times 3.27 \times 4.00$	0.1739
Autopilot	$5.90 \times 1.80 \times 1.50$	0.0159
Servo	$2.70 \times 1.30 \times 2.50$	0.0088
S-band antenna	$4.40 \times 4.40 \times 0.50$	0.0097
S-band transceiver	10.6 x 5.08 x 1.27	0.0684
UHF-band antenna	12.95 x 2.29 x 11.43	0.3385
UHF-band transceiver	$6.00 \times 3.30 \times 1.00$	0.0198
See and Avoid	$5.00 \times 15.0 \times 2.00$	0.1500
Batteries		3.8000
Total required volume		5.4883
Wing (single)		2.8000
Body		4.8100
Total available volume		10.410

FLIGHT PERFORMANCE AND AERODYNAMIC CHARACTERISTICS

In this chapter the different aspects of the ASAP UAV are analyzed with respect to the different aerodynamics characteristics. The chapter will start with defining an additional requirement for the performance of the UAV in Section 8.1. Then in Section 8.2 the required flight performance of the UAV is discussed, the requirements are elaborated and the influence of the Aspect Ratio (AR) and wing loading is discussed. This is done with both estimated and realistic input variables. In Section 8.3 the characteristics of tailless aircraft are discussed in addition to a number of airfoils that could be applicable to the final design. Subsequently, the influence of the remaining planform parameters is discussed in Section 8.4. Finally, in Section 8.5, a quantitative analysis is made in order to choose values for all geometrical parameters of the UAV using planform and airfoil characteristics. As presented in Figure 8.1 the entire external design process is highly iterative and a better result is expected for every iteration.

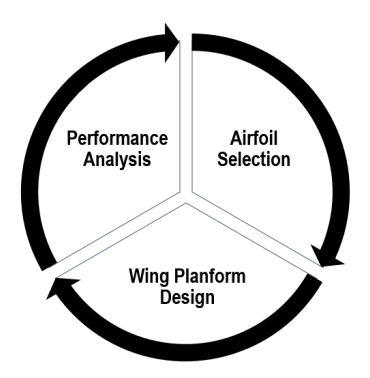


Figure 8.1: The iterative process to optimize the design for mission performance

8.1. ADDITIONAL REQUIREMENTS

The entire list of requirement can be found in the MTR [2] and in the compliance matrix in Chapter 12. Compared to the MTR a new requirement is set for the aerodynamic performance based on the circling capability of the ASAP UAV which is described in this section.

After a victim is detected the UAV will circle over this victim at endurance speed ($V_{endurance}$) in order to maximize its duration. During turns, the aerodynamic efficiency decreases due to the fact that the lift vector is now pointing inwards with the bank angle. Without increasing the pitch angle, the turn will result in altitude decrease. However, this increased angle of attack results in higher drag and an increase in required thrust to maintain the same airspeed. Finally the increase in thrust results in more power required. The ASAP UAV is designed in such a way that it can perform this circling for 3 hours, hence the increased power during circling should be taken into account. The equation for the increase in power during a turn is given by Equation 8.1.

$$P_r = \sqrt{\frac{n^3 \cdot W^3 \cdot 2 \cdot C_d^2}{S \cdot \rho \cdot C_L^3}} \tag{8.1}$$

Where n is the load factor given by equation 8.2 where ϕ is the bank angle.

$$n = \frac{1}{\cos(\phi)} \tag{8.2}$$

These load factors are applied to the power required curves, created for the ASAP UAV in the MTR. It can be seen that power required gradually increases until 20 degrees angle of bank. After this angle the required power increases significantly. This can be seen in Figure 8.2 where the power required curves are plotted for bank angles between 0 and 60 degrees. This increase in power is plotted in comparison with normal flight condition and the increase in power is calculated as a percentage which can be seen in Figure 8.3. To

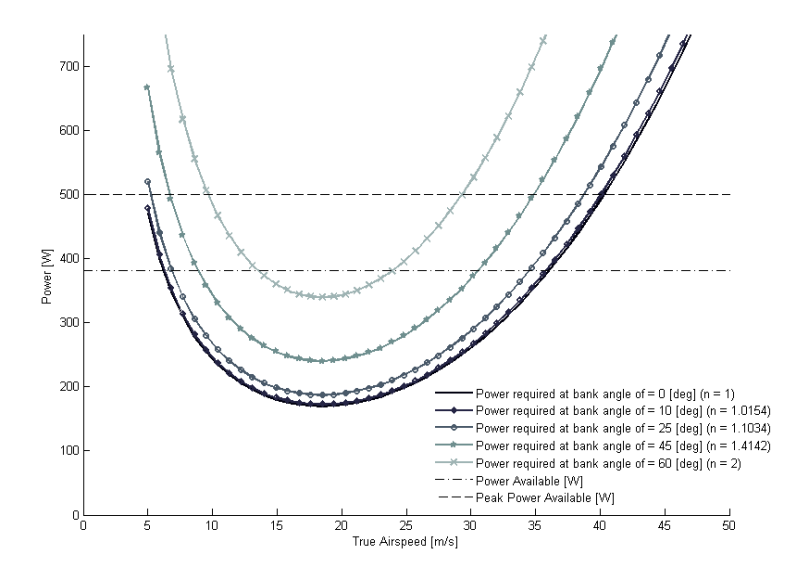
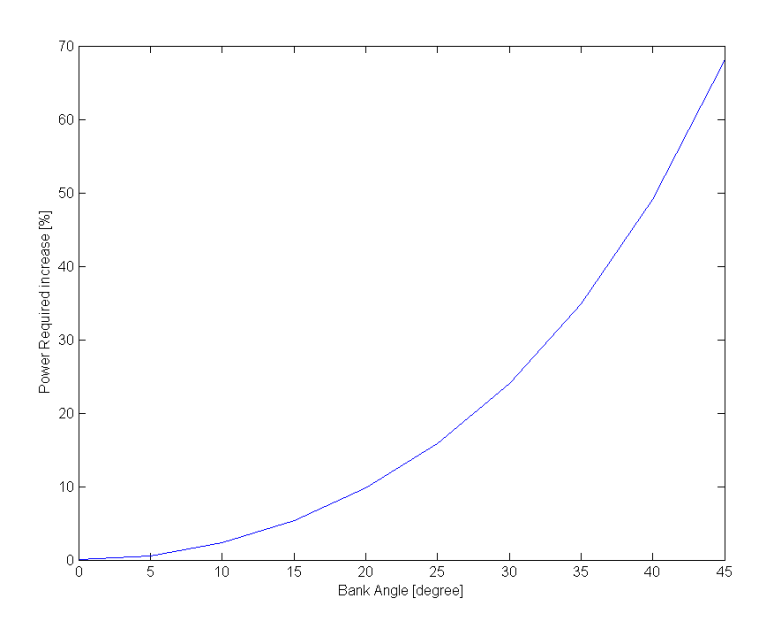


Figure 8.2: Power required increased when making a turn



Figure~8.3: Increase~in~power~required~in~turn~compared~to~normal~flight~expressed~in~percentage

conclude the performance analysis during the tracking of the victim, the turn radius is examined. The turn radius is calculated using Equation 8.3.

$$r = \frac{V}{g \cdot \sqrt{n^2 - 1}} \tag{8.3}$$

Where V is the flight speed during the turn. As the flight speed increases the turn radius increases. The steeper the bank angle the smaller the turn radius. The turn radius is plotted against the load factor for speeds varying

between 18 and 26 m/s in Figure 8.4. Finally, a requirement is set that the UAV turn radius is smaller or equal

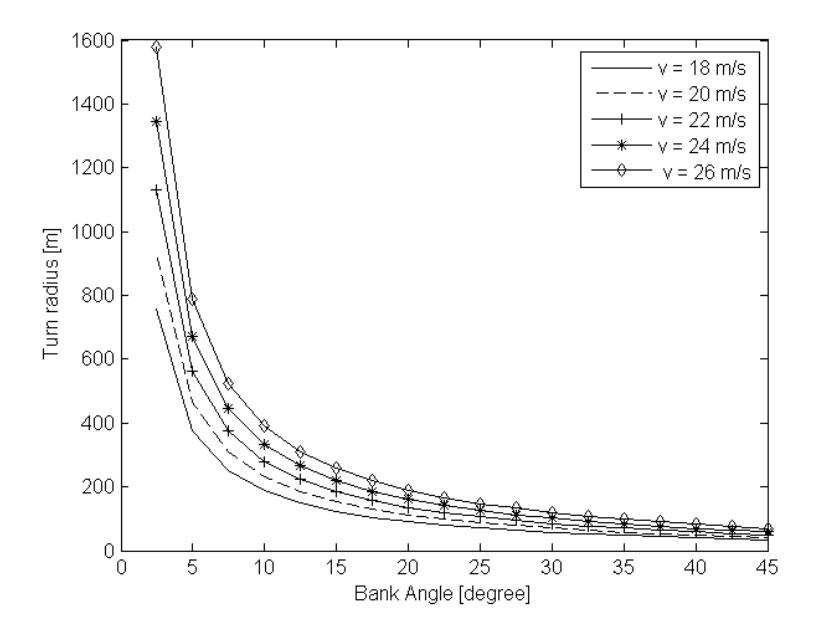


Figure 8.4: Turnradius vs bank angle for speed varying between 18 and 26 m/s

to the flight altitude of 150 m. This will result in an elevation angle of 45° between the victim and the UAV. However, the camera needs to correct for a larger angle due to the bank angle. Additionally a maximum of 20° bank angle is taken which results in a required power increase of almost 10%. Looking at Figure 8.4, this angle limitation shows a maximum $V_{endurance}$ of 23 m/s. This results in the following requirement: *PERF-13:* The UAV shall have an endurance velocity of at most 23 m/s.

8.2. FLIGHT PERFORMANCE

The performance of the ASAP UAV is optimized for finding the victim as fast as possible in all-weather conditions. This optimization is explained in this section. First the parameters involved are described, followed by the criteria on which the design is chosen. The design sensitivity is also discussed in this section, explaining how certain values will change with a change in design parameters.

As mentioned before, the first results are obtained from estimated airfoil and planform parameters. The result from the code is a matrix containing performance characteristics for different wing loading designs and for every wing loading a range of aspect ratios and taper ratios. Another varying parameter is the leading edge sweep angle. The effects of both taper and sweep are explained in Section 8.4. Design options resulting in an UAV that is unable to perform the mission are immediately discarded. These design rejections are based on the endurance at the cruise speed ($H_{V_{range}}$) which should be at least 180 minutes. The endurance velocity is another requirement on which the design can be immediately discarded. As explained earlier in Section 8.1, this velocity may not be larger than 23 m/s due to the limitation on the turn radius during circling. After applying these requirements to the matrix the number of design options is significantly decreased.

The reasoning behind the selection of a design is that the most optimal design in terms of mission performance is the design with the highest possible wing loading and for that wing loading the lowest possible aspect ratio. The wing loading is critical because of the all-weather requirement for the UAV. A lower aspect ratio results in a more compact design which is favorable for all-weather operation as well. A contradiction exists since an increase in wing loading results in a higher aspect ratio for the design in order to remain capable of enduring flight for three hours. However the wing loading is more influential on the design performance shown in Equation 8.4 [87].

$$a_{gust} = \frac{C_{L,alpha} \cdot \rho}{2} \left(\frac{AR}{AR + 2.4} \right) \left(\frac{VS}{m} \right)$$
(8.4)

The performance tool shows that a slightly higher aspect ratio combined with a higher wing loading results in a more compact design. This can be contributed to the fact that the wing loading increase is resulting from a decrease in wing surface area because the weight of the UAV is fixed. A design with a small surface area and a large aspect ratio shows a smaller wing span and chord length compared to a lower wing loading and lower aspect ratio design. This can pose another threat on the design since the smaller wing will provide less internal space for the UAV subsystems. The available internal volume needs to be at least 5 liters for the wing according to requirement M&S-8 (Chapter 12). The rationale behind the amount of liters necessary in the wing is further explained in Chapter 7.

For the performance characteristics of the design, the conversion from a two-dimensional (infinite) to a three-dimensional wing is necessary. The two-dimensional airfoil and infinite wing characteristics are described in Section 8.3. For determining the 3D lift coefficient (C_L) Equation 8.5 is used.

$$C_L = \frac{2W}{\rho V^2 S \cdot \cos^2\left(\Lambda_{LE}\right)} \tag{8.5}$$

The required lift coefficient is increasing for an increasing leading edge sweep angle (Λ_{LE}). This is due to the component of the free-stream velocity vector perpendicular on the leading edge. Directly, this means that for an increase in sweep angle the airspeed or the wing surface should be increased or the UAV will have to fly at higher angles of attack. Since the design target is an as large as possible wing loading, it is preferred to increase the airspeed over the wing surface or increase the angle of attack. Both these countermeasures result in a lower lift-to-drag ratio compared to an unswept wing, meaning the required power in flight is increasing for increasing sweep angle. For this reason it is desirable to use an as low as possible sweep angle. The benefits and reasoning of applying sweep is discussed in Section 8.3.

The speed range of the UAV is shifting to higher velocities as the wing loading increases. The minimum airspeed, the endurance airspeed (at $(C_L^3/C_D^2)_{max}$), the range airspeed (at $(C_L/C_D)_{max}$) and the maximum airspeed all increase for an increase in wing loading. This can be explained with Equation 8.5. As the wing loading (W/S) is increasing the velocity should increase in order to keep the lift coefficient at a constant value. The minimum airspeed is directly defined by the maximum lift coefficient and the wing loading and is unaffected by aspect ratio. The airspeeds for maximum endurance and range are increasing for a decrease in aspect ratio due to the lower lift-to-drag ratio associated to a lower aspect ratio. This lower lift-to-drag ratio is due to the induced drag coefficient which increases linearly with a decrease in aspect ratio as can be seen in Equation 8.7 [88]. The maximum airspeed is reached when the available power equals the required power. The required power is strongly influenced by the total drag on the wing meaning that an increase in wing loading (decrease of wing surface area) results in a higher maximum airspeed. The aspect ratio influences the maximum airspeed in two ways: on the one hand the induced drag coefficient is decreasing for an increasing aspect ratio as described by Equation 8.7. On the other hand the zero-lift drag coefficient will increase for an increase in aspect ratio since the Reynolds number and the wetted surface of the wing will change as shown in Equation 8.11.

$$C_D = C_{D,0} + C_{D,i} (8.6)$$

$$C_{D,i} = \frac{C_L 2}{\pi A R e} \tag{8.7}$$

$$c_f = \frac{0.455}{\log(Re)^{2.58}} \tag{8.8}$$

$$Re = \frac{V\bar{c}}{v} \tag{8.9}$$

$$S_{wet} = 2S\left(1 + 0.2\frac{t}{c}\right) \tag{8.10}$$

$$C_{D,0} = k \cdot c_f \left(\frac{S_{wet}}{S_{ref}}\right) \tag{8.11}$$

Where k is a constant equal to 1.2, c_f is the skin friction coefficient, Re the Reynolds number, \bar{c} the mean chord length, v the kinematic viscosity of 1.568 · 10⁻⁵ m^2/s and t/c the thickness in percentage of the airfoil.

With the design rationale and sensitivity presented in this section the final external layout is selected. This is done by varying aspect ratio, taper ratio and wing loading. Applying the criteria as explained below will result in non-feasible designs. The order of selection is based on the all-weather requirement where wing loading is most critical. Designs that do not satisfy the set requirements are eliminated, after which the design with the lowest aspect ratio is chosen. For this highest possible wing loading and corresponding lowest aspect ratio the taper ratio is selected such that the volume of the wing is at least 5 liters. The final design parameters are described in Section 8.5, after the airfoil and planform selection approach is presented.

8.3. AIRFOIL SELECTION

Flying wings require a different sort of airfoil due to the lack of a horizontal stabilizer. If the flying wing stalls, there is no recovery option because there is no re-stabilizing moment exerted by the tail, which only incorporates two vertical stabilizers. However there are some 'reflex' airfoils, which tend to pitch down when the angle of attack becomes too large. This is because the moment coefficient at the Aerodynamic center (a.c.) is positive and is counteracted by the negative moment induced by the lift force. As the lift force rises due to an increased angle of attack, the negative nose-down moment will increase as well, bringing the flying wing back to its equilibrium position [89].

The main difference within the range of reflex airfoils are the types. Stated below are most of the reflex airfoils which can be used for a flying wing model [90] [91] [92].

- 5-digit reflexed NACA airfoils
- Martin Hepperle MH44 to MH84 airfoils
- Eppler E325 to E344 airfoils
- · Fauvel airfoil
- Horten brothers airfoils
- Roncz/Marske-7 low drag airfoil

All of these airfoil types differ from one another in a very eccentric way concerning their basic shape, however the airfoils may differ within a specific airfoil type as well. In the latter case, the differences between the airfoils are determined by the two-dimensional design lift coefficient $C_{l_{des}}$, the maximum airfoil thickness and the location of the camber & reflex location on the chord length.

As mentioned before, the ASAP UAV should be as neutrally stable as possible. None of these 'reflex' airfoils are truly neutrally stable, but some approach it very closely. The Eppler airfoils however, perform the worst in terms of neutral stability, while the Horten airfoils are nearly neutrally stable, but generate a very low $C_{l_{max}}$. The Roncz/Marske-7 airfoil has a very low drag coefficient but is outperformed by the NACA- and MH-profiles in terms of $C_{l_{max}}$ and stability. The Fauvel airfoil has a too positive C_m , which is incompatible with the desired characteristics of the ASAP UAV's airfoil. Compared to the other airfoils, the NACA- and MH-types resulted in the highest $C_{l_{max}}$ and they are close to the desired stability. Using the program XFLR5, the most viable NACA- and MH- airfoils were evaluated. Figures 8.5, 8.6 and 8.7 depict the $C_m-\alpha$, $C_l-\alpha$ and C_l-C_d curves for each airfoil.

The C_m – α – curves for MH profiles are curved the same way and only differ in size and position along the y-axis. Other MH profiles had the same, or even slightly better moment characteristics than the MH 81 airfoil, however their lift was much lower. The MH 81 airfoil incorporates both near neutral stability and a decent $C_{l_{max}}$. Due to a wide range in variation, there are several viable 5-digit NACA airfoils. The NACA34110 and NACA44113 airfoils approximate neutral stability closest and have the highest $C_{l_{max}}$ of these 5-digit NACA airfoils. A cross-sectional view of the three airfoils can be seen in Figure 8.8. Note that Figures 8.5a till 8.7c are the result of two-dimensional analysis, hence they need to be converted in order to determine the three-dimensional values for the final design. The ASAP UAV will operate at Reynolds numbers between 300.000 and 500.000 meaning there will be a minimum and maximum value for the $C_{l_{max}}$. This value can be evaluated using the High-aspect-ratio-method, since the wing satisfies the high-aspect ratio criteria as stated by Equation 8.12 and Figure 8.9 [93].

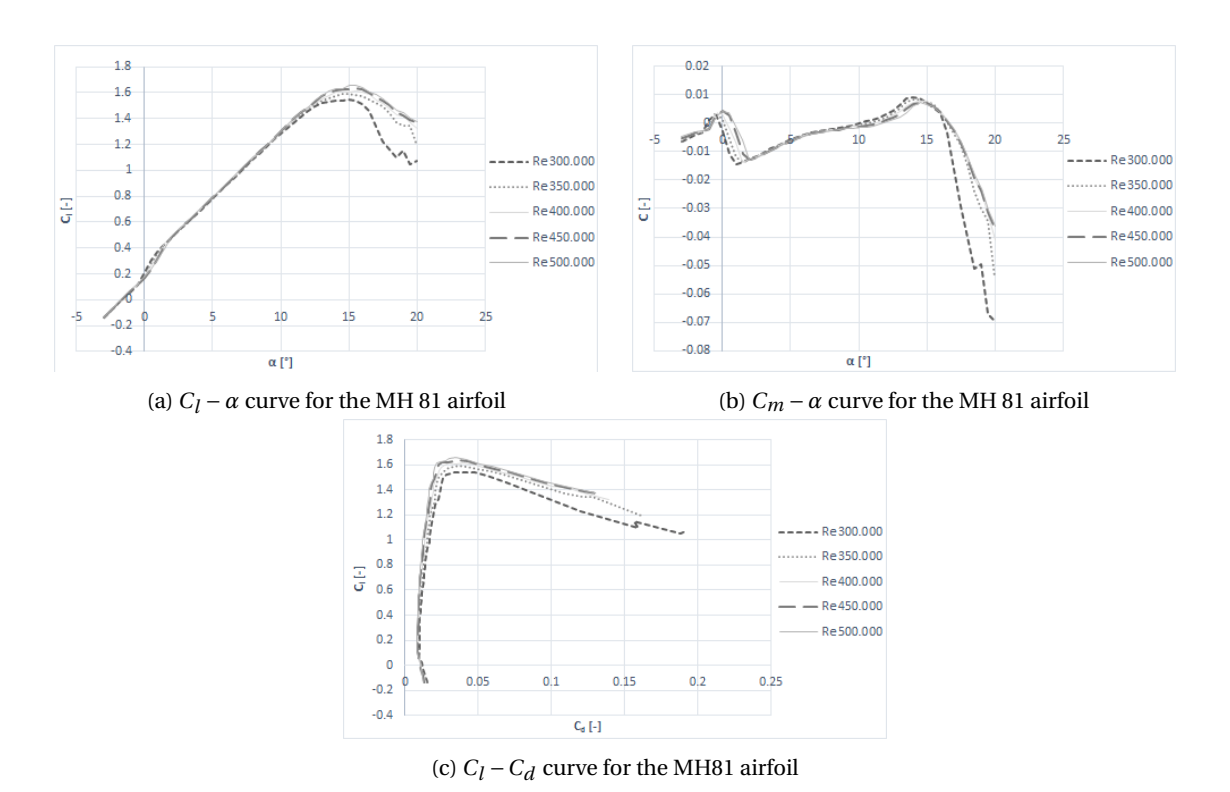


Figure 8.5: Martin Hepperle 81, 13% max thickness

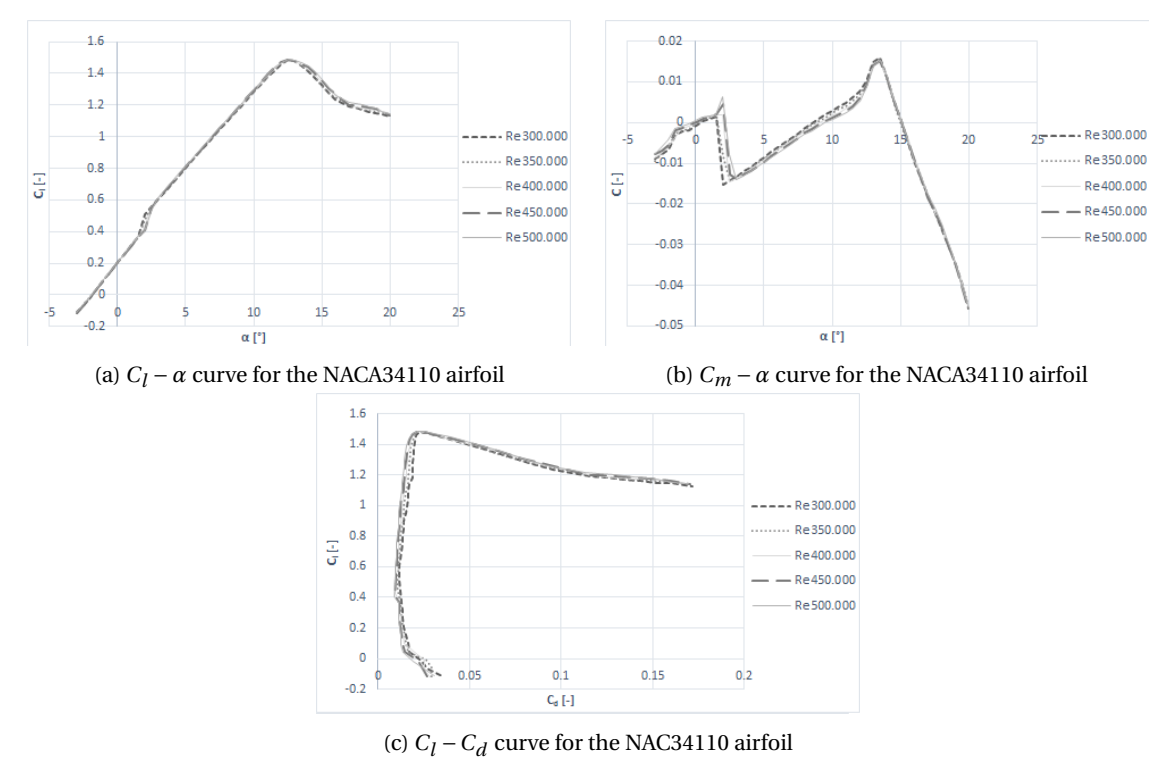
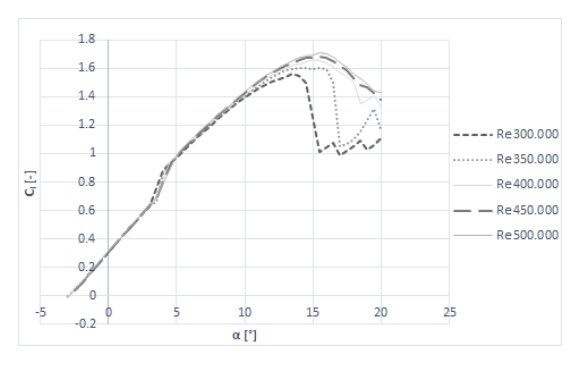
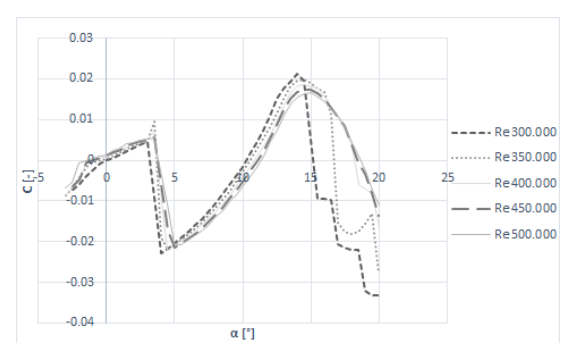


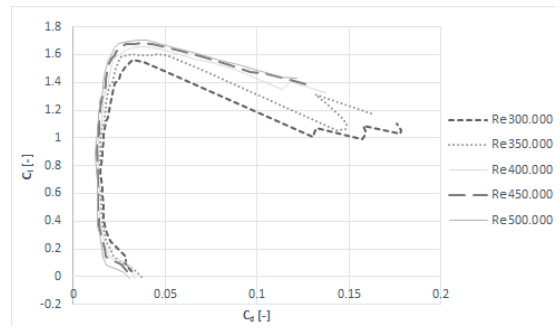
Figure 8.6: NACA34110 airfoil, 10% max thickness





(a) $C_l - \alpha$ curve for the NACA44113 airfoil

(b) $C_m - \alpha$ curve for the NACA44113 airfoil



(c) $C_l - C_d$ curve for the NACA44113 airfoil

Figure 8.7: NACA44113 airfoil, 13% max thickness

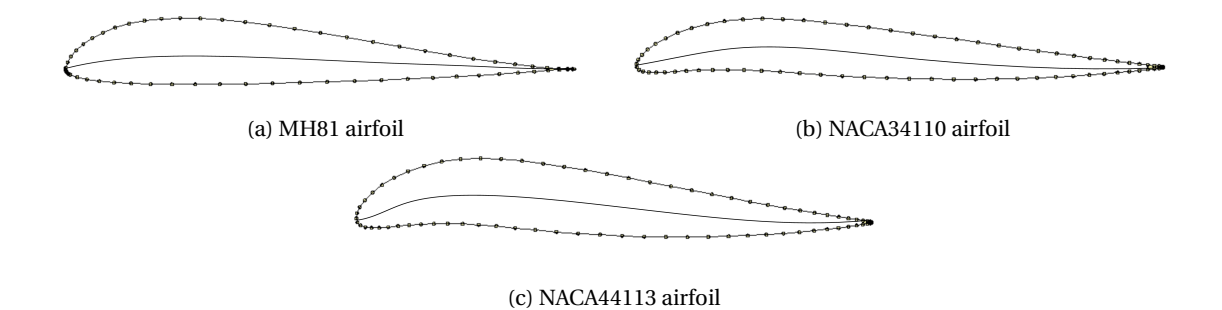


Figure 8.8: Airfoil candidates

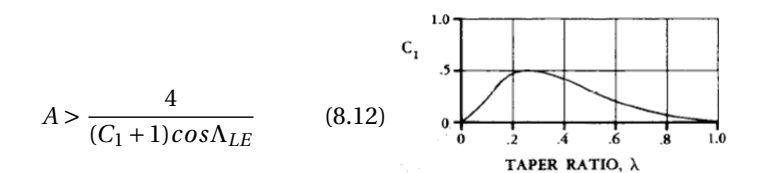


Figure 8.9: High aspect ratio C_1 coefficient

After the airfoil selection the $C_{l_{max}}$ can be derived from the two-dimensional analysis. The three-dimensional lift coefficient using Equation 8.13 where the $[\frac{C_{l_{max}}}{C_{l_{max}}}]$ ratio can be derived from Figure 8.10. The leading edge sharpness parameter Δy is dependent on the chosen airfoil, particularly on the camber line which defines the sharpness of an aifoil. A smal Δy denotes a relatively sharp airfoil [93].

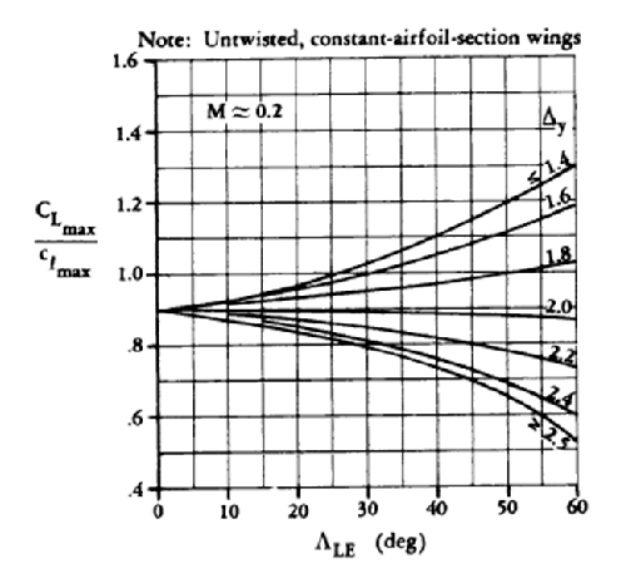


Figure 8.10: $\frac{C_{L_{max}}}{C_{l_{max}}}$ in function of ΔY and Λ_{LE} for high-aspect ratio wings without twist

$$C_{L_{max}} = \left[\frac{C_{L_{max}}}{C_{l_{max}}}\right] C_{l_{max}} \tag{8.13}$$

This final three-dimensional $C_{L_{max}}$ is used to evaluate the minimum airspeed V_{min} necessary for take-off. This V_{min} is used in Chapter 4 in order to size the UAV launcher and the landing procedure. This process is iterative meaning that the final V_{min} will be determined by several parameters such as the size of the launcher, the $C_{L_{max}}$ and the wing loading W/S. This is considered during the selection of a final airfoil.

8.4. PLANFORM PARAMETERS

In addition to the airfoil selection, the planform parameters must be chosen. The AR, surface area and taper ratio are the variables used to evaluate the different designs, as specified in 8.2. Therefore the remaining parameters are the sweep (Λ), angle of twist (ϵ), incidence angle (i_w) and the dihedral angle (Γ). The taper ratio (λ) is also included to check the sensitivity of the design for changing taper. For all these parameters the qualitative effects of an increase on the ASAP UAV in particular are summarized in Table 8.1. As can be seen in Table 8.1, the main effects of the planform parameters concern controllability, wing weight, tip stall, lift distribution efficiency and stability. A number of notes are to be made however to elaborate on the different aspects of planform parameters.

Controllability versus Finite Wing Effects; The longitudinal control of a flying wing without horizontal tailplane is provided by the elevons. The controllability of the UAV depends entirely of the location of the elevons w.r.t. the c.g. and the size of the elevons. Therefore, increasing the sweep angle has a direct positive effect on the controllability of the UAV.

 $Table \ 8.1: The \ planform \ parameters, the \ effect \ of \ an \ increase \ of \ these \ parameters \ and \ the \ effect \ particular \ to \ the \ ASAP \ UAV$

Parameter	Effect of increase	Notes
Sweep	Increase of longitudinal control due to increase in aileron/elevon arm w.r.t. the c.g.	Crucial for a flying wing without horizontal stabilizer.
	Increase in lateral stability due to increase in fin/winglet arm w.r.t. c.g.	Lateral stability will be ensured by the vertical stabilizers in the tail. Therefore this effect is of small influence.
	Decrease in lift due to decrease of the normal airspeed component.	Will have significant impact on the L/D ratio and thus the power required. In addition C_{Lmax} will decrease which has an negative effect on V_{min} .
	Increase in tip loading due to upwash from inboard wing sections.	May lead to inefficient lift distribution and may lead to tip stall.
Taper	Weight reduction due to lower bending moment.	The bending stresses have been determined to be low. In addition, without taper more batteries can be stored in the wing, counteracting bending moment.
	Decrease in wing tip loading.	Possible to increase lift distribution efficiency.
	Increase of tip stall due to reduction in tip chord length.	Due to low Reynolds number of small size aircraft this should be taken into account.
Angle of twist	Decrease of the effective Angle of Attack (AoA) towards the wing tip.	Can be used to reduce tip stall and increase the lift distribution efficiency.
Incidence angle	Will increase the difference in AoA between the wing root and tip.	Allows for a better lift distribution efficiency.
Dihedral angle	Will result in more lateral stability.	As backswept wings have a natural dihedral effect, the stability of the UAV might increase so that it becomes too stable. Therefore an anhedral might be required.

The wing sweep angle however, also has a direct negative effect on the lift produced by a wing, as described in Section 8.2. This is due to the fact that lift is only produced by the airspeed component that is parallel with the airfoil sections. It can be concluded that the sweep angle should be chosen to be as small as possible, but large enough so that sufficient controllability is provided.

Tip Stall; Due to the fact that the longitudinal control of a flying wing without horizontal stabilizer is provided solely by its elevons, tip stall is a very undesirable quality of the ASAP UAV. It decreases the effectiveness of the elevons and may even result in a positive pitching moment. This may result in an uncontrollable stall situation.

A number of parameters add to the tip stall characteristics of the UAV and should be minimized. Adding taper will reduce the Reynolds number at the wing tips, which has a negative impact on the tip stall characteristics. As the relatively low operating flight speed and small wing chord of the ASAP UAV result in a low Reynolds number, this is of concern to the design process. Therefore the amount of taper should be as small as possible.

Another planform parameter that increases tip stall behavior is the amount of wing sweep. The inboard wing sections create an upwash which affects the effective AoA of the wing tips. Therefore, tip stall is another reason to limit the amount of wing sweep of the UAV. Note that for low AR UAVs the effect of sweep on tip stall is smaller.

One particular adjustment to the wing may help to improve the tip stall characteristics, namely adding negative wing twist to the tips. This way, the effective stall angle of the wing tips will occur at a higher total angle of attack. Hence the elevons will remain more effective at higher angles of attack.

Lift Distribution Efficiency; As concluded in the previous sections, the chance of tip stall can be decreased by reducing the amount of taper and sweep of the wing. This will however have a adverse effect on the lift distribution efficiency. In general, not adding taper to a wing will increase the $C_{d,i}$ with approximately 7% [94]. The result would be a significant increase in the required power, especially in combination with the fact that the wing sweep will decrease the amount of lift produced. Therefore, the remaining wing planform parameters, the wing twist and the incidence angle, should be designed to increase the lift distribution effectiveness.

Giving the wing a positive incidence angle will increase the amount of lift produced at the root of the wing. In addition, giving the wing a negative angle of twist will decrease the amount of lift produced at the tip. By combining these measures the lift distribution is optimized for a given sweep angle and taper.

8.5. Final Flight Performance and Aerodynamic Characteristics

Now all design approaches are described in detail, the final design can be determined. As stated in the introduction to this chapter the process of creating a design is highly iterative. Describing all iterations is omitted and only the final design parameters are described. First a trade-off for the airfoil selection is performed in Subsection 8.5.1. After this the wing planform parameters are presented in Subsection 8.6. Both of these selections result in the necessary input to obtain the performance parameters for the final design as presented in Subsection 8.7.

8.5.1. AIRFOIL TRADE-OFF

The airfoil is chosen using Table 8.2 which is based on the $C_l - \alpha$, $C_m - \alpha$ and $C_l - C_d$ curves for each airfoil as shown in Figures 8.5, 8.6 and 8.7. The three most important criteria which are used to grade each airfoil are the $C_{l_{max}}$, the $C_{m_{\alpha}}$ and the maximum thickness t/c of the airfoil. As mentioned before, the $C_{l_{max}}$ is a pivotal parameter for take-off, hence it has a heavy weight in the trade-off table. However, the fact that the airfoil needs to be as close to neutral stability as possible makes the $C_m - \alpha$ the most important trade-off criterion for the airfoil selection. Because of the high required internal volume, the maximum thickness t/c is included since thickness impacts the storage capacity. The NACA34110 is outperformed on all aspects by the other two airfoils, hence this choice will be eliminated. Although the NACA44113 airfoil has the highest $C_{L_{max}}$, its $C_m - \alpha$ curve performs the worst in terms of neutral stability. The MH81 airfoil has a slightly lower $C_{L_{max}}$, however it performs better in terms of stability and it has a high thickness which is useful for battery storage in the wing. As mentioned in Chapter 6 this can also be beneficial because of bending relief. The MH81 airfoil is chosen for the ASAP UAV. The three-dimensional values of the MH81 airfoil are determined using Figure 8.5

5

 Criteria
 Weight
 MH81
 NACA34110
 NACA43112

 Cm α
 10
 10
 7
 4

 Cl max
 7
 8
 6
 9

8

196

137

143

Table 8.2: Airfoil trade-off table

and Equation 8.13 and can be found in Table 8.6.

Total points

8.5.2. STABILITY ANALYSIS

t/c

In order to choose a proper wing planform, a stability analysis needs to be performed in order to choose the wing sweep. In general a flying wing needs a high Leading Edge sweep angle Λ_{LE} when using a standard airfoil in order to maintain longitudinal stability. When using reflex airfoils however, this sweep does not need to be as large as usual because the airfoil itself creates a stabilizing nose-down moment close to the trailing edge of the airfoil. This requires the c.g. to be in front of the a.c., which coincides with the Neutral Point (n.p.) in a flying wing due to the lack of a horizontal stabilizer [95]. The c.g. will move more aft of the wing when the sweep angle increases, hence it should be kept as low as possible [95]. The internal layout has been determined in Chapter 7 and it can be used to determine the c.g. location. This may vary slightly with the addition of redundancies concerning the electronics, however its influence on the c.g. position is minimal due to its relatively low weight.

Note that the root chord of the wing $C_{r,wing}$ is slightly smaller than the root chord of the main body $C_{r,body}$ due to the extension of the engine at the trailing and the nose at the leading edge. According to Figure 7.1, the c.g. positions of all the individual blocks are calculated in terms of their percentual distance from the nose of the main body. Their respective weights and positions are stated in Table 8.3 Note that there is no c.g. envelope considered because the total weight of the UAV will remain virtually the same throughout the entire duration of a mission. The c.g. is positioned at the 32.12% of the root chord of the body $C_{r,body}$. The

Subsystem	Name	Mass [g]	Distance from front, along $C_{r,body}$ [%]
Camera	Cobalt 90	660	22.80
Motor control	Hacker A30-14L-V3	143	
	Servos	114	78.43
Flight control	GNC	85	42.10
Communications	S-band Antenna	55	
	S-band Transceiver	71	
	UHF-band Antenna	75	
	UHF-band Transceiver	14	68.63
See and Avoid	(TBD)	200	5.88
Batteries	LiPo batteries	5100	37.53
Structure	Total structure	2200	
Total		8717	CG location from front, along $C_{r,body}$ [%]: 32.12 CG location from front, along $C_{r,wing}$ [%]: 21.34

Table 8.3: Weight distribution of all elements, including their respective c.g. location

root chord of the wing $C_{r,wing}$ however, has its leading edge positioned 10.08% aft of the nose. This means that the c.g. of the entire UAV is positioned at 21.34% of $C_{r,wing}$. The n.p. needs to be aft of the c.g. and the

UAV still needs to be controllable using only its control surfaces and vertical stabilizers due to its lack of a horizontal stabilizer. These two reasons have resulted in a leading edge sweep angle Λ_{LE} of 15°. Its effect on the location of the n.p. is stated in Equation 8.14 [95].

$$x_{np} = \frac{C_r}{4} + \frac{b(1+2\lambda)}{6(1+\lambda)} \tan \Lambda_{0.25c}$$
 (8.14)

Using the parameters from Table 8.6, a n.p. location at 44% of the root chord C_r is obtained, which is well aft of the c.g.. The airplane shall be longitudinally and statically stable. Figure 8.11 shows how a reflex airfoil stabilizes the airplane in a disturbed state [95]. In the equilibrium position the positive M^* created by the

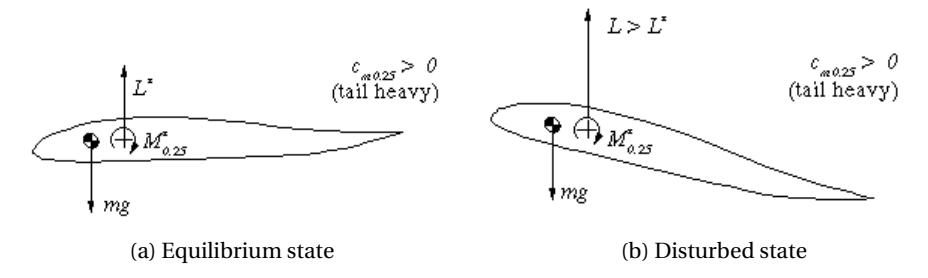


Figure 8.11: Stability of a reflex airfoil

negative lift at the trailing edge of the airfoil is counteracted by the lift force while still allowing a pitching up motion. When the airfoil is disturbed and pitches too far up, the lift force increases enough to fully counteract the positive aerodynamic moment and bring the airfoil back to its equilibrium position. The aerodynamic moment itself is given by Equation 8.15 [96].

$$C_{m_{ac}} = C_L(\frac{x_{np} - x_{cg}}{\bar{c}}) \tag{8.15}$$

Note that the MH81 airfoil is nearly neutrally stable, so its correcting effect will be minimal, though still present which is key for longitudinal stability. This near neutral stability is necessary for the minimal gust responsivity, and it will make the UAV more controllable as well.

8.6. FINAL WING PLANFORM SELECTION

Now that a basic stability analysis has been performed. The control surfaces and vertical stabilizers can be sized in order to determine a final wing planform. The sizing of these control surfaces is performed according to the control surface design of a conventional aircraft. This leads to certain limitations in the analysis of some control surfaces, as well as some possible errors that are mentioned and discussed in the next subsections.

8.6.1. ELEVONS

The ailerons can be determined using a full analysis of the necessary deflections and roll moments. The elevators however, can be only partially analyzed because the used method for analysis in only valid for a flying wing up until a certain point. The fact that both control surfaces are combined in the design by using elevons makes the analysis more complex. And the use of reflex airfoils needs engineering sense to estimate how the elevons can be determined using limited analysis tools. The use of two elevons was chosen over the use of four different control surfaces, namely two elevators and two ailerons, because of the reduced complexity during assembly and because elevons are more than sufficient enough in order to guarantee effective control of a flying wing. Although the use of four control surfaces will definitely add more controllability to the design, it will add more complexity which is not reconcilable with its added advantages to the mission.

AILERONS

The aileron analysis is performed in a very similar manner to that of a conventional aircraft. The first step when performing an aileron analysis is calculating the three-dimensional $C_{L_{\alpha}}$ slope using Equation 8.17 [97]. Equation 8.16 calculates the half chord sweep which is necessary for Equation 8.17.

$$\tan \Lambda_{0.5c} = \tan \Lambda_{LE} - \frac{1}{2} \frac{2C_r}{b} (1 - \lambda)$$
 (8.16)

$$C_{L_{\alpha_w}} = \frac{2\pi AR}{2 + \sqrt{4 + (\frac{AR\beta}{\eta})^2} (1 + \frac{\tan^2 \Lambda_{0.5c}}{\beta^2})}$$
(8.17)

The second task is choosing an effectiveness parameter for the control surface angle. This depends on the aileron chord to wing chord ratio C_A/\bar{C} which needs to be chosen in terms of the effectiveness of the ailerons, as shown in Figure 8.12 [97]. This means the designing process is iterative in the sense that parameters need be chosen to calculate the given performance of the ailerons, checking that they fulfill the stated roll requirements and adjust the chosen parameters until the ailerons do fulfill the requirements. A sensible depth of

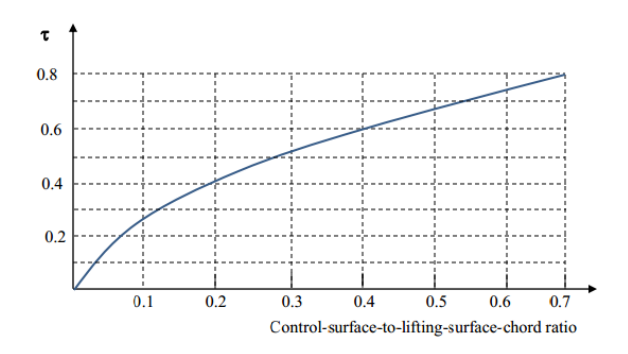


Figure 8.12: Control surface angle of attack effectiveness parameter τ

the ailerons is at 20 % of the chord length, resulting in an effectiveness parameter of $\tau = 0.41$. The spanwise location of the ailerons is initially chosen between 65% and 95% of the half span b/2 of the wing, starting from the root. These locations are geometrically denoted by $y_i = 0.65b/2$ and $y_o = 0.95b/2$. The root chord C_r , the surface area of the wing S and the wing span b are already determined. Equation 8.18 uses all of these parameters to calculate the rolling moment coefficient per deflection angle of the ailerons, namely the $C_{\ell_{\delta_A}}$ slope [97].

$$C_{\ell_{\delta_A}} = \frac{2C_{L_a}\tau C_r}{Sh} \left[\frac{y^2}{2} + \frac{2}{3} \left(\frac{1-\lambda}{h} \right) y^3 \right]_{y_i}^{y_o}$$
 (8.18)

In order to find the acting rolling moment on the UAV, the maximum deflection angle δ_{max} of the aileron must be chosen. Because the deflection angles of both ailerons have a different sign and may differ in magnitude as well, the total δ_{max} is the average of the absolute values of both aileron deflections. This value is taken as 20° , which is a general value for utility aircraft [97].

$$C_{\ell} = C_{\ell_{\delta_A}} \delta_A \tag{8.19}$$

This rolling moment coefficient is used to calculate the rolling moment itself, using the approach speed V_{app} of the UAV as shown in Equation 8.20 [97].

$$V_{app} = 1.2 V_{min} \rightarrow L_A = \frac{1}{2} \rho V_{app}^2 SC_{\ell} b$$
 (8.20)

The steady state roll rate P_{ss} is the roll rate the aircraft experiences when the ailerons are not deflected back to their zero-deflection angle position [97].

$$P_{ss} = \sqrt{\frac{2L_A}{\rho(S_w + S_v)C_{D_R}y_D^3}}$$
 (8.21)

The bank angle at which the aircraft achieves P_{ss} is found using Equation 8.22. This is used in Equation 8.23 to calculate the aircraft's rate of roll rate \dot{P} [97].

$$\Phi_I = \frac{I_{xx}}{\rho y_D^3 (S_w + S_v) C_{D_R}} \ln P_{ss}^2$$
 (8.22)

$$\dot{P} = \frac{P_{ss}^2}{2\Phi_I} \tag{8.23}$$

Finally the time t_2 necessary to achieve the required bank angle Φ_{des} is calculated using Equation 8.24 [97]. This is the major parameter when evaluating the effectiveness of the designed ailerons. If they fail to achieve

the required bank angle within the designated time frame, the ailerons will be resized and the entire analysis process needs to be repeated until the ailerons do satisfy the requirements. The same is true when the ailerons are overdesigned. The required roll capabilities of the ASAP UAV are set at a bank angle of 30° , with an acting time t_2 of 1 sec. This is quite fast compared to other utility aircraft, however this fast reaction time is necessary in order to quickly recover from an asymetric gust interference without loosing sight of possible victims in the water [97]. The fact that the aircraft is near neutral stable allows a relatively fast reaction time. And considering the ailerons act as elevators as well, this requires them to have a slightly larger surface area than regular sized ailerons to compensate for the necessary pitching moment.

$$t_2 = \sqrt{\frac{2\Phi_{des}}{\dot{P}}} \tag{8.24}$$

Note that in the final comparison in Table 8.4, a safety factor is added to the acting time t_2 of the UAV because of redundancies taken for the elevator function. And the fact that the analysis is performed using conventional aircraft methods justifies the use of a generous safety factor.

ELEVATORS

The analysis of the elevators is unconventional in the sense that they are based on conventional elevator design techniques, which incorporate a tail with a horizontal stabilizer. Keeping this in mind, and the fact that elevons are chosen for the ASAP UAV resulted in a minimal analysis of the elevators. Since the ASAP UAV will fly within a limited altitude range of a 100 m, the climb and descent capabilities are secondary to the trim condition at which the UAV will be able to fly steadily.

Since their size is already determined in the ailerons section, their trim condition is the most relevant aspect in keeping the UAV stable in cruise flight. When considering a conventional design, the first step is determining the moments that will act about the location of the main landing gear x_{mg} . There is no landing gear on the ASAP UAV, however it will land at the rear of its faring, as discussed in Chapter 4. In the elevator analysis, the rear position of the faring is taken as x_{mg} , which is at roughly 80% of the body span l_{body} . The lift at take-off is calculated in Equation 8.25 with the maximum lift coefficient $C_{L_{max}}$ and the linear forward speed of the aircraft during take-off V_R , which can be taken as the minimum flight speed V_{min} .

$$L_{to} = \frac{1}{2} \rho V_R^2 S_{ref} C_{L_{max}}$$
 (8.25)

Equations 8.26 and 8.27 are used for calculating the drag and aerodynamic moment during take-off. Calculating the induced drag requires an estimation of the Oswald efficiency factor e. Figure 8.13 [98] shows the relation between the e and the aspect ratio A for conventional aircraft. Due to its aerodynamic simplicity, the Oswald efficiency factor of a flying wing is slightly higher than for conventional aircraft. An aspect ratio of 8, results in an Oswald efficiency factor for flying wings of approximately 0.9. The parasitic drag coefficient

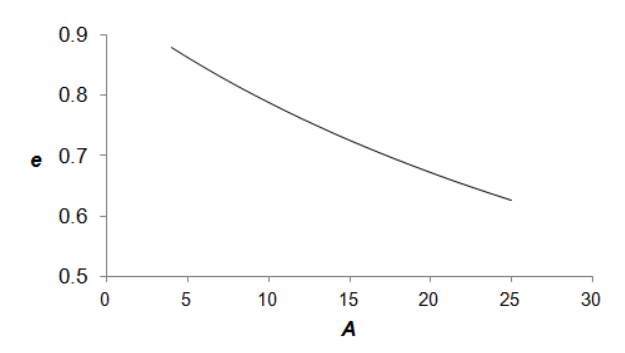


Figure 8.13: Oswald efficiency factor \boldsymbol{e} in function of a spect ratio \boldsymbol{A}

 $C_{D_{0,to}}$ and the moment coefficient $C_{mac_{wf}}$ were derived from the $C_m - \alpha$ curves and a basic three-dimensional analysis performed with the program xflr5. The $C_{L_{max}}$ was derived from the $C_{l_{max}}$ of the airfoil using Equation 8.13.

$$C_{D_{to}} = C_{D_{0,to}} + \frac{C_{L_{max}}^2}{piARe} \rightarrow D_{to} = \frac{1}{2}\rho_0 V_R^2 S C_{D_{0,to}}$$
 (8.26)

$$M_{ac_{wf}} = \frac{1}{2}\rho_0 V_R^2 S C_{mac_{wf}}$$
 (8.27)

The thrust T during take-off was determined using the very straightforward Equation 8.28 [99]. The maximum boost power P_{boost} which will be used during take-off was stated as 500W [2].

$$T = \frac{P_{boost}}{V_{min}} \tag{8.28}$$

There are several contributions to the total moment of an aircraft. However, because of the flying wing shape of the ASAP UAV, an assumptions are justified. The vertical distance from z_{mg} to $z_{c.g.}$ is the same as the vertical distance from the thrust and drag location to z_{mg} , because they all act roughly in the same plane. A second assumption is the fact that the UAV will be launched at a certain angle of attack close to the stall angle. This means the UAV will have very low angular acceleration $\ddot{\theta}$ close to zero, hence canceling out this term when calculating the necessary lift force of the elevators in Equation 8.29.

$$L_{h} = \frac{L_{to}(x_{mg} - x_{ac_{w}}) + M_{ac_{wf}} + ma(z_{cg} - z_{mg}) - mg(x_{mg} - x_{cg}) + D_{to}(z_{cg} - z_{mg}) - T(z_{cg} - z_{mg}) - I_{yy}\ddot{\theta}}{x_{ac_{h}} - x_{mg}}$$
(8.29)

Equation 8.30 determines the three-dimensional lift coefficient of the elevators. Although the formula requires the surface area of the horizontal stabilizer S_h , this is approximated with the trailing edge surface area at 80% of the local chord, along the entire span of the wing. This is a reasonable approximation because that part of the MH81 reflex airfoil generates negative lift and so can be considered as the horizontal stabilizer.

$$C_{L_h} = \frac{2L_h}{\rho V_R^2 S_h} \tag{8.30}$$

The required C_{L_h} is -0.0777 for the calculated parameters and the ones stated in Table 8.6. Although there is no verifiable ratio between the positive lift generated at the a.c. of the airfoil and the negative one generated at the twisted trailing edge, this can be considered as a reasonable value. In order to precisely determine the trim angle of the elevator, a further elevator analysis is to be performed in the Post-DSE section, Chapter 13.

The elevators and ailerons are now combined in one type of control surface, namely the elevons. This reduces the structural complexity of the control surfaces on the wing. The number of servos in the wing are reduced from four to two, however four servos are used for redundancy reasons, as discussed in Chapter 5. The size of the servos can be found in Chapter 3. The final size and the rolling characteristics of the elevons are stated in Table 8.4. A graphic representations of the elevons on the UAV can be seen in Figure 8.14

Elevon parameters	[%]	w.r.t.
y_i	65	half wing span $b/2$
y_o	95	half wing span $b/2$
$C_A/ar{C}$	20	Local chord length c
Elevon performance	value	units
Φ_{des}	30	[°]
t_{des}	1	[sec]
t_2	0.6023	[sec]
$t_2 * 1.5$	0.9034	[sec]
C_{L_h}	-0.0777	[-]

Table 8.4: Elevon characteristics

TAIL SIZING

For initial tail sizing Equation 8.31 is used to determine the tail area. In Equation 8.31 V_{ν} is the volume fraction coefficient, S_{ν} is the tail area and l_{ν} is the distance from the CG of the UAV to the 25% Mean Aerodynamic Chord (M.A.C.) of the tail chord. S and b are the wing area and the wing span. A problem occurred while searching for a volume fraction coefficient of reference UAVs with 2 vertical tails. No volume fraction coefficients are found for reference UAVs, therefore reference data of single propeller airplanes with single tail is

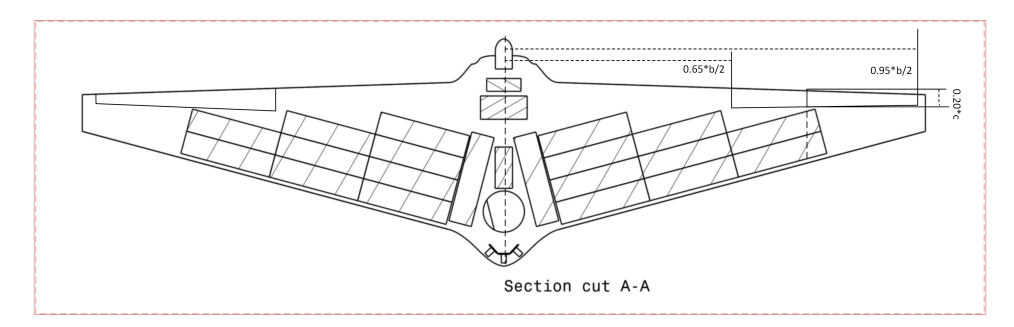


Figure 8.14: Elevon locations on the main wing of the ASAP UAV

used[100]. A V_v of 0.040 is used for this calculation, while it is assumed that l_v is 0.25 m. The area of one large tail S_v is calculated at 0.0817 m^2 , which is used as initial value for the design of the rudder. Since this is the area for one large tail, this value is divided by 2 and then multiplied by 1.1 for redundancy reasons.

$$V_v = \frac{S_v l_v}{Sh} \tag{8.31}$$

RUDDER DESIGN

In the design process of the rudder one large tail is used as explained in Section 8.6.1. Different design steps are followed as described in [97] to design the rudder for the ASAP UAV. Because the UAV is flying in heavy wind conditions, the rudders are designed to withstand the crosswinds during landing. A minimum velocity of 20 m/s is taken from Section 4.3 while the crosswind v_w is 24 m/s at 9 Beaufort. According to Mr. Stefan Knijnenburg, performance expert Air Traffic Control Netherlands, the gust crosswind will have a maximum angle of 30 degrees at the most flight extreme conditions during landing. Since the wind velocity vector is known, the wind force F_w on the UAV is calculated using Equation 8.32. Here ρ is the density of the air during landing and C_{D_y} is the side drag coefficient of the fuselage. The side drag coefficient for a flying wing is estimated at 0.3, while a conventional fuselage side drag coefficient is 0.6. A conventional fuselage is cylindrical shaped, while the fuselage of a flying wing is integrated with the wings. The protected side area (S_s) of the UAV is the side area of the fuselage and the area of one small tail. In Equations 8.33 and 8.34 the total velocity and the side slip angle are calculated.

$$F_w = \frac{1}{2} \rho v_w^2 S_s C_{D_y} \tag{8.32}$$

$$v_t = \sqrt{v_{min}^2 + v_w^2} \tag{8.33}$$

$$\beta = atan(\frac{V_{min}^2}{v_{iw}^2}) \tag{8.34}$$

Now the distance between the center of the projected side area and the UAVs c.g. d_c is determined. The rudder-span-to-vertical-tail-span ratio and the rudder-to-vertical-tail-chord ratio are initially taken as 1 and 0.3. From the rudder-to-vertical-tail-chord ratio the control surface angle of attack effectiveness parameter τ is determined at 0.51, see Figure 8.12.

The next step is to calculate the stability derivatives in y-axis and the yaw stability derivatives w.r.t the side slip angle β and the deflection angle of the rudder δ_R as shown in Equations 8.35, 8.36, 8.37 and 8.38. C_α is a function of the aspect ratio, sweep and taper of the vertical tail wing as seen in Equations 8.17 and 8.16. K_{f_1} and K_{f_2} are both fuselage parameters which describe the reaction of the fuselage to a different velocity vector. K_{f_1} is typically between 0.65 and 0.85 for conventional aircraft and K_{f_2} varies between -1.3 and -1.4. In a flying wing the effect of a fuselage is less than typical conventional aircraft because the fuselage has a more aerodynamic design and is more incorporated in the wings. Because there is no reference UAV data available, the K_{f_1} and K_{f_2} are estimated at 0.3 and -0.8.

$$C_{n_{\beta}} = K_{f_1} C_{L_{\alpha_{\nu}}} (1 - \frac{d\sigma}{d\beta}) \eta_{\nu} \frac{l_{\nu_t} S_{\nu}}{bS}$$
(8.35)

$$C_{Y_{\beta}} = K_{f_2} C_{L_{\alpha_v}} (1 - \frac{d\sigma}{d\beta}) \eta_v \frac{S_v}{S}$$
(8.36)

$$C_{Y_{\delta_R}} = C_{L_{\alpha_v}} \eta_v \tau \frac{b_R}{b_v} \frac{S_v}{S}$$
(8.37)

$$C_{n_{\delta_R}} = -C_{L_{\alpha_v}} V_v \eta_v \tau \frac{b_R}{b_v}$$
(8.38)

These stability derivatives in conjunction with equations 8.39 and 8.40 are used to calculate the rudder deflection and the side wash angle. Equation 8.39 represents the yaw moment, while Equation 8.40 gives the yaw force. A maximum rudder angle deflection of 30 degrees is given as requirement.

$$\frac{1}{2}\rho v_t^2 Sb(C_{n_\beta}(\beta - \sigma) + C_{n_{\delta_R}}\delta_R) + F_w d_c cos(\sigma) = 0$$

$$\tag{8.39}$$

$$\frac{1}{2}\rho v_w^2 S_s C_{D_Y} = \frac{1}{2}\rho v_t^2 S(C_{Y_\beta}(\beta - \sigma) + C_{Y_{\delta_R}} \delta_R)$$
 (8.40)

It is desired to have a small tail area to decrease the influence of gust and drag on the UAV, so the tail area is minimized in the design of the rudder. After iterating the tail area and the tail planform data, the tail size is determined for a side wash angle of 29.9 degrees. The rudder deflection calculated with this method is at 5 degrees. This deflection is much lower than the expected outcome. If the rudder deflection is sized for 30 degrees, the side wash angle would be 80 degrees. Therefore the tail is sized for a maximum side wash angle of 30 degrees. The tail area of one small wing is calculated at $0.0068 \ m^2$, while the width and height of the tail are 0.0673 and 0.1010 m respectively. It is expected that a mistake is made in the rudder deflection calculation. In the post DSE phase a thorough analysis should be performed to size the rudder.

A sensitivity analysis is performed to see how the rudder deflection angle reacts on a difference in UAV parameters. The data are design parameters of the UAV as shown in Table 8.5. Important design parameters are the wing area, wing span and landing velocity. Also the shape of the fuselage can easily be changed. In Equations 8.41 and 8.42, the Equations 8.39 and 8.40 are circumscribed to δ_R . These equations show the influence of the different parameters to δ_R . An increase in rudder deflection should lead to a larger control surface.

$$\delta_R = \frac{\frac{-F_w d_c \cos(\sigma)}{\frac{1}{2}\rho v_t^2 S b} - C_{n_{\beta}}(\beta - \sigma)}{C_{n_{\delta,p}}}$$
(8.41)

$$\delta_R = \frac{v_{w}^2 S_s C_{D_Y} v_t^2 - C_{Y_{\beta}} (\beta - \sigma)}{C_{Y_{\delta_R}}}$$
(8.42)

From the sensitivity analysis in Table 8.5 is concluded that there is a possibility that a mistake has been made. It is expected that the rudder deflection angle changes as the wing area or the wing span differs. It is also unexpected for the deflection angle to switch signs when there is more fuselage drag. In the post DSE phase a thorough analysis should be done to size the tail and rudder of the ASAP UAV.

8.7. FINAL PARAMETERS AND CHARACTERISTICS

The final design parameters and characteristics are presented in Table 8.6. The table is divided in multiple categories. The first, planform, presents the wing planform parameters. The second category shows the speed range of the UAV and the last category presents the UAV's aerodynamic performance and power consumption. The rationale and equations are described in the preceding sections of this chapter.

Table 8.5: The final aerodynamic and planform parameters for the ASAP UAV

Parameter	Effect on rudder deflection angle
S	An increase in the wing area has zero effect on the deflection angle. This could be explained by the multiple equations in which the wing area is used.
b	An increase in span width has also zero effect on the deflection angle. This can be explained in the same manner as the wing area.
Fuselage length	An increase in fuselage length causes d_c to decrease. This change in d_c shifts the deflection angle from positive angle towards a negative angle. A fuselage length increase by a factor 1.5 shifts the deflection angle from 1.5 to -2.8 degrees. In a conventional airplane, the tail is mounted on the fuselage. Therefore the distance from the tail to the c.g. of the UAV scales with the size of the fuselage. On the ASAP UAV, the tails are mounted on the wings and therefore there is instead of an increase in distance to the c.g. a decrease in length.
V_{min}	An increase in V_{min} is combined an increase in V_t . A multiplication of 1.5 with the minimum velocity decreases the deflection angle from 1.5 to 0.9 degrees, which is expected.
C_{D_Y}	An increase in drag coefficient of the fuselage makes the UAV more sensitive to wind force. Therefore an increase by a factor 1.5 led to a higher deflection angle of 2.2 degrees.
K_{f_1}	An increase in K_{f_1} leads to a negative increase in $C_{n_{\beta}}$. Because $C_{n_{\beta}}$ is a positive value, the deflection angle shifts, by a multiplication of 1.5 times K_{f_1} , from a positive to a negative angle, see Equation 8.41.
K_{f_2}	An increase in K_{f_2} has led to a negative increase in $C_{Y_{\beta}}$. Because $C_{Y_{\beta}}$ is a negative value the deflection angle increases, see Equation 8.42.

Table 8.6: The final aerodynamic and planform parameters for the ASAP UAV

Explanation	Parameter	Value	Unit
Planform			
Aspect ratio	AR	8	-
Leading edge sweep	Λ_{LE}	15	deg
Taper ratio	λ	0.25	-
Twist angle (tip)	ϵ_{tip}	-2	deg
Incidence angle	i_w	1	deg
Dihedral angle	Γ	0	deg
Spanwidth	b	1.602	m
Mean chord	c_{mean}	0.20	m
Wing area	S	0.321	m^2
Tip chord	C_t	80.132	mm
Root chord	C_r	320.527	mm
Volume	ν	2.803	L
Speed Range			
Minimum speed	V_{min}	18.4	m/s
Endurance Speed	$V_{endurance}$	22.2	m/s
Max range speed	V_{range}	29.2	m/s
Maximum speed	V_{max}	40.2	m/s
Performance and Power			
Acceleration due to gust	a_{gust}	2.769	m/s^2
Wing loading	$\frac{W}{S}$	275	N/m^2
Minimum power	$\overset{\circ}{P}_{min}$	223	W
Power required in turn	$P_{turn}(20^{\circ})$	247	W
Power for V_{range}	$P_{V_{range}}$	254	W
Maximum endurance	$H_{V_{endurance}}$	225	mins
Endurance for V_{range}	$H_{V_{range}}$	180	mins
Oswald factor	e	0.9	_
Glide ratio	$\left(\frac{L}{D}\right)_{max}$	20.123	_
Profile drag coefficient	$C_{D,0}$	0.014	_
Maximum lift coefficient	$C_{L,max}$	1.421	_
Lift coefficient for max endurance	$C_{L,endurance}$	0.976	_
Lift coefficient for max range	$C_{L,range}$	0.564	_
Lift coefficient for V_{max}	$C_{L,V_{max}}$	0.298	-

MANUFACTURING, ASSEMBLY AND INTEGRATION

In this chapter the manufacturing, assembly and integration of the various parts and subsystems will be analysed. The material and structure discussed in Chapter 6 need to be manufactured and assembled in a way that the structural integrity can be guaranteed during the lifetime of the UAV. Also the manufacturing and assembly has to be done in an effective matter to avoid waste and extra cost. The integration of all onboard systems is discussed here as well.

9.1. MANUFACTURING

This section will describe the manufacturing process for the ASAP UAV. First the focues will be on the molding of the composites followed by the structural components. A trade-off will be made regarding the assembly and the way the cuts will be positioned.

9.1.1. MOLDING OF COMPOSITES

It was decided in Chapter 6 to use PLA and Flax fibers for the structure of the UAV. Their individual manufacturing process will not be discussed here, however their molding process will be elaborated upon. For chopped PLA/30%Flax composites with a fiber length of 2 mm, two different molding methods can be used. Other composite production techniques will not be discussed because the products are overdesigned.

- *Injection Molding*; During injection molding, molten PLA together with the short Flax fibers are pushed into a mold by an extruder. The tapered screw in the extruder mixes the heated monomers with the reinforcements and with possible color agents. The mold, where the liquid monomers and the reinforcements are extruded in, is cooled in order to cure the composite. The advantage of this process is the quick forming of the products and the fact that a lot of different shapes can be produced. However, this method is only usable when the fiber length is less than or equal to 2 mm [101], [102].
- Long-fiber Direct Injection Molding; Long-fiber Direct Injection Molding uses the same principle as
 'regular' Injection Molding. However, the main difference between the two production processes is the
 fact that with Long-fiber Direct Injection Molding composites with fibers up to 50 mm can be produced.
 In order to achieve that, the fibers are directly seam into the extruder and a higher pressure is required.
 Disadvantages of this production method are higher complexity and higher required energy compared
 to Injection Molding.

Injection Molding is less energy intensive and less complex than Long-fiber Direct Injection Molding. Furthermore, Long-fiber Direct injection Molding has no obvious advantages over Injection Molding because very short fibers that are used in the structure of the UAV. Hence Injection Molding will be the best production method for the required composites.

9.1.2. COMPONENTS

The production processes are known, hence the manufacturing process per component can be defined. The initial challenge is deciding on the most optimal way to assemble the UAV. This is done by defining several options of assembly for the UAV and subsequently choosing the most suitable option by means of a trade-off matrix.

STRUCTURAL COMPONENTS TRADE-OFF

There are multiple ways to assemble the UAV depending on lay-out of the seams. This will be done using five trade-off criteria with assigned weights, mimicking the same technique used in the Mid-term report [2]. The

trade-off criteria and respective weighs are listed in Table 9.1. The different methods to assemble the UAV will be described in Table 9.2.

Table 9.1: Definition of the trade-off criteria of the assembly

Trade-off criteria	Definition	Weight	Explanation
Stress concentra- tions	The location of the seams w.r.t. the stress concentrations defines if the assembly lines are concentrated around stress concentrations.	10	When the seams run through the stress concentrations, additional reinforcements to the design are required to maintain structural integrity. This adds weight and complexity to the UAV that can be avoided.
Maintenance	Is the UAV easily accessible for maintenance?	8	As the UAV will need regular maintenance, its inboard systems should be easy to access.
Total seam length	The total length of the seam at which the UAV will be assembled.	6	The UAV needs to be waterproof, when the seam length is optimized, there are less problem areas for water to enter the UAV.
Manufacturability	The ease of manufacturing the parts of the UAV	5	Some parts are more difficult to manufacture than others. Therefore it is desirable to keep the complexity of the parts as low as possible.
Integrated design	This criterion defines the level of the part integration of the UAV structure.	3	Integration of different parts of the structure are beneficial for assembly and weight reduction.

Table 9.2: Assembly methods

Description	Figures	Explanation
Option 1: 2 wing parts + a top fuse-lage or removable lids (3 parts)		The wing is divided in three parts. Two of the parts consist of a wing and half of the bottom part of the fuselage as can be seen in the first figure. The top part is then used to seal the UAV.
Option 2: 2 wing parts + top and bottom fuselage (4 parts)		The fuselage exists of 2 parts, a bottom skin and a top skin seen respectively. The two wings are added to the sides to complete the assembly.
Option 3: 2 wings (2 parts)		This assembly exists of 2 symmetrical parts. The fuselage is seam in the middle and will be assembled by attaching the sides to each other.

The assembly methods described in Table 9.2 are evaluated in the trade-off table displayed in Figure 9.1.

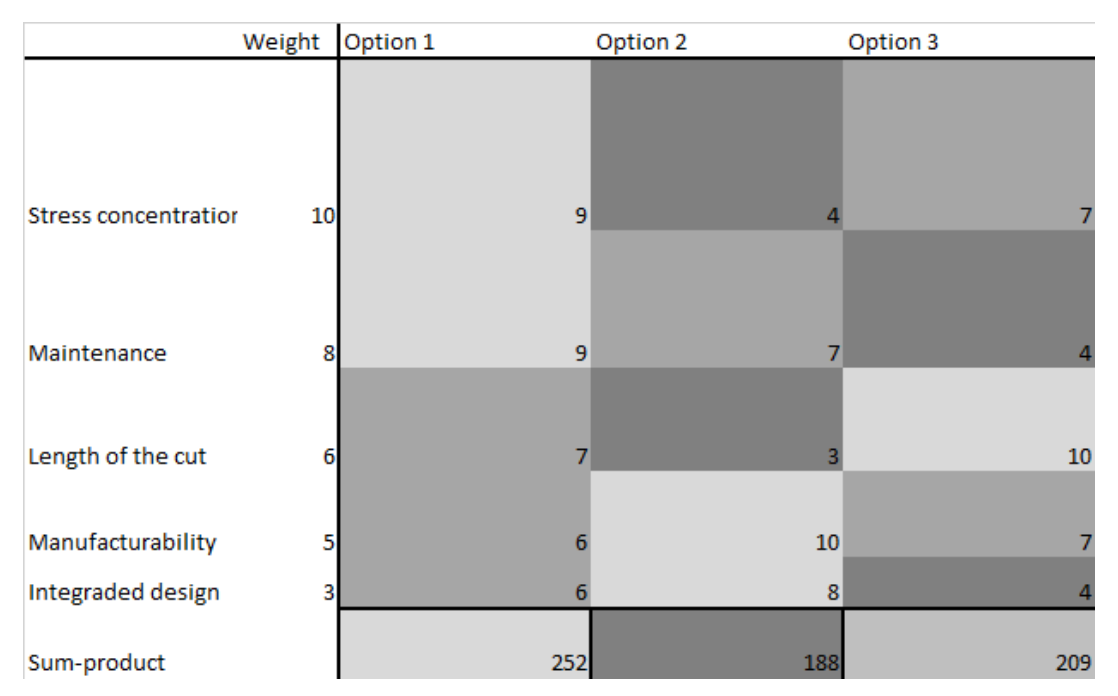


Figure 9.1: Trade-off table for the assembly of the ASAP UAV

It is clear that the best option of the trade-off is the assembly with 3 parts. An advantage is that the locations of stress concentration are not located on the seams. The location of the horizontal seams (on the

wings) can be moved further out or closer in, compared to the shown variant in Table 9.2, in order to lower the stresses at the connection, to lower seam length or to improve integration of the tail. The locations of the seams as they are in the UAV are visible in Figure 9.2.

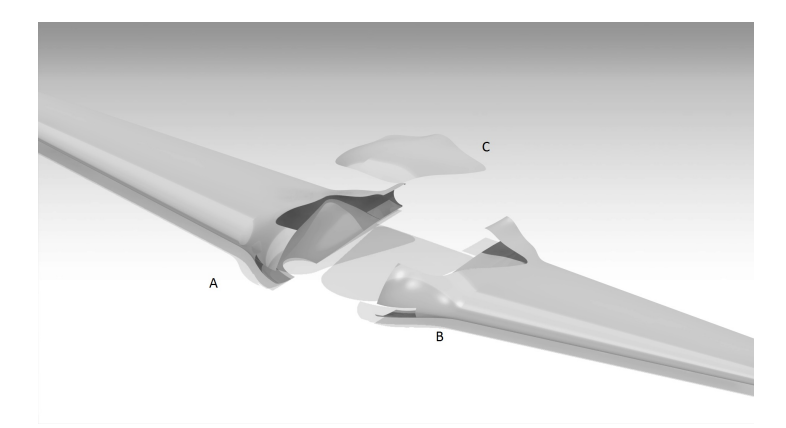


Figure 9.2: Lay-out where the chosen assembly method, showing all separate components

The three parts are made by injection molding. An outer mold will ensure a smooth outside of the wing, while a second mold will determine the thickness of the wing. This second mold is placed inside the first one and is used as a 'gate' for the composite. With the relatively high length of the wing it might be necessary to design multiple entries for the composite. Also due to these parts' complexity and size, the production cycle will be relatively long compared to the other parts. On the other hand, the top part of the fuselage has a relatively short cycle, due to its simplicity.

Besides these three main parts, also other parts have to be manufactured. These parts are:

- Camera, led light and see and avoid fairing; The fairing for the main camera as well as the 'window' for the see and avoid system can both be made separately of the other parts. Since they need to be transparent, they cannot be made from the same material as the fuselage, since PLA/Flax composites generally have a brown color. Afterwards, the fairing and window can be joined with the fuselage. Both the fairings for the see and avoid, the led lights and the camera on the underside will be made of seethrough PLA. Since the shapes of these fairings are relatively simple, producing these shapes will have a short production cycle.
- *Tails*; Each tail consists of a left section and a right section and since both tails have the same size, it is possible to make one large mold for all tail sections. Due to the small size of the tail sections, the production cycle will be short.

9.2. ASSEMBLY

In this section the assembly of the UAV will be discussed. As described in chapter 6 it is important that the joining of the different parts does not create significant extra stresses due to secondary bending or stress concentrations due to the creation of holes. The joining must guarantee structural integrity during the UAV's life time.

9.2.1. MECHANICAL FASTENING

To attach the different parts of the UAV to each other, mechanical fasteners can be used. To fulfill the all-polymer requirement, metal fasteners will be avoided. Therefore, a good polymer fastener is required, e.g. Extreme Bolt & Fastener® designs polymer bolts. A good replacement for metal fasteners is found with the PEEK Fasteners.[103] The tensile stress of polymer bolts is closely related to the temperature of the environment. Figure 9.3 shows the relation between the temperature and the tensile stress of the PEEK fasteners. With a maximum temperature of 60° C, the tensile stress of the weakest compound is still 70MPa. If this would prove to be insufficient, a glass fiber reinforcement will be used to improve the tensile stress to 300MPa. The joints are waterproof by the use of a waterproof rubber seals.

SECTION 9.2. ASSEMBLY 89

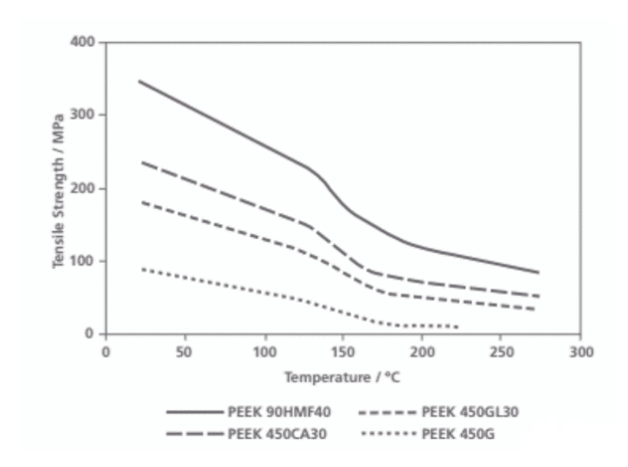


Figure 9.3: Tensile stress of PEEK fasteners dependent on fasteners and compound (addition of FG for example)[103]

9.2.2. ADHESIVE BONDING

When possible, mechanical fasteners are be avoided. Adhesive bonding is be the preferred solution, because this bonding method gives a better stress distribution then fasteners and is waterproof without extra measures. Two options are possible, an adhesive film and an adhesive paste. The maximum shear stress of these materials is explained in Section 6.1.4. The 3M Scotch-Weld Epoxy Adhesive EC-2792 B/A paste has the best thermal properties of the selection and is the only solution of the three proposed solutions that can cure on room temperature. This adhesive also performs best at low and high temperatures. Therefore this adhesive will be used to bond the components of the UAV that need adhesive bonding.

9.2.3. ATTACHMENT OF SEPARATE WINGS (CONNECTION A & B)

On the bottom side of the UAV an important connection exists between the two separate wings of the UAV, as can be seen in Figure 9.2. It is important for the structural integrity that the attachment of these two parts is made without creating significant stress concentrations which could lead to failure of the component. The options left are mechanical fastening e.g. riveting and the use of bolts and nuts or screws or adhesive bonding using a paste or films. An adhesive paste will be used. It is preferred over mechanical fastening since the stress concentrations are better for adhesive bonding.

To prevent secondary bending from the fastening, symmetric butt joints will be used to bond the two wings to each other, as can be seen in Figure 9.4. A small plate of PLA/flax composite will be attached to the upper and lower side of the joint to join the two parts to each other of 2 mm thick. The reinforcements will bonded as can be seen in figure 9.5.

For the adhesive bond an epoxy paste will be used between the reinforcement plates and the two wing parts.

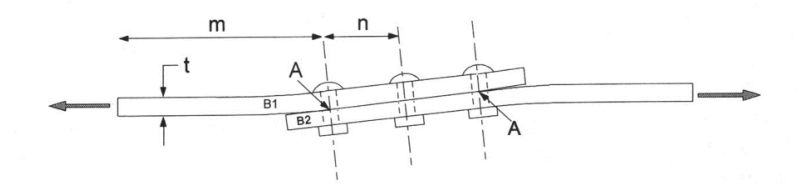


Figure 9.4: Secondary bending of shear joint

The advantage is that the reinforcement plats can be smaller and thinner because of the lack of stress concentrations and the entire reinforcement plate can be used as contact surface. The reinforcement plates can be made out of 1 mm thick plates, this is beneficial for the weight of the structure. Another advantage of adhesive bonding is that no extra waterproof matters have to be taken into account. The disadvantage of an adhesive bond is that the part cannot be removed again after bonding. However polymers possess several

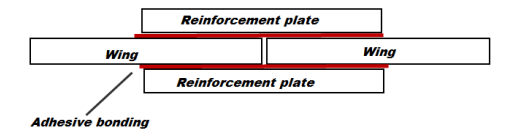


Figure 9.5: Symmetric bonded joint connecting the wing

repairing options in case of damage. The PLA resin can be again molten in a crack or the damaged part can be seam out and a new part can be bonded into its place.

Because of the advantages of bonding, the minimum weight increase and lack of stress concentrations by not creating any holes in the structure, it is chosen to bond the wings to each other.

9.2.4. ATTACHMENT FUSELAGE TOP PANEL TO WINGS (CONNECTION A AND B TO C)

The top part of the fuselage is a seam out made for maintenance reasons for easy accessibility of the engine, flight computer and other electronics. Between flights, it can be removed to check these internal components. The connection with the wing is a non-permanent joint and should be easily removed. The 2 wings at the sides are already mounted before the fuselage top panel and for this reason the location of the wings are already fixed. The fuselage top plate will be joined by a single butt joint. A reinforcement plate will be adhesively bonded on the inner side of the wing, this can be seen in Figure 9.6. On the inner side of this reinforcement plate, nuts will be fixed so that the top plate can be placed on the reinforcement panel and the bolts can be insert from outside. A seal will be placed between the connecting pars to prevent water from entering the UAV. The bolts will be sealed by putting sealing tape round the thread so also here the water is blocked from entering.

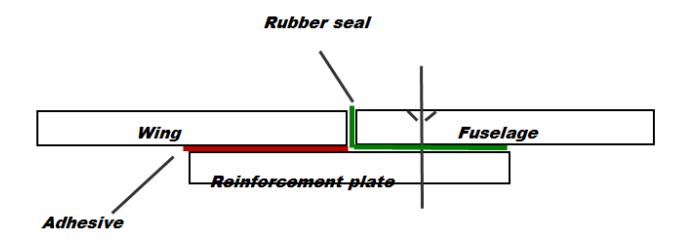


Figure 9.6: Single butt joint connecting the wings to the fuselage top plate

9.2.5. ATTACHMENT OF FAIRING

The fairing protects the camera from impact stresses during landing and gives the UAV an aerodynamic profile. It is not structural when considering lift loads but needs to be waterproof nonetheless. It is attached on both wings with an adhesive connection since it makes the connection waterproof and removal is not a requirement. The joint with the wing will be a single joint. This suffices since the main loading will be compression during landing.

9.2.6. ATTACHMENT OF TAILS AND RUDDER

There are multiple possibilities for attaching the tails to the wing surface. Using nuts and bolts, adhesive bonding or different welding methods. The main problem with nuts and bolts however is the difficulty reaching inside the wing for bolt attachment. Another possibility is to use ultrasonic, laser or solvent welding. The main disadvantage is however that the welding plants are very expensive compared to adhesive bonding. Using fillers would be preferred over welding techniques. The main problem with this is however that the vertical tail should be replaceable and maintainable. The solution for attaching the vertical tails to the wing surface is a combination of using adhesive bonding and a slide system for attachment. A local patch of polymer will be bonded to the wing surface upon which the vertical tail can then slide into place. With this system, the vertical tail will be secured to the wing during flight and can be detached afterwards. The wing will not be punctured or disturbed by nuts or welding techniques. The servos can be placed in the fairing of

the vertical tail and the wires can either be guided from the tail to the fuselage (from the outside) or a small watertight hole can be made at the location of the vertical tail. The tail will be attached and detached on multiple occasions and thus the durability can become an issue. Extra research needs to be performed to check the structural integrity of the connection considering fatigue.

9.2.7. ATTACHMENT OF ELEVONS

The control surfaces will manufactured separately and placed into the wings before the joining of the 2 main wing parts so that it is easier to access for assembly. A small shaft will be placed through the elevons

and into the wing at the inner and outboard side of the elevons. A servo at the innerside connection of the elevon will be place inside the wing and will directly drive the shaft. The shaft will be sealed at the connection to the wing and the elevon so no water can enter the UAV structure.

9.3. INTEGRATION

The last step in the production phase, is integrating the sub-systems inside the ASAP UAV's structure. These sub-systems have to be integrated step by step. These steps are:

- *Battery integration*; The batteries will be ordered at the manufacturer in battery packs. These pack will have five strings of batteries in series providing a voltage of 18.5 V. In total six packs will be placed in the UAV: two packs in each wing and two packs in the fuselage, one on each side of the camera. The battery packs in the wing will be clamped in to the wing structure and Velcro will be placed on the underside of the package to attach it to the wing. In the fuselage the same method will be applied using velcro to attach the battery pack. The batteries will be placed inside the fuselage and wing. However the operating temperatures of the battery varies between -10 and 60 degrees. The glass transition temperature of PLA is about the same temperature, 60 degrees, and this may impose some problems. The mechanical properties of the PLA degrades significantly with increasing temperature. The total heat generation of the batteries is only 0.95 *W* as explained in Section 3.6. This means that the heat generated from the batteries imposes no problem to the structural integrity of the wings. Simultaneously with the battery packs, the wiring (data and power) and the buck and boost converters will be placed inside the UAV's structure.
- *flight computer integration*; The flight computer will be placed in the middle of the UAV just behind the hole of the camera. In order to protect the flight computer from the vibrations induced during the flight, it has to be placed upon a sprung platform. For the sake of maintenance, an easy attachment and detachment method is required. Therefore, the platform together with the platform will be attached to the UAV using velcro. After the flight computer is placed inside the UAV, it will be connected to a 12*V* buck converter and therefore the battery.
- *Pitot tube*; The Pitot tube will be placed on the nose of the ASAP UAV. The best way to do that, is drilling a small hole through the UAV's nose, insert the Pitot tube from the inside through the hole and simultaneously seal the hole with a rubber ring. Finally the Pitot tube is connected with a plastic tube to the differential pressure sensor of the autopilot. Besides that, the heater of the Pitot tube is connected to flight computer and to the 12*V* buck converter, which is connected to the battery.
- Engine and engine controller integration; The engine and engine controller will be placed in the back of the UAV. First the engine controller is attached with velcro to the fuselage. Second the engine with propeller is mounted at the end of the fuselage with bolts and nuts. After the engine controller and the engine are placed, the engine controller can directly be connected to the battery and the flight computer. Subsequently the engine is connected to the engine controller.
- *Servos*; The tail servos will be inserted inside the casing of the vertical tail in order to control to have a direct connection with the rudders. The elevon servos will be inserted inside the wing between the elevon and the fuselage. After inserting the servos in the UAV, they are connected to the 12*V* Buck converter and to the engine controller.
- Communication system integration; Between the engine controller and the flight computer the transceivers will be placed. Just like the flight computer, the transceivers are sensitive for vibrations. Therefore the transceivers also will be placed on a sprung platform, which is attached to the UAV using velcro. The UHF-band antenna, which is only a small plate, will be positioned above the engine together

with the S-band antenna, which is a fin. Both antennas are connected to the fuselage with bolts and nuts. After placing the communication systems, first the transceivers are directly connected to the flight computer. Subsequently the UHF-band transceiver is connected to the 12V Buck converter and the S-band transceiver to the 4V Buck converter. The UHF band antenna is connected to the UHF-band transceiver and is directly connected to battery. Subsequently the S-band is connected to the S-band transceiver and to a 32V boost converter, which is subsequently connected to the battery.

- *S&A payload integration*; In the front of the UAV the S&A payload will be positioned. This SD payload comprises 5 cameras and a FPGA board. These cameras will be clamped between the top part of the fuselage and the bottom parts of the fuselage. The FPGA board of the S&A payload will be placed on a sprung platform, which is attached to the fuselage using velcro. After placing the S&A payload, it will be connected to the flight computer and to a 7.5V Buck converter, which is connected to the battery.
- *Led lights*; At the wingtips the led lights will be placed by adhesive bonding. Subsequently the transparent cover, made from PLA, will be glued to the wingtip. Finally the LED lights will be connected to the flight computer and to the 4V Buck converter and therefore the battery.
- *Imaging payload integration*; The last subsystem to be placed is the FLIR Cobalt 90 gimbal camera. This camera is bonded to the circular bulging by adhesives. After inserting the camera to the structure, it will be connected to the flight computer and the 12V Buck converter.

BUDGET ALLOCATION

This chapter will describe the ASAP UAVs budget allocation. The result will be coupled back to the estimations and limits posed in the Baseline Report (BR) and MTR. The chapter will commence with the weight budget breakdown in Section 10.1 followed by the total cost estimation as described in Section 10.2

10.1. WEIGHT BUDGET

Since the weights of almost all the UAV's components are known, a final weight estimation can be made. First this estimation is shown in Section 10.1.1. This is followed by the sensitivity analysis of the design in Section 10.1.2. Finally the polymer content of the design is calculated in Section 10.1.3.

10.1.1. COMPONENT WEIGTHS

The only weights that are approximated are the exact weights of the wiring and converters. Since it is hard to make an exact estimation, it was chosen to add a weight fraction of 5% to the total weight. This weight fraction equals approximately $450 \ gr$. In Table 10.1 the total weight estimation is shown. The final weight for

Components	Weight	
Engine + controller	190	gr
Servos	108	gr
S-band antenna	55	gr
UHF-band antenna	5.7	gr
S-band transceiver	71	gr
UHF-band transceiver	14	gr
See & Avoid payload	200	gr
Imaging payload	660	gr
NavStik mainboard	5.4	gr
NavStik interface board	8.6	gr
Watchdog timer	2.9	gr
Led lights	1	gr
SD card	0.5	gr
Pitot tube	58	gr
Wiring+converters+other systems	447	gr
Battery	5100	gr

Table 10.1: Component weight breakdown

the ASAP UAV equals approximately 9.4~kg. This is below the estimated weight budget of 10.5~kg from the Baseline report [1] and below the design weight of 10~kg from the Midterm report [2]. However, it is about 400 grams more than the 9~kg estimated in the Midterm report [2]. This is due to the fact that several sub-systems and the battery degradation were not yet taken into account.

2200

300

35

53

9452

gr

gr

gr

gr

Wing + Fuselage

Redundancy weight

Fairing Tails

Total

10.1.2. SENSITIVITY OF THE DESIGN

The weight breakdown presented here is very detailed, up to component level and including uncertainties for wiring and converters. However, the weight could increase rapidly if some of the COTS-systems are deemed insufficient after testing in the post-DSE phase as described in Chapter 13. The famous snowball-effect will result in even more weight since more batteries will be needed to account for increased weight. However, since the external layout of the wing is also dependant on the internal systems by setting a lower limit on internal volume (Chapter 8, an increase in system weight will also change the external layout. This can result in more structural mass or lower aerodynamic performance which in turn requires the use of extra power, thus weight. As one can observe the design is very sensitive to small increases in system weight or power consumption and therefore special care must be taken to verify the estimated performance of all internal systems.

10.1.3. POLYMER CONTENT OF FINAL DESIGN

With the total weight shown the polymer content of the ASAP UAV is determined. Requirement CUS-20 (Chapter 12) stipulates that the maximum non-polymer content in the construction will be 5%, including the propulsion installation. Using Table 10.1 one can calculate the total polymer content which equals over 81%. The structural polymer content is approximately 98%, calculated with the propulsion installation consisting of motor, propeller and batteries.

10.2. COST BUDGET

The cost estimation for the ASAP UAV is performed using empirical relations. These relations are adapted from the cost estimation methods of Roskam, RAND and DACPA and must be used within the applicable range for the results to be valid [104]. The adaptations for the cost estimation are there to provide indicative equations for UAVs smaller than manned aircraft. For larger UAVs as the Predator or Global Hawk the method shown is not valid [104]. The estimation method is a bottom-up estimation which requires full knowledge of the UAV.

The estimation of costs is performed for the entire UAS rather than just the UAV. This system includes support systems like launchers and ground stations. The cost estimation can generally be divided in 4 different categories, being:

- Research, Development, Testing and Evaluation (RDT&E) (Section 10.2.1)
- Manufacturing and production (Section 10.2.4)
- Operational cost (Section 10.2.5)
- Disposal

The total life cycle cost is given by Equation 10.1. Usually disposal costs are not included in the life cycle cost. This disposal cost will also be omitted this chapter.

$$C_{LC} = C_{RDTE} + C_{Manf} + C_{Ops} + C_{Disp}$$

$$(10.1)$$

Since the empirical relations were established using data from the year 2004 there will be a factor called Cost Escalation Factor (CEF), which accounts for inflation. This CEF is shown in Equation 10.2. The Producer Price Index (PPI) is retrieved from the Bureau of Labor Statistics: the average PPI in aerospace manufacturing was around 150 in 2004 where the PPI for 2014 is estimated to equal roughly 220 [105]. This gives a CEF_{2004} equal to 1.4667.

$$CEF_{TY} = \frac{PPI_{now}}{PPI_{TY}} \tag{10.2}$$

10.2.1. RESEARCH, DEVELOPMENT, TEST AND EVALUATION (RDTE) COST ESTIMATE

This phase involves all services, materials and personnel necessary to design, integrate and test the development of a single UAS. The total costs related to Research, Development, Testing & Evaluation (RDTE) are given by Equation 10.3.

$$C_{RDTE} = C_{Des,RDTE} + C_{HW,FT,RDTE} + C_{FTO,RDTE}$$
(10.3)

Where the first term on the right are the design costs, followed by the hardware and operation prices to perform the flight test(s) required to validate the design. These separate costs are described in the following subsections.

DESIGN

The costs related to the design can again be split up into several other aspects. These are presented in Equation 10.4. The design costs are the engineering labor cost Including UAV, payload, ground control stations, Aircraft Launch & Recovery Equipment (ALRE) and support equipment.

$$C_{Des,RDTE} = C_{AV,Des,RDTE} + C_{PL,Des,RDTE} + C_{GS,Des,RDTE} + C_{ALRE,Des,RDTE}$$
(10.4)

Where the engineering labor ($C_{AV,Des,RDTE}$) is calculated using Equation 10.5. Hr is the amount of hours spent on the design project and R_{Engr} is the burdened hourly rate. For the DSE design team, the man-hours equal to the amount of hours per week (40) multiplied with the number of weeks (10) and the number of designers (10), resulting in 4000 man-hours. A typical burdened rate for starting engineers is \$ 100 resulting in the engineering labor cost of \$ 400,000 [106].

$$C_{AV,Des,RDTE} = Hr \cdot R_{Engr} \tag{10.5}$$

The payload cost ($C_{PL,Des,RDTE}$) is zero, as well as the ALRE development costs due to the purchase of commercial off-the-shelf (COTS) systems.

For the estimation of the ground control station design costs $C_{GS,Des,RDTE}$ Equation 10.6 is used. This equation shows an empirical relation between the empty weight of the UAV (almost 5 lbs for the ASAP UAV) and the ground control costs, including testing and software design. This cost needs to be corrected for the inflation using the CEF based on 2004. Equation 10.6 is based on statistics involving large and military UAVs, among others. This results in an overestimation of the ground station design costs. The ASAP UAV ground control station should be as simplistic as possible, making the UAV controllable by a controller with minimal training. Therefore a correction factor of 0.7 is applied to this equation [104]. A more thorough study of the ground station characteristics should be performed for a more accurate design cost estimation, resulting in a ground station design cost of approximately to \$ 100,000.

$$C_{GS,Des,RDTE} = $20,000 \cdot W_E \cdot CEF_{2004}$$
 (10.6)

Finally, all these costs can be added using Equation 10.4 to obtain the total costs related to the Design of the ASAP UAV. This results in a $C_{Des,RDTE}$ equal to \$500,000.

DEVELOPMENT TESTS

This section describes the costs involved in testing during the development phase. Examples of tests are wind tunnel tests, structural tests, software tests and tests to check the interference between different subsystems. It will likely be costly to perform tests in specialist facilities and since the UAV falls in the mini-UAV category most test will be performed using a prototype. The cost associated to the hardware to perform a flight test is given by Equation 10.7.

$$C_{HW,FT,RDTE} = C_{AV,Sys,RDTE} + C_{Manf,RDTE} + C_{Matl,Manf,RDTE} + C_{QC,RDTE} + C_{GS,HW,RDTE}$$
(10.7)

Here the $C_{AV,Sys,RDTE}$ are the critical components for the flight test. For first tests the imaging system, which is the most expensive COTS system, could be replaced with a cheap weight to simulate the presence of this system. Table 10.2 (excluding the Imaging payload) is used giving a total cost equal to \$ 1748. Note that components may decrease in price per unit for bulk purchases. However, this effect is not incorporated in the cost estimation.

Components	Cost (\$)	
Engine + controller	100.00	[107]
Servos	95.00	[108]
S-band antenna	25.00	
UHF-band antenna	80.00	
S-band transceiver	10.00	[109]
UHF-band transceiver	200.00	[109]
See & Avoid payload	450.00	[5]
Imaging payload	30,000.00	[21]
NavStik mainboard	213.00	[20]
SD card	59.00	[35]
Wiring+converters+other systems	unknown	
Battery	516.00	[110]
Total	31,748.00	

Table 10.2: Cost for Commercial off-the-shelf (COTS) systems on board of the ASAP UAV

The manufacturing costs of the prototype for flight test are estimated using statistics from home-built and small UAS. These costs are calculated using Equation 10.8.

$$C_{Manf,RDTE} = 10.4W_E^{0.605} f_{Matl} \cdot R_{Manf}$$
 (10.8)

Where the empty weight is again equal to 5lbs, f_{Matl} is equal to 1.98 for composite airframes (making the equation applicable for different material types) and R_{Manf} is equal to \$ 100 (hourly rate for the manufacturer) [104]. This relation assumes that the airframe of the UAV is comparable with model aircraft of the same empty weight which may be inaccurate for the monocoque design of the ASAP UAV. The resulting prototype cost estimate will be \$ 5500 in terms of manufacturing, excluding material and subsystems.

The material costs are \$ 8.89 for the PLA and \$ 1.36 for flax for the airframe of 5 *lbs* [111], resulting in total material costs equal to \$ 10.25.

The ground station costs for the flight test can be lower than the final ground station costs since the functionality of this station can be limited for flight tests. Here it is assumed that a laptop with controller is sufficient so the ground station costs for the flight test will not be more than \$ 2000. Finally, a factor due to quality control will be involved. It is derived from reference [104] that a total of 10% of the labor hours are spent on quality control, or \$ 550 when comparing with manufacturing costs above. This results in a total flight test hardware cost equal to \$ 9810.

FLIGHT-TEST OPERATIONS

Flight tests will be used as a testing environment for the ASAP UAV and will include launch from rail, flight envelope testing and landing. Estimating the costs related to this testing is only possible when it is fully known how this test will be performed. The number of people involved for the flight test, the flight test interval and duration, the location and the additional safety precautions all influence the final costs associated.

10.2.2. FINANCING

In the RDTE phase of the project there will also be considerable costs arising mainly from the possible project financing, due to interest on taken loans. The exact costs can only be estimated after an accurate estimation of the total RDTE costs of the project and if the interest rate is known. Financing can add as much as 10% to the RDTE costs of a project.

10.2.3. TOTAL RDTE COST

Now all costs involving the RDTE costs are estimated, the total RDTE cost estimation is calculated using Equation 10.3. The final value for C_{RDTE} is equal to \$510,000. The sidenote is that this value may be very conservative and that due to financing or unexpected design throwbacks this cost may increase rapidly.

10.2.4. MANUFACTURING COST

The next phase in the cost estimation for aircraft is the manufacturing phase. The total manufacturing costs are described by Equation 10.9 where C_{Matl} equals the material cost of flax-PLA composite for a single UAV. The payload costs C_{PL} can be directly obtained from Table 10.2 and equal \$ 31,748. The mold cost for injection molding and the labor cost of manufacturing and assembling the ASAP UAV are estimated using [112].

$$C_{Manf} = C_{Matl} + C_{PL} + C_{Mold} + C_{Labor}$$

$$(10.9)$$

These molding costs are estimated from the size of the required mold. As explained in Chapter 9 the UAV fuselage will be constructed from 3 separate cast parts; two halves of the wing/fuselage and a top panel. The mold should be 75 mm larger than the to-be-cast shape in every possible direction [112]. This way the total volume of the mold is calculated. The price follows directly from the dimensions of the mold described by the relation shown in Equation 10.10.

$$C_{Mold} = \$1000 + 0.45 A_{mold} t^{0.4} \tag{10.10}$$

Where A_{mold} is the largest surface area of the mold and t is the smallest length of the molds exterior dimensions. For the three molds in total a price of \$12,000 is calculated. However, since these molds will be produced from quality steel it will be possible to manufacture multiple UAV parts from one set of molds, reducing the mold cost per UAV. The amount of UAVs from one set of molds is set to 1000 which is a realistic value [112].

The man hours related to the production of the UAV is directly related to the dimensions of the object to be molded as well as the complexity of the object [112]. The equation for these costs, C_{Labor} , is given by Equation 10.11.

$$C_{Labor} = 45(X_i + X_o)^{1.27} \cdot R_l abor$$
 (10.11)

The values X_i and X_o are the internal and external complexity of the injection molded parts, respectively, and R_labor is set to 50 \$/hr. The complexity factors can be directly determined from the complexity of the part using Equation 10.12.

$$X_i = 0.01 N_{curve} + 0.04 N_{hole} (10.12)$$

Where the number of curves and the number of holes can be counted from the three-dimensional parts. Finally, the total costs related to labor required for manufacturing equals \$4300.

Now all manufacturing costs are calculated, the cost per UAV is calculated and equals \$48,000. Note that this is the price of a single UAV, including a new mold and excluding the learning effect which will be present. These effects will be described for the final cost in Section 10.2.6.

10.2.5. OPERATIONAL COSTS

The operational costs of the ASAP UAV will be estimated per 200 flight hours as described in Chapter 5. The operational costs are determined using Equation 10.13 (adapted from [104]).

$$C_{Ops} = C_{Fuel} + C_{Pers,Dir} + C_{ConMatl} + C_{ALRE} + C_{Replace}$$
(10.13)

First the cost for fuel C_{Fuel} will be calculated. Since the ASAP UAV is entirely powered by batteries the fuel cost, is the cost per kWh of electricity, multiplied by the amount of flight hours per year and the battery capacity. With an average electricity price of 0.2 kWh and an average mission duration of 2 hours for 365 missions every year, the annual power cost equals \$ 186.15 for a 1250 kWh battery pack.

The largest contribution to operational costs are the personnel costs (C_{Pers}). In total 3 roles can be identified: one UAV operator trained to pilot the UAV, if necessary, in the ground control station. This person will be present for the 200 flight hours at a rate of almost \$ 90 per hour [104]. The second person will perform maintenance every 20 flight hours and will monitor a flight envelope test. The rate of this person equals \$ 60 per hour [104]. The last person involved is, in the case of KNRM operation, a volunteer which will perform post-flight maintenance as described in Chapter 5. This person will not be paid, however the industry cost for employee delay is equal to $\[\]$ 15.80 per hour, equivalent to \$ 21.50 per hour [113]. Total personnel costs for 200 flight hours of the ASAP UAV will equals almost \$ 32,000.

Next the cost for consumable parts is determined. This cost is determined by the replacement parts necessary to maintain the UAV as described in Chapter 5. The replacement parts and corresponding rates are described in that chapter as well. Using the costs of the parts as described before in 10.2.4, the total cost for consumables $C_{ConMatl}$ equals \$ 1420.

Next the costs for the ALRE is estimated. This cost is purely based on supplier prices since no statistics exist due to the broad range of options for ALRE. As stated in Chapter 4, the chosen launch method is a pneumatic catapult supplied by Troy. The purchase price for this COTS system is equal to \$ 22,000 [44]. The additional systems required for landing are negligible in price when compared to the take-off systems and are thus not included here.

Finally the replacement cost of the UAV is included in operational costs. As described in Chapter 5 it is expected an ASAP UAV is lost every 2220 hours. In the case of UAV loss a replacement needs to be manufactured for the aforementioned manufacturing costs equal to \$48,000. This gives a replacement cost of \$4300 per 200 flight hours.

Now all elements contributing to the operational costs are determined, the total operational costs, C_{Ops} , can be calculated. The total costs for the operational phase of the ASAP UAV equals \$ 38,000 per 200 flight hours. A note here is that some elements, like support system maintenance & replacement or training programs are not included in these costs. Therefore the number presented here is deemed conservative for the ASAP UAV.

10.2.6. RETURN ON INVESTMENT AND BUSINESS STRATEGY

After the elements determining the life cycle cost are all determined, the Return on Investment (RoI) can be developed. Since this is a commercially initialized project, the target is to make a profit from the ASAP UAV. In order to determine a selling price, an estimation has to be made regarding the amount of UAVs to be sold. However, as pointed out in the market analysis in the BR and MTR, there are multiple uncertainties. This makes it close to impossible to estimate the amount of UAVs to be sold at this point; a more thorough market analysis should be performed in the post-DSE phase. For now the amount of UAVs is varied in order to give an estimation. This variation of cost is presented in Table 10.3. Table 10.4 presents the results of the cost estimation in euros instead of US dollars by applying the following rate: 1 USD equals 0.73 EUR as of June 29, 2014.

From these tables, the following points of interest should be taken. First, the row showing the costs for a

Table 10.3: Total cost per phase of design as well as service contract price per flight hour for the ASAP UAV, per number of UAV sales, in US dollar

				UAV Sales	UAV Service contract
Number of sales	RDT&E (<i>US</i> \$)	Manufacturing (US\$)	Operations (US\$)	Total costs (US\$)	US\$/flight hour
1	531,808.25	47,910.58	400,034.18	979,753.01	489.88
10	531,80.83	38,271.64	400,034.18	491,486.65	245.74
100	5,318.08	36,574.17	400,034.18	441,926.44	220.96
1000	531.81	35,755.04	400,034.18	436,321.03	218.16
10000	53.18	35,131.67	400,034.18	435,219.03	217.61
100000	5.32	35,131.67	400,034.18	435,171.17	217.59

single UAS directly correspond to all aforementioned costs for RDT&E, Manufacturing and Operations. The operational cost is calculated for 3 years in which 10 cycles of 200 flight hours are expected as mentioned in Chapter 5. The column showing total cost is a simple addition of all category costs. The cost per flight hour is calculated by dividing the total costs through the expected number of flight hours.

Also, one can easily see the total cost decreases when the number of UAS sales increases. This is due to a couple of reasons. First, as mentioned before, the injection molds can be used for multiple UAVs. For the cost

$Table 10.4: Total \ cost \ per \ phase \ of \ design \ as \ well \ as \ service \ contract \ price \ per \ flight \ hour \ for \ the \ ASAP \ UAV, \ per \ number \ of \ UAV \ sales, \ in$
Euro

	UAV Sales	UAV Service contract
Number of sales	Total costs (€)	€/flight hour
1	715,219.70	357.61
10	358,785.25	179.39
100	322,606.30	161.30
1000	318,514.35	159.26
10000	317,709.89	158.85
100000	317,674.95	158.84

estimation it is expected that one set of molds will produce 1000 UAVs. Secondly, the learning curve means that the manufacturing costs will decrease rapidly and stagnate at a lower price at approximately 1000 UAVs. The learning factor assumed for the ASAP UAS equals 0.95. This means that for a doubling in produced units the cost will have decreased by 5%. For aircraft the learning factor is usually between 0.7 to 0.9 but since the ASAP UAV is not as complicated and will comprise of relatively few parts it is assumed that there is a low learning effect [114]. The large decrease in cost is due to the fact that the RDTE costs can be split between several UASs. As one can see this cost varies rapidly when producing 1 or 5 UASs but will decrease to only a small contribution to the total costs in the case of several hundred UASs. Finally, a customer may decrease the cost per UAS even more by using multiple UAVs on the same ALRE and ground station. These effects on cost are not incorporated since this scenario is very customer specific.

For the market integration of the ASAP UAS, two strategies could be followed. The first method is to sell the UAS directly to the customer, thereby requiring this customer to invest heavily. A second and more realistic way of providing the ASAP UAS may be with a service contract. This way the customer buys the rights to use the UAS, not to own it. The maintenance will be conducted by the contractor and this does not require a large investment up front by the customer. The service contract will also replace the UAV, should it have failed. From Chapter 5 it was concluded that the ASAP UAV will catastrophically fail every 2220 flight hours. This statistic is used to incorporate the expected replacement costs of a lost ASAP UAV. Since the manufacturing price (without learning effect) is equal to almost \$48,00 and a UAV needs to be completely replaced after 2220 hours the additional cost per flight hour is equal to \$21.60.

Coupling back this cost estimation to the preliminary cost estimation as performed in the BR, one can see that the total costs are significantly higher. However, when comparing the manufacturing price for one UAV (learning effect excluded) one can see that the aforementioned \$ 48,000 can compare to the maximum estimated \$ 57,000 (€42,000) in the BR. The operational costs do not correspond as well. The total comparison between the preliminary cost budget and the final cost estimation can be seen in Table 10.5. Finally it can

Table 10.5: Comparison between Baseline Report (BR) Cost Budget and Final Report (FR) Cost Estimation

Cost	Unit	Min	Max
Manufacturing (BR)	\$	38,000	57,000
Manufacturing (FR)	\$	35,000	48,000
Cost per flight hour (BR)	\$	475	610
Cost per flight hour (FR)	\$	n.a.	n.a.
Total cost per flight hour (BR)	\$	1060	1360
Total cost per flight hour (FR)	\$	207	468

be said that Mr. Moleman, head of operations of the Koninklijke Nederlandse Reddings Maatschappij, has expressed his general interest in the design due to its low cost and innovative solution and thinks the UAS as presented can be a viable option in future Search & Rescue operations.

SUSTAINABILITY

Sustainability of the ASAP UAS is an essential aspect of both the design phase as well as the production phase. Product sustainability has as a primary influence on the environment but it also has social and economic impacts [115]. This makes it vital that the designer or design team makes a clear sustainability development strategy which is spread out over both material selection and manufacturing and distribution systems, keeping the required performance and costs demanded by the client. The sustainability of a product can be improved by design changes such as a different material selection, reduction in energy usage, lean manufacturing, etc.

This section will start with a short recap of the sustainability described earlier this report. This is followed by a description of the environmental sustainability of the production process. Sustainability of the total project can only be achieved by sustainability in all three categories, social, economic and environmental. For a more theoretical approach on sustainability, including the methods to reach social and economic sustainability, the reader is referred to the chapter Sustainability in the MTR [2].

11.1. DESIGN RECAP

This section describes the sustainability as described in preceding chapters. Special attention is paid to the biodegradability of the Flax-PLA bio composite in Chapter 6. Furthermore, the lithium-polymer battery is completely recyclable after its lifetime as described in Chapter 5. According to Chapter 4 the charging of this battery should preferably be executed using electricity from renewable sources as wind or solar. Sustainability is also obtained by minimizing the power consumption of the UAV by selecting power-efficient subsystems (Chapter 3 and selecting an efficient planform and airfoil (Chapter 8).

Concluding, all components of the ASAP UAV are categorized in one of three categories: a subsystem or component will either be recycled, treated as waste or degrade over time. The result for the entire UAV is shown in Figure 11.1. As shown only 5% of the total UAV will be considered waste. This 5% is mainly made

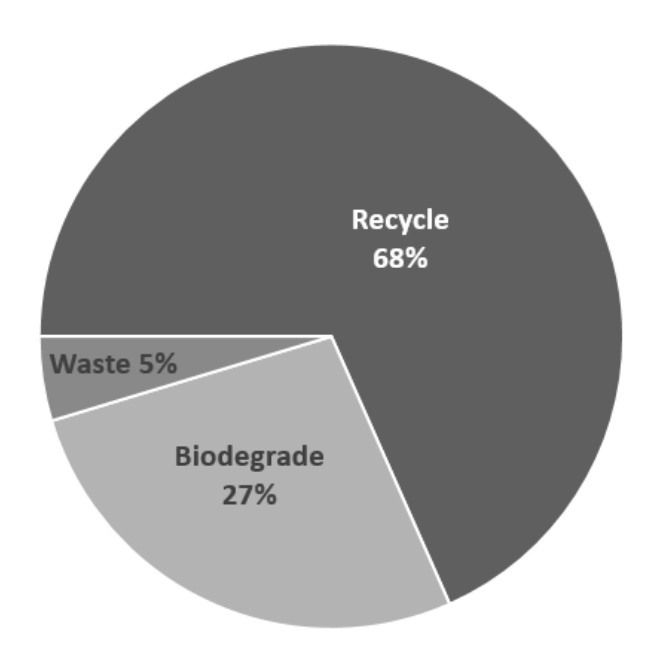


Figure 11.1: Pie-chart showing the mass-percentage of the UAV in terms of recyclable, biodegradable and waste creating

up from PCBs which will in practice not be recycled. However, 95% of the UAV is either re-used or degraded over time. The airframe will, as mentioned, completely degrade whilst systems as the engine, batteries and imaging payload will be completely recycled.

11.2. Environmental sustainability in UAV production

The most common aspect of sustainability is the environmental sustainability. For the ASAP UAS the effect on the environment of the subsystems is described in 11.1. What remains is an analysis of the production process in terms of environmental sustainability. This analysis is performed using the EIO-LCA.-method from Carnegie-Mellon University [116]. This method incorporates economic share per category and uses this as a factor to calculate the environmental impact in terms of carbon cost, emissions and power consumption. For the analysis of the ASAP UAV the category 'Aircraft Manufacturing' as well as 'Other Aircraft Parts Manufacturing' were used, using a producer price value of one million US Dollar (USD). This data was then filtered to only include relevant categories for the all polymer ASAP UAV since the supply chain includes the mining, refining and shaping of metal materials. Since the ASAP UAV will be a non-metal aircraft these categories will not be included in the supply chain. Also all categories having a 0% effect in aircraft manufacturing are omitted. The resulting table is added in Appendix A and not shown here for clarity.

After obtaining the output data from the EIO-LCA.-method the environmental results were analyzed. The results can be found in Figure 11.2. This figure shows the emissions for the nine top contributors to aircraft manufacturing. The total emission in metric tonne is shown in the figure legend. As one can see, carbon dioxide is by far the largest emission category for the production of the UAV. Most of the carbon dioxide emission is due to power generation and component transportation, which is also visible in Figure 11.2. These contributions could be reduced by producing and assembling the UAV in one location, minimizing the need for transport, and by using energy from a sustainable source as solar or wind. This will also directly decrease CO, SO2 and NOx emissions in the production process. The main CO emissions are due to tools and machines used in aircraft manufacturing. By minimizing the need of complex machinery for the production (only an injection molding facility is needed) this contribution is minimized for the ASAP UAV.

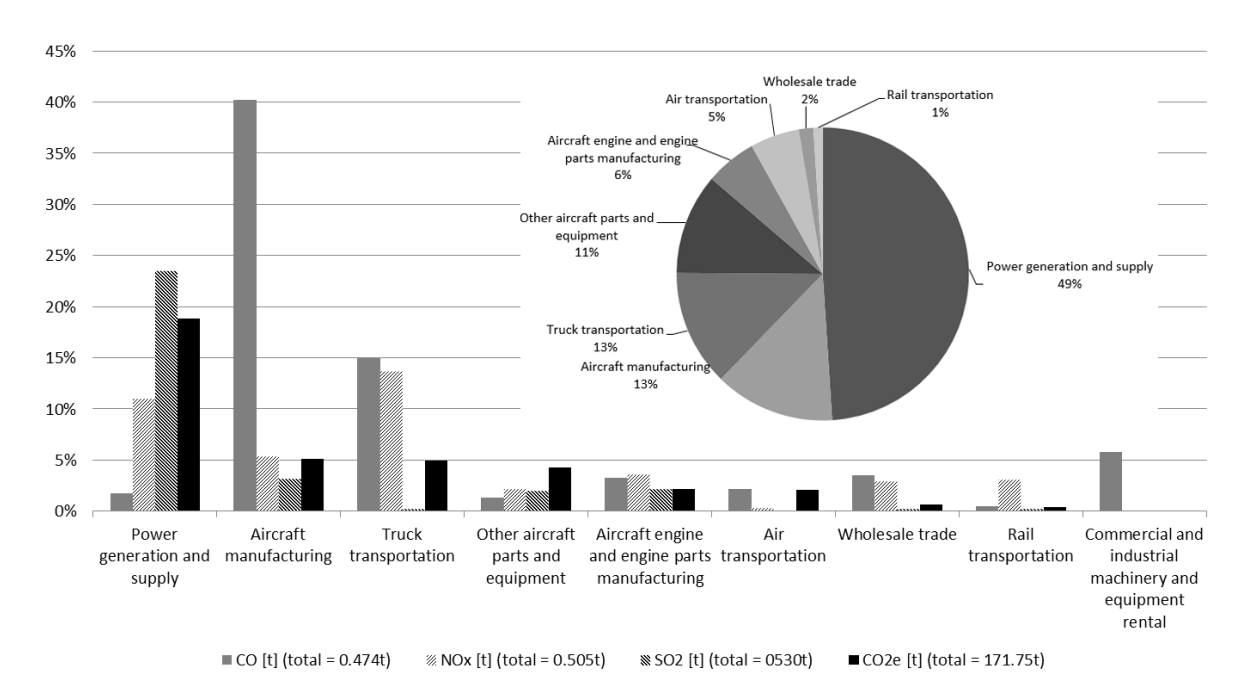


Figure 11.2: CO, NOx, SO2 and CO2 emissions for the nine largest contributors to the Aircraft Manufacturing sector and a pie chart showing the CO2 contributions of different industries

Concluding one can say that the environmental impact of the production process should be minimized by decreasing the transport and power consumption during this process. Furthermore the power necessary can be drawn from a renewable source as wind or solar. Lastly, by minimizing the amount of machining and tools the emissions as well as the additional materials for these machines can be decreased.

VERIFICATION AND VALIDATION

This chapter concerns the verification and validation of the design tools and the final design. First, the performance tool is verified in Section 12.1 following by the verification of the rule of mixture and the structures tool in Sections 12.2 and 12.3. In section 12.4, the design is verificated with the requirements.

12.1. PERFORMANCE TOOL

The UAV performance tool is based on an iterative script that calculates the required power for different airspeeds. This tool is also described in the MTR [2]. In order to verify the correctness and accuracy of the results, two test cases are calculated analytically and compared with the power tool output.

First, assuming steady symmetric flight where lift (L) equals weight (W), the required power is expressed as a function of C_L and C_D using Equations 12.1, 12.2 and 12.3.

$$L = \frac{1}{2} \cdot \rho \cdot V^2 \cdot S \cdot C_L \tag{12.1}$$

$$C_D = C_{D,0} + \frac{C_L^2}{\pi \cdot AR \cdot e} \tag{12.2}$$

$$P_{req} = \sqrt{\frac{2 \cdot W^3 \cdot C_D^2}{\rho \cdot S \cdot C_L^3}} \tag{12.3}$$

Next, the power required for optimal cruise flight is given for the minimal thrust required, or maximal $\frac{C_L}{C_D}$ as explained in [117]. The minimum thrust required is obtained by differentiating the required power with respect to the airspeed, as demonstrated in Equation 12.4. The optimal cruise speed is obtained by solving Equation 12.5 for airspeed (V).

$$T_{req} = \frac{P_{req}}{V} \tag{12.4}$$

$$\frac{dT_{req}}{dV} = 0 ag{12.5}$$

Now the cruise speed is known, the lift and drag coefficients are evaluated using Equations 12.1 and 12.2. The total power required for sustaining cruise flight is found by evaluating 12.3. The total power demand from the batteries is obtained from Equation 12.6 where all efficiency factors and a safety factor for extra power demand caused by disturbances are incorporated.

$$P_{cr} = \frac{P(V_{opt})}{\mu \cdot \nu} \tag{12.6}$$

Next, these calculations are performed for two different designs and the results are compared. The constant values in both the computational model and analytical verification model are listed in Table 12.1 Given Table 12.2, the computed characteristic cruise flight values show only minor deviations from the analytical computed values. These deviations are most likely caused by round-off errors due to the finite resolution in the matlab script. Therefor the flight performance tool is verified.

12.2. RULE OF MIXTURE

The next step in the verification and process, is validating the material properties calculated with the Rule of Mixture. In Table 12.3 a comparison is made between the calculated properties of certain composites and the properties of the same composites given by the manufacturer. For the chopped, unidirectional and woven

Table 12.1: Constants for the verification of the flight performance tool

Parameter	Value	Dimension
Oswald factor	0.9	[-]
Grav. acc. (g)	9.81	$\left[\frac{m}{s^2}\right]$
UAV mass	9.0	[kg]
ρ	1.225	$\left[\frac{kg}{m^3}\right]$
$C_{D,0}$	0.014	[-]
Drivetrain efficiency (μ)	0.60	[-]
Payload buffer (v)	0.90	[-]

Table 12.2: Performance tool verification results

Input	Tool	Verification	Tool	Verification	Dimension
Aspect Ratio (AR) Wing loading (W/S)	8 275	8 275	10 400	10 400	
Results					
$V_{cruise} \ C_L \ P_{cruise}$	29.2 0.564 254	29.2 0.563 254	33.3 0.631 258	33.4 0.629 259	[\frac{m}{s}] [-] [W]

Table 12.3: Material properties of several calculated composites and existing composites

Material	Tensile stress	Young's modulus	Density
	[MPa]	[GPa]	$[g/cm^2]$
Calculated:			
woven PLA/40%Flax	105	10.5	1.31
UD PLA/40%Flax	200	20.1	1.31
woven PP/40%Flax	79	8	1.06
UD PP/40%Flax	175	17.4	1.06
chopped PLA/30%Flax	57	6.6	1.3
Manufacturer:			
woven PLA/40%Flax [67]	102	13.2	1.33
UD PLA/40%Flax [67]	160	27.4	1.33
woven PP/40%Flax [67]	57	8.1	1.04
UD PP/40%Flax [67]	130	19	1.04
chopped PLA/30%Flax [61]	53	8.1	1.3

fibers, an orientation efficiency of respectively 0.3, 1 and 0.4 is chosen. As can be seen in Table 12.3, the Rule of Mixture of Cox-Krenchel [66] gives a particularly good estimate for the Young's modulus and the density. However, the estimate for the tensile stress is most of the time quite optimistic. A possible improvement for the tensile stress calculation is using the theory of Kelly-Tyson [66]. This theory takes the volume fraction of the fibers, which are longer than the critical fiber length, and the volume fraction of the fibers, which are shorter than the critical fiber length, into account. However, these volume fractions can only be retrieved by a more elaborated research to Flax fibers.

Besides that, the Rule of Mixture of Cox-Krenchel only calculates the ideal properties, without material defects, which especially result in a decrease in tensile strength [66]. How the flax fibers are woven, and production errors cause deterioration of all the material properties

As can be seen in Table 12.3, the calculated composites could have a tensile stress about 40% percent higher than the tensile stress given by the manufacturer. For the material chosen for the ASAP UAV this could result in a real tensile stress of approximately 30 MPa instead of the ideal 55.9 MPa. However, this tensile stress is still larger than the structure's maximum stress.

12.3. STRUCTURES TOOL

This section contains the verification of the structural tool used for the sizing of the wing. Based on the geometry of the wing, a wing box is modelled and analyzed under an elliptical lift distribution. It is not certain that a wing box will be used within the design, but this is merely a tool to calculate the range of stresses and is thus subjected to uncertainties. Assuming the width of the wing box is approximately 40% of the local chord and the lift acts at a quarter chord, the resulting lift distribution acts on the front spar of the wing box. The height of the wing box is assumed to be 9%. These values are estimated based on the shape of the airfoil and the amount of space other subsystems will need.

Because the weight of the battery and the structure itself can induce bending relief, this is also included. The Lithium polymer battery can be placed within the wing box section, resulting in bending relief all over the wing span. The code is also used to calculate the volume of the structure and can thus be used to estimate the weight of the structure. This is done to enable including a rough estimate of bending relief due to structural weight. Because this method of estimating the weight is highly uncertain, this will not be used for the final weight breakdown and will thus not be verified. Note also that this verification is done before the project is actually finished. This is done to see whether the code calculates the correct thing, forces may be added.

Figure 12.1 shows the distribution of forces and moments along the span of the wing. As was explained in Section 6.2, all forces and moments behave as expected. The moments and forces however show differences due to the fact that the weight of the structure was not included during verification and validation of the tool. With the help of an analytic tool, the wing box is checked on two different locations. First at a distance of 0.25 m from the span to check whether the geometry of the wing box is modelled correctly and secondly at the root, to check if the forces, moments and stresses are calculated correctly. The analytic results are obtained using resulting forces and centroids to compute the moments and stresses. Table 12.4 shows the results and also the difference between the code and the analytic results. All the individual checks are unit test of pieces of the code. The system test of the code is actually the testing of the Von Mises stress. When this is correct or within respectable margins, the code is deemed verified. Basic debugging to make the code work (Matlab errors) was done throughout the creation of the program. During the verification of the structures code, a couple of errors were found. The distribution of the batteries along the wing span was mirrored and the weight of the structure was incorrectly calculated. After debugging there were no more errors to be found. Looking at the differences, all are under a 10% error margin which makes this a reliable tool for stress calculations. Only deviation in the moment around Y is present, causing the error in the shear stress.

12.4. REQUIREMENTS COMPLIANCE MATRIX

The objectives and requirements for the ASAP UAV have been defined during the entire design process. In addition they have changed and were adapted to suite the customers and the mission better. Therefore, the design should be checked for compliance with respect to each requirements. Note that this can also be viewed as the verification and procedure for the final design. Verification of the design is performed with the requirements that are derived from the customer requirements. These are provided in Table 12.5. Validation of the design is done with the customer requirements themselves, which were provided in the DSE Informational

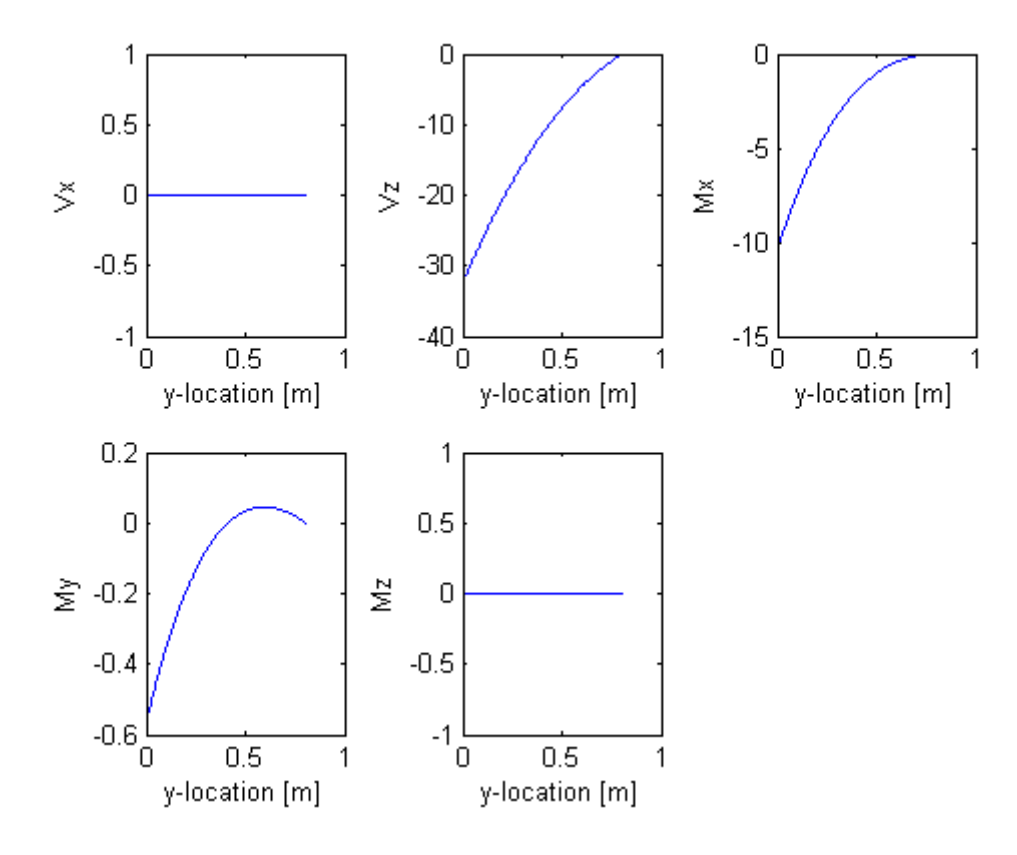


Figure 12.1: Distribution of Forces and Moments along the span of the wing box $\,$

Table 12.4: Verification results for the structures tool

	Result using tool	Analytic result	Error margin (%)
y [m]	0.25		
\bar{c} [m]	0.215	0.215	0
\bar{x} [m]	0	0	0
$ar{z}$ [m]	0	0	0
$I_{xx}[m^4]$	$2.32 * 10^{-08}$	$2.34 * 10^{-08}$	0.86
$I_{zz}[m^4]$	$2.90*10^{-07}$	$2.92 * 10^{-07}$	0.62
$I_{xz}[m^4]$	0	0	0
$\xi[m]$	0	0	0
$\eta[m]$	0	0	0
y[m]	0.801		
$V_x[N]$	0	0	0
$V_z[N]$	-32.31	-32.31	0
$M_x[Nm]$	-10.32	-10.35	0.29
$M_{\nu}[Nm]$	-0.56	-0.62	9.7
$M_z[Nm]$	0	0	0
$\sigma[Pa]$	$-1.76*10^{06}$	$-1.75*10^{06}$	0.31
$\tau[Pa]$	$-4.71*10^{05}$	$-4.36*10^{05}$	7.97
$\sigma_{VM}[Pa]$	$1.94*10^{06}$	$1.91*10^{06}$	1.55

Booklet [118], the Project Description [119], the kick-off meeting and the regular customer status updates.

12.4.1. DESIGN VERIFICATION

Table 12.5 contains all derived requirements from Table 12.6. The requirement code, the requirement description and the customer requirement and/or references they are based on, in addition to a checkmark if they have been achieved by the design. If a requirement has not been achieved, it will be discussed. If a requirement has an empty entry in the 'derived from' column, it means that it has not been derived directly from the customer requirements, but it has been obtained during the process, or from other derived requirements. Furthermore, not all requirements satisfy the V.A.L.I.D. criteria, as specified in the Baseline Report [1]. In these cases, the design team has evaluated if the design has achieved the requirement, or the evaluation of the requirement has been moved to the post-DSE phase.

Table 12.5: Derived requirements compliance matrix

Code	Description	Achieved	Derived from
PAY-1	The UAV shall carry an electro-optical camera system on board	√	CUS-13
PAY-2	The UAV shall carry a thermal camera system on board	\checkmark	CUS-13
PAY-3	The electro-optical camera shall have at least 35 pixels in a single direction	\checkmark	CUS-15, CUS-16 & [120]
PAY-4	The thermal imaging camera shall have at least 4 pixels in a single direction	\checkmark	CUS-15, CUS-16 & [120]
PAY-5	The frame rate of the camera shall be at least 24 fps	\checkmark	CUS-11 & CUS-14
PAY-6	The camera system shall have a state of the art vibrational damping system	\checkmark	CUS-14
PAY-7	The UAV shall carry a see-and-avoid camera system	\checkmark	CUS-18 & CUS-19
PAY-7.1	The see-and-avoid camera system shall be able to respond to an incoming	\checkmark	CUS-18 & CUS-19 & [121]
	airborne object so that a collision is avoided by at least $500 ft$, or $153 m$		
PAY-7.2	The see-and-avoid camera system shall have a horizontal angle of at least 220	\checkmark	CUS-18 & CUS-19 & [121]
	deg		
PAY-7.3	The see-and-avoid camera system shall have a vertical angle of at least 30 deg	\checkmark	CUS-18 & CUS-19 & [121]
PAY-8	The UAV shall have a light source on each wingtip	\checkmark	
COMM-1	The UAV shall have a continuously stable uplink with the control base	√	CUS-14
COMM-2	The UAV shall have a continuously stable downlink with the control base	,	C03-14
COMM-2	The signal range shall be at least $20km$ w.r.t. the launch vehicle	√	CUS-2
COMM-3	The UAV shall be able to operate at the UHF for UAV and S-band frequencies	∨ ✓	CUS-12
COMM-5	The UAV shall contain two transmitters and two transceivers	∨ ✓	CUS-12 & COMM-4
		V	
CTRL-1	The UAV shall be equipped with a state of the art Flight Computer (F/C)	√	CUS-2
CTRL-1.1	The F/C shall be programmed to fly the mission autonomously	\checkmark	-
CTRL-1.2	The F/C shall be programmed with a see and avoid sequence	\checkmark	CUS-18 & CUS-19
CTRL-1.3	The F/C shall be programmed with a manual take-over sequence	\checkmark	CUS-10
CTRL-1.4	The F/C shall be programmed with a bystander avoidance sequence	\checkmark	CUS-17
CTRL 1.5	The F/C shall be programmed with all failure mode response sequences	\checkmark	CUS-17
CTRL-2	The mission commands shall be pre-programmable	\checkmark	-
CTRL-3	The UAV shall be controllable during all flight conditions	\checkmark	-
CTRL-4	The UAV shall be equipped with a state of the art GNC system	√	-
CTRL-4.1	The GNC shall contain a 3-axis gyroscope	√	-
CTRL-4.2	The GNC shall contain a 3-axis accelerometer	√	-
CTRL-4.3	The GNC shall contain a 3-axis magnetometer	√	-
CTRL-4.4	The GNC shall contain a barometer	√	-
CTRL-4.5	The GNC shall contain a GPS system	√	-
CTRL-4.6	The GNC shall contain a differential pressure sensor	\checkmark	-
PERF-1	The UAV shall be operational during heavy rain	√	CUS-1
PERF-2	The UAV shall remain operational after hail strike with a maximum size of $5cm$	\checkmark	CUS-1
	diameter		
PERF-3	The UAV shall be operational during icing conditions	±	CUS-1
PERF-4	The UAV shall remain operational after a lightning strike	±	CUS-1
PERF-5	The UAV shall be operational in temperatures from -20 deg Celsius to 60 deg	\checkmark	CUS-1
	Celsius		
PERF-6	The UAV shall provide power for the entire mission	\checkmark	CUS-2
PERF-7	The mission shall be performed between 50 m and 150 m altitude	\checkmark	CUS-3
PERF-8	The UAV shall be able to operate at a continuous wind speed of 21 m/s	\checkmark	CUS-7
PERF-9	The UAV shall be able to sustain gusts with a wind speed of 30 m/s	\checkmark	CUS-7
PERF-10	The UAV shall have a minimum airspeed of at most $14.3 m/s$	_	CUS-7
PERF-11	The UAV shall have at least a maximum velocity of at least 30 m/s	\checkmark	CUS-7 & CUS-8
PERF-13	The UAV shall have a maximum endurance velocity of at most $23m/s$	\checkmark	-
PERF-13	The rudder angle shall not exceed an angle of 30 degrees	\checkmark	-
PERF-14	The UAV shall have a sufficient UAV reliability	\checkmark	-
PERF-15	The UAV shall have a sufficient mission reliability	\checkmark	-
PERF-16	The UAV shall have a roll rate of at least $0.5 rad \cdot s^{-1}$	\checkmark	-
PERF-17	The location of the c.g. shall be in front of the neutral point	\checkmark	-

Table 12.5: Mission requirements for the SAR UAV (continued)

Code	Description	Achieved	Elaboration
		,	
M&S-1	The UAV shall consist for 95% out of polymers including structure and propulsion system	✓	CUS-20
M&S-2	The materials chosen for the fuselage UAV shall be biodegradable	√	CUS-22, CUS-9
M&S-4	The materials selected for the UAV shall be sufficiently resistant to fatigue	,	CUS-9
M&S-5	The UAV shall maintain structural integrity during entire flight envelope	, ,	-
M&S-6	The UAV shall maintain structural integrity during transportation	· ✓	=
M&S-8	The UAV structure shall provide sufficient space for the onboard systems	✓	_
M&S-9	The UAV structure shall withstand operations during heavy rain	✓	CUS-1 & PERF-1
M&S-10	The UAV structure shall withstand hail impact up to 5 <i>cm</i> diameter	\checkmark	CUS-1 & PERF-2
M&S-11	The UAV structure shall withstand operations under icing conditions	\checkmark	-
M&S-12	The UAV structure shall withstand a lightning strike	_	CUS-1 & PERF-4
M&S-13	The UAV structure shall maintain structural integrity trough out the	\checkmark	-
	operational temperature range		
M&S-14	The UAV shall have a high visibility coating	\checkmark	-
TRNSPT-1	The transport vehicle shall provide protected storage for UAV	±	-
TRNSPT-2	The transport vehicle shall provide launch system for UAV	\checkmark	CUS-6
TRNSPT-3	The transport vehicle shall provide landing system for UAV	_	CUS-6
CMND 1	A controller shall always be an stand by		
CMND-1 CMND-2	A controller shall always be on stand-by The command station shall have state of the art person detection software	√	-
	1	V	-
CMND-3	The command station shall have sufficient processing power for continuous data analysis	✓	-
CMND-4	A state of the art manual control interface shall be available	\checkmark	-
CMND-4	A state of the art manual control interface shall be available	√	-

- *PERF-3: The UAV shall be operational during icing conditions.* The success of the UAV to achieve this requirement is based on the performance of the super hydrophobic coating as anti-icing agent. The coating seems like a viable solution, but not enough information is available to make a definite conclusion. Therefore the coating must be tested during the post-DSE phase.
- PERF-4: The UAV shall remain operational after a lightning strike. In all likelihood the UAV will
 not be able to continue operations after a experiencing a lightning strike. However, as has been
 described in Chapter 5, lightning does not occur often enough to make adjustments to the UAV.
- PERF-10: The UAV shall have a minimum airspeed of at most 14.3 m/s. This requirement was determined by calculation of the take-off speed, using maximum launch load and launch rail length as input. However, as reducing the minimum airspeed results a reduction of the cruise speed, the speed with which the victim can be found will also decrease. As this is the primary goal of the ASAP UAV, a conscious choice has been made to choose for a high cruise speed and tolerate a higher minimum speed. The take-off load has been increased to reach the take-off speed.
- M&S-12: The UAV structure shall withstand a lightning strike. See the explanation of PERF-4.
- TRNSPT-1: The transport vehicle shall provide protected storage for UAV. No designs have been made in order to satisfy this requirement, as the vessels on which the ASAP UAV will operate differ in size. It is however treated in the post-DSE planning.
- TRNSPT-3: The transport vehicle shall provide landing system for UAV. As has been discussed in Chapter 4, it is too dangerous to land the UAV on board of a ship. The decision has been made to land the ASAP UAV in the water, and to pick it up.

It can be concluded, that the design is verified and it will likely satisfy the customer needs/requirements to a large extent. In addition, a number of (derived) requirements that have not been fully met, will be treated in the post-DSE phase.

12.4.2. DESIGN VALIDATION

Now that the design has been verified, it should be validated using the customer requirements. In Table 12.6 all user requirements have been collected. A checkmark is provided if the design has achieved the requirements, a minus is assigned if a requirement is not achieved, and a plus minus sign is assigned if the results are still inconclusive. The requirements that are not achieved and those of which the conclusion is inconclusive are discussed below.

Table 12.6: Customer requirement matrix

Code	Description	Achieved
CUS-1	The UAV shall be able to operate in all-weather conditions	±
CUS-2	The UAV shall be able to perform at least 3 hours of autonomous search	\checkmark
CUS-3	The UAV shall operate at a flight altitude low enough not to bother local air traffic and high enough not to be caught by kites	✓
CUS-4	The UAV shall have (limited) hover capabilities or perform slow circling flight	\checkmark
CUS-5	The UAV shall be operational during day and nighttime	\checkmark
CUS-6	The UAV shall be able to take-off and land from a ship	_
CUS-7	The UAV shall be operational up to including wind conditions of 7 Beaufort and wind gusts up to 9 Beaufort	✓
CUS-8	Local winds at the cruise altitude must be taken into account	\checkmark
CUS-9	Special attention must be spent on the degradation of plastics and polymers over time	\checkmark
CUS-10	Manual take-over of the UAV will be possible	✓

Code Description Achieved Human operator must be able to look for a victim using the UAV CUS-11 CUS-12 Communications and data handling system must be completely designed CUS-13 Payload must be able to detect both in the visual and infrared range CUS-14 Payload shall be able to support a stable live video feed Payload shall be able to survey from 100m height and send information CUS-15 CUS-16 Payload shall have adequate resolution in order to spot drowning persons from the operating flight altitude CUS-17 In case of emergency the UAV may never result in a threat for bystanders CUS-18 The UAV shall be able to operate in the vicinity of other objects CUS-19 The UAV shall incorporate a see and avoid system CUS-20 Maximum non-polymer content in the construction will be 5%, including the propulsion installation. The UAV shall be affordable enough to allow a couple to be on-board of a CUS-21 \pm ship, so that larger search areas can be covered by multiple UAVs CUS-22 The UAV shall be safely disposable \pm

Table 12.6: Customer and mission requirements for the SAR UAV

- CUS-1: The UAV shall be able to operate in all-weather conditions. The ASAP UAV is operational during 10 Bft continuous wind and 12 Bft gusts, it can withstand impact of hail with a maximum size of 6 cm diameter and is operational in a temperature range from -20 deg Celsius to 60 deg Celsius. Protection against lightning strikes is considered until it was clear that this would drive the design to an unacceptable level. Although harsher weather conditions can be encountered, it is very unlikely that the ASAP UAV will be required to operate in these conditions. Therefore, this requirement is achieved.
- CUS-6: The UAV shall be able to take-off from and land on a ship. As has been discussed in Chapter 4 the UAV cannot land on the transportation vessel. Although the UAV is designed to be reusable and can be picked up from the water, this requirement is not met.
- CUS-21: The UAV shall be affordable enough to allow a couple to be on-board of a ship so that larger search areas can be covered by multiple UAVs. This requirement cannot be achieved due to the requirement formulation. However, Mr. Moleman, head of operations of the KNRM, has expressed his interest in the ASAP UAV due to its reasonable pricing and promised performance. Therefore, the design team considers this requirement to be achieved.
- CUS-22: The UAV shall be safely disposable. Although a very large part of the UAV is safely disposable (either by degradation or recycling), there are a number of components (totaling 5% of the UAV weight) that are not. These consist mainly of the imaging payload and a number of PCBs. As these components are required for the mission and degradable or recyclable replacements are non-existing, the design team believes it has achieved the best possible result.

12.5. RISK ANALYSIS

After completion of the validation of the product, the technical risk assessment for the final stage of the project can be updated. Risk assessment is an important and ever changing part of the project. The possibility to identify bottlenecks and delays before they occur provide the team with room to find solutions for these identified risks.

The risk analysis will start with a description of the project schedule risk, followed by a section on mis-

sion risk analysis. In this section all risks which negatively affect the capability of the UAV to perform the proposed where the contingencies for the rest of the project will be treated. Because the product is now validated, old risks might disappear and new risk could emerge. This section will thus show an updated risk map.

12.5.1. MISSION RISK ANALYSIS

In this section risk will be discussed which will negatively affect the mission of the UAV. These risks have been assigned to four categories. Risk related to the structure, the power and propulsion, the control and the on-board systems of the UAV which can be found in Tables 12.7 to 12.10. The risk map, risk mitigation strategy and contingency management are included in this section.

Table 12.7: Structural Mission Risk Analysis

ID	Risk
S1	Not feasible to produce the UAV out of 95 % polymers
S2	Structural integrity (also due to the T_g) of the structure cannot be maintained during flight
S3	UAV structure suffers of fatigue within its life time cycle
S4	Storability of the UAV is impossible from its deployment location
S5	Degradability of the UAV is not possible after operation or failure
S6	Stiffness of structure of the UAV is too low to perform entire flight envelope
S7	c.g. Range of the UAV is too large to maintain controllability
S8	Sustainability of the structure is not feasible
S9	Internal space of the structure is too small to equip operational equipment
S10	Durability of the UAV's structure is not feasible
S11	UAV's structure can not withstand all weather conditions, severe rain, hail, snow,
	lightning and wind and other severe weather conditions

Table 12.8: Power and Performance Mission Risk Analysis

ID	Risk
P1	UAV underpowered for flight in constant wind speed of 7 beaufort
P2	UAV unable to fly for at least 3 hr
P3	UAV does not have sufficient power for take off and landing
P4	Lift is less than required in any part of the mission
P5	Aerodynamic thrust force is insufficient in any part of the mission
P6	Propulsive power is insufficient to provide the required mechanical power for the propulsion device
P7	Energy storage is insufficient to provide energy to UAV (sub)systems
P8	The power and propulsion system is not sustainable in design, production, usage and/or end-of-life
P9	Total loss of the generator or power supply.
P10	Battery sensor indicates wrong power level.

MISSION CONSEQUENCE RISK MAP AND MITIGATION

For every identified risk the probability of occurrence and the consequence for the mission is identified and presented in the risk map, table 12.11. The risk map is an updated version of the presented

Table 12.9: Control Mission Risk Analysis

ID	Risk
C1	UAV is no longer controllable with wind gusts of 9 bft
C2	Maneuverability of the UAV is too low to perform the mission
C3	Controllability of the UAV is insufficient to perform mission
C4	UAV is not stable during mission
C5	Computing Power of the control board is not sufficient to control the UAV
C6	Guidance & Navigation of the UAV is insufficient to control the track of the UAV
C7	UAV is not able to avoid obstacles
C8	Remote control of the UAV is not possible during operation
C9	C.g. range of the UAV too large to control the UAV at all times
C10	Hover/Slow Flight of UAV is not possible at all conditions e.g. weather and loading conditions

Table 12.10: On-board Systems Mission Risk Analysis

ID	Risk
01	UAV is not able to Up-link data
O2	UAV is not able to Down-link data
О3	Camera quality of UAV is not sufficient to perform the mission
O4	Computing Power of the control board is not sufficient to control the UAV
O5	Guidance & Navigation of the UAV is insufficient to control the track of the UAV
O6	On board data storage is insufficient
O7	The on board systems are not (sufficiently) sustainable
8O	Loss of communications
O9	Sensor measurement out of range
O10	Loss of redundancy
O11	Insufficient processing speed on board computer
O12	Unstable Gimball

risk map in the Midterm report [2]. Table 12.11 is clearly divided into three sections. These are the

		Mission Consequence			
		Negligible	Marginal	Critical	Catastrophic
				O4, O6	
				P4, P5, P6, O3,	
Pr			O10, C7	S11, C2, C9, P1,	C8 O5 O8
Probability	Proven flight design	Green: S7	Green: O7,	Green: S6, S9,	Orange: P6 P9
abi	existing flight design			C1, O1, O2, P2	
lit,	Extrapolated from			Orange: S3, S4,	Red: P1
Jo /	engineering				
00.	non-flight				
<u>5</u>	Based on existing		Orange: S5	Red: S8	
occurance	model				
Se	Working laboratory				
	Feasible in theory				

Table 12.11: Mission Consequence Risk Map

high-, medium- and low risks, indicated by the colors red, orange and green respectively. The purpose of the risk map is to get a clear overview of all high risks and to try to mitigate these. This is the main focus of the risk mitigation strategy, explained briefly for the high risks in the next paragraph.

Changes with previous risk map There are multiple risks neglected because these risks were based on requirements which are achieved. Some examples are the structural risks like 95% polymer, the integrity of the design, sustainability of the material or controllability and stability for wind gusts up to 9 Bft. These are all removed for the recent risk map. Other risks are moved in the risk map, primarily from right to left. This means mission consequence is, in general, decreased while the probability of occurance is unchanged. Looking at the power and propulsion of the UAV, it is computed that the UAV contains enough power for launch and propulsive power during its mission. Looking at the risk map, only two red risks remain. These are the power needed during all-weather conditions and sustainability of the overall design. Because these risks are still very uncertain they are kept in the red risk mitigation zone.

13

POST DSE

After this DSE the detailed design of the ASAP UAV is not yet finished. There are quite a number of activities left before this UAV can go into production and service. This chapter contains the flow diagram and Gantt chart for all these activities. In the first section the project design and development logic is presented. After that the post DSE Gantt chart is shown.

13.1. Project Design & Development Logic

This section shows the logical order of activities to be executed in the post-DSE phases of the project. Since there are multiple post-DSE activities related to each aspect of the UAV, the upcoming activities are related to prior chapters. The flowchart showing the post-DSE activities is given in Figure 13.1

Subsystems One of the most important post DSE activities is the testing of all the hardware and software of all the subsystems. This includes communications, see and avoid and the autopilot. Also, the link budget may suffer from discrepancies because of the unknown ground station characteristics. That being said, the communication flow from and towards the ground station still needs to be investigated. The UAV is controlled via the boat by the ground station, and it is important that the boat does not interrupt the flow of communication and surpasses any information smoothly.

Operations & Logistics In Chapter 4 the *whiskering* of the camera has been discussed. This sweeping motion of the camera can increase the search area without flying extra kilometers and can improve search efficiency. However, to make sure this is an effective way of using the camera and if the camera is able to do this at all, testing has to be performed. The manufacturer does not provide sufficient data to make accurate predictions regarding this manoeuvre. Additional information regarding the payload life cycle is required.

Second, the landing load case has to be carefully analyzed. To ensure the UAV can land on water an accurate FEM model or real time testing has to be performed. In the first case additional validation is in order while in the latter test setups have to be constructed.

Third, the logistic part of the operation has to be evaluated. Seeing as the UAV is stored on board of a ship that can crash into waves causing 7g decelerations, a protective storage unit might be necessary.

A final activity that is required regarding Operations & Logistics is a more elaborate literature study concerning maneuverability in severe weather conditions. The aircraft might respond differently when flying in 9 Beaufort winds and therefore has to be investigated. Finally the retrieving of the UAV using nets must be evaluated and tested. Especially testing in rough weather is necessary.

Life Cycle As discussed in Section 5.1.1, there are multiple parts where an accurate MTBF is missing. Two options exist here: either a MTBF is set to which the part has to comply, or an accurate MTBF is requested from the manufacturer and the impact is analyzed afterwards. More redundancy to increase the life time of the UAV might be implemented if deemed necessary.

116 CHAPTER 13. POST DSE

Materials and Structure There are lots of load cases left to analyze when it comes to the structure of the ASAP UAV. Besides landing and take-off several other behavior has to be evaluated; vibration, fatigue, flutter and impact resistance. Several tests concerning degradation of the materials have to be performed to ensure the UAV 'performs' as desired at end-of-life. Looking at the connection of wings to fuselage, the pitch of the nuts has to be further analyzed. The connection is most probably overdesigned, due to uncertain stresses because of boundary effects.

Internal Layout Depending on the results from Life Cycle the internal layout might be changed; if more redundancy of systems will extend the life cycle tremendously the layout of the internal systems might be adjusted to accommodate all the extra parts.

Manufacturing, Assembly and Integration A detailed design of the packaging system has to be performed. Module casings for the batteries have to be designed and the methods to keep the other systems in place have to be validated.

To ensure the assembly of the different parts is not just easy but also a safe process, tests have to be performed. Not just the strength of the attachments has to be tested, but the water tightness and maintainability as well.

Flight Performance and Aerodynamic Characteristics Before the external layout is finalized it is beneficial to perform Computational Fluid Dynamics (CFD) calculations and/or wind tunnel tests. Depending on these results (multiple) iterations can be performed to optimize the design from an aerodynamic point of view.

Cost The cost breakdown is an ongoing process and will give more and more accurate cost estimates over time. At this point the cost estimate for future processes (test flights, designing ground stations, etc.) is still inaccurate because they have not been planned/designed yet. Also, a more detailed market analysis should be performed in order to narrow down the cost range of the UAS.

Verification & Validation If and when FEM and CFD models are used, proper validation is in order. Besides validating numerical tools, there are still requirements that have to be validated. Some requirements are not yet met and need additional attention, while others are still not specified (<TBD>) and need more research.

Testing This will be the largest phase after the detailed design is finished. Testing includes building prototypes of the aircraft as well as ground station, performing test flights and re-iterate on design aspects if necessary.

Legislation As the design is finished it needs to be certified by the authorities. This test includes a performance and quality assurance test and the ASAP UAV has to meet qualification criteria as stated in the legislation documents by the different aviation authorities, e.g. JAR for Europe and FAR for the US.

13.2. POST-DSE PLANNING

For the post-DSE activities, a Gantt chart was made. This Gantt chart is presented in Figure 13.2 and shows the time distribution of the several post-DSE activities that need to be performed.

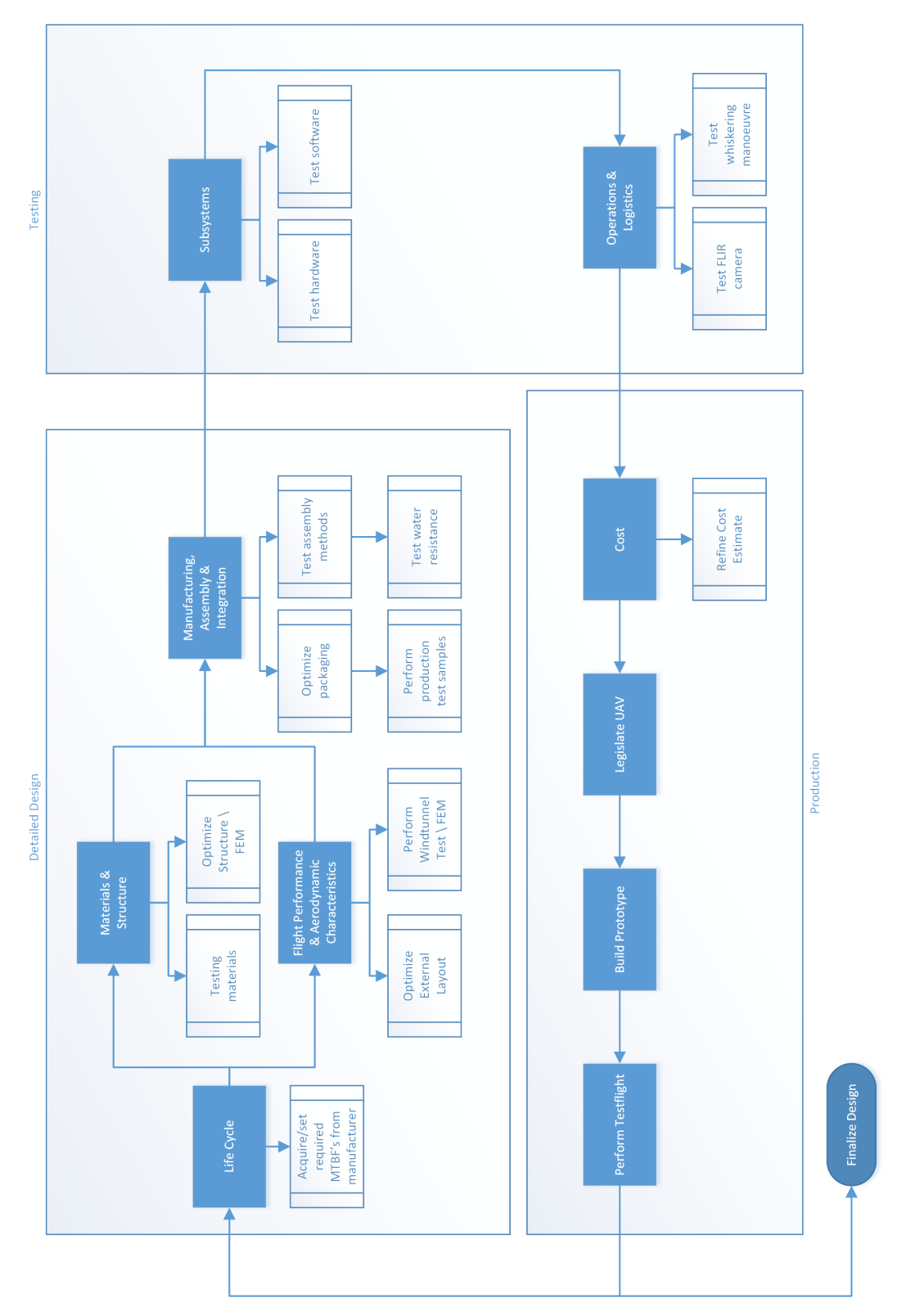


Figure 13.1: The post-DSE project design and development logic flow diagram

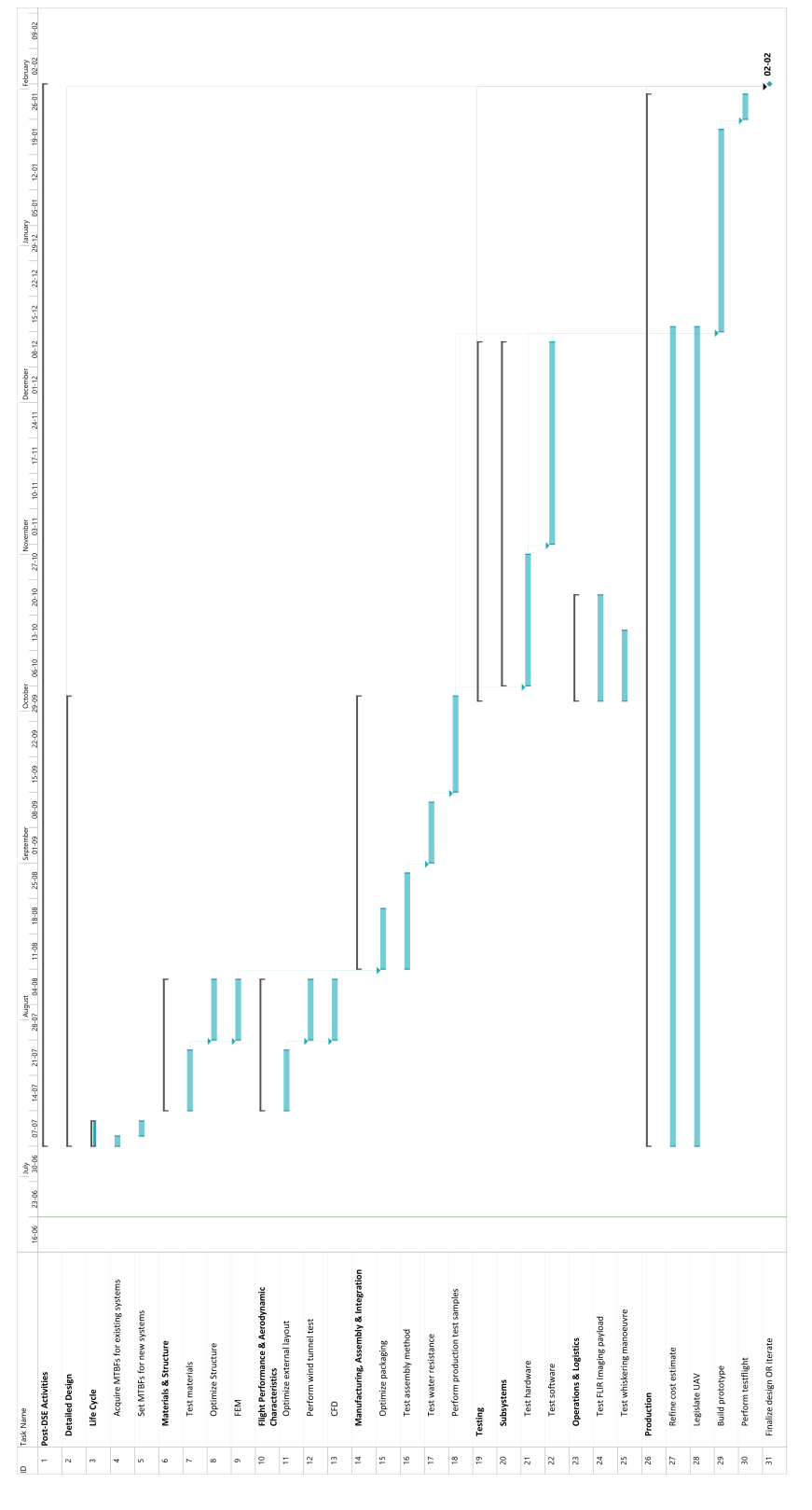


Figure 13.2: The post-DSE project planning

CONCLUSION & RECOMMENDATIONS

In this chapter the conclusion of the Final Report is presented. It contains a description of the final design. Furthermore, a number of recommendations are made for the post-DSE phase.

14.1. CONCLUSION

The purpose of this report is to present the design of an all-polymer biodegradable autonomous Unmanned Aerial System (UAS) with which a person or object can be located at sea in any weather conditions, which can transfer its location to its remote command center, and is deployable from a ship. In addition, its support equipment, construction, maintenance, disposal and operation are presented. The final result is called the 'Autonomous Search All-Polymer (ASAP) UAV'.

By analysis of the customer needs, the market and the mission, a list of requirements is created. All possible design configurations are then evaluated on their likely performance with respect to the requirements. By means of an elaborate trade-off the best result is chosen and further developed. For the mission that is to be performed, a flying wing with a small tail and a single rear-mounted battery driven propeller is considered the optimal configuration. In addition, lithium-polymer based batteries are chosen in order to achieve a maximal polymer content as requested by the customers.

In order to perform its mission, the ASAP UAV carries a payload and a number of other subsystems. These consist of:

- an electro-optical imager, in order to perform daytime search missions.
- an infrared (IR) imager, in order to perform nighttime search missions.
- a motor
- batteries
- an autopilot, containing a GNC system and a flight computer.
- · a communication system.
- · a see and avoid system.

These systems, including their interaction, are designed and are incorporated in the internal layout provided in Figure 14.1.

The structure of the UAV will consist of a monocoque, a reinforced shell, with a constant thickness of $2.0\ mm$. As the polymer content of the UAV should be maximized and as sustainability should be taken into account, the material chosen for the structural components is a polymer composite consisting of a bio-based resin called poly-lactic acid (PLA) and Flax fibers. This combination of PLA and natural fibers enables the UAV to disintegrate in seawater within approximately 18 months. In addition, when using these materials, the deflections and stresses are far within the allowable limits.

The ASAP UAV is deployable from a ship by means of a Troy pneumatic catapult with a four meter rail. The UAV will perform a belly landing, flying into the wind in order to decrease its ground speed velocity, after which it will need to be retrieved from the ocean.

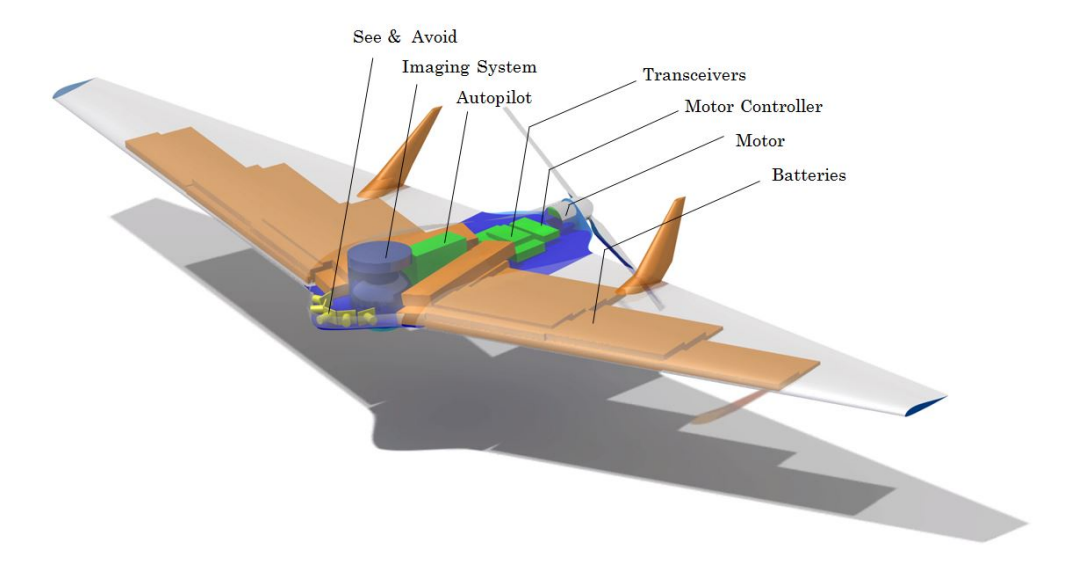


Figure 14.1: The internal layout of the ASAP UAV

The reliability of the UAV has been evaluated for two aspects; mission reliability, which expresses how often a mission cannot be completed, and the UAV reliability, which expresses how often a UAV is lost. The reliability has been increased by adding a redundant autopilot and motor controller. The results are that on average, every 120 missions a mission cannot be completed, and every 1100 missions an UAV is lost. In addition, a maintenance plan has been developed in order to keep the UAV operational. Finally, each part of the end-of-life disposal method has been developed.

In order to optimize accessibility and manufacturability and to make the UAV as waterproof as possible, it consists of only three components. In addition, the location of the seams are chosen so that they do not coincide with the location of the highest stress concentrations. The components are shown below, in Figure 14.2. The bottom parts are bonded together by means of an adhesive, whereas the top is fastened using bolts in order to allow for easy access during maintenance.

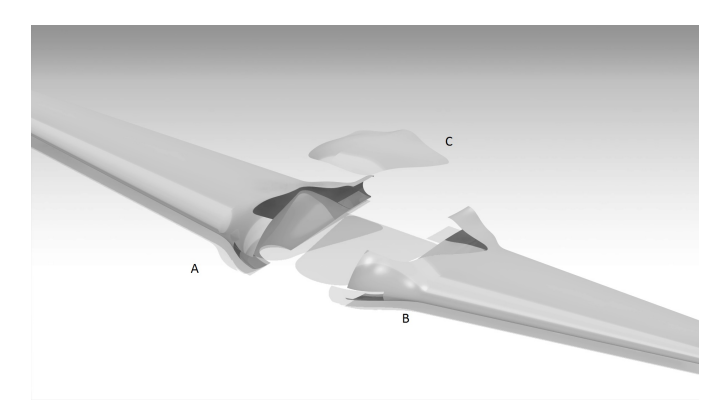


Figure 14.2: Lay-out where the chosen assembly method, showing all separate components

The aircraft aerodynamic parameters, such as the airfoil and the planform dimensions, are chosen in such a way that the UAV's aerodynamic performance is optimized for the required mission. The results, both the performance parameters as well as the geometric parameters, are provided in Table 14.1.

The cost of the ASAP UAV consists not only of the purchase price of a single UAV, but also of the research and development cost, the ground station equipment, launcher and other general operating costs. It can therefore be stated that the cost of the Unmanned Aerial System (UAS) is approximately \$120.000 per year after one hundred sales. An increase in sales will not bring down the cost much further. As a leasing system is also being considered, the cost per flight hour has been calculated to be \$210,- per hour. Mr. Moleman, head of operations of the Koninklijke Nederlandse Redding Maatschappij (KNRM), has expressed his general interest in the design due to its low cost and innovative solution compared to other UAS projects the KNRM has considered.

It should be noted that special attention is paid to the biodegradability of the Flax-PLA bio-composite. Furthermore, the lithium-polymer battery is completely recyclable after its lifetime. To maintain a high degree of sustainability, the charging of the batteries should be executed using electricity from renewable sources such as wind or solar. Finally, all components of the ASAP UAV are categorized in one of three categories: a subsystem or component will either be recycled, treated as waste or degrade over time. The result for the entire UAV is shown in Figure 14.3. It can be seen that only 5% of the UAV is considered waste, which consists mainly of Printed Circuit Boards (PCBs) and wiring which in practice will not be recycled.

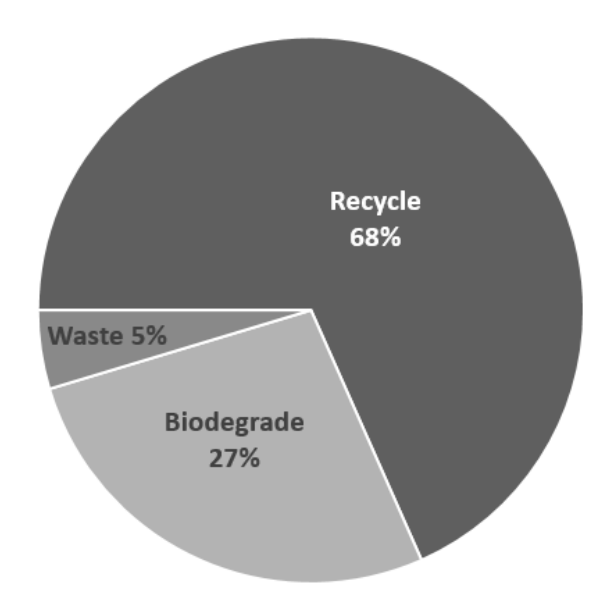


Figure 14.3: Pie-chart showing the mass-percentage of the UAV in terms of recyclable, biodegradable and waste creating

14.2. RECOMMENDATIONS

Due to the restricted amount of time available for the design of the ASAP UAV, a number of aspects have not yet been (adequately) covered. The design team recommends the following aspects to be evaluated further during the post-DSE phase:

Table 14.1: The final aerodynamic and planform parameters for the ASAP UAV

Explanation	Parameter	Value	Unit
Planform			
Aspect ratio	AR	8	-
Leading edge sweep	Λ_{LE}	15	deg
Taper ratio	λ	0.25	-
Twist angle (tip)	ϵ_{tip}	-2	deg
Incidence angle	i_w	1	deg
Dihedral angle	Γ	0	deg
Spanwidth	b	1.602	m
Mean chord	c_{mean}	0.20	m
Wing area	S	0.321	m^2
Tip chord	C_t	80.132	mm
Root chord	C_r	320.527	mm
Volume	υ	2.803	L
Speed Range			
Minimum speed	V_{min}	18.4	m/s
Endurance Speed	$V_{endurance}$	22.2	m/s
Max range speed	V_{range}	29.2	m/s
Maximum speed	V_{max}	40.2	m/s
Performance and Power			
Acceleration due to gust	a_{gust}	2.769	m/s^2
Wing loading	$rac{a_{gust}}{S}$	275	N/m^2
Minimum power	P_{min}	223	W
Power required in turn	$P_{turn}(20^{\circ})$	247	W
Power for V_{range}	$P_{V_{range}}$	254	W
Maximum endurance	$H_{V_{endurance}}$	225	mins
Endurance for V_{range}	$H_{V_{range}}$	180	mins
Oswald factor	e	0.9	-
Glide ratio	$\left(\frac{L}{D}\right)_{max}$	20.123	-
Profile drag coefficient	$C_{D,0}$	0.014	-
Maximum lift coefficient	$C_{L,max}$	1.421	-
Lift coefficient for max endurance	$C_{L,endurance}$	0.976	-
Lift coefficient for max range	$C_{L,range}$	0.564	-
Lift coefficient for V_{max}	$C_{L,V_{max}}$	0.298	-

- Structural analysis of the UAV during take-off and landing. Furthermore, the results of different types of impact loading should be evaluated.
- Aerodynamic performance should be verified, validated and optimized.
- Extensive controllability tests should be performed. In addition the autopilot must be programmed to cope with high wind operations.
- The hydrophobic coating should be tested for durability and anti-icing performance
- Production and assembly tests should be performed.
- The UAV should be checked for legislative compliance.

The next step in the designing process of the ASAP UAV is applying the recommendations and refining the design further.

BIBLIOGRAPHY

- [1] D. van den Bergen et al. *Baseline Report. Design Synthesis Exercise*. Technical Report. Delft University of Technology, 2014.
- [2] D. van den Bergen et al. *Midterm Report. Design Synthesis Exercise*. Technical Report. Delft University of Technology, 2014.
- [3] Marine Traffic. *Marine traffic overview*. [Online; accessed April 25, 2014]. 2014. URL: http://www.marinetraffic.com.
- [4] U.S. Coast Guard. U.S. Coast Guard SAR Program Information. [Online; accessed April 24, 2014]. 2014. URL: http://www.uscg.mil/hq/cg5/cg534/SAR_Program_Info.asp.
- [5] A. Zarandy et al. *On-board-see-and-avoid-system*. Technical Report. Hungarian Academy of Sciences, 2012.
- [6] University of Washington. *Relationship Between Head Mass and Circumference in Human Adults*. [Online; accessed June 30, 2014]. URL: http://www.smf.org/docs/articles/pdf/chingtechbrief.pdf.
- [7] Night vision. *How Thermal Imaging Works*. [Online; accessed July 1, 2014]. URL: http://www.nightvision.com.au/library/how-thermal-imaging-works.
- [8] Hacker Brushless Motors. Specification sheet. [Online; accessed May 20, 2014]. URL: http://www.hacker-motor.com/download/hacker-antriebsfinder/.
- [9] Hacker Brushless Motors. A30-14 L V3. [Online; accessed May 20, 2014]. URL: http://www.hacker-motor-shop.com/e-vendo.php?shop=hacker_e&SessionId=&a=article&ProdNr=15716903&t=3&c=6514&p=6514.
- [10] Hacker Brushless Motors. Speed Controller X-40-SB-Pro. [Online; accessed May 20, 2014]. URL: http://www.hacker-motor-shop.com/e-vendo.php?shop=hacker_e&a=article&ProdNr=87200004&t=7&c=46&p=46.
- [11] Servo Database. NARO super FD. [Online; accessed May 21, 2014]. URL: http://www.servodatabase.com/servo/gws/naro-super-fd.
- [12] Battery University. How to Prolong Lithium-based Batteries. [Online; accessed June 2, 2014].

 URL: http://batteryuniversity.com/learn/article/how_to_prolong_lithium_based_batteries.
- [13] Marshall Brain. *How Lithium-ion Batteries Work*. [Online; accessed June 2, 2014]. URL: http://electronics.howstuffworks.com/everyday-tech/lithium-ion-battery2.htm.
- [14] B. Scrosati, F. Croce, and S. Panero. "Progress in lithium polymer battery R&D". In: *Journal of Power Sources* (1-2 Nov. 2001). [Online; accessed May 19, 2014], pp. 93–100. DOI: 10.1016/S0378-7753(01)00886-2.
- [15] Amicell. *Li-Polymer batteries*. [Online; accessed June 2, 2014]. URL: http://www.amicell.co.il/batteries/rechargeable-batteries/li-polymer-batteries/.
- [16] Verdant. S-Band Blade Antenna. [Online; accessed May 15, 2014]. URL: http://www.verdanttelemetry.com/product-details.php?id=50&prdtcat_id=167.

126 Bibliography

[17] PHARAD. *UHF to C-band UAV Antenna* 800 – 6000 MHz. [Online; accessed May 13, 2014]. 2014. URL: http://www.pharad.com/uhf-to-c-band-uav-antenna.html#.

- [18] L-3 communications. MICRO SDDL. 2012. URL: http://www2.l-3com.com/scm/pdf/datasheets/ML628_MICRO%20SDDL_MICRO%20Secure%20Digital%20Data%20Link_SCMRev%20A.PDF.
- [19] Avalon RF. 1W High Speed Wireless Digital Link. [Online; accessed May 15, 2014]. URL: http://www.avalonrf.com/literature/pdf/TR430%20Brochure.pdf.
- [20] NavStik. [Online; accessed June 19, 2014]. URL: http://navstik.org/home/.
- [21] FLIR. COBALTTM90 gimbal system. 2010. URL: http://www.flircms.com/uploadedfiles/gs/datasheets/a_ltr_cobalt_90.pdf.
- [22] OCZ technology. OCZ 2.5inch SATA2 SSD (Solid State Drive). [Online; accessed June 10, 2014]. URL: http://www.ocztechnology.com/res_old/ssd/OCZ_Core_Series_SSD_SPEC.pdf.
- [23] UAV factory. *Heated Pitot-Static Probe for UAVs.* [Online; accessed June 26, 2014]. URL: http://uavfactory.com/product/28.
- [24] Cree. XLamp XP-E. [Online; accessed June 19, 2014]. URL: http://www.cree.com/LED-Components-and-Modules/Products/XLamp/Discrete-Directional/XLamp-XPE.
- [25] Hon Hai Precision Industry Co. *Voltage adjusting device for solid state drive*. [Online; accessed June 10, 2014]. URL: http://www.google.com/patents/US20130119959.
- [26] On semiconductor. NCP1129, 12 Watt, Off-line Buck Regulator. [Online; accessed June 10, 2014]. URL: http://www.onsemi.com/pub_link/Collateral/DN05053-D.PDF.
- [27] Marshall Brain. *How Microprocessors Work*. [Online; accessed June 10, 2014]. URL: http://www.howstuffworks.com/microprocessor.htm.
- [28] J.L. Henessy and D.A. Patterson. *Computer Architecture: A Quantitative Approach.* ISBN 0-12-383872-X. 2011.
- [29] AMD. AMD's 10-bit Video Output Technology. [Online; accessed June 10, 2014]. URL: http://ati.amd.com/products/pdf/10-Bit.pdf.
- [30] Peter Torr. *High Definition Facts*. [Online; accessed June 10, 2014]. URL: http://blogs.msdn.com/b/ptorr/archive/2006/03/15/hdfacts.aspx.
- [31] Peter Forret. Video bitrate calculator. [Online; accessed June 10, 2014]. URL: http://web.forret.com/tools/video_fps.asp?width=768&height=240&fps=24&space=rgb444&depth=4.
- [32] Logitech. *The H.264 Advanced Video Coding (AVC) Standard*. [Online; accessed June 6, 2014]. URL: http://www.logitech.com/assets/45120/logitechh.pdf.
- [33] SkyCircuit. *Autopilots*. [Online; accessed June 17, 2014]. URL: http://www.skycircuits.com/autopilots/.
- [34] ST. STWD100. [Online; accessed June 19, 2014]. URL: http://docs-europe.electrocomponents.com/webdocs/0dbf/0900766b80dbfeae.pdf.
- [35] Samsung. Samsung MicroSDXC Pro 64GB Class 10. [Online; accessed June 19, 2014]. URL: http://www.samsung.com.
- [36] Jay Gundlach. *Designing unmanned aircraft systems a comprehensive approach*. .16 Command, control, tasking, processing, exploitation and dissemination. 978-1-160086-843-6. AIAA, 2012.

BIBLIOGRAPHY 127

[37] PHARAD. *Ultrathin Peel & Stick Appliqué Antenna 420 - 450 MHz.* [Online; accessed June 11, 2014]. 2014. URL: http://www.pharad.com/420-450-mhz-peel-stick-applique-antenna.html#.

- [38] A. Rashidian et al. *Development of polymer-based dielectric resonator antennas for millimeter-wave applications.* Technical Report. University of Saskatchewan, 2010.
- [39] National Data Buoy Center (NDBC). *Ocean current velocities*. [Online; accessed June 13, 2014]. National Oceanic and Atmospheric Administration (NOAA). URL: http://www.ndbc.noaa.gov/adcp.shtml.
- [40] G. Elert. Speed of Ocean Currents. [Online; accessed April 29, 2014]. URL: http://hypertextbook.com/facts/2002/EugeneStatnikovs.shtml.
- [41] R. (Canadian Coast Guard) Fitzgerald. *Drift of common search and rescue objects: Phase II.* The Centre, 1993.
- [42] Koninklijke Nederlandse Redding Maatschappij (KNRM). *Instructieboek*. .7 Zoeken. 2010.
- [43] N. Timmer. Introduction to wind energy Lecture 3. Delft University of Technology, 2013, p. 57.
- [44] Troy. *UAV pneumatic catapult.* [Online; accessed June 9, 2014]. URL: http://wrww.troybuiltmodels.com/items/UAVPEN-ACC-CATAPULT4.html.
- [45] Robonic. *Robonic pneumatic catapult.* [Online; accessed June 17, 2014]. URL: http://zen. yritysposti.com/wordpress/wp-content/uploads/2012/10/MC0315L.pdf.
- [46] Eli. *Eli pneumatic catapult*. [Online; accessed June 17, 2014]. URL: http://www.eli.ee/products/7/uav-pneumatic-catapult.
- [47] AMSA. Wind & Waves. [Online; accessed June 12, 2014]. URL: https://www.amsa.gov.au/forms-and-publications/search-and-rescue/publications/documents/Wind_&_Waves.pdf.
- [48] Affluent page. Dornier Seaplane Prepares Launch of \$ 6 Million Seastar. [Online; accessed June 17, 2014]. 2013. URL: http://www.affluentpageluxuryindex.com/new-and-noteworthy/dornier-seaplane-prepares-launch-of-6-million-seastar/.
- [49] Bourns. Datasheet 12 mm Rotary Position Sensor. [Online; accessed June 16, 2014]. URL: http://www.bourns.com/data/global/pdfs/3382.pdf.
- [50] V. Severson, P. Murray, and Heeter J. "Establishing cause and effect relationships between lightning flash data and airplane lightning strike damage". In: *Vaisalia* (2014).
- [51] G. Sweers, B. Birch, and J. Gokcen. *PLA Resin Raw Material*. [Online; accessed June 24, 2014]. URL: http://www.boeing.com/commercial/aeromagazine/articles/2012_q4/4/.
- [52] E.R. Weibel and R.J. Hansman. "Safety considerations for operation of unmanned aerial vehicles in the national airspace system". In: MIT Report No. ICAT-2005-1 (2005). URL: http://dspace.mit.edu/bitstream/handle/1721.1/34912/Weibel%20-%20ICAT%20Report%20-%20UAV%20Safety.pdf.
- [53] INC. HARDING ENERGY. Harding Battery Handbook For Quest. 2014. URL: http://hardingenergy.com/wp-content/uploads/2012/06/6-Lithium-Polymer.pdf.
- [54] Ainsley Henry. *Marine Pollution*. [Online; accessed June 16, 2014]. URL: http://www.nepa.gov.jm/student/resource-material/pdf/Marine_Pollution.pdf.
- [55] R. Dortwegt. The chemistry of copper in water and related studies planned at the advanced photon source. [Online; accessed June 16, 2014]. URL: http://accelconf.web.cern.ch/accelconf/p01/PAPERS/TPAH106.PDF.

128 Bibliography

[56] Lenntech B.V. Aluminum and water: reaction mechanisms, environmental impact and health effects. [Online; accessed June 16, 2014]. URL: http://www.lenntech.com/periodic/water/aluminium/aluminum-and-water.htm.

- [57] Environmental Health & Safety Online. *Battery Recycling and Disposal Guide for Households*. [Online; accessed June 16, 2014]. URL: http://www.ehso.com/ehshome/batteries.php#Summary.
- [58] Kristen Hall-Geisler. Can Electric Car Batteries Be Recycled? [Online; accessed June 16, 2014].
 URL: http://auto.howstuffworks.com/can-electric-car-batteries-be-recycled.
 htm
- [59] A.K. Mohanty, M. Misra, and G. Hinrichsen. "Biofibres, biodegradable polymers and biocomposites: An overview". In: *Macromolucular Materials and Engineering* (2000). [Online; accessed May 14, 2014].
- [60] L. Yan, N. Chouw, and K. Jayaraman. "Flax fibre and its composites A review". In: *Elsevier composites* (2013). [Online; accessed May 14, 2014].
- [61] K. Oksman, M. Skrifvars, and J.F. Selin. "Natural fibres as reinforcement in polylactic acid (PLA) composites". In: *Composites Part A: Applied Science and Manufacturing* 27 (1996).
- [62] John Scheirs. Compositional and failure analysis of polymers. John Wiley.
- [63] Jinchun Zhu et al. "Recent Development of Flax Fibres and Their Reinforced Composites Based on Different Polymeric Matrices". In: *Materials* 6.11 (2013). ISSN: 1996-1944. DOI: 10.3390/ma6115171. URL: http://www.mdpi.com/1996-1944/6/11/5171.
- [64] K. Madhavan Nampoothiri, Nimisha Rajendran Nair, and Rojan Pappy John. "An overview of the recent developments in polylactide (PLA) research". In: Bioresource Technology 101.22 (2010), pp. 8493-8501. ISSN: 0960-8524. DOI: http://dx.doi.org/10.1016/j.biortech. 2010.05.092. URL: http://www.sciencedirect.com/science/article/pii/S0960852410009508.
- [65] I. Widiastuti, I. Sbarski, and S.H. Masood. "Creep Behavior of PLA-Based Biodegradable Plastic Exposed to a Hydrocarbon Liquid". In: *Journal of Applied Polymer Science* (2013).
- [66] H. Bos. *The Potential of Flax Fibres as Reinforcement for Composite Materials.* 90-386-3005-0. University Press Facilities, Eindhoven, 2004.
- [67] Composite Evolution. *Biotex Flax/PLA*. [Online; accessed June 13, 2014]. URL: http://www.compositesevolution.com/Products/Biotex/BiotexFlaxPLA.aspx.
- [68] J.L. Thomason and Vlug M.A. "Composites". In: *Composites Part A: Applied Science and Manufacturing* 27 (1996).
- [69] Caroline Baillie. Green Composites: Polymer Composites and the Environment. John Wiley.
- [70] Composite Evolution. Nonwoven Flax Fibre Reinforced PLA biodegradable Composites. [Online; accessed June 13, 2014]. URL: https://www.escholar.manchester.ac.uk/api/datastream?publicationPid=uk-ac-man-scw:220581&datastreamId=FULL-TEXT.PDF.
- [71] K. Krasowska1 et al. "Environmental Degradation of Ramie Fibre Reinforced Biocomposites". In: *Polish J. of Environ*. 937-945 19 (2010).
- [72] Chyanbin Hwu Mengchun Yu. Free Vibration Analysis of Tapered Composite Wings. 2013. URL: http://www.iaa.ncku.edu.tw/~chwu/PDFfile/PDF_Conference/C061_AMDP_Auckland.pdf.

BIBLIOGRAPHY 129

[73] I. Widiastuti, I. Sbarski, and S.H. Masood. "Fatigue Behavior of Unidirectional Jute Spun Yarn Reinforced PLA". In: *Advanced Composite Materials* (2012).

- [74] E.G. Bilham and E.F. Relf. "The Dynamics of Large Hailstones". In: *Quarterly Journal of the Royal Meteorological Society* 63 (1937).
- [75] ultraeverdry. *Ultra Ever Dry*. [Online; accessed June 5, 2014]. URL: http://www.ultraeverdrystore.com.
- [76] Taber Industries. *Taber Industries*. [Online; accessed June 5, 2014]. URL: http://www.taberindustries.com/taber-abrading-wheels.
- [77] Tencate. EF72. [Online; accessed June 30, 2014]. URL: http://www.ambercomposites.com/ef72-adhesive-film.
- [78] Master Bond. Master Bond polymer system EP31. [Online; accessed June 30, 2014]. URL: http://pdf.directindustry.com/pdf/master-bond/master-bond-ep31-epoxy-adhesive-structural-bonding-featuring-extraordinarily-high-shear-peel-strengths/17407-13454.html.
- [79] 3m. 3M Scotch-Weld Epoxy Adhesive EC-2792 B/A. [Online; accessed June 30, 2014]. URL: http://multimedia.3m.com/mws/mediawebserver?mwsId=SSSSufSevTsZxtU5xt10x_UevUqevTSevTSeSSSSSS--&fn=TDS_EC-2792BA.pdf.
- [80] Huntsman. *Users guide adhesives*. [Online; accessed June 27, 2014]. URL: http://www.freemansupply.com/datasheets/adhesivesguide.pdf.
- [81] J.A. Mulder, W.H.J.J. Staveren, and J.C. Vaart. *Flight Dynamics. Lecture Notes AE3202*. Faculty of Aerospace Engineering.
- [82] Evco. *Thin wall packaging*. [Online; accessed June 19, 2014]. URL: http://www.evcoplastics.com/thin-wall-plastic-packaging.
- [83] Efunda. Design standards plastic design. [Online; accessed June 18, 2014]. URL: http://www.efunda.com/designstandards/plastic_design/wall.cfm.
- [84] Adhesives toolkit. *Design guidance, stress distributions*. [Online; accessed June 29, 2014]. URL: http://www.adhesivestoolkit.com/Toolkits/DesignGuidance/StressDistributions.xtp.
- [85] A. I. Shutov and V.G. Strukov. "A method for calculating the impact strength of sheet glass". In: *Glass and ceramics* 53 (1996).
- [86] R. B. Charlton and R. List. "Hail size distributions and accumulation zones". In: *Journal of the atmospheric sciences* 29 (1972).
- [87] R. Kelm and M. Grabietz. *Method of reducing wind gust loads acting on an aircraft.* US Patent 6,161,801. 2000.
- [88] Ilan Kroo. "Simple Performance Estimation". In: AA241X Spring (2009).
- [89] Dr. Martin Hepperle. Basic Design of Flying Wing Models. 2002.
- [90] aerospace department UIUC. *UIUC airfoil coordinates database*. [Online; accessed June 5, 2014]. URL: http://aerospace.illinois.edu/m-selig/ads/coord_database.html.
- [91] Jean-Claude Etiemble. *airfoils database*. [Online; accessed June 5, 2014]. URL: http://tracfoil.free.fr/airfoils/h.htm.
- [92] Airfoiltools.com. *NACA 5 digit airfoil generator*. [Online; accessed June 5, 2014]. URL: http://airfoiltools.com/airfoil/naca5digit.

130 Bibliography

[93] G. La Rocca. *Systems engineering and aerospace design - Lecture 3*. Delft University of Technology, 2014, p. 20.

- [94] G. La Rocca. *Aerospace Design and Systems Engineering Elements II Wing Design part 2.* Delft University of Technology, 2011, p. 71.
- [95] Martin Hepperle. *Basic design of flying wing models*. [Online; accessed June 16, 2014]. URL: http://www.mh-aerotools.de/airfoils/flywing1.htm.
- [96] G. La Rocca. *Requirement Analysis and Design principles for A/C stability & control (Part 2).* Delft University of Technology, 2011, p. 40.
- [97] Mohammed Sadraey. Aircraft Design. J. Wiley & Sons, 2013.
- [98] D. Sholz M. Nita. *Estimating the Oswald factor from basic aircraft geometrical parameters.* Technical Report. Hamburg University of Applied Sciences, 2012.
- [99] Martin Hepperle. *How a Propeller Works*. [Online; accessed June 20, 2014]. URL: http://www.mh-aerotools.de/airfoils/propuls4.htm.
- [100] G La Rocca. Tail plane design, Weight & Balance. Delft University of Technology, 2013, p. 7.
- [101] J. Sinke. Production of Aerospace Materials. Delft University of Technology, 2013.
- [102] Arburg. Long-fibre direct injection moulding. [Online; accessed June 17, 2014]. URL: http://www.arburg.com/fileadmin/redaktion/Sonstiges/ARBURG_long-fibre_direct_injection_moulding_680867_en_GB.pdf.
- [103] Extreme bolts & fasteners. *PEEK Fasteners / Victrex*® *Fasteners*. [Online; accessed June 19, 2014]. URL: http://www.extreme-bolt.com/Materials-PEEK.html.
- [104] Jay Gundlach. *Designing unmanned aircraft systems a comprehensive approach*. .19 Cost Analysis. 978-1-160086-843-6. AIAA, 2012.
- [105] United States Department of Labor. Bureau of Labor Statistics Databases, Tables & Calculator per Subject PPI Database. [Online; accessed June 18, 2014]. URL: http://www.bls.gov/ppi/#data.
- [106] Bureau of labor statistics. *Occupational Employment and Wages, May 2013.* [Online; accessed June 24, 2014]. URL: http://www.bls.gov/oes/current/oes172011.htm.
- [107] Conrad. Motor price. [Online; accessed May 23, 2014]. URL: http://www.conrad.nl/ce/.
- [108] Servo Database. *Robbe FS-550 servo*. [Online; accessed May 20, 2014]. URL: http://www.servodatabase.com/servo/robbe/fs-550-bb.
- [109] Furunousa. S-Band Transceiver price. [Online; accessed May 23, 2014]. URL: http://www.furunousa.com/ProductDocuments/FLYKITFAR28X5SBAND%20FAR28x5%20S-Band%20Transceivers%20Service%20Kit.pdf.
- [110] Energytrend. *Battery price*. [Online; accessed May 23, 2014]. URL: http://www.energytrend.com/battery-price.html.
- [111] PZC. Productschap: prijs van lange vlas vezels herstelt. [Online; accessed June 24, 2014]. URL: http://www.vandebiltzadenvlas.com/assets/files/Pers-PZC/101123.pdf.
- [112] G. Boothroyd, P. Dewhurst, and W. Knight. *Product Design for Manufacture and Assembly*. Marcel Dekker, Inc., 2002.
- [113] S. Hoogendoorn. *Traffic management and ITS, CT3080LR. Lecture Notes.* Delft University of Technology, 2012, p. 18.
- [114] K. Hartley. "The Learning Curve and Its Application to the Aircraft Industry". In: *The Journal of Industrial Economics* 13 (1965).

BIBLIOGRAPHY 131

[115] G. Howarth and M. Hadfield. "A sustainable product design model". In: *Elsevier Materials and Design* 27 (10 2006), pp. 1128–1133.

- [116] Carnegie Mellon University Green Design Institute. *Economic Input-Output Life Cycle Assessment (EIO-LCA), US 2002 Producer Price model.* [Online; accessed June 3, 2014]. 2008. URL: http://www.eiolca.net.
- [117] J.D. Anderson. Introduction to Flight. 0-07-100496-3. McGraw-Hill, 1989.
- [118] J.A. Melkert and T.J. Dingemans. *Project Guide Design Synthesis Exercise. All weather, all polymer Search and Rescue(SAR) UAV with hover capability.* Faculty of Aerospace Engineering.
- [119] J.A. Melkert and T.J. Dingemans. *AE3200 Project Description. All weather, all polymer Search and Rescue(SAR) UAV with hover capability.* Faculty of Aerospace Engineering.
- [120] AIS Security Solutions. Long-range surveillance cameras & Johnson's criteria. [Online; accessed April 28, 2014]. URL: http://www.aissecuritysolutions.com/white-paper-on-long-range-surveillance-cameras.pdf.
- [121] ASTM. Historical Standard: ASTM F2411-04e1 Standard Specification for Design and Performance of an Airborne Sense-and-Avoid System. ASTM.

A

EIO-LCA FOR AIRCRAFT MANUFACTURING

Table A.1 [116] shows the total result from the Economic Input-Output Life Cycle Assessment as used for the environmental sustainability of the ASAP UAS (Section 11.2).

Table A.1: The EIO-LCA. result

	Category	Direct Economic	CO	DIRECT CO	NOx	DIRECT Nox	SO2	Direct SO2	CO2e	Direct CO2e
		%	t	t	t	1	<i>t</i>	t	<i>t</i>	t
ID	Total for all sectors	80.481	0.589	0.474	0.627	0.505	0.658	0.530	213.654	171.951
221100	Power generation and supply	20.700	0.036	0.007	0.258	0.053	0.575	0.119	139.000	28.773
336411	Aircraft manufacturing	99.800	0.169	0.169	0.026	0.026	0.016	0.016	7.840	7.824
484000	Truck transportation	39.900	0.157	0.063	0.166	0.066	0.003	0.001	18.900	7.541
336413	Other aircraft parts and equipment	92.900	900.0	900.0	0.011	0.010	0.011	0.010	7.050	6.549
336412	Aircraft engine and engine parts manufacturing	71.900	0.019	0.014	0.024	0.017	0.015	0.011	4.630	3.329
481000	Air transportation	46.800	0.019	0.009	0.003	0.001	0.000	0.000	6.830	3.196
334413	Semiconductor and related device manufacturing	22.600	0.000	0.000	0.000	0.000	0.000	0.000	2.580	1.486
550000	Management of companies and enterprises	20.000	0.001	0.001	0.001	0.001	0.001	0.001	2.370	1.185
420000	Wholesale trade	45.700	0.032	0.015	0.031	0.014	0.002	0.001	2.060	0.941
334511	Search, detection, and navigation instruments	93.100	0.000	0.000	0.001	0.001	0.000	0.000	0.748	0.696
482000	Rail transportation	18.300	0.011	0.002	0.082	0.015	0.000	0.001	3.330	0.609
541700	Scientific research and development services	37.100	0.016	900.0	0.001	0.000	0.002	0.001	1.250	0.464
562000	Waste management and remediation services	9.340	0.003	0.000	0.002	0.000	0.000	0.000	3.830	0.358
32619A	Other plastics product manufacturing	46.700	0.007	0.003	0.001	0.000	0.002	0.001	0.554	0.259
332800	Coating, engraving, heat treating and allied	32.500	0.003	0.001	0.001	0.000	0.000	0.000	0.690	0.224
	activities									
336300	Motor vehicle parts manufacturing	65.400	0.005	0.003	0.001	0.001	0.000	0.000	0.334	0.218
325940	All other chemical product and preparation	42.700	0.008	0.003	0.002	0.001	900.0	0.003	0.496	0.212
	manufacturing									
493000	Warehousing and storage	35.700	0.004	0.001	0.001	0.000	0.000	0.000	0.361	0.129
325190	Other basic organic chemical manufacturing	2.560	0.006	0.000	0.009	0.000	0.007	0.000	3.830	0.098
332500	Hardware manufacturing	34.300	0.000	0.000	0.000	0.000	0.000	0.000	0.242	0.083
33451A	Watch, clock, and other measuring and controlling	94.400	0.000	0.000	0.000	0.000	0.000	0.000	0.087	0.082
	device manufacturing									
533000	Lessors of nonfinancial intangible assets	23.800	0.000	0.000	0.000	0.000	0.000	0.000	0.316	0.075
334220	Broadcast and wireless communications	79.700	0.000	0.000	0.000	0.000	0.000	0.000	0.080	0.064
	equipment									
335920	Communication and energy wire and cable	45.100	0.000	0.000	0.000	0.000	0.000	0.000	0.141	0.064
	manufacturing									
335930	Wiring device manufacturing	73.200	0.000	0.000	0.000	0.000	0.000	0.000	0.085	0.062
332710	Machine shops	34.200	0.000	0.000	0.000	0.000	0.000	0.000	0.159	0.054
517000	Telecommunications	10.400	0.002	0.000	0.000	0.000	0.000	0.000	0.492	0.051
532400	Commercial and industrial machinery and	33.500	0.072	0.024	0.001	0.000	0.000	0.000	0.108	0.036
	equipment rental									
325211	Plastics material and resin manufacturing	1.090	0.003	0.000	0.002	0.000	0.002	0.000	2.660	0.029
325510	Paint and coating manufacturing	37.600	0.002	0.001	0.000	0.000	0.000	0.000	090.0	0.023
261900	Other support services	20.600	0.000	0.000	0.000	0.000	0.000	0.000	0.081	0.017

Table A.1: (continued)

	Category	Direct Economic	00	DIRECT CO	NOx	DIRECT Nox	SO2	Direct SO2	CO2e	Direct CO2e
E		%	t	+	+	t	1	t	1	1
333515	Cutting tool and machine tool accessory	43.200	0.000	0.000	0.000	0.000	0.000	0.000	0.037	0.016
	manufacturing									
5419A0	All other miscellaneous professional and technical	22.700	0.000	0.000	0.000	0.000	0.000	0.000	090.0	0.014
	services									
541512	Computer systems design services	30.000	0.000	0.000	0.000	0.000	0.000	0.000	0.044	0.013
811300	Commercial machinery repair and maintenance	22.600	900.0	0.001	0.000	0.000	0.000	0.000	0.058	0.013
541511	Custom computer programming services	64.000	0.000	0.000	0.000	0.000	0.000	0.000	0.018	0.012
323110	Printing	2.960	0.000	0.000	0.000	0.000	0.000	0.000	0.136	0.011
334418	Printed circuit assembly (electronic assembly)	29.300	0.000	0.000	0.000	0.000	0.000	0.000	0.035	0.010
	manufacturing									
531000	Real estate	4.660	0.000	0.000	0.000	0.000	0.000	0.000	0.219	0.010
518200	Data processing, hosting, and related services	29.400	0.000	0.000	0.000	0.000	0.000	0.000	0.033	0.010
325188	All other basic inorganic chemical manufacturing	0.774	0.001	0.000	0.001	0.000	900.0	0.000	1.200	0.009
811200	Electronic equipment repair and maintenance	26.800	0.000	0.000	0.000	0.000	0.000	0.000	0.018	0.005
334417	Electronic connector manufacturing	16.500	0.000	0.000	0.000	0.000	0.000	0.000	0.028	0.005
334419	Other electronic component manufacturing	11.400	0.000	0.000	0.000	0.000	0.000	0.000	0.040	0.005
326110	Plastics packaging materials, film and sheet	2.410	0.000	0.000	0.000	0.000	0.000	0.000	0.133	0.003
334412	Bare printed circuit board manufacturing	3.430	0.000	0.000	0.000	0.000	0.000	0.000	0.044	0.002
325220	Artificial and synthetic fibers and filaments	0.107	0.001	0.000	0.002	0.000	0.004	0.000	0.286	0.000
	manufacturing									
334111	Electronic computer manufacturing	9.180	0.000	0.000	0.000	0.000	0.000	0.000	0.003	0.000
313100	Fiber, yarn, and thread mills	0.083	0.000	0.000	0.000	0.000	0.000	0.000	0.068	0.000

B

PERSONAL APPENDICES

This appendix contains the personal appendices of all team members. The purpose of these is to provide the tutor and coaches with feedback about the design and the team process. Each team member will elaborate on:

- his functioning in the design team,
- the project as a whole,
- the design team and team cooperation,
- the project organisation and
- · the tutor and coaches.

B.1. D. VAN DEN BERGEN

Personal activities After the mid-termreview we started with correcting the mid-term report. Also in this week I wrote the quality control sheet (in this excel sheet all used values were stored) of the mid-termreport and the final report. Also I wrote this week the concept generation part of the chapter "baseline and midtermreport recap". At the end of this I started with the electrical block diagram of the UAV.

The next week I did some quality control and finished the electrical block diagram. Besides that I wrote the section "battery" of the chapter "sub-systems" together with Bram and made the data handling and communication diagrams. At the end of the week I wrote about the sub-systems in general and started to do some research to polymers. In the third week I started a vast research to biodegradable materials and polymers together with Nico en Tim. In this week I wrote about creep of PLA, the Rule of Mixture, chopped fiber composites and continuous fiber composites. Also I built a small script in order to calculate the properties of several Flax-PLA composites. In the fourth week I finished my part of materials and started with the manufacturing part of the MAI plan. After finishing the manufacturing part, I started with the integration part of the MAI plan. Besides that, I also helped Tom a bit with the cost analysis. During the final design Tom and I were responsible for the quality control.

The last week before the deadline of the draft report we started with editing the report. Also I wrote about the final weight analysis and about the Pitot tube, warning lights and flight computer. In the last weeks before the deadline of the final report I did a research to adhesive bonding and wrote about. Also I wrote the part about detecting drowning victims in the water. Besides these activities we had weekly meetings with the team, status updates and the Final review.

Project, Team and Staff After the mid-termreview I noticed the motivation of the team was a little bit decreased, nevertheless high enough to deliver a high quality final design. Still, I think this motivation is our team's major advantage. Everyone takes their tasks serious and is trying to do their tasks as conscientious as possible. Still there is a bit of chaos inside the team, however normally this is fixed with semi-weekly meetings and by hard working. I still think that the staff functions professional, since their technical background is really good and they respond fast to questions. On the other hand the OSSAs were sometimes not really helpful. Of all the project's subjects I think materials was the most interesting.

Personal functioning I am still convinced that I am doing everything I can to deliver high quality work and as fast as possible. I think advantage of me in the team are the willingness to work hard. The main disadvantages of me in the team is the fact that sometimes I have to take more initiative and sometimes I could be too quiet, however I think this has improved.

B.2. T. BLONDEEL

My activities for the final report existed of the structural elements in the DSE. I cooperated with the recap, the reliability, the selection of the materials and with the manufacturing, assembly and integration and with the battery configuration. I am happy to say that my input in these parts was good. I tried to improve my writing skills after the feedback of the first half of the project and I feel that I grew in being a team member and an engineering and that my writing skills have improved.

The group was the best project group I have had during my bachelor aerospace engineering. There were no problems about other elements then design choices and these are necessary to find an optimal solution. All the work is done in time and the level of quality is also very high in my opinion. There was also a good task description and focus on the parts that had be performed.

The project was fun. It was challenging yet achievable. It was a nice change to be on a design team once instead of learning about how a design should be. The concept of a meeting was known to me, but I never participated in one and I can say now that I have. However, I expected more calculations and less literature study. A lot of the work came forth from other sources where a method was replicated instead of designed. The technical input of the final design was higher than for the mid-term report but still under my expectations. The technical content that was present, was a good challenge.

The OSSA's where available and a number of books was available through them. A negative point was the noise in the Fellowship. During the final design, a working crew started with construction work and this gave a loud, annoying sound that irritated me on multiple occasions. Another building was foreseen but this was not finished on time. By the time it was finished, I already became familiar with the noise and a transmigration was not necessary anymore. Overall, I was happy with the organization in the Fellowship since there were also meeting rooms that could be reserved multiple times per week.

Contact with the tutors went great. Every week, there was a meeting where the current problems were explained. These sessions where always helpful. The tutors helped with this problems and gave new problems with critical questions which improved the overall design.

The subject of the project was fun. During my Bachelor, I did not learn a lot about UAVs and now I was part of a team that designed one. I am happy that the DSE is part of the Bachelor since such a design exercise is extremely educational and the scope of the work is not achievable through lectures.

B.3. B. DURIEUX

The second part of the project was about finalizing the trade-off performed in the midterm report and working out the final design in detail.

Personally, I started the second phase with elaborating on the trade-off for the final concept where I focused on the difference in flight performance of the different concepts and the structural aspects of the joined wing concept.

When the final trade-off was finished and the detailed design phase started I worked on the flight performance part. It was quite a challenge to find a more or less optimal solution because of all the contradictory performance elements. It was a highly iterative process.

When the technical aspects of the UAV were more or less determined it was time to start on the less technical aspects. I primarily focused on the energy storage of the UAV and the life cycle plus RAMS analysis. This last chapter was far more extensive than we thought it would be and it took a large bulk of our time. On a final note, I was a bit disappointed that the team roles we put ourselves to in the first week were abandoned. I was to work on the control and operations part, a field of expertise I committed myself to for a MSc Systems and Control. Although I feel everyone experienced the same, we eagerly took on other problems without much complaints.

Our team really gave the subject our personal touch. We managed to come up with a unique solution for a difficult challenge. Where we found quite a few UAV projects which shared some similarities with ours, our solution is truly unique.

In this second part of the project, the team motivation dropped a bit. I think it is mainly due to the fact that the midterm review was conceived as disappointing by many. I think the motivational drop is reflected in the second peer review where I expect everyone scored a few tenths of points lower than in the first peer. However, we continued working and we managed to deliver a great product.

I am very happy with the way the tutors handled our group. We were given a great amount of freedom to define our project ourselves. With the status updates and during the reviews, they asked critical and honest questions which helped our team to improve the quality of the report. I feel our team is very satisfied with the level of commitment of the tutors.

B.4. D.N.E. MAXENCE

At first the group was a bit hesitant about one another, though some people already knew each other before the project started. However the enthusiasm for the project itself was immense from day one. I believe the group was even too enthusiastic in the beginning because it was one uncoordinated chaos of brainstorming ideas without any straight lineout for the project. However we tried to get a project structure going as fast as possible.

The functions were divided as fast as possible. I volunteered to keep the logbook going and started sending out mails to external third parties asking for any additional input that may be of use. That way I became the secretary of external communication which has proven to be quite beneficial to the group as we managed to set up an interview with the KNRM as well as additional communication with the UAV and materials departments of NLR. Information gathered from the KNRM was a major driver in some important decisions throughout the report.

As for contributions to the baseline report, I mainly worked on the organogram, the market analysis, mission analysis and the budget breakdown. The feedback of the baseline report was mainly positive and after the presentation, we immediately started correcting the baseline report. After that, the concept generation was made, which was a team effort. This was done in the universal library which was beneficial for these kind of group sessions because there was no interference from other groups.

After the concept generation, everybody started on their individual contributions to the mid-term report. My main contributions were the communication systems, the RAMS analysis and the development of the aero-dynamics tool. I also contributed to other parts to a smaller extent. I also continued to keep the external communication going and tried to gather as much reference material as possible. This was because the literature studies performed online were not always successful, and even frustrating sometimes because of the incompatibility of the found information to the project.

The mid-term presentation went well, including the feedback. However a drastic change has been made in the design. Because of the insufficiently argumented choice to go for a boxwing design, a revision of the final trade-off table has been made. This was also a team effort, as a definite choice on the design had to be made in order to continue with the project. Everybody worked on one specific part of the trade-off table. I worked on the stall characteristics, and after that I completed the aerodynamic characteristics, airfoil selection, stability analysis and the sizing of the elevens . I also performed a link budget analysis, and contributed to other sections in a minor way.

I believe the end result is quite decent, because the entire group had a say in its design. Major design choices were always discussed within the group during the semi-weekly group meetings or with improvised team meetings. No definite design choice was made until everybody had discussed it. There are people that talk more than others off course, but I believe that everybody had a chance to do their say. This improved greatly after the first peer evaluation, which helped improve the dynamic within the group. The effectiveness of the team also rose after the peer evaluation, and I believe we have a quite effective team towards the end of the project. There were no major disagreements within the group, everybody got along quite well and the work proceeded fluently.

The coordinators had relevant feedback during the status updates and the review sessions. Although not every coordinator could always be present during these meetings, there was no lack of guidance when it was necessary. However, we as a team were also stimulated to think for ourselves without relying too much on the coordinators for guidance. We were motivated to solve our own problems independently and use logic thinking and engineering sense to come to a solution. This engineering mentality and the improved dynamic of the team work are the most important things I have acquired during the duration of the project.

B.5. J.M. VAN MOURIK BROEKMAN

My personal appendix starts with my own tasks and functioning during the project, followed by a short description of the team and cooperation between the group members. Finally I will give some notes on the project, the organization and the staff.

My **activities** during the second half of the project consisted of designing the aerodynamics of the UAV, determining the life cycle and the verifying and validating the final design. I am proud to say that I have made a significant contribution to all three. Furthermore, I am responsible for the symposium presentation together with Nico and this is something I look forward to.

I believe that, although I was less motivated the second hald of the project, my **functioning** within the group has improved. I have taken the remarks on my functioning by the group, as well as my own remarks, seriously and I have progressed as both a chairman and an engineer. From being over concerned and too involved as chairman, I now feel that I know when to let go and when it is necessary for me to step in and take charge. In addition, I have put much time and effort in my technical output, which was my main goal for the second half.

Not a lot has changed to the **team** dynamic since the first half of the project. We have made this project into a success, which is what we all set out to do. The main improvement within the group with respect to the first half is that we have learned to embrace our strengths and weaknesses, and we have divided the work so that everyone could use their strengths. However, I do believe everyone had a more difficult time to keep working hard and everyone was slightly less motivated, as a full time project of 10 weeks requires a lot of energy. A different aspect of the groups dynamic is that no one in the group shies away from confrontation and during these confrontations, the group members keep their positivity and respect for each other. Finally, all major decisions are left up to the group which I see as a good sign of good group dynamic.

I believe that the **cooperation** within the team is one of our strong points. We stay positive under deadline stress and everyone is willing to jump in when someone is having difficulty finishing his task on time.

The entire **project** has been a pleasurable and highly educational experience. It was a large challenge and the level of autonomy was high, which I enjoyed. There is only one aspect that I did not like. If one wants to design an exceptional search and rescue device, it should not be 'limited' by other requirements, such as the polymer content or disposal methods. I understand this is what makes it a challenge. Somewhere during the project I got the realization that this is simply not a viable product and much more an exercise than I first expected.

The **organization** of the DSE is done very well. All informational documents are complete and clearly written and the timetable is useful. My only complaint is about the working environment; the Fellowship is very noisy with 70 people in one room. More important is that the table is too small for 10 people to work at. It is warm and badly ventilated, even when the windows are open, which has not been the case.

The **staff** has been coaching us well. The weekly meetings allow for us to have a large amount of freedom and I find this very educational. In addition the points of criticism have been more thorough compared to the first half, which for us has been helpful. And just as previous half, I want to mention that the speed with which our inquiries are replied to is great.

B.6. T.J.E. SCHOUTEN

My personal appendix will start with my activities since the Midterm Report. Next, I will evaluate my personal functioning and the group performance. After this I will describe my experience with the DSE and organization before concluding with my feedback on the coaching.

After the Midterm review the team started working on the revision of the Midterm Report. For this revision the main focus was selecting a concept on an engineering basis since the trade-off performed before was weak. I was mainly focused on including contingency in the final trade-off to indicate the unavoidable uncertainties which were present at that project stage. After the Midterm Revision I have been primarily working on the external layout and propulsive performance of the UAV by continuing my work from before the Midterm. This proved to be more work than I initially expected due to the iterative and multi-disciplinary approach with structures, airfoil selection and internal systems. I enjoyed being part of this process and I believe I made a quality contribution to one of the key aspects of aircraft design. The work on aircraft design and optimization also resulted in confirmation for myself that the Flight Performance & Propulsion master will be the right choice for me

When the external layout was determined I have worked on several sections of the project, some more technical than others. First, I described the UAV search patterns and described the movement of objects in water in Operations & Logistics. Next I worked on sustainability and the cost estimation which were less popular among team members. However, I set myself to deliver and I am proud of the results in these chapters. I was unfamiliar with performing a technical cost estimation and therefore I also found this an educational part.

I was happy with the mostly positive feedback I received for the Midterm peer evaluation. I tried to keep the positives while working on my weaknesses. One of these weaknesses was identified by myself as being too engaged by multiple subjects and I think I did well in keeping mostly to subjects were I was expected to work on. A second critique was that I can be loud and distracting at the project table. On the one hand I think I managed to be less distracting to others by being more thoughtful before saying something about whether it will add something to the discussion. On the other hand I think some may still have experienced me as a distraction from time to time. This is also due to the fact that the entire team was more expressive throughout the second part of the project.

Which brings me to the group dynamic after the Midterm. I think the group has really bonded and shown that we are all willing to work for a result to be proud of. No-one turned their back on responsibilities and everyone took feedback in a constructive manner. However, I think the concentration on the project decreased as more weeks went by. After an explosive start and an intense couple of weeks leading to the Midterm Review I think the team has settled at a slower pace. This is completely understandable for such an energy-intensive project as the DSE and therefore I don't think the team is to blame. We all worked with the same goal in mind: achieving a beautiful and as complete as possible design of the ASAP UAV. I want to thank all group members for working hard, setting high standards and enjoying the project as it went.

I think the experience I obtained from the DSE can bring me further in my career. Not only did the DSE solidify my feeling to apply for the FPP MSc but it also showed me what a group of ten motivated people is capable of with limited resources. I know more of my personal strengths and weaknesses in a group setting and will try to keep working on shortcomings in future stages. Overall, I really liked the DSE and experienced it as a challenging closing of the BSc.

The organization of the DSE was professional with clear deadlines, instruction documents on deliverables and resources. The only side-note I would like to make here is that the Fellowship is an unpleasant facility to work in due to poor ventilation and the limited space, thereby making it crowded and noisy. There was an opportunity to work in another building but this building was lacking in support equipment as printers.

Finally, I want to thank all three coaches. After the Midterm their comments on our work were more constructive and detailed whilst keeping a very critical view on our presented results during the weekly status updates. The team was able to work autonomously due to the hands-off approach of the coaches during the entire DSE. In despite of this hands-off approach, questions posed by the team were always quickly and adequately replied and the coaches were always available for support.

SECTION B.7. S. VIAL

B.7. S. VIAL

This personal appendix will start with my functions within the team and the project. After that I will elaborate on the functioning of the team itself. Finally, I will make some comments about the project organisation and tutor and coaches.

After the mid-term report I have had lots of different task, spending time at various aspects of this project. Besides the normal 'engineering' and reporting, I have been working on Finite Element Models, Matlab scripts, CAD drawings, posters, renders and animations. Also, at the time of writing this I am still trying to get a 3D model printed. This is, however, difficult as we're not the only group who would like to use the 3D printers.

Having spend time on so many different things was rewarding. Especially since each and everyone of them gave a satisfying, tangible output. Constantly working on Matlab scripts and documenting everything was something I got a little bit tired off, to be honest. This was also the reason for a motivational 'dip' for the first half of the second part of the DSE. And I think I was not the only one. In the end, though, I think no one really underperformed and we delivered something we can be really proud off. I have contributed most to the structural design, internal lay-out and the post-dse activities.

My positive memories about this project did not only originate from the research topic. I believe that every DSE exercise could have been fun/interesting as long as you have proper guidance (tutor/coaches/other contact) and above all, a nice team. We were lucky to have both. The tutors gave us some great feedback during the reviews and the weekly status updates that we arranged. Any questions at hand could be answered during these meetings, via email or just simply by hopping by. We've had some advice that was most certainly game changing and pushed our final design in a different direction than we initially intended. The team adapted great and together we've pushed the design as far as I think is possible within the DSE time span.

There were also some (relatively small) hiccups that cause irritation. First off, there is the accommodation. Simply put, the project tables are too small for 10 people with laptops. This could be solved by sitting at one of the 'overflow' tables, but this would only diminish the effectiveness of communication. And then there was the ramming of poles across the street. This would cause people to close the windows, making it quite warm inside, or everyone would put on music, making it even harder to communicate. There was the option to go to the new building, but with so little time left we did not want to acclimate to our new surroundings. The time we had was something we wanted to spend on our project. This all might sound bad, but it was bearable and quite frankly the only negative remarks I have about the past 10 weeks.

B.8. R.S. DE WIT

The last halve of the DSE project began by looking at the comments made on the midterm review/report. The most critical comment was about the trade-off we made for the configuration. This was not technically sufficient and this was improved. I worked on the gust stability criteria for this trade off and I really tried to make this more sound. After this was completed, I recapped the mission analysis and market analysis for the final report. In every report this should shortly be outlined and referenced. After this I started working on the subsystems of the UAV. I explained the workings of the payload and summed up what was said in the midterm report. From this point on, I worked on the placement and integration of several subsystems in the UAV. How can the batteries be integrated into the design, what about maintenance etc. I worked on this together with Bram and Stijn. During the status update of the 3rd of June, we got the feedback that we should really start looking at the structures and materials part of the UAV. From this point onwards, I became responsible for the structural analysis of the entire report. I began by first verifying the tool to know whether the calculations were indeed correct. I did that with the help of analytic calculations. Simplifying the loads and exactly calculating what should be the result and comparing this to what the Matlab code computed. I did the entire structural analysis, looking at the wings, the way the connection is designed for attaching the wings to the fuselage, the way a maintenance hatch can be integrated in the design and many other structural components. I also worked on the risk analysis, materials part and manufacturability, availability and integration.

In the personal appendix I made for the midterm report, I indicated that I can be a little bit quieter than others. This was also something that came out of the peer review and I took it as productive advice. I really tried to let my opinion be more apparent and I think it really paid off. Looking back at the period between midterm and final, I do not find myself as one of the quiet guys anymore. There is however that I can be a little bit too much focused on my responsibilities within the group. The quality that I deliver is, I think also because of this, usually good enough but I could take a bit more initiative. I think the problem with this was also that the summer holiday was getting closer and closer and the end was really in sight. A couple of us just lacked a bit of motivation towards the end. This is also seen when looking at the productivity before and after the midterm report.

Looking at the team itself, I can honestly say that this was one of the best teams I worked with during my bachelor at aerospace. The organization was very good; everyone was focused but not uptight. It was just about right. I have only one comment about the staff and organization. During the final review, it was a bit annoying that we were constantly interrupted. The feedback was however very good and I know it is better to immediately give feedback because otherwise one might forget and the presenter could not better himself during. But this was the final review, we were all a bit nervous about it because there is a lot at stake and being interrupted could really make things worse for the ones that are already susceptive for their nerves.

I really enjoyed designing the ASAP UAV, it was a wonderful project and I would do it again if I had the opportunity. I really enjoyed being part of this team and appreciate the way we were supported by the organization and staff. There was however some trouble with borrowing books from the OSSAs. This was a weak point in their management.

SECTION B.9. M. WOLKEN 145

B.9. M. WOLKEN

For the final report I have worked on the following subjects: RAMS, coating, operations & logistics and vertical stabilizer. I did not like working on RAMS and operations and logistics. Problem with these subjects is the large non-technical part. When I was searching for the coating, I did not find much detailed information. All the coatings I found were from companies selling these coating, therefore not much negative information was given. Also all these coatings are not tested on biodegradable polymers, so testing is needed to verify the viability for our UAV. This is not a satisfying conclusion. The last subject I worked on were the vertical stabilizers of the UAV. These are initially designed based on reference aircraft. Since there is no data of reference UAVs, the design is based on a single propeller aircraft. Because the vertical stabilizers are based on a propeller aircraft with fuselage, the final conclusion of the vertical stabilizers was also not satisfying. Unfortunately because of the time constraint the mistake is not found. The program worked for conventional airplane, unfortunately not for a twin tail flying wing.

I like the subject of this project, but I am not content with the execution of this project. Personally I had expected to perform more calculations instead of writing all the time. It is possible that I have a wrong impression of a design project, but I am disappointed about the lack of calculation steps.

There is a positive attitude in our project group. The fact that we are all Dutch and Belgian guys helps to achieve this attitude. The cooperation within the group was going well. I think communication could be better, but this is difficult within a group of 10 people. We have planned meetings, but here we spoke about important subjects with the whole group. It is sometimes helpful to have a group member check your work for completeness.

The organization of the project was well organized. But there is a lot of noise in the Fellowship. We sat in a large room with 60 students. All these student created a lot of noise, therefore I had to put in earplugs with music to concentrate. However these earplugs made it hard to communicate. But without these earplugs I was really annoyed by the sound.

In 10 weeks it happened 3 or 4 times that we were with 13 people in one room. I think it is a shame this has not happened more often, because the comments received during a meeting were useful. I would choose this project again, bacause I really liked the subject and the project group.

B.10. N.J. VAN WONDEREN

In this personal appendix I'm first going give input on my personal impressions and functioning, I will then address the functioning of the team and finally the cooperation with staff.

To start I want to address first I enjoyed the DSE project and learned a lot during this period of 10 weeks. Not only about the topic but also as working in a team for 10 weeks. At the beginning of the project I asked the team I could take the role of chief engineer and in my opinion I have fulfilled this position successfully. I like being involved in many parts of the design and I like to know as much as possible in every topic. For this reason I read a lot of articles about the different topics and try to stay up to date with everyone in the project. I was fully aware of the topics every team member was working on and help them in case of any problems. My activities after the midterm report where first determining the drag of the UAV and the sizing of the UAV. Also during this time I was determining the aerodynamic properties by first selecting the airfoil and afterwards analyzing the UAV using CFD program. Because the materials and structures part was getting behind of schedule I joined this team and the group had formed a focus group to get back on schedule. With this focus group I belief we had finished the materials and structures parts within time. Before the project I only had little knowledge of the properties of polymers and the manufacturing methods. I found it very interesting to read about the bio-composites and their possibilities in the future.

In group discussions I therefore have the feeling my opinion is respected and many ideas or arguments I use are implemented in the project. For this reason I belief I had a significance influence on the design process and the DSE project in general.

As said before there is a good working atmosphere in the group, everybody wants to make the best out of it and win the DSE symposium at the end. The communication between the team members is extensive and everybody knows what everybody is doing. Synergy is the term used when the effort of multiple part is greater than the cumulative of the individual parts, I think this is the case within the team. The different personalities and different backgrounds make the team complete and provide the team with different inputs. Sometimes a different point of view of a team member can provide a new input in the problem and finally solve it. Only negative point I can give is we could have more effective working hours during the day and could take more initiative when people think they are finished. But again this is only a minor point of complaint.

Finally I'm going to provide some feedback on the cooperation between the group and the staff. I like the fact the staff gives freedom to the team and let us struggle through the different problems. The weekly meetings give the opportunity to ask questions and present the progress. The staff possesses a wide technical background with experts in different fields. Their knowledge has helped us finish the project with good ideas and helpful resources.